

**TRACING METABOLISM FROM SUGARS
AND ONE-CARBON SUBSTRATES USING STABLE ISOTOPES**

by

Jacqueline Eve Gonzalez

A thesis submitted to the Faculty of the University of Delaware in partial fulfillment of the requirements for the degree of Doctor of Philosophy in Chemical Engineering

Spring 2018

© 2018 Jacqueline Eve Gonzalez
All Rights Reserved

**TRACING METABOLISM FROM SUGARS
AND ONE-CARBON SUBSTRATES USING STABLE ISOTOPES**

by

Jacqueline Eve Gonzalez

Approved: _____
Eric M. Furst, Ph.D.
Chair of the Department of Chemical and Biomolecular Engineering

Approved: _____
Babatunde A. Ogunnaike, Ph.D.
Dean of the College of Engineering

Approved: _____
Ann L. Ardis, Ph.D.
Senior Vice Provost for Graduate and Professional Education

I certify that I have read this dissertation and that in my opinion it meets the academic and professional standard required by the University as a dissertation for the degree of Doctor of Philosophy.

Signed:

Maciek R. Antoniewicz, Ph.D.
Professor in charge of dissertation

I certify that I have read this dissertation and that in my opinion it meets the academic and professional standard required by the University as a dissertation for the degree of Doctor of Philosophy.

Signed:

Eleftherios T. Papoutsakis, Ph.D.
Member of dissertation committee

I certify that I have read this dissertation and that in my opinion it meets the academic and professional standard required by the University as a dissertation for the degree of Doctor of Philosophy.

Signed:

Wilfred Chen, Ph.D.
Member of dissertation committee

I certify that I have read this dissertation and that in my opinion it meets the academic and professional standard required by the University as a dissertation for the degree of Doctor of Philosophy.

Signed:

Bryan Tracy, Ph.D.
Member of dissertation committee

ACKNOWLEDGMENTS

There are many people that I must thank and acknowledge for contributing both directly and indirectly to the completion of this dissertation. First, I have to thank my thesis advisor, Maciek Antoniewicz. Thank you for constantly challenging me and pushing me beyond what I thought I was capable of. Thank you for giving me the freedom to try new things and the opportunity to explore multiple research areas. I can only hope to emulate your unwavering positive attitude and genuine curiosity in my future career. I must also thank my committee members Wilfred Chen and Bryan Tracy. I had the pleasure of meeting with both of you several times over the past few years during ARPAE meetings. Thank you for all of your valuable feedback and discussion as well as general advice.

I would like to specifically thank Terry Papoutsakis, one of my committee members. You acted like a second advisor and mentor for me, bringing a new perspective to my work and always willing to give research and life advice. I want to thank you for spending that time on me and my research even though that was not your obligation. To the members of the Papoutsakis lab, thank you for letting me use all of your equipment and lab space and for treating me as a member of the group. Specifically, I have to thank Kyle Bennett. You taught me everything I know about genetic engineering. Thank you for being a constant source for discussion and for being one of the best colleagues I've had the pleasure of working with. I also have to acknowledge other members of the ARPAE team, Lisa Steinberg, Brian Whitaker, Vanessa Falara, Andrew Jones, and others who have provided valuable feedback and were always available for scientific (and sometimes non-scientific) discussions.

Thank you to Fraser Russell for granting me the opportunity to be a teaching fellow and thank you to Josh Enszer and Doug Buttrey for mentoring me through that fellowship. It will be an experience I will never forget and has helped me grow in my teaching abilities. Also, thank you to all CBE department staff, especially Chil and Kathie, who always knew the answer to any question I had and were always available for very unproductive conversations.

I also have to acknowledge my mentors from Cornell. My academic advisor Thomas M. Duncan pushed me to apply to UD, a school that I wasn't considering applying to. Without his advice, I would not have attended graduate school at UD. I also have to thank Bo Ri Seo, my graduate student mentor from the Fischbach lab. Bo, you cultivated my interest in research. Thank you for spending your valuable time mentoring me and teaching me how to do good research. I especially enjoyed our non-scientific conversations and endeavors and all the wisdom you've shared with me. And thank you to all Fischbach lab members for creating an innovative, intellectual, and entertaining research environment and for shaping me into the researcher I am today.

I definitely would not have made it through this PhD without my lab group, both past and present members, especially Jen, Niko, Chris, Camil, Brian and Ellie. I'm grateful to have spent these past few years with this great group of people who constantly make me laugh and smile. Each of you brought a unique perspective (and personality) to the group as well as to my experience in graduate school. I can only hope to find another group of people to spend everyday with that is as fun, intelligent, and crazy as you all are. Also, thank you to any of you who took ODs for me or took samples off the heating blocks.

Thank you to all my UD friends who have made this entire experience enjoyable. To my fellow classmates, who have been there since first year classes, and to all of my other UD friends, especially Bassil, Elisa, Chen-yuan, Amber, Trishelle, Ru, Hannah, Camil, Ellie, and Victoria, thank you for providing the life to my work-life balance with movie nights, lunches, adventures (haunted houses, six flags, UD creamery runs, escape rooms, music bingo and trivia and so many more) and just conversations in the halls of Colburn. You all have no idea how much all of these experiences have meant to me and I am grateful to have spent this time with this amazing group of people.

Lastly, I have to thank my non-UD family. Thank you to my parents who have unconditionally supported me throughout this entire process even though they have no idea what I'm doing or why I'm doing it. Thank you to Lauren for being my non-ChemE connection to the world and for sticking with me since the first day of college. And finally, I have to thank my partner Cesar. You're in this section because I consider you now as part of my family. Thank you for being there for me since the beginning (literally since the first day of graduate school). The only reason I made it to the end was because of your patience and constant support. Thank you for going along with all of my weird shenanigans and for dealing with my endless naps. Thank you for being honest and genuine and for always knowing what to say to make me laugh. I couldn't have asked for a better person to spend these last few years with.

TABLE OF CONTENTS

LIST OF TABLES	xi
LIST OF FIGURES	xiv
ABSTRACT	xxiii

Chapter

1	INTRODUCTION	1
1.1	Studying Metabolism of Renewable and Waste Feedstocks	1
1.1.1	Metabolism of Lignocellulosic Biomass	2
1.1.2	Native and Synthetic Pathways for Conversion of Renewable Feedstocks	5
1.2	Tracing Metabolism with Isotopic Tracers.....	8
1.2.1	Measuring Metabolism with ¹³ C- Metabolic Flux Analysis.....	9
1.3	Aims and Outline of Thesis	14
2	COMPREHENSIVE ANALYSIS OF GLUCOSE AND XYLOSE METABOLISM IN <i>Escherichia coli</i> UNDER AEROBIC AND ANAEROBIC CONDITIONS BY ¹³ C-METABOLIC FLUX ANALYSIS....	18
2.1	Introduction	18
2.2	Materials and Methods	20
2.2.1	Materials	20
2.2.2	Strains and Growth Conditions	20
2.2.3	Analytical Methods	21
2.2.4	Biomass composition analysis.....	22
2.2.5	Gas chromatography-mass spectrometry	22
2.2.6	Metabolic network model and ¹³ C-metabolic flux analysis	23
2.2.7	Goodness-of-fit analysis	25
2.3	Results and Discussion	25
2.3.1	Growth characteristics	25
2.3.2	Biomass composition analysis.....	27
2.3.3	Turnover of biomass macromolecules.....	29
2.3.4	Growth of β -oxidation knockouts.....	34
2.3.5	Validation of metabolic network models	35

2.3.6	¹³ C-Metabolic Flux Analysis	35
2.3.7	Quantitative analysis of co-factor balances	40
2.4	Conclusion	44
3	CHARACTERIZATION OF GLUCOSE AND XYLOSE CO- CONSUMING STRAINS AIDS IN IDENTIFICIATION OF IDEAL DESIGN FOR SUGAR CO-UTILIZATION	46
3.1	Introduction	46
3.2	Materials and Methods	47
3.2.1	Materials	47
3.2.2	Strains and growth conditions	48
3.2.3	Analytical methods	48
3.2.4	Gas chromatography-mass spectrometry	49
3.2.5	Tracer simulations	49
3.2.6	Metabolic network model and ¹³ C-metabolic flux analysis	50
3.2.7	Goodness-of-fit analysis	51
3.3	Results and Discussion	51
3.3.1	Knockouts of PTS respond to feed composition	51
3.3.2	Engineered strains for co-utilization exhibit various uptake profiles	54
3.3.3	Comprehensive analysis of engineered strains for co-utilization	56
3.3.4	Ideal co-utilizing strain demands linear uptake profile	61
3.4	Conclusion	63
4	METHANOL ASSIMILATION IN <i>Escherichia coli</i> IS IMPROVED BY CO-UTILIZATION OF THREONINE AND DELETION OF LEUCINE- RESPONSIVE REGULATORY PROTEIN	66
4.1	Introduction	66
4.2	Materials and Methods	69
4.2.1	Materials	69
4.2.2	Strains and growth conditions	69
4.2.3	Analytical methods	71
4.2.4	Amino acid quantification	71
4.2.5	RNA and glycogen quantification	71
4.2.6	Gas chromatography-mass spectrometry	72

4.3	Results	73
4.3.1	¹³ C-labeling demonstrates that yeast extract is a superior co-substrate compared to glucose in enhancing methanol assimilation.....	73
4.3.2	Threonine as a co-substrate leads to high ¹³ C-labeling and enhanced growth.....	75
4.3.3	A potential role for the leucine-responsive protein (Lrp) in methylotrophy.....	80
4.3.4	Deletion of the Lrp gene enhances methanol assimilation	81
4.4	Discussion and Conclusions	84
5	METABOLIC MODEL VALIDATION AND ¹³ C-METABOLIC FLUX ANALYSIS OF THE METHANOGENIC ARCHAEON <i>Methanosarcina acetivorans</i>	87
5.1	Introduction	87
5.2	Materials and Methods	90
5.2.1	Materials	90
5.2.2	Strain and growth conditions.....	90
5.2.3	Analytical methods.....	91
5.2.4	Gas analysis by mass spectrometer	91
5.2.5	Gas chromatography-mass spectrometry	91
5.2.6	Metabolic network model.....	92
5.2.7	¹³ C-Metabolic flux analysis.....	92
5.2.8	Goodness-of-fit analysis	93
5.3	Results and Discussion	94
5.3.1	Characterization of growth on ¹³ C-methanol	94
5.3.2	Network model validation	96
5.3.3	¹³ C-Metabolic flux analysis.....	102
5.4	Conclusion.....	105
6	APPLICATION AND EVALUATION OF METABOLIC FLUX ANALYSIS METHODS FOR METABOLIC AND ISOTOPIC NON-STEADY STATE.....	106
6.1	Introduction	106
6.2	Methods	107

6.2.1	Metabolic Network Model	107
6.2.2	Simulation of labeling using EMU balances	108
6.2.3	Calculation of parameter sensitivities	110
6.2.4	Extension of EMU balances to include metabolite C.....	111
6.2.5	Estimation of parameters	112
6.2.6	Statistical Analysis	113
6.3	Results and Discussion	114
6.3.1	Simulation of labeling patterns.....	114
6.3.2	Application of metabolic flux analysis methods to a simple model	116
6.3.3	Effect of including additional measurements	121
6.3.4	Testing the limits of ¹³ C-DMFA.....	125
6.4	Conclusions	128
7	CONCLUSIONS AND FUTURE WORK.....	130
7.1	Summary of Conclusions	130
7.2	Future work	133
	REFERENCES	138
Appendix		
A	SUPPLEMENTARY DATA FOR CHAPTER 2.....	153
B	SUPPLEMENTARY DATA FOR CHAPTER 3.....	179
C	SUPPLEMENTARY DATA FOR CHAPTER 4.....	224
D	SUPPLEMENTARY DATA FOR CHAPTER 5.....	239
E	REPRINT PERMISSION LETTERS.....	250

LIST OF TABLES

Table 2.1	Physiological characteristics of <i>E. coli</i> grown in batch culture on glucose and xylose under aerobic and anaerobic conditions in MOPS minimal medium at 37°C.	27
Table 6.1	¹³ C-Metabolic flux analysis methods and the parameters estimated in each method.	117
Table A.1	Biomass composition (% Dry Weight) of <i>E. coli</i> grown on glucose or xylose under aerobic and anaerobic conditions.	153
Table A.2	Fatty acid composition (umol/gFA) of <i>E. coli</i> grown on glucose or xylose under aerobic and anaerobic conditions.	153
Table A.3	Amino acid composition (umol/gProtein) of <i>E. coli</i> grown on glucose or xylose under aerobic and anaerobic conditions.	154
Table A.4	Metabolic network models for ¹³ C-metabolic flux analysis of <i>E. coli</i> grown on glucose or xylose under aerobic and anaerobic conditions. ...	154
Table A.5	Mass isotopomer distributions from parallel labeling experiments with <i>E. coli</i> grown on glucose under aerobic and anaerobic conditions.	159
Table A.6	Mass isotopomer distributions from parallel labeling experiments with <i>E. coli</i> grown on xylose under aerobic and anaerobic conditions.	165
Table A.7	Results of ¹³ C-MFA for <i>E. coli</i> grown on glucose under aerobic and anaerobic conditions. The reaction numbers correspond to the reactions listed in Table A.4. The fluxes are normalized to a substrate uptake rate of 100. 95% confidence intervals of fluxes (LB95 = lower bound, UB95 = upper bound) were determined by evaluating the sensitivity of the minimized SSR to flux variations.	170
Table A.8	Results of ¹³ C-MFA for <i>E. coli</i> grown on xylose under aerobic and anaerobic conditions. The reaction numbers correspond to the reactions listed in Table A.4. The fluxes are normalized to a substrate uptake rate of 100. 95% confidence intervals of fluxes (LB95 = lower bound, UB95 = upper bound) were determined by evaluating the sensitivity of the minimized SSR to flux variations.	173

Table B.1	¹³ C-labeling (in %) of proteinogenic amino acids and carbohydrates for $\Delta cr r$, $\Delta pts G$, $\Delta pts H$, and $\Delta pts I$ knockouts during growth on [U- ¹³ C]glucose and unlabeled xylose. The condition indicates the ratio of glucose to xylose. “Avg” indicates the average carbon labeling.	179
Table B.2	Metabolic network models for ¹³ C-metabolic flux analysis of GX50 and LMSE2 strains grown on mixtures of glucose and xylose or on glucose/xylose alone.....	184
Table B.3	Results of ¹³ C-MFA of LMSE2 grown on glucose and xylose at the specified ratios. The reaction numbers correspond to the reactions listed in Table B.2. The fluxes are normalized to a total substrate uptake rate of 100. 95% confidence intervals of fluxes (LB95 = lower bound, UB95 = upper bound) were determined by evaluating the sensitivity of the minimized SSR to flux variations.....	188
Table B.4	Results of ¹³ C-MFA for GX50 grown on glucose and xylose at the specified ratios. The reaction numbers correspond to the reactions listed in Table B.2. The fluxes are normalized to a total substrate uptake rate of 100. 95% confidence intervals of fluxes (LB95 = lower bound, UB95 = upper bound) were determined by evaluating the sensitivity of the minimized SSR to flux variations.....	193
Table B.5	Mass isotopomer distributions from parallel labeling experiments with LMSE2 grown on glucose and xylose at the specified ratio.	203
Table B.7	Mass isotopomer distributions from parallel labeling experiments with GX50 grown on glucose and xylose at the specified ratio.	208
Table C.1	¹³ C-labeling (%) in biomass components during growth on glucose, yeast extract, casamino acids, or tryptone and ¹³ C-methanol (average of two replicates).	224
Table C.2	OD ₆₀₀ for growth on co-substrates both with and without ¹³ C-methanol (average of two replicates)	226
Table C.3	¹³ C-labeling (%) in biomass components during growth on a co-substrate and ¹³ C-methanol after 72 hours for the non-degradable amino acids (average of two replicates).	227
Table C.4	¹³ C-labeling (%) in biomass components during growth on a co-substrate and ¹³ C-methanol at 72 hours for degradable amino acids (average of two replicates)	229

Table C.5	^{13}C -labeling (%) in biomass components during growth on a co-substrate and ^{13}C -methanol at 72 hours for non-amino acids (average of two replicates)	231
Table D.1	Metabolic network model used for ^{13}C -metabolic flux analysis in <i>M. acetivorans</i> . “2e” represents two electrons.	239
Table D.2	Results from ^{13}C -MFA of <i>M. acetivorans</i> grown on methanol and methanol + acetate. The reaction numbers correspond to the reactions listed in Table D.1. The fluxes are normalized to a methanol uptake rate of 1000. 95% confidence intervals of fluxes (LB95 = lower bound, UB95 = upper bound) were determined by evaluating the sensitivity of the minimized SSR to flux variations. Data from a ^{13}C -methanol + acetate and methanol + [U- ^{13}C]acetate were fit simultaneously to estimate fluxes.....	241
Table D.3	Mass isotopomer distributions from labeling experiments using ^{13}C -methanol, ^{13}C -methanol + acetate, or methanol + [U- ^{13}C]acetate as substrates.	244

LIST OF FIGURES

Figure 1.1	Conversion of lignocellulose-derived sugars into substrates of central carbon metabolism.	4
Figure 1.2	Native and synthetic metabolic pathways for conversion of renewable feedstocks into value-added products.....	8
Figure 1.3	Comparison of different designs of isotopic labeling experiments to quantify co-utilization of multiple substrates using classical ^{13}C -MFA (left) and integrated ^{13}C -MFA based on parallel labeling experiments (right).....	12
Figure 2.1	Biomass composition analysis of wild-type <i>E. coli</i> grown aerobically and anaerobically on glucose and xylose.	29
Figure 2.2	Expected (black bars) and measured (red bars) mass isotopomer distributions for five metabolites (valine, serine, phenylalanine, aspartate, and palmitate) from tracer experiments with $[\text{U-}^{13}\text{C}]$ glucose and $[\text{U-}^{13}\text{C}]$ xylose. Presence of incompletely labeled mass isotopomers, especially under anaerobic conditions, indicates significant biomass turnover.	30
Figure 2.3	Mass isotopomer distributions for the glycolytic intermediates 3-phosphoglycerate (3PG), phosphoenolpyruvate (PEP), and pyruvate (Pyr) from tracer experiment with $[\text{U-}^{13}\text{C}]$ glucose and $[\text{U-}^{13}\text{C}]$ xylose. Presence of unlabeled mass isotopomers (M+0), especially during anaerobic growth on $[\text{U-}^{13}\text{C}]$ xylose, indicates that significant biomass turnover occurs.	33
Figure 2.4	(A) β -oxidation pathway with genes encoding each reaction. (B) Growth rates of wild-type <i>E. coli</i> and knockout strains $\Delta fadD$, $\Delta fadK$, $\Delta fadD\Delta fadK$ grown aerobically and anaerobically on glucose and xylose as substrates. The double-knockout strains $\Delta fadD\Delta fadK$ did not grow on xylose under anaerobic conditions	36
Figure 2.5	Validation of metabolic network models for ^{13}C -MFA. Sum of squared residual (SSR) values are shown for models containing various dilution reactions. For the aerobic cultures, inclusion of CO_2 dilution was necessary to obtain an acceptable SSR value (below the dotted line). For the anaerobic cultures, CO_2 and lipid dilution were necessary to achieve an acceptable SSR value.....	37

Figure 2.6	Metabolic flux maps for <i>E. coli</i> grown in batch culture at four growth conditions: aerobic and anaerobic growth on glucose and xylose, respectively. Fluxes were determined using integrate ^{13}C -MFA by simultaneously fitting labeling data from two tracers for each substrate. For glucose, [1,2- ^{13}C]glucose and [1,6- ^{13}C]glucose tracers were used. For xylose, [1,2- ^{13}C]xylose and [5- ^{13}C]xylose tracers were used. Complete flux results are provided in Tables A.7 and A.8.....	39
Figure 2.7	Production and consumption of key co-factors in metabolism NADH/FADH ₂ , NADPH, and ATP, during aerobic and anaerobic growth on glucose (Gluc) or xylose (Xyl). “Other” in NADPH panel represents the contribution of malic enzyme to NADPH production. “Other” in ATP panel represents the estimated ATP maintenance cost (here, assuming P/O ratio = 2.0).....	43
Figure 3.1	Characterization of growth and sugar allocation in PTS knockouts. The growth rate and ^{13}C -labeling of glycogen, RNA, and alanine were measured for each PTS knockout at different ratios of glucose to xylose, as indicated by the color. For the ^{13}C -labeling experiment, [U- ^{13}C]glucose and unlabeled xylose were used as tracers. The growth rates of both $\Delta ptsH$ and $\Delta ptsI$ vary depending on the ratio of glucose to xylose. As the ratio of glucose to xylose increases, the relative uptake of glucose also increases. Based on the ^{13}C -labeling of alanine, $\Delta ptsG$, $\Delta ptsH$, and $\Delta ptsI$ all prefer xylose over glucose (<50% labeling in alanine) while Δcrr prefers glucose (>50% labeling in alanine. Error bars indicate standard error (n =3).	53
Figure 3.2	Comparison of two co-utilizing strains and WT <i>E. coli</i> . For each strain, the initial uptake rates of glucose and xylose were measured. The ratio of these rates (% Xylose Uptake) was plotted versus initial fraction of xylose in the culture (% Xylose Concentration). Additionally, using these uptake profiles, we were able to simulate the glucose and xylose concentrations and compare this simulation to the measured concentrations. In WT, diauxic growth was observed, as expected, with the uptake rate of glucose being unaffected by the presence of xylose. The ratio of uptake rates for LMSE2 remained constant at 60% xylose uptake and no growth was observed when glucose or xylose were the sole substrate. The uptake rates in GX50 varied, depending on the initial concentrations of the two sugars, with a general preference for xylose. Error bars indicate standard error (n=3).	55

Figure 3.3	Precision of estimated fluxes for various tracer schemes. Improved precision is observed using parallel labeling experiments with each sugar isotopically labeled. Poor precision is observed in single labeling experiments or when only one substrate is isotopically labeled.	57
Figure 3.4	Metabolic flux map for strains LMSE2 and GX50 grown in a 1:1 ratio of glucose to xylose. Fluxes were estimated using ^{13}C -MFA, including measurements from parallel labeling experiments using [1,2- ^{13}C]glucose + [1,2- ^{13}C]xylose and [1,6- ^{13}C]glucose and [5- ^{13}C]xylose as tracers.	59
Figure 3.5	Comparison of estimate fluxes for various glucose/xylose mixtures. Highlighted changes indicate at least a 15% relative increase (blue) or decrease (red) compared to the fluxes estimate for a 1:1 glucose/xylose mixture. Changes in the TCA cycle fluxes are observed for LMSE2 while changes in the PPP fluxes are observed for GX50.	60
Figure 3.6	Production and consumption of key co-factors in metabolism. Using fluxes estimated by ^{13}C -MFA, utilization of NADH/FADH ₂ , NADPH, and ATP was quantified for each strain. GX50 and LMSE2 differ in the consumption of NADH and production of NADPH by the transhydrogenase as well as the production of NADPH by the PP pathway. ATP allocation remains relatively constant for both strains....	61
Figure 3.7	Simulation of theoretical uptake profiles. The uptake profiles examined were diauxic (A), parabolic (B), linear (C), and constant (D). Each profile was used to simulate the consumption of glucose and xylose for different starting concentrations in batch culture. It is clear that the only profile resulting in an efficient process is the linear profile, with simultaneous consumption and no residual sugar.	63

- Figure 4.1 Synthetic methylotrophy in *E. coli* and its relation to the global regulator Lrp. To achieve a methylotrophic phenotype in *E. coli*, three heterologous genes were expressed methanol dehydrogenase (mdh), 3-hexulose-6-phosphate synthase (hps), and 6-phospho-3-hexuloisomerase (phi). Methanol enters the pentose phosphate pathway and through various rearrangement reactions, Ru5P is generated for another round of formaldehyde fixation. In this work, we demonstrate that increased methanol assimilation is associated with increased flux from threonine (Thr) to glycine (Gly) and serine (Ser). To improve incorporation of methanol, the leucine-responsive protein (Lrp), which negatively regulates reactions denoted with (-) and positively regulates reactions denoted (+), was deleted. 68
- Figure 4.2 Yeast extract is a better co-substrate for methanol assimilation than glucose. (A) The increase in OD₆₀₀ in the presence of methanol compared to the absence of methanol was determined for growth with the co-substrates glucose (red bars) and yeast extract (blue bars). (B) ¹³C-labeling in biomass components (amino acids, RNA, and glycogen) from ¹³C-methanol was measured for both co-substrates after 48 hours. Overall, yeast extract was the superior co-substrate for methanol assimilation as indicated by higher labeling and improved growth in the presence of methanol. Error bars indicate standard error (n=2). 74
- Figure 4.3 Growth is improved in the presence of methanol for several co-substrates. Growth profiles for *E. coli* on leucine (A), threonine (B), acetate (C), and glucose (D) as co-substrates in the presence (dashed line) or absence (solid line) of methanol. The number of cell doublings in both the presence and absence of methanol was determined for each co-substrate (E). In the presence of methanol, growth was improved for many co-substrates, however, the extent of improvement varied, generally decreasing with increased growth. Error bars indicate standard error (n = 2). 76
- Figure 4.4 Threonine as a co-substrate leads to high ¹³C-methanol incorporation in biomass components. Isotopic labeling from ¹³C-methanol was measured for 25 co-substrates. Here, mass isotopomer distributions (MID) of glycogen (A), RNA (B), valine (C), alanine (D), glutamate (E), and serine (F) are shown. Relative abundances are the measured mass isotopomer distributions that have been corrected for natural isotope abundances. High labeling in biomass components was observed when threonine was the co-substrate. Error bars indicate standard error (n = 2). 78

Figure 4.5	Deletion of <i>lrp</i> increases biomass concentration in both the absence and presence of methanol. The base (A) and Δ <i>lrp</i> (B) strains were grown in 1.5 g/L yeast extract with (dashed line) and without (solid line) 60 mM ^{13}C -methanol. Both strains reached a higher OD ₆₀₀ in the presence of methanol. The OD ₆₀₀ of the Δ <i>lrp</i> strain was consistently higher than that of the base strain. Error bars indicate standard error (n = 3). An asterisk indicates a statistically significant difference (p < 0.05) between the conditions with and without methanol for each strain.	82
Figure 4.6	^{13}C -labeling in RNA and glycogen from ^{13}C -methanol are significantly enhanced when <i>lrp</i> is deleted. Isotopic labeling of RNA (A, B) and glycogen (C, D) from ^{13}C -methanol was measured for both the base strain and the Δ <i>lrp</i> strain. Relative abundances are the measured mass isotopomer distributions that have been corrected for natural isotope abundances. Absolute amounts of ^{13}C -RNA (E) and ^{13}C -glycogen (F) were also measured and are represented here as % dry weight (DW). ^{13}C -labeling of glycogen and RNA in the Δ <i>lrp</i> strain was significantly higher than that of the base strain at each respective timepoint (p < 0.05). While the total amount of ^{13}C -RNA was similar for both strains, the amount of ^{13}C -glycogen was significantly higher in the Δ <i>lrp</i> strain. Error bars indicate standard error (n = 3). An asterisk indicates a statistically significant difference (p < 0.05).	83
Figure 5.1	Physiological characterization of <i>M. acetivorans</i> during growth on ^{13}C -methanol. (A) Growth and methanol consumption were monitored until all methanol was consumed. (B) CO_2 , $^{13}\text{CO}_2$, CH_4 , and $^{13}\text{CH}_4$ were also monitored over the course of the culture, normalized to the N_2 in the headspace.	95
Figure 5.2	Carbon and electron balances. The majority of carbon and electrons from methanol are used for production of methane. Both balances close (> 90%).....	95
Figure 5.3	Biomass composition analysis of <i>M. acetivorans</i> compared to <i>E. coli</i> ...	97
Figure 5.4	Network model for <i>M. acetivorans</i> and annotated genes based on KEGG and Biocyc databases and genome-scale models.	98
Figure 5.5	Mass isotopomer distributions for the amino acids alanine (Ala), serine (Ser), glutamate (Glu), aspartate (Asp), and threonine (Thr) during growth on ^{13}C -methanol. The difference in labeling between glutamate and aspartate indicate the presence of an incomplete TCA cycle.....	99

Figure 5.6	^{13}C -labeling from [1,4- ^{13}C]aspartate and [U- ^{13}C]glutamate tracer experiments reveal presence of incomplete TCA cycle (A) and threonine aldolase (B). (C) If threonine aldolase is active, a [1,4- ^{13}C]aspartate tracer will result in labeling of the 246 m/z fragment of glycine but not the 216 m/z fragment of glycine, which is indeed observed in (B).	99
Figure 5.7	Metabolic flux map for <i>M. acetivorans</i> during growth on ^{13}C -methanol. Fluxes were determined using ^{13}C -MFA.....	101
Figure 5.8	Allocation of electrons and ATP across different pathways during growth on methanol.....	102
Figure 6.1	Simple metabolic network model that will be used for evaluating metabolic flux analysis methods.	108
Figure 6.2	Changes in fluxes v_3 and v_4 . Shown here are changes of 0%, 10%, and 20%. Additionally 5%, 15%, and 25% changes were also tested. Flux v_3 decreases over time and flux v_4 increases over time.....	115
Figure 6.3	Simulated MIDs of metabolite D. (A) shows the MIDs when the fluxes are constant over time for pool sizes 1, 5, and 20. (B) shows the MIDs when the fluxes change by 0%, 10%, and 20% for a pool size of 10. The grey dashed lines indicate the timepoints used to estimate parameters.	116
Figure 6.4	Comparison of flux estimation for each MFA method using a pool size of 10 and a flux change of 25%. The estimated parameters as well as the uncertainties of those estimates are shown for both v_3 (A) and v_4 (B). The shaded regions indicate the uncertainty. ^{13}C -MFA was used to estimate fluxes at each of the six timepoints. ^{13}C -NMFA estimated one flux value for the entire duration of the experiment. ^{13}C -DMFA estimated the initial and final flux values.	118
Figure 6.5	Comparison of MFA methods using labeling measurements of metabolites B and D. Each heat map corresponds to a different statistical value for each method: SSR, precision, or accuracy. Precision and accuracy are determined with respect to the estimated values of the fluxes v_3 and v_4	120

Figure 6.6	Comparison of MFA methods using labeling measurements of metabolites B, C, and D. Each heat map corresponds to a different statistical value for each method: SSR, precision, or accuracy. Precision and accuracy are determined with respect to the estimated values of the fluxes v_3 and v_4	122
Figure 6.7	Comparison of flux estimation using ^{13}C -NMFA after including labeling measurements of metabolites B and D as well as pool size measurements of metabolites B, C, and D with different uncertainties in the measurement (5%, 20%, 100%). Each heat map corresponds to a different statistical value for each method: SSR, precision, or accuracy. Precision and accuracy are determined with respect to the estimated values of the fluxes v_3 and v_4	123
Figure 6.8	Comparison of flux estimation using ^{13}C -DMFA after including labeling measurements of metabolites B and D as well as pool size measurements of metabolites B, C, and D with different uncertainties in the measurement (5%, 20%, 100%). Each heat map corresponds to a different statistical value for each method: SSR, precision, or accuracy. Precision and accuracy are determined with respect to the estimated values of the fluxes v_3 and v_4	124
Figure 6.9	Simulated MIDs of metabolite D. (A) shows the MIDs when the fluxes are constant over time for pool sizes 10, 100, and 200. (B) shows the MIDs when the fluxes change by 0%, 40%, and 80% for a pool size of 100. (C) shows the MIDs when the fluxes change by 0%, 40%, and 80% for a pool size of 10. The grey dashed lines indicate what timepoints were used to estimate parameters.	126
Figure 6.10	Comparison of flux estimation using ^{13}C -DMFA after including labeling measurements of metabolites B and D, measurements of B, C, D, and measurements of B, C, D and pool sizes (uncertainty in measurement is 20%). Each heat map corresponds to a different statistical value for each method: SSR, precision, or accuracy. Precision and accuracy are determined with respect to the estimated values of the fluxes v_3 and v_4	127
Figure 6.8	Summary of MFA methods and when to apply them. When choosing a method, one must consider if the system is at metabolic or isotopic steady state. ^{13}C -MFA and ^{13}C -MFAg can be used for isotopic steady state. ^{13}C -NMFA can be used for isotopic non-steady state. ^{13}C -DMFA can be used for metabolic and isotopic non-steady state.	128

Figure A.1	Analysis of ^{13}C -MFA goodness-of-fit for various metabolic network models. Sum of squared residual values are shown here for models containing different dilution reactions in the model. Overall, including dilution reactions that account for RNA turnover, glycogen turnover, and amino acid turnover (here, glutamate turnover) did not improve the goodness-of-fit.....	177
Figure A.2	Representative growth curves for each condition: Aerobic Glucose (A), Aerobic Xylose (B), Anaerobic Glucose (C), Anaerobic Xylose (D).	178
Figure B.1	Growth rates for wild-type <i>E. coli</i> , GX50 and LMSE2 for various glucose:xylose concentrations. Error bars indicate standard error ($n>3$).	220
Figure B.2	Representative growth curves for LMSE2 grown on a (A) 1:1, (B) 2:2, (C) 1:2, or (D) 2:1 ratio of glucose to xylose.	221
Figure B.3	Representative growth curves for GX50 grown on a (A) 1:1, (B) 2:2, (C) 1:2, (D) 2:1, (E) 1:0, (F) 2:0, (G) 0:1, or (H) 0:2 ratio of glucose to xylose.....	222
Figure B.4	Comparison of estimated fluxes for various glucose/xylose mixtures. Highlighted changes indicate at least a 15% relative difference compared to the fluxes estimated for the 1x case. Fluxes highlighted blue indicate a flux increase while fluxes highlighted red indicate a flux decrease. No significant change was observed when the glucose or xylose concentration was doubled.	223
Figure C.1	Yeast extract as a co-substrate results in improved growth when methanol is present. Growth was characterized in medium containing 1.5 g/L glucose (A) or 1.5 g/L yeast extract with (dashed line) or without (solid line) 60 mM ^{13}C -methanol. A substantial improvement in growth was observed when yeast extract was the co-substrate. Error bars indicate standard error ($n = 2$).	234
Figure C.2	High ^{13}C -labeling is observed in fructose 6-phosphate, a key intermediate in methanol assimilation via the RuMP pathway. ^{13}C -labeling of fructose 6-phosphate was measured for the base strain grown on 1.5 g/L yeast extract and 60 mM ^{13}C -methanol at 24 and 48 hour timepoints. Error bars indicate standard error ($n = 2$).	234

Figure C.3	Amino acids are the major components of casamino acids, tryptone, and yeast extract. The relative amount of amino acids, both as free amino acids and in peptide form, was measured for casamino acids, tryptone, and yeast extract. Amino acids composed >52% of the total dry weight. Error bars indicate standard error ($n = 4$).....	235
Figure C.4	Casamino acids, tryptone, and yeast extract affect growth similarly when methanol is present. The increase in OD ₆₀₀ in the presence of methanol was compared to control experiments without methanol. Error bars indicate standard error ($n = 2$).....	235
Figure C.5	¹³ C-methanol assimilation is enhanced when casamino acids, tryptone, or yeast extract are used as co-substrates. ¹³ C-labeling of biomass components from ¹³ C-methanol was measured for each co-substrate at 48 hours. Error bars indicate standard error ($n = 2$).....	236
Figure C.6	Deletion of <i>lrp</i> has a similar effect as adding threonine to yeast extract in the base strain. The base strain and the Δ <i>lrp</i> strain were both grown in 1.5 g/L yeast extract + 60 mM ¹³ C-methanol, or 1.5 g/L yeast extract + 5 mM threonine (Thr) + 60 mM ¹³ C-methanol. The ¹³ C-labeling of RNA and glycogen were measured by GC-MS. Adding threonine to yeast extract in the base strain resulted in similar labeling as Δ <i>lrp</i> strain grown in yeast extract alone as the co-substrate. Error bars indicate standard error ($n = 3$).	237
Figure C.7	Yeast extract and threonine as co-substrates also results in improved growth with methanol present. Growth of the base strain was characterized in medium containing 1.5 g/L yeast extract and 5 mM threonine with (dashed line) or without (solid line) 60 mM methanol. An improvement in growth was observed when methanol was present. Error bars indicate standard error ($n = 3$).....	238
Figure D.1	Metabolic flux map for <i>M. acetivorans</i> grown on methanol and acetate. Parallel labeling experiments were performed using ¹³ C-methanol + acetate and methanol + [U- ¹³ C]acetate.....	249

ABSTRACT

The production of chemicals through bioconversion has received much attention over the past decade. Focus is now shifting towards the utilization of cheap, renewable and waste feedstocks for chemical production. With the availability of these feedstocks, metabolic engineering efforts are targeted towards engineering organisms to utilize one or more of these substrates and produce value-added chemicals. Therefore, it is of critical importance to evaluate the economic feasibility of bioprocesses, determine the capabilities of microbial systems, identify targets for improvements, and select ideal candidates for industrial implementation.

A powerful method for characterizing *in vivo* metabolism is through the use of ^{13}C -labeled substrates (or ^{13}C -tracers). Tracing techniques allow quantitative evaluation of the flow of carbon from feedstocks to central metabolism and further into the desired products. Additionally, advanced techniques, such as ^{13}C -metabolic flux analysis (^{13}C -MFA), can be applied to gain a fine-grained picture of native metabolism and metabolic changes that result from genetic manipulations. Isotopic tracers are easy to implement and can be used to achieve a wealth of new information about metabolism. However, there has been limited application of tracers and therefore, their potential has not been realized. We aim to demonstrate how tracers can be applied to various systems to gain a detailed understanding of pathway utilization. The systems studied here include ones with multiple substrates, engineered pathways, and one-carbon substrates. Additionally, we develop new methods of MFA that allow for its application to a broader range of systems.

Sugars are the main product of lignocellulose hydrolysis and a common feedstock for bioprocesses. While glucose and xylose are the two most abundant

sugars derived from the breakdown of lignocellulosic biomass, there have been few studies of their metabolism under various environmental conditions. In the absence of this experimental data, constraint-based approaches cannot be used to guide new metabolic engineering designs. In this work, we have addressed this critical gap by performing comprehensive characterizations of glucose and xylose metabolism under aerobic and anaerobic conditions, including applying ^{13}C -MFA, measuring biomass composition and biomass turnover, and quantifying co-factor requirements. Additionally, we examine more efficient *E. coli* strains that can co-utilize these two sugars through application of ^{13}C -MFA and interrogation of their sugar uptake profile. Through this analysis, we identified the ideal uptake profile to be linear and non-biased towards a specific substrate, focusing future efforts towards the development of novel transport systems.

Another interesting feedstock, methane, the main component of natural gas, can be used to produce methanol which can be further converted to other valuable products. There is increasing interest in using biological systems for the production of fuels and chemicals from methanol, termed methylotrophy. Here, we first examine methanol assimilation metabolism in a synthetic methylotrophic *E. coli* strain. Through our investigations, we proposed specific metabolic pathways that, when activated, correlated with increased methanol assimilation. These pathways are normally repressed by the leucine-responsive regulatory protein (*lrp*), a global regulator of metabolism associated with the feast-and-famine response in *E. coli*. By deleting *lrp*, we were able to further enhance the methylotrophic ability of our synthetic strain, as demonstrated through increased incorporation of ^{13}C carbon from ^{13}C -methanol into biomass.

Additionally, we study the methanogen, *Methanosarcina acetivorans*, a model organism for studying the conversion of various substrates into methane and a possible host for the conversion of methane into value-added products. Here, we characterize this organism during growth on the one-carbon substrate, methanol. Typically, estimating fluxes during growth on one-carbon substrates requires more advanced computational approaches and precise sampling of metabolic intermediates compared to ^{13}C -MFA. Here, we applied classical ^{13}C -MFA to validate the network model and generate the first flux map for *M. acetivorans*, demonstrating the successful application of classical ^{13}C -MFA to a one-carbon system.

Lastly, we aim to extend the reach of metabolic flux analysis. To apply ^{13}C -MFA, it is assumed that the system being interrogated is at metabolic and isotopic steady state, where fluxes and isotopic labeling remain constant over time. This assumption limits the application of ^{13}C -MFA to systems where these assumptions do not hold. Here, we address the need for metabolic flux analysis methods that can be used for atypical systems, ones that are not at isotopic or metabolic steady state. We present an extension of DMFA to include isotopic labeling measurements (^{13}C -DMFA) and evaluate established MFA methods (^{13}C -MFA, ^{13}C -NMFA, and ^{13}C -DMFA) and their ability to estimate fluxes for various conditions. It was concluded that ^{13}C -MFA can be used for systems at isotopic steady state, ^{13}C -NMFA can be used for systems at metabolic steady state, and ^{13}C -DMFA can be used for metabolic and isotopic non-steady state. This work is the first demonstration of ^{13}C -DMFA and clearly outlines how and when each established method should be applied, substantially increasing the range of systems and organisms that can be studied.

Chapter 1

INTRODUCTION

1.1 Studying Metabolism of Renewable and Waste Feedstocks

The production of chemicals through bioconversion has received much attention over the past decade (Himmel and Bayer, 2009). Focus is now shifting towards the utilization of cheap, renewable and waste feedstocks, ultimately leading to reduced operating costs, reduced reliance on non-renewable feedstocks and feedstocks that compete with food supply, and reduced environmental impact (Elkins et al., 2010; Liao et al., 2016). Renewable and waste feedstocks include lignocellulosic biomass and gaseous substrates such as syngas, methane, hydrogen gas, and carbon dioxide. The primary renewable feedstock, lignocellulosic biomass, is composed of three main components, two of which, cellulose and hemicellulose, can be hydrolyzed to C6 and C5 sugar monomers and used as substrates in fermentations. Alternatively, biomass can be gasified to produce syngas, a mixture of carbon dioxide, carbon monoxide and hydrogen, for use in mixotrophic fermentations (Jones et al., 2016; Munasinghe and Khanal, 2010). Moreover, biological processes such as anaerobic digesters produce large quantities of methane, yet another potential source of carbon and energy. With the availability of these feedstocks, metabolic engineering efforts are geared towards engineering organisms to utilize one or more of these substrates and produce value-added chemicals. These efforts have consisted of introducing new metabolic capabilities into model organisms, such as *E. coli* and *S. cerevisiae*, and engineering

promising new organisms capable of metabolizing these feedstocks at higher rates and yields (Cordova et al., 2015; Liao et al., 2016).

With this wide range of potential substrates and products, it is of critical importance to evaluate the economic feasibility of bioprocesses, determine the capabilities of microbial systems, identify targets for improvements, and select ideal candidates for industrial implementation. Significant efforts have been directed at understanding cellular metabolism of microbes and identifying key regulatory mechanisms and potential kinetic limitations. A powerful method for characterizing *in vivo* metabolism is through the use of ^{13}C -labeled substrates (or ^{13}C -tracers). Tracing techniques allow quantitative evaluation of the flow of carbon from feedstocks to central metabolism and further into the desired products. Additionally, advanced techniques, such as ^{13}C -metabolic flux analysis (^{13}C -MFA), can be applied to gain a fine-grained picture of native metabolism and metabolic changes that result from genetic manipulations. In this introduction, there will be an overview of the wide range of pathways that are being implemented to convert renewable and waste substrates into value-added products as well as the methods for elucidating metabolism through these pathways using advanced ^{13}C -tracing techniques.

1.1.1 Metabolism of Lignocellulosic Biomass

The major costs in biological processes are substrate-related (Papoutsakis, 2015). Thus, organisms which can utilize a broad spectrum of renewable and waste substrates offer a major competitive advantage in the development of technologies for the production of next-generation fuels and chemicals. The primary renewable feedstock, lignocellulosic biomass, is composed of cellulose, hemicellulose, and lignin. Cellulose is a polymer of glucose, while hemicellulose is composed of both C6

(glucose, mannose, galactose) and C5 (xylose, arabinose) sugars. Metabolism of these sugars starts with transport of the sugar into the cells followed by activation (phosphorylation). The main mechanisms for sugar transport are active transport (via the PTS transport system, or ATP-dependent ABC transporters), and passive transport by permeases. For example, in *E. coli*, glucose is transported and phosphorylated simultaneously via the PTS system at the expense of one ATP equivalent, while two ATPs are expended when xylose serves as the carbon source, i.e. one for transport (high-affinity ABC transporter) and the second for activation (phosphorylation). Other sugars, e.g. lactose, are transported by permeases. The two classical pathways for sugar catabolism are glycolysis and the pentose phosphate pathway (Figure 1.1). Hexoses feed directly into glycolysis at glucose 6-phosphate (G6P) or fructose 6-phosphate (F6P), while pentoses feed into the pentose phosphate pathway at xylulose 5-phosphate (X5P). Many organisms are capable of catabolizing more than one sugar; however, in most cases, carbon catabolite repression (CCR) results in preferential utilization of certain sugars over others.

Various engineering strategies have been employed to eliminate CCR, often resulting in more efficient bioprocesses. A successful strategy has been knocking out components of the PTS system and applying adaptive evolution to improve sugar co-utilization. For example, Balderas-Hernandez et al. adaptively evolved *E. coli* lacking a functional PTS system under anaerobic conditions to achieve a glucose/xylose co-utilizing *E. coli* strain (Balderas-Hernández et al., 2011). Adaptive evolution was also successfully applied to generate an improved strain of the thermophile *Thermus thermophilus* that efficiently co-utilized glucose and xylose without CCR (Cordova et al., 2016). In another study, the *ptsG* gene was removed in *E. coli* to relieve CCR and

allowed production of 3-hydroxypropionic acid from both glucose and xylose in fed-batch fermentations (Jung et al., 2015). The model anaerobic organism *Clostridium acetobutylicum* was also evaluated for sugar co-utilization (Aristilde et al., 2015). Analysis of CCR genes in *C. acetobutylicum* identified targets for engineering simultaneous utilization of glucose and xylose (Grimmler et al., 2010). When glucose repression of xylose catabolism was removed, product titers from co-utilization of both substrates were comparable to wild-type titers (Ren et al., 2010).

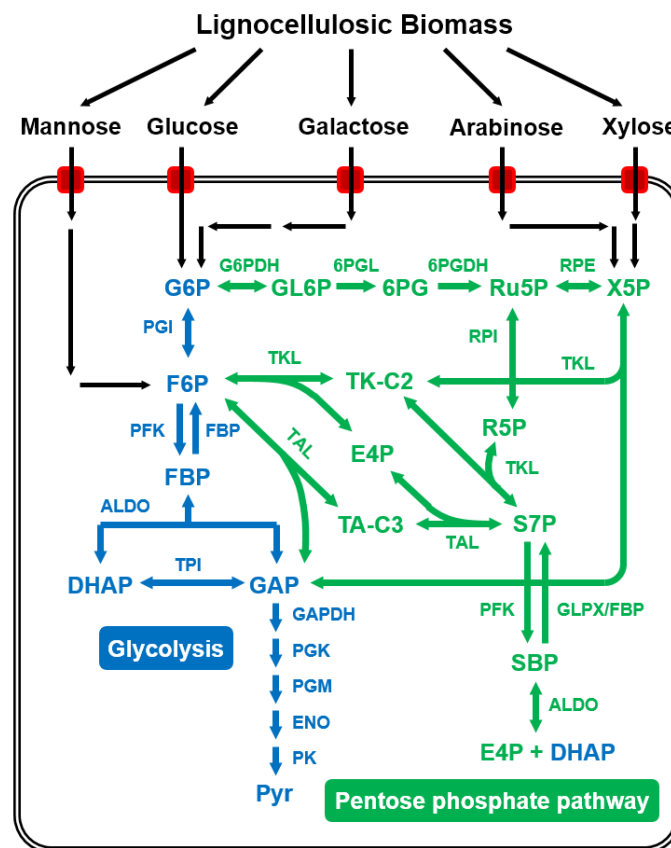


Figure 1.1 Conversion of lignocellulose-derived sugars into substrates of central carbon metabolism.

There has also been interest in broadening the substrate range for organisms that have the potential to produce high titers and yields of valuable products. Both *S. cerevisiae* and *Zymomonas mobilis*, major ethanol producers, have been engineered to use pentoses, such as arabinose and xylose, to achieve more efficient conversion of lignocellulose to product (Becker and Boles, 2003; He et al., 2014). There also exist organisms that express enzymes capable of hydrolyzing lignocellulose into sugars. *Clostridium thermocellum*, and several other thermophilic organisms, produces cellulases and hemicellulases; however, this organism cannot utilize the pentoses produced by hemicellulose degradation (Liao et al., 2016). Therefore, there's interest in engineering these organisms to consume a wider range of sugars. Unfortunately, due to the lack of genetic tools, little progress has been made towards this end. Instead, co-cultures have been designed that allow for breakdown of lignocellulose and consumption of all sugars by combining organisms that excel in each of these strategies (Fu et al., 2009; Lin et al., 2011).

1.1.2 Native and Synthetic Pathways for Conversion of Renewable Feedstocks

Glycolysis and the pentose phosphate pathway are the main routes for sugar catabolism in microbes; however, these pathways result in significant loss of carbon (CO₂ released), which reduces theoretical yields (Jones et al., 2016). Recent metabolic engineering strategies have focused on integrating alternative catabolic pathways into host organisms with the goal of producing more efficient bioconversions. Figure 1.2 provides an overview of the wide range of alternative metabolic pathways that are being considered for conversion of various feedstocks.

Gaseous substrates are increasingly evaluated as potential co-substrates for the production of chemicals (Fast et al., 2015; Hu et al., 2016). These gases include

carbon dioxide, carbon monoxide, and hydrogen gas derived from biomass gasification, and methane derived from anaerobic digestion of organic wastes or natural gas waste. Multiple avenues are considered to increase the ability of microorganisms to utilize gaseous substrates. Two well studied carbon fixation pathways are the Calvin cycle and the Wood-Ljungdahl pathway (Fast and Papoutsakis, 2012). The Calvin cycle fixes CO₂ to the C5 sugar ribulose biphosphate (RuBP) forming two molecules of 3-phosphoglycerate (3PG), catalyzed by ribulose1,5-biphosphate carboxylase–oxygenase (RubisCO), an enzyme that is essential in the process of photosynthesis. While the Calvin cycle is most prevalent in photosynthetic organisms, it is also found in some bacteria such as the *Sulfobacillus* and *Oscillochloris* species (Berg et al., 2010). Compared to other carbon fixation pathways, however, the Calvin cycle is more energy demanding as it consumes seven ATP and five reducing equivalents to form one molecule of pyruvate (Fast and Papoutsakis, 2012). Regardless, there have been many reports of using autotrophic organisms to produce chemicals such as isopropanol, isoprene, and sugars from CO₂ (Ducat et al., 2011). There is also the potential to introduce this pathway into non-carbon fixing organisms, which could effectively increase product yields and decrease carbon loss (Antonovsky et al., 2016; Gong et al., 2015; Li et al., 2015). In a recent study, it was demonstrated that expression of the Calvin cycle in *S. cerevisiae* resulted in higher ethanol yields and eliminated glycerol by-product formation (Guadalupe-Medina et al., 2013).

In addition to the Calvin cycle, the Wood-Ljungdahl (WL) pathway is a widely studied carbon fixation route that can utilize both CO₂ and CO as substrates (Abubackar et al., 2015; Munasinghe and Khanal, 2010). In the WL pathway, one

molecule of CO₂ is converted to CO by carbon monoxide dehydrogenase, and a separate cascade of steps forms a methyl group from CO₂. The enzyme acetyl-CoA synthase then brings the CO and methyl group together to form AcCoA. Depending on the carbon source, electrons can be obtained from H₂ or CO. The WL pathway, which is more energetically efficient than the Calvin cycle, is found exclusively in anaerobic organisms (Jones et al., 2016; Kopke et al., 2010).

Methane is another potential substrate that can be converted into fuels and chemicals (Fei et al., 2014; Haynes and Gonzalez, 2014). Methane is first converted to methanol and then to formaldehyde, which gives the cell access to several carbon assimilation pathways. Two of these pathways are depicted in Figure 1.2, the ribulose monophosphate (RuMP) pathway and the xylulose monophosphate (XuMP) pathway. The RuMP pathway uses two enzymes to fix formaldehyde to ribulose 5-phosphate (Ru5P) and enter central carbon metabolism as F6P. Similarly, the XuMP pathway attaches formaldehyde to a C5 sugar, X5P, and forms GAP and dihydroxyacetone phosphate (DHAP), which are intermediates of glycolysis. The RuMP pathway is found in methylotrophic bacteria such as *Mycobacterium gastri* and *Bacillus methanolicus*, while the XuMP pathway is found natively in methylotrophic yeasts. Additionally, the serine cycle uses the conversion of glycine to serine as the entry point of formaldehyde, and uses the cofactor, tetrahydrofolate, as the one carbon carrier. Methanol is an attractive substrate because it contains more electrons per carbon than sugars. Thus, theoretical yields of reduced products are higher with methanol as a substrate. So far, it has been difficult to generate a non-native fully methylotrophic microbe. Engineering co-utilization of methanol and sugars has been more successful (Whitaker et al., 2017). For example, *Corynebacterium glutamicum* was engineered to

consume methanol and ribose and produce cadaverine (Leßmeier et al., 2015), and *Pichia pastoris* was shown to produce recombinant proteins from methanol and glucose (Jordà et al., 2012).

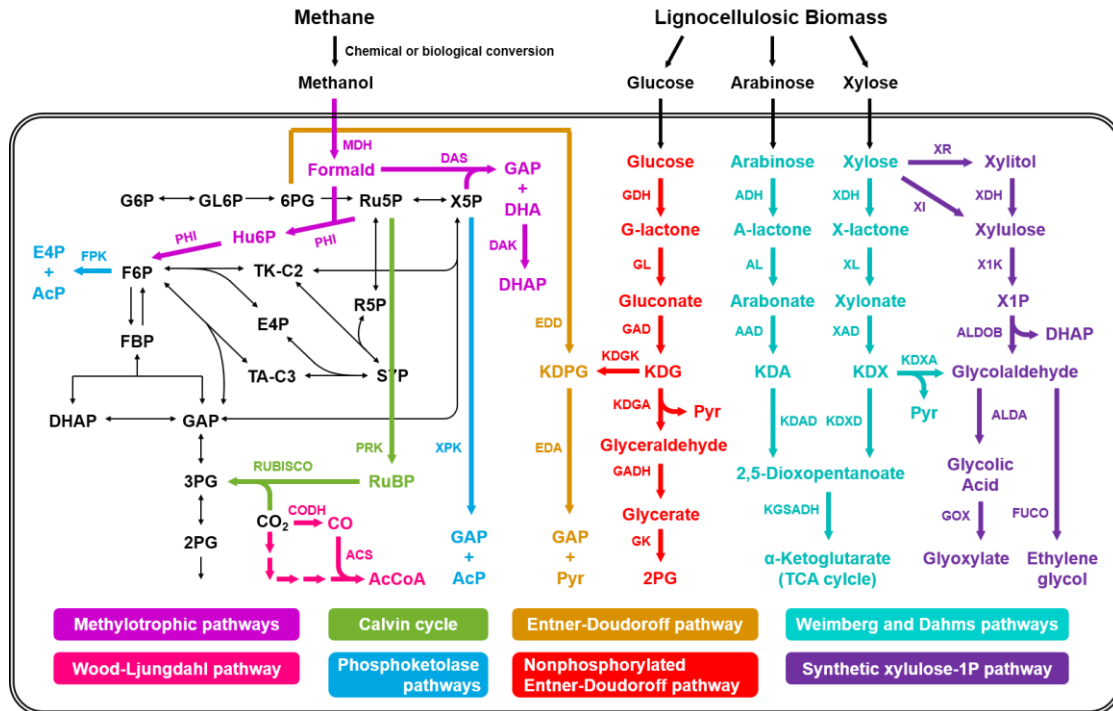


Figure 1.2 Native and synthetic metabolic pathways for conversion of renewable feedstocks into value-added products

1.2 Tracing Metabolism with Isotopic Tracers

Tracing how substrates are utilized and converted into products is critical in assessing the efficiency of engineered pathways and guiding further metabolic engineering strategies. Stable-isotope labeling techniques (primarily with ^{13}C -tracers) are widely used in metabolic engineering to quantify carbon flux for this purpose (Antoniewicz, 2015; Gebreselassie and Antoniewicz, 2015). In tracer experiments, an isotopically labeled substrate is added to the culture, e.g. $[\text{U-}^{13}\text{C}]$ glucose, resulting in

the incorporation of ^{13}C atoms into intermediates of cellular metabolism and eventually into products. By quantifying fractional ^{13}C -labeling of various metabolites, the contribution of a particular substrate can be determined. Tracer experiments are especially useful when examining non-native substrate utilization. When an engineered pathway is expressed in a host organism, the ability of the pathway to use the non-native substrate can be quantified by feeding a ^{13}C -labeled isotope of that substrate and measuring labeling in metabolites. This labeling can also be used as a method for detecting how further modifications to metabolism or the engineered pathway itself affect uptake of that substrate. Additionally, tracer experiments are particularly informative when multiple substrates are present, and when complex additives such as yeast extract are used in fermentations. By measuring ^{13}C -labeling over time, it is possible to elucidate relative rates of substrate utilization. For example, a constant isotopic labeling indicates that substrates are consumed simultaneously (Jones et al., 2016). On the other hand, if labeling changes in time, then the rate at which the labeling changes can be translated into relative flux changes (Iwatani et al., 2007).

1.2.1 Measuring Metabolism with ^{13}C - Metabolic Flux Analysis

In order for biological processes to be economically viable, substrates must be converted to products at near-theoretical yields (Papoutsakis, 2015). This generally requires significant rewiring of cellular metabolism. Compared to native metabolism, which has evolved to optimize cell growth, product formation will require a different balance of pathway activities to maximize the flow of carbon and electrons from feedstocks to products. ^{13}C -Metabolic flux analysis (^{13}C -MFA) is the best approach to gain quantitative insights into cellular metabolism (Antoniewicz, 2015). Knowledge of

metabolic fluxes is important to identify bottlenecks in metabolism and determine specific changes in pathway utilization resulting from genetic manipulations (Long and Antoniewicz, 2014). Experimentally validated fluxes are also used in constraint-based modeling approaches, and fluxes are critical for parameterizing kinetic models of metabolism (Khodayari et al., 2014), which are increasingly applied for analyzing metabolic pathways and predicting the outcomes of metabolic engineering interventions given the poor performance of traditional constraint-based approaches (Long et al., 2016b).

Methods for ^{13}C -MFA have advanced significantly in the past few years (Antoniewicz, 2015). With current state-of-the-art approaches, it is possible to measure intracellular fluxes with a precision of about 1-3% (Crown et al., 2015). The ability to generate high-resolution flux maps presents unprecedented opportunities to gain a much more detailed understanding of the regulation of metabolic pathways and *in vivo* enzyme kinetics. Current best approaches for flux estimation are based on the concept of parallel labeling experiments and integrated ^{13}C -MFA (Figure 1.3) (Antoniewicz, 2015). A good example of the power of parallel labeling experiments is the study by Crown et al. (Crown et al., 2015), where 14 parallel labeling experiments were successfully integrated to generate a detailed flux map for *E. coli*. Parallel labeling was also successfully applied for analysis of *Clostridium acetobutylicum* (Au et al., 2014), *Geobacillus* spp. (Cordova and Antoniewicz, 2015), and various mammalian systems (Ahn and Antoniewicz, 2013; Ahn et al., 2016; Crown et al., 2016; Crown et al., 2015).

The design of optimal labeling experiments is a critical step in ^{13}C -MFA. It is now well recognized that traditional tracers such as $[1-^{13}\text{C}]$ glucose and $[\text{U}-$

^{13}C]glucose, although relatively cheap, are suboptimal for quantifying precise metabolic fluxes (Crown and Antoniewicz, 2012). For example, it was demonstrated that doubly labeled tracers such as [1,2- ^{13}C]glucose and [1,6- ^{13}C]glucose are more optimal for ^{13}C -MFA, i.e. these tracers produce fluxes with much smaller confidence intervals (Crown et al., 2016b). For xylose, optimal tracers include [1,2- ^{13}C]xylose and [5- ^{13}C]xylose (Cordova and Antoniewicz, 2015).

The choice of tracers becomes even more critical when multiple substrates are present. When studying glucose and xylose co-utilization, the combination of [1- ^{13}C]glucose and unlabeled xylose has been commonly used (e.g. to elucidate pentose phosphate pathway fluxes in a *creA*-mutant of *Aspergillus nidulans* (David et al., 2005), and to study the effect of a modified redox pathway in *S. cerevisiae* (Grotkjær et al., 2005). A limitation of this tracer scheme is, however, that it only works well when the labeled substrate (in this case glucose) is the main carbon source. If xylose becomes the main carbon source, then ^{13}C -labeling becomes dramatically reduced and flux estimation fails. It is therefore advantageous to design labeling experiments that are less dependent on specific fluxes. Logically, it follows that both substrates should be labeled. A number of optimized tracer schemes have been successfully applied, including [1,2- ^{13}C]glucose + [1,2- ^{13}C]xylose to elucidate glucose and xylose co-utilization in *E. coli* (Long et al., 2016a), and [1,6- ^{13}C]glucose + [5- ^{13}C]xylose for flux analysis in *T. thermophilus* (Cordova et al., 2016).

Metabolic fluxes from other lignocellulosic sugars have also been studied. For example, Fonseca et al. used [2- ^{13}C]arabinose to study arabitol production in arabinose-utilizing yeast strains (Fonseca et al., 2008), and Sund et al. used [1- ^{13}C]glucose, [1- ^{13}C]xylose, and [1- ^{13}C]arabinose to estimate phosphoketolase fluxes in

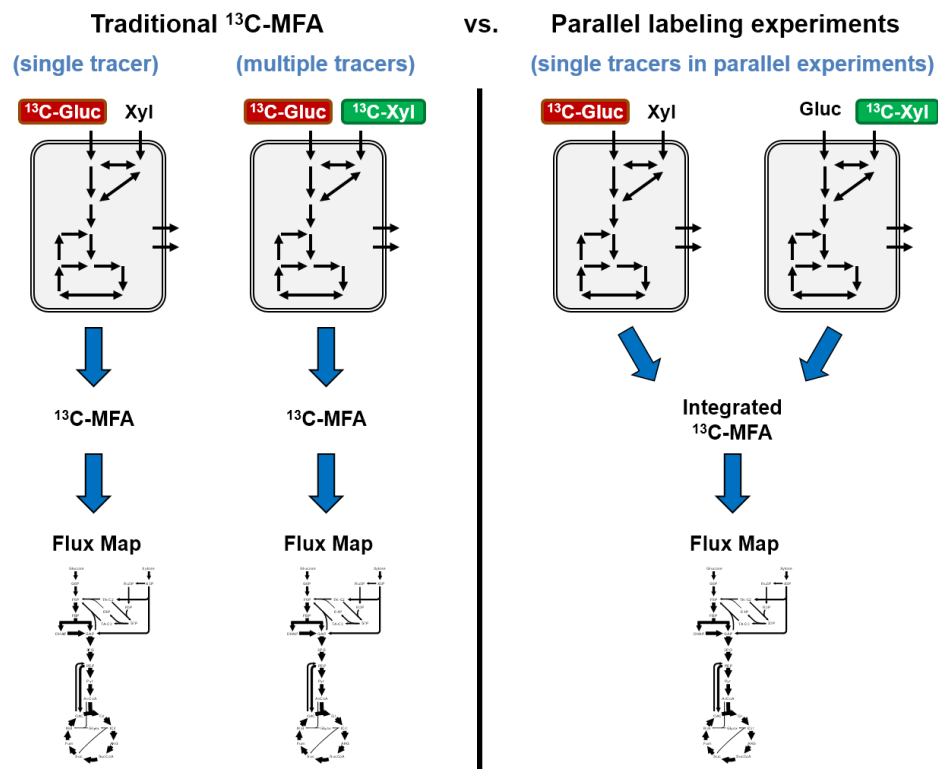


Figure 1.3 Comparison of different designs of isotopic labeling experiments to quantify co-utilization of multiple substrates using classical ¹³C-MFA (left) and integrated ¹³C-MFA based on parallel labeling experiments (right).

Clostridium acetobutylicum (Sund et al., 2015). Similarly, Fendt and Sauer used ¹³C-glucose, ¹³C-galactose, and ¹³C-mannose tracers to elucidate sugar metabolism of *S. cerevisiae*. Earlier studies with *Fibrobacter* also focused on elucidating catabolism of more complex substrates, including cellulose and cellobiose (Fendt and Sauer, 2010). By examining the dilution of [1-¹³C]glucose and quantifying the labeling of products during growth on cellulose or cellobiose, the authors were able to determine how glucose was utilized in the presence of cellulose (Matheron et al., 1998).

Investigation of the metabolism of gaseous and one carbon substrates has also been performed using ^{13}C -tracers. Several CO_2 -utilizing organisms have been studied. Specifically, the model cyanobacteria, *Synechocystis* sp., has been the focus of many works examining the dynamics of photosynthesis using $^{13}\text{CO}_2$ as a tracer and applying ^{13}C -nonstationary metabolic flux analysis (Young et al., 2011). Additionally, $^{13}\text{CO}_2$ incorporation has also been studied in organisms that have been engineered to use CO_2 . For example, $^{13}\text{CO}_2$ was used to evaluate the autotrophic ability of *E. coli* before and after adaptive evolution, when expressing of RubisCO (Antonovsky et al., 2016; Herz et al., 2017). Through this investigation, it was shown that all sugar-phosphate intermediates were completely derived from CO_2 . The metabolism of ^{13}CO and $^{13}\text{CO}_2$ has been quantified in several organisms that can use the WL pathway in an attempt to evaluate the potential of mixotrophic production of chemicals (Jones et al., 2016).

Metabolism of methane, and its subsequent derivatives (methanol, formaldehyde, formate), has also been studied with the goal of creating new and improving existing methanotrophic and methylotrophic organisms (Bennett et al., 2018). Kalyuzhnaya et al assess the ability of *Methylobacterium alcaliphilum* to convert $^{13}\text{CH}_4$ into product under both anaerobic and microaerobic conditions (Kalyuzhnaya et al., 2013). An engineered strain of the methanogen *Methanosarcina acetivorans*, an organism that typically produces methane, was demonstrated to instead use $^{13}\text{CH}_4$ for the production of acetate (Nazem-Bokaei et al., 2016). ^{13}C -methanol has also been used to quantify the ability of native methylotrophs, such as *Bacillus methanolicus* and *Pichia pastoris* (Jordà et al., 2012; Pluschkell and Flickinger, 2002), and engineered methylotrophs, such as *E. coli* and *Corynebacterium glutamicum* (Leßmeier et al., 2015; Whitaker et al., 2017), to use methanol for growth

and production of specialty chemicals. More recently, *E. coli* has been modified to use formate as a carbon source for growth. ^{13}C -formate was used to demonstrate successful design of this auxotrophic strain in which formate was required for the synthesis of several amino acids, including methionine and glycine (Yishai et al., 2017).

1.3 Aims and Outline of Thesis

Isotopic tracers are easy to implement and can be used to achieve a wealth of new information about metabolism. However, there has been limited application of tracers and therefore, their potential has not been realized. In this dissertation, we aim to demonstrate how tracers can be applied to various systems to gain a detailed understanding of pathway utilization, one that cannot be achieved without this analytical technique. The systems studied here include ones with multiple substrates, engineered pathways, and one-carbon substrates. Specifically, we first examine sugar utilization in *E. coli* and demonstrate how to choose and apply tracers to *E. coli* strains that can co-utilize sugars. We then use tracers to study and improve *E. coli* that has been engineered to consume a non-native substrate, methanol. We next show that classical ^{13}C -MFA can be used to study the metabolism of a one-carbon substrate in the model methanogen, *Methanosarcina acetivorans*. Lastly, we present new and evaluate existing metabolic flux analysis methods.

- **Chapter 2** shows the analysis performed of glucose and xylose metabolism under both aerobic and anaerobic conditions in *E. coli*. Here, we aim to aid the design and validation of constraint-based approaches by providing a wealth of new information of the metabolism of these two widely studied substrates. We applied ^{13}C -MFA using optimal tracers for

glucose and xylose. It was found that under anaerobic conditions, there is significant turnover of lipids. Specifically, under anaerobic growth on xylose, this biomass turnover was critical for growth. Analysis of fluxes and co-factor allocation revealed key differences in pathway utilization for each condition.

- **Chapter 3** demonstrates how we applied tracers to a multi-substrate system. Here we examine knockouts of the phosphotransferase system in *E. coli* and quantify their ability to co-utilize glucose and xylose. Additionally, we characterize two successfully engineered co-utilizing strains, GX50 and LMSE2. We apply ^{13}C -metabolic flux analysis to elucidate the metabolism of glucose/xylose co-consumption and interrogate the sugar uptake profile for each strain. It was found that the PTS knockouts and GX50 are sensitive to the relative extracellular concentrations of glucose and xylose. Specifically, as the fraction of one sugar increases, so does its relative uptake rate. Unlike GX50, LMSE2 is stoichiometrically limited, constraining the relative uptake rates to a constant ratio. Through this analysis, we identified the ideal uptake profile to be linear and non-biased towards a specific substrate, focusing future efforts towards the development of novel transport systems.

- **Chapter 4** describes how we examined and improved methanol assimilation in a synthetic methylotrophic *E. coli* strain. Specifically, we applied ^{13}C -tracers and evaluated 25 different co-substrates for methanol

assimilation. It was found that co-utilization of threonine significantly enhanced methylotrophy and led to increased activity of specific metabolic pathways. These pathways are normally repressed by the leucine-responsive protein (*lrp*). By deleting *lrp*, we further enhanced the methylotrophic ability of our strain, as demonstrated through increased incorporation of ^{13}C carbon from ^{13}C -methanol. Here, we demonstrate the value of using tracers to study engineered pathways as well as the importance of studying and interrogating regulation when attempting to engineer substrate metabolism.

- **Chapter 5** presents the characterization of the methanogen, *Methanosarcina acetivorans*, a model organism for studying the conversion of various substrates into methane and a possible host for the conversion of methane into value-added products. Here, we characterize this organism during growth on the one-carbon substrate, methanol. A network model was created, consisting of reactions from central carbon metabolism, amino acid biosynthetic pathways, and methanogenesis. Typically, estimating fluxes during growth on one-carbon substrates requires more advanced computational approaches and precise sampling of metabolic intermediates compared to ^{13}C -MFA. Here, we applied classical ^{13}C -MFA to validate the network model and generate the first flux map for *M. acetivorans*, demonstrating the successful application of classical ^{13}C -MFA to a one-carbon system.

- **Chapter 6** addresses the need for metabolic flux analysis methods that can be used for atypical systems, ones that are not at isotopic or metabolic steady state. Here, we present an extension of DMFA to include isotopic labeling measurements (^{13}C -DMFA). Additionally, we evaluate all established MFA methods (^{13}C -MFA, ^{13}C -NMFA, and ^{13}C -DMFA) and their ability to estimate fluxes for various conditions. It was concluded that ^{13}C -MFA and ^{13}C -MFAg can be used for isotopic steady state, ^{13}C -NMFA can be used for isotopic non-steady state, and ^{13}C -DMFA can be used for metabolic and isotopic non-steady state. This work is the first demonstration of ^{13}C -DMFA and clearly outlines how and when each established method should be applied.

- **Chapter 7** reviews the major conclusions and implications of the described work and addresses possible directions for future work.

Chapter 2

COMPREHENSIVE ANALYSIS OF GLUCOSE AND XYLOSE METABOLISM IN *Escherichia coli* UNDER AEROBIC AND ANAEROBIC CONDITIONS BY ^{13}C -METABOLIC FLUX ANALYSIS

2.1 Introduction

Biological conversion of lignocellulosic biomass into fuels and other chemicals has gained much attention in recent years (Choi et al., 2015). Lignocellulosic biomass is composed mainly of cellulose and hemicellulose, both of which can be broken down to carbohydrate monomers such as glucose, xylose, mannose, and galactose (Gírio et al., 2010). With glucose and xylose as the major products of lignocellulose breakdown, conversion of these two sugars into value-added products has been the focus of many metabolic engineering efforts (Hasona et al., 2004; R. Liu et al., 2012; Tao et al., 2001). While progress in metabolic engineering has allowed the generation of unique strains for improved glucose and xylose fermentations, detailed knowledge regarding changes in cellular metabolism as a result of these modifications is lacking and this limits further rational strain design (Long and Antoniewicz, 2014; Woolston et al., 2013).

Constraint-based reconstruction and analysis (COBRA) methods have been widely used in metabolic engineering for strain design (Becker et al., 2011; King et al., 2015). These methods include flux balance analysis (FBA) (Edwards et al., 2002), minimization of metabolic adjustment (MOMA) (Segre et al., 2002), regulatory on/off minimization of metabolic flux changes (ROOM) (Shlomi et al., 2005), and relative optimality in metabolic networks (RELATCH) (Kim and Reed, 2012), which can be implemented for strain design in algorithms such as OptKnock (Burgard et al., 2003).

An important requirement for COBRA methods is the presence of experimentally validated reference flux maps. ^{13}C -Metabolic flux analysis (^{13}C -MFA) is the most robust technique for determining precise intracellular metabolic fluxes (Antoniewicz, 2015; Antoniewicz et al., 2006; Crown and Antoniewicz, 2013a). In the past decade, ^{13}C -MFA has been applied extensively to investigate aerobic metabolism of glucose in *E. coli* (Chen et al., 2011; Perrenoud and Sauer, 2005; Toya et al., 2012); several ^{13}C -MFA studies have also focused on elucidating anaerobic glucose metabolism in *E. coli* (Chen et al., 2011; Choudhary et al., 2011), and other microbes (Au et al., 2014). In contrast, relatively little is known about xylose metabolism. To our knowledge, there have been no prior ^{13}C -MFA studies on xylose metabolism in *E. coli*, and only a handful of ^{13}C -MFA studies have been published on xylose metabolism in other organisms (Cordova and Antoniewicz, 2015; Cordova et al., 2016; Feng and Zhao, 2013; L. Liu et al., 2012; Wasylenko and Stephanopoulos, 2015).

To address this gap in current knowledge, we have in this work applied advanced methods for ^{13}C -flux analysis based on parallel labeling experiments and integrated ^{13}C -MFA (Antoniewicz, 2015; Leighty and Antoniewicz, 2013) to comprehensively quantify metabolism of glucose and xylose in *E. coli* under aerobic and anaerobic growth conditions. Fully ^{13}C -labeled tracers were also applied to measure changes in biomass composition and turnover of macromolecules under all growth conditions. Results from this work provide valuable new insights into metabolism of *E. coli* that can serve as the basis for future model building efforts and new strain designs using COBRA approaches.

2.2 Materials and Methods

2.2.1 Materials

Media and chemicals were purchased from Sigma-Aldrich (St. Louis, MO). Tracers were purchased from Cambridge Isotope Laboratories: [1,2-¹³C]glucose (99.9 atom% ¹³C), [1,6-¹³C]glucose (99.6%), [U-¹³C]glucose (99.3%), [1,2-¹³C]xylose (99.3%), [5-¹³C]xylose (99.6%), and [U-¹³C]xylose (99.3%). The isotopic purity of all glucose tracers was determined by GC-MS (Long et al., 2016a). MOPS minimal medium was used for all experiments.

2.2.2 Strains and Growth Conditions

For labeling experiments, a single colony of *E. coli* BW21135 (GE Healthcare Dharmacon) was first suspended in MOPS medium containing either 40 mM glucose or 40 mM xylose and grown overnight at 37°C in a shaker flask. The pre-culture was then re-suspended in fresh MOPS medium containing a particular tracer (40 mM initial concentration). For labeling experiments with [U-¹³C]glucose and [U-¹³C]xylose the cells were first washed with glucose-free and xylose-free medium. The initial OD₆₀₀ of inoculated cultures was 0.15 ± 0.02 (an inoculation ratio of approximately 1:10 was used). Cells were grown at 37°C in parallel mini-bioreactors with a working volume of 10 mL, as described before for aerobic *E. coli* cultures (Crown et al., 2015). Air was sparged into the liquid at a rate of 12 mL/min to provide oxygen and to ensure sufficient mixing of the culture by the rising gas bubbles. For anaerobic cultures, nitrogen was sparged into the headspace of the mini-bioreactors at 5 mL/min to maintain anaerobic conditions (Au et al., 2014), and mixing was achieved by continuous stirring with a stirrer bar. The pH of the anaerobic cultures was maintained at $\text{pH } 7.0 \pm 0.15$ through automatic addition of 1N NaOH. In all cases,

glucose pre-cultures were used for glucose tracer experiments, and xylose pre-cultures for xylose tracer experiments. The following tracers were used for ^{13}C -MFA (40 mM initial concentration): [1, 2- ^{13}C]glucose, [1, 6- ^{13}C]glucose, [1, 2- ^{13}C]xylose, [5- ^{13}C]xylose. Labeling experiments were also performed with 40 mM of [U- ^{13}C]glucose and [U- ^{13}C]xylose to determine turnover of biomass macromolecules (including proteins, lipids and RNA) during aerobic and anaerobic growth of *E. coli*. Growth characterization of the knockout strains $\Delta fadD$, $\Delta fadK$, and $\Delta fadD\Delta fadK$ was performed as described above for wild-type *E. coli*. The strains $\Delta fadD$ and $\Delta fadK$ were obtained from the Keio collection (GE Healthcare Dharmacon) and $\Delta fadD\Delta fadK$ strain RMK58 was obtained from Dr. John Cronan (University of Illinois at Urbana-Champaign) (Campbell et al., 2003).

2.2.3 Analytical Methods

Samples were collected at multiple times during the exponential growth phase to monitor cell growth, substrate uptake and product formation. Cell pellets and supernatants for isotopic labeling analysis were collected at an OD_{600} of 0.85 ± 0.02 . Cell growth was monitored by measuring the optical density at 600nm (OD_{600}) using a spectrophotometer (Eppendorf BioPhotometer). The OD_{600} values were converted to cell dry weight concentrations using previously determined OD_{600} -dry cell weight relationship for *E. coli* ($1.0 \text{ OD}_{600} = 0.32 \text{ gDW/L}$; molecular weight of dry biomass = 24.6 gDW/C-mol) (Long et al., 2016b). After centrifugation of the samples, the supernatant was separated from the biomass pellet. Acetate, formate, succinate, ethanol, and xylose concentrations in the supernatant were determined using an Agilent 1200 Series HPLC (Au et al., 2014). Glucose and lactate concentrations were determined using a YSI 2700 biochemistry analyzer (YSI, Yellow Springs, OH).

2.2.4 Biomass composition analysis

The methods used for quantifying biomass composition were described in (Long and Antoniewicz, 2014). Briefly, samples were prepared by three respective methods: hydrolysis of protein and subsequent TBDMS derivatization of amino acids; hydrolysis of RNA and glycogen and subsequent aldonitrile propionate derivatization of sugars (ribose and glucose, respectively); and fatty acid methyl ester derivatization for fatty acid. In total, 17 amino acids were quantified. The amino acids arginine, cysteine and tryptophan are degraded during hydrolysis and were thus not detected. For total protein quantification, we assumed the values previously reported for these three amino acids (Neidhardt, 1987). Glutamine and asparagine were deaminated to glutamate and aspartate, respectively, during hydrolysis; thus, we report the combined pools of each. Quantification of all components was achieved by isotope ratio analysis using an isotopically labeled standard and a naturally labeled sample. In this study, the standard was generated by growing wild-type *E. coli* on [U-¹³C]glucose and aliquoting identical (1 mL of an OD₆₀₀ = 1.0) samples of this “fully labeled” biomass. These were centrifuged and washed twice with M9 medium. The composition of the fully labeled biomass was characterized using unlabeled chemical standards, and subsequently these were used as standards by co-dissolving with the unlabeled samples at the beginning of each respective analytical method.

2.2.5 Gas chromatography-mass spectrometry

GC-MS analysis was performed on an Agilent 7890B GC system equipped with a DB-5MS capillary column (30 m, 0.25 mm i.d., 0.25 μm-phase thickness; Agilent J&W Scientific), connected to an Agilent 5977A Mass Spectrometer operating under ionization by electron impact (EI) at 70 eV. Helium flow was maintained at 1

mL/min. The source temperature was maintained at 230°C, the MS quad temperature at 150°C, the interface temperature at 280°C, and the inlet temperature at 250°C. GC-MS analysis of *tert*-butyldimethylsilyl (TBDMS) derivatized proteinogenic amino acids was performed as described in (Antoniewicz et al., 2007a). Labeling of glucose and xylose were determined after aldonitrile propionate derivatization as described in (Antoniewicz et al., 2011; Sandberg et al., 2016). Labeling of fatty acids was determined after derivatization to fatty acid methyl esters (FAME) (Crown et al., 2015). Labeling of glucose (derived from glycogen) and ribose (derived from RNA) were determined as described in (Long et al., 2016a; McConnell and Antoniewicz, 2016). In all cases, mass isotopomer distributions were obtained by integration (Antoniewicz et al., 2007a) and corrected for natural isotope abundances (Fernandez et al., 1996).

2.2.6 Metabolic network model and ¹³C-metabolic flux analysis

The metabolic network models used for ¹³C-MFA for all four growth conditions, i.e. aerobic and anaerobic growth with glucose and xylose as carbon source, are provided in Supplemental Materials. The models are based on the *E. coli* model described in (Crown et al., 2015). The models include all major metabolic pathways of central carbon metabolism, lumped amino acid biosynthesis reactions, and a lumped biomass formation reaction. Because we cannot distinguish between the NAD-dependent (*meaA*) and NADP-dependent (*meaB*) malic enzymes, we included only one of the two malic enzymes in the models, the NADP-dependent malic enzyme. Previous studies have demonstrated that neither enzyme is expressed during growth on glucose, and that only the NADP-dependent (*meaB*) malic enzyme is significantly expressed during growth on xylose (Schmidt et al., 2016). The

stoichiometries for the biomass formation reactions were derived using the measured biomass composition for each growth condition. The models also accounted for dilution of intracellular labeling from unlabeled CO₂ (Leighty and Antoniewicz, 2012), and dilutions resulting from the turnover of lipids as described in the text.

All ¹³C-MFA calculations were performed using the Metran software (Yoo et al., 2004) which is based on the elementary metabolite units (EMU) framework (Antoniewicz et al., 2007b). Fluxes were estimated by minimizing the variance-weighted sum of squared residuals (SSR) between the experimentally measured and model predicted external rates and mass isotopomer distributions of biomass amino acids, glucose derived from glycogen, ribose derived from RNA, and external succinate (anaerobic cultures only) using non-linear least-squares regression (Antoniewicz et al., 2006). All measured mass isotopomers are provided in Table A.5 and A.6. For integrated analysis of parallel labeling experiments, the data sets were fitted simultaneously to a single flux model as described previously (Leighty and Antoniewicz, 2013). Flux estimation was repeated 10 times starting with random initial values for all fluxes to find a global solution. At convergence, accurate 95% confidence intervals were computed for all estimated fluxes by evaluating the sensitivity of the minimized SSR to flux variations. Precision of estimated fluxes was determined as follows (Antoniewicz et al., 2006)

$$\text{Flux precision (stdev)} = [(\text{flux}_{\text{upper bound 95\%}}) - (\text{flux}_{\text{lower bound 95\%}})] / 4 \quad (2.1)$$

To describe fractional labeling of metabolites, G-value parameters were included in ¹³C-MFA. As described previously (Antoniewicz et al., 2007c), the G-

value represents the fraction of a metabolite pool that is produced during the labeling experiment, while $1-G$ represents the fraction that is naturally labeled, i.e. from the inoculum. By default, one G -value parameter was included for each measured metabolite in each data set. Reversible reactions were modeled as separate forward and backward fluxes. Net and exchange fluxes were determined as follows: $v_{\text{net}} = v_f - v_b$; $v_{\text{exch}} = \min(v_f, v_b)$.

2.2.7 Goodness-of-fit analysis

To determine the goodness-of-fit, ^{13}C -MFA fitting results were subjected to a χ^2 -statistical test. In short, assuming that the model is correct and data are without gross measurement errors, the minimized SSR is a stochastic variable with a χ^2 -distribution (Antoniewicz et al., 2006). The number of degrees of freedom is equal to the number of fitted measurements n minus the number of estimated independent parameters p . The acceptable range of SSR values is between $\chi^2_{\alpha/2}(n-p)$ and $\chi^2_{1-\alpha/2}(n-p)$, where α is a certain chosen threshold value, for example 0.05 for 95% confidence interval.

2.3 Results and Discussion

2.3.1 Growth characteristics

Growth characteristics of wild-type *E. coli* grown in MOPS minimal medium at 37°C were determined at four growth conditions: aerobic and anaerobic growth with glucose and xylose as the carbon source. For the anaerobic cultures, controlling the pH at 7.0 was necessary to maintain exponential growth; no pH control was required for the aerobic cultures (up to OD_{600} of about 1.0). Table 2.1 shows the measured growth rates, biomass and product yields, and the corresponding biomass specific product

secretion rates for all conditions. The aerobic growth rates for both substrates (0.70 ± 0.01 and $0.50 \pm 0.02 \text{ h}^{-1}$ for glucose and xylose, respectively) were more than 2-fold higher than the corresponding anaerobic growth rates (0.33 ± 0.02 and $0.13 \pm 0.02 \text{ h}^{-1}$, respectively). The aerobic biomass yields (0.44 ± 0.02 and $0.35 \pm 0.03 \text{ g}_{\text{DW}}/\text{g}$ for glucose and xylose, respectively) were also several-fold higher compared to anaerobic biomass yields (0.14 ± 0.01 and $0.08 \pm 0.01 \text{ g}_{\text{DW}}/\text{g}$, respectively). Under aerobic growth conditions, acetate was the only secreted product. Under anaerobic conditions acetate, ethanol, formate and succinate were produced. Acetate, ethanol and formate were secreted at a relatively constant ratio of about 1:1:2 for both substrates. No lactate was detected in any of the cultures. The biomass specific glucose uptake rate was 50% higher during anaerobic growth ($13.1 \pm 1.0 \text{ mmol}/\text{g}_{\text{DW}}\cdot\text{h}$) compared to aerobic growth ($8.8 \pm 0.5 \text{ mmol}/\text{g}_{\text{DW}}\cdot\text{h}$), consistent with previous reports (Chen et al., 2011). In contrast, the biomass specific xylose uptake rate was only 13% higher during anaerobic growth ($10.8 \pm 1.1 \text{ mmol}/\text{g}_{\text{DW}}\cdot\text{h}$) compared to aerobic growth ($9.5 \pm 0.5 \text{ mmol}/\text{g}_{\text{DW}}\cdot\text{h}$). The carbon and electron recoveries (not accounting for CO_2 and O_2 , which were not measured) for the aerobic cultures were 77% for glucose and 57% for xylose (Table 1), which suggests that a relatively larger fraction of xylose was catabolized to CO_2 compared to glucose. The carbon and electron recoveries for the anaerobic cultures were 87% for glucose and 81% for xylose, suggesting that a non-negligible fraction of both substrates must have been converted to e.g. CO_2 and a reduced product such as H_2 . Indeed, in sealed flask cultures we detected net accumulation of CO_2 and H_2 in the head-space that could account for the missing 13-19% of carbons and electrons.

Table 2.1 Physiological characteristics of *E. coli* grown in batch culture on glucose and xylose under aerobic and anaerobic conditions in MOPS minimal medium at 37°C.

	Aerobic Glucose	Aerobic Xylose	Anaerobic Glucose	Anaerobic Xylose
μ (1/h)	0.70 ± 0.01	0.50 ± 0.02	0.33 ± 0.02	0.13 ± 0.02
Y_x (g _{DW} /g)	0.44 ± 0.02	0.35 ± 0.03	0.14 ± 0.01	0.08 ± 0.01
Y_{Ac} (mol/mol)	0.65 ± 0.01	0.33 ± 0.01	0.56 ± 0.02	0.51 ± 0.02
Y_{Form} (mol/mol)	-	-	1.25 ± 0.05	1.00 ± 0.03
Y_{EtOH} (mol/mol)	-	-	0.61 ± 0.04	0.56 ± 0.01
Y_{Suc} (mol/mol)	-	-	0.15 ± 0.02	0.10 ± 0.01
q_{Gluc} (mol/g _{DW} h)	8.8 ± 0.5	-	13.1 ± 1.0	-
q_{Xyl} (mol/g _{DW} h)	-	9.5 ± 0.5	-	10.8 ± 1.1
q_{Ac} (mol/g _{DW} h)	5.7 ± 0.2	3.2 ± 0.2	7.3 ± 0.7	5.5 ± 0.8
q_{Form} (mol/g _{DW} h)	-	-	16.4 ± 0.9	10.8 ± 0.8
q_{EtOH} (mol/g _{DW} h)	-	-	8.0 ± 0.5	6.1 ± 0.5
q_{Suc} (mol/g _{DW} h)	-	-	2.0 ± 0.1	1.1 ± 0.1
Carbon Recovery (%)	75 ± 7%	56 ± 9%	87 ± 5%	81 ± 7%
Redox Recovery (%)	78 ± 8%	58 ± 9%	86 ± 6%	81 ± 8%

The data shown are biomass yield (Y_x), yields of secreted products (Y_i), specific growth rate (μ), specific uptake rate (q_{Gluc} and q_{Xyl}), and specific production rate (q_i) for secreted metabolites acetate (Ac), formate (Form), ethanol (EtOH) and succinate (Suc).

2.3.2 Biomass composition analysis

In nearly all flux studies performed to date, a constant *E. coli* biomass composition has been assumed. However, it is well known that the composition of biomass can change in response to environmental and genetic perturbations (Long et al., 2016b). This in turn can have a non-negligible impact on the accuracy of flux

predictions. To ensure that flux results generated in this study are as accurate as possible, biomass composition was measured for all growth conditions using the methods described in (Long and Antoniewicz, 2014). This information was then used to generate condition-specific growth stoichiometries for ^{13}C -MFA.

The results of the biomass composition analyses are summarized in Figure 2.1 (complete results are provided in Table A.1). Proteins were the most abundant component of biomass for all conditions. The protein content of dry biomass was slightly higher for xylose as the substrate (57 wt% and 61 wt% for aerobic and anaerobic cultures, respectively) compared to glucose as the substrate (51 wt% for both aerobic and anaerobic cultures). RNA was the next most abundant component of biomass. For both substrates, the RNA content was higher during aerobic growth (18 wt% for both substrates) compared to anaerobic growth (11 wt% for glucose and 9% for xylose). It is well known that the RNA content of biomass positively correlates with the growth rate of cells (Long et al., 2016b), which is consistent with the results presented here. The lipid content was relatively constant at about 6 wt% for all growth conditions. Glycogen content varied significantly, ranging from 2 wt% for aerobic growth on glucose to 9 wt% for anaerobic growth on glucose. Figure 1B shows the distribution of fatty acids in biomass, which varied notably depending on the specific growth condition. For example, the relative abundance of C18:1 was reduced by more than 2-fold when cells were grown anaerobically on xylose, compared to the other three growth conditions. No significant changes were observed in the relative amino acid profiles (Table A.3). The composition for the aerobic glucose condition is consistent with previous reports (Long and Antoniewicz, 2014; Long et al., 2016b).

Small differences in the fatty acid distribution, particularly higher C16:1 levels here, may be the result of the media conditions (MOPS here, M9 previously).

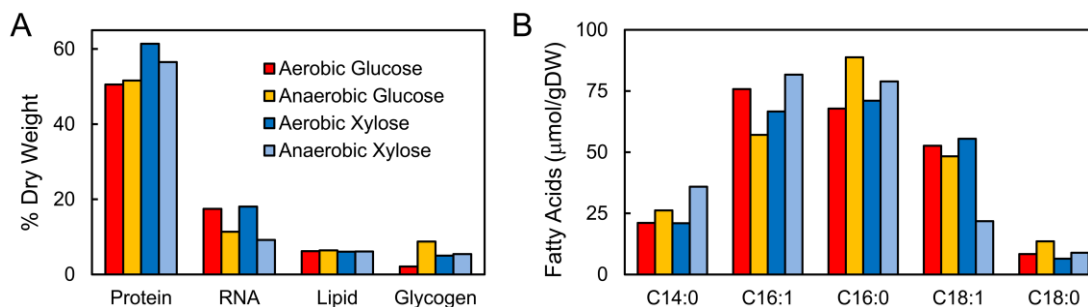


Figure 2.1 Biomass composition analysis of wild-type *E. coli* grown aerobically and anaerobically on glucose and xylose.

2.3.3 Turnover of biomass macromolecules

A common assumption in ^{13}C -MFA is that turnover of biomass macromolecules such as proteins, lipids and RNA can be neglected; however, this assumption has not been validated rigorously under all relevant growth conditions. To investigate the presence or absence of biomass turnover, cells were first pre-cultured in medium containing unlabeled glucose or xylose (i.e. natural abundance of ^{13}C), washed with sugar-free medium, and then transferred to medium containing fully labeled glucose [$\text{U-}^{13}\text{C}$]glucose, or fully labeled xylose [$\text{U-}^{13}\text{C}$]xylose. The initial OD_{600} of the cultures was 0.15 ± 0.02 and cells were harvested for GC-MS analysis when OD_{600} reached 0.85 ± 0.02 . Assuming that no turnover of biomass occurs, the expected labeling profile of biomass components at the time of harvesting would be: 18% ($=0.15/0.85$) fully unlabeled (M+0), and 82% fully labeled (M+N, where N is the number of C-atoms in the measured compound). Since isotopic tracers are not 100%

^{13}C -labeled (for example, here, we determined that $[\text{U-}^{13}\text{C}]$ glucose and $[\text{U-}^{13}\text{C}]$ xylose tracers both had an isotopic purity of about 99.3 atom% ^{13}C), some incompletely

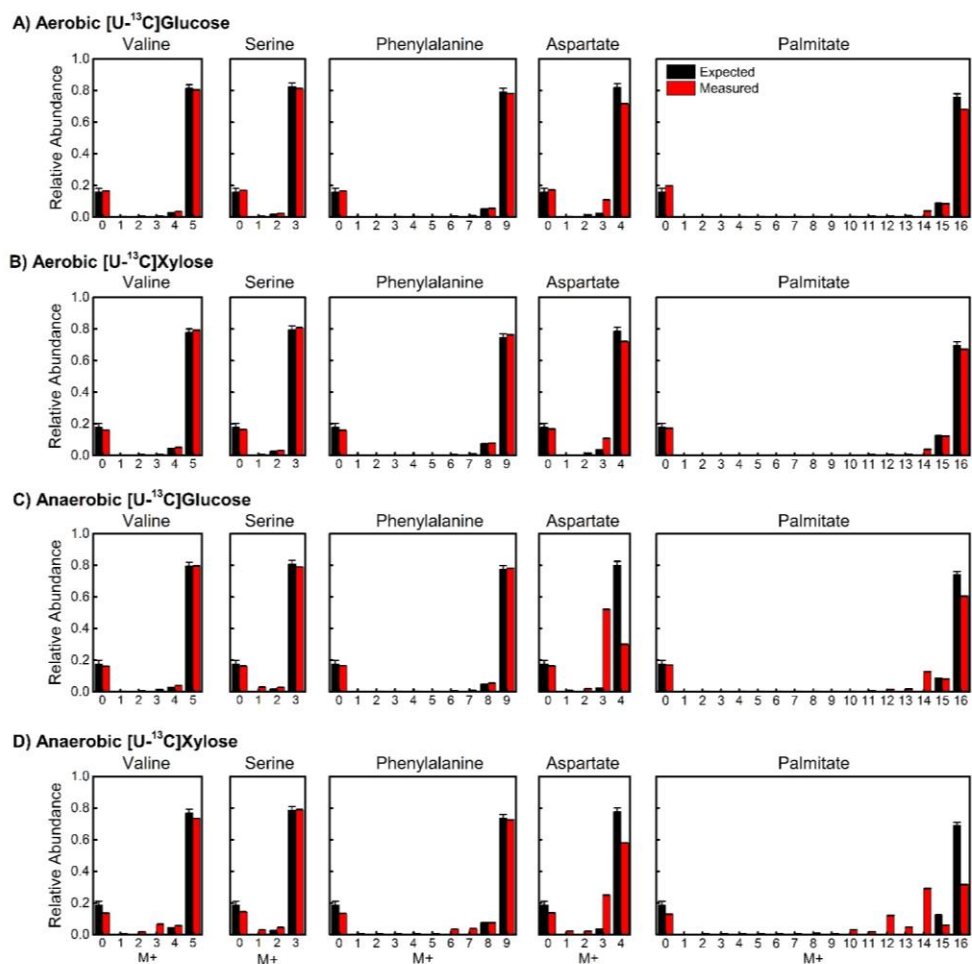


Figure 2.2 Expected (black bars) and measured (red bars) mass isotopomer distributions for five metabolites (valine, serine, phenylalanine, aspartate, and palmitate) from tracer experiments with $[\text{U-}^{13}\text{C}]$ glucose and $[\text{U-}^{13}\text{C}]$ xylose. Presence of incompletely labeled mass isotopomers, especially under anaerobic conditions, indicates significant biomass turnover.

labeled mass isotopomers ($M+N-1$) are also expected. On the other hand, if biomass turnover does occur, then we would expect unlabeled carbon from the initially unlabeled biomass to enter central carbon metabolism, which would subsequently result in increased abundances of incompletely labeled mass isotopomers. Figure 2 shows the expected and measured mass isotopomer distributions (after correction for natural isotope abundances), for five representative metabolites: valine, serine, phenylalanine, aspartate and palmitate. The complete set of GC-MS measurements are provided in Table A.5 and A.6.

For aerobic glucose and xylose cultures, the measured mass isotopomers matched well with the expected mass isotopomers assuming no biomass turnover (Fig. 2.2A and 2.2B). The notable exceptions were aspartate, glutamate and related amino acids (see Tables A.5 and A.6), which displayed higher than expected abundances of $M+N-1$ mass isotopomers. In a previous study using $[U-^{13}C]$ glucose (Leighty and Antoniewicz, 2012), we noted similar dilutions of labeling which could be explained by the incorporation of unlabeled (atmospheric) CO_2 via the anaplerotic reaction: phosphoenolpyruvate + $CO_2 \rightarrow$ oxaloacetate (i.e. oxaloacetate is the precursor for aspartate, glutamate and related amino acids). The inlet air in this study contained $\sim 0.04\%$ CO_2 . The partial labeling observed here for both aerobic cultures is thus not related to biomass turnover, but results from the incorporation of unlabeled atmospheric CO_2 .

For anaerobic glucose and xylose cultures, the measured mass isotopomers differed more significantly from the expected mass isotopomers (Fig 2.2C and 2.2D). Most striking were the very high abundances of $M+N-1$ mass isotopomers of aspartate, glutamate and related amino acids, suggesting significant incorporation of

unlabeled CO₂. For example, for the anaerobic [U-¹³C]glucose experiment, the M+N-1 mass isotopomer of aspartate (M+3) was the most abundant mass isotopomer in the mass spectrum (>50% relative abundance). We validated that the nitrogen gas used in the anaerobic cultures did not contain any CO₂ (less than 0.001%). Thus, all of the unlabeled CO₂ must have originated from turnover of unlabeled biomass. These results further suggest that under anaerobic conditions not enough CO₂ is generated in central carbon metabolism and amino acid biosynthesis pathways to support anaplerosis (phosphoenolpyruvate + CO₂ → oxaloacetate), but instead that a large fraction of CO₂ originates from biomass turnover.

For the anaerobic cultures, we also noted that palmitate had significantly higher than expected abundances of incompletely labeled mass isotopomers. This was especially pronounced for the anaerobic xylose culture, where we detected significant abundances for M+10, M+12, and M+14 mass isotopomers, in addition to the expected M+16 mass isotopomer of palmitate. The presence of M+N-2, M+N-4, and M+N-6 mass isotopomers suggests incorporation of unlabeled AcCoA (M+0) that originated from biomass turnover, e.g. via β-oxidation of initially unlabeled fatty acids.

Moreover, we found evidence that unlabeled phosphoenolpyruvate (PEP) was present. For example, we observed significant M+6 (=M+N-3) and M+7 (=M+N-2) mass isotopomers in the mass spectrum of phenylalanine for the anaerobic xylose culture. Phenylalanine is produced from the condensation of erythrose 4-phosphate, PEP_{C1-C2} and PEP_{C1-C3}. If unlabeled PEP (M+0) is present, then we would expect to observe equal abundances of M+6 and M+7 mass isotopomers for phenylalanine, consistent with our GC-MS measurements (Figure 2.2). To further validate that

unlabeled PEP was present, we measured directly the labeling of three intracellular metabolites in glycolysis, 3PG, PEP and pyruvate. For the anaerobic xylose culture, 7% of 3PG was fully unlabeled (M+0), and 5% of PEP and pyruvate were fully

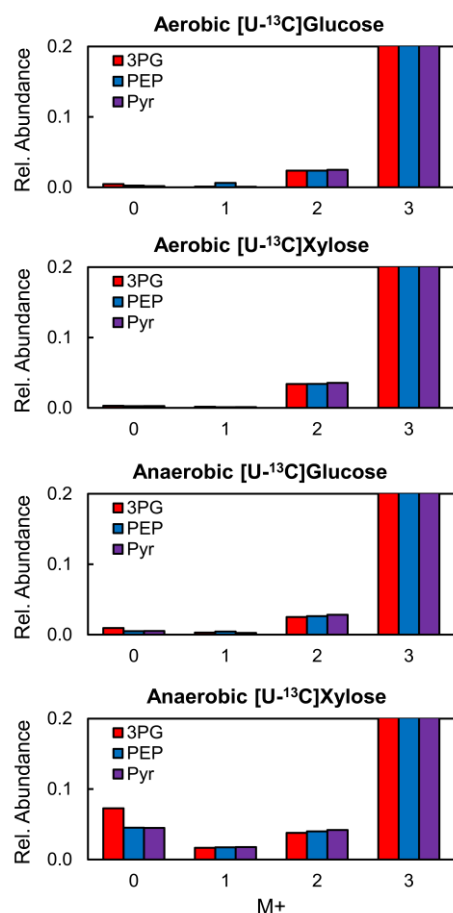


Figure 2.3 Mass isotopomer distributions for the glycolytic intermediates 3-phosphoglycerate (3PG), phosphoenolpyruvate (PEP), and pyruvate (Pyr) from tracer experiment with [U-¹³C]glucose and [U-¹³C]xylose. Presence of unlabeled mass isotopomers (M+0), especially during anaerobic growth on [U-¹³C]xylose, indicates that significant biomass turnover occurs.

unlabeled (Figure 2.3). For the other three growth conditions, the M+0 abundances of these metabolites were less than 1%. A possible explanation for the presence of

unlabeled PEP is that it originated from the glycerol moiety of unlabeled lipids that turned over. Taken together, the labeling data presented here provide strong evidence that biomass turnover occurs under anaerobic growth conditions and that this cannot be neglected when analyzing labeling data.

2.3.4 Growth of β -oxidation knockouts

The results described above suggest that lipid turnover could be a characteristic feature of anaerobic growth on xylose. To determine if β -oxidation is strictly necessary for cell growth under this condition, the effect of gene knockouts of key enzymes in the β -oxidation pathway were investigated. Specifically, we determined growth characteristics for the strains $\Delta fadD$, $\Delta fadK$, and $\Delta fadD\Delta fadK$ under aerobic and anaerobic conditions for both substrates. The genes *fadD* and *fadK* encode for acyl-CoA synthetase, the first step in the β -oxidation pathway (Fig. 2.4A). It is believed that *fadD* is mainly involved in aerobic fatty acid oxidation, while *fadK* is active during anaerobic fatty acid oxidation (Campbell et al., 2003). Figure 2.4B compares the growth rates of wild-type *E. coli* and each of the knockout strains for the four growth conditions. No significant differences in growth rates were observed for the aerobic cultures, and for the anaerobic glucose culture. However, for the anaerobic xylose culture, the growth rates of the single gene knockout strains were significantly lower compared to wild-type (~40-70% reduction in growth rate). Moreover, the double-knockout $\Delta fadD\Delta fadK$ failed to grow on xylose. These results provide additional support that β -oxidation is indeed necessary for anaerobic growth on xylose.

2.3.5 Validation of metabolic network models

To statistically validate the proposed metabolic network models for ^{13}C -MFA (Leighty and Antoniewicz, 2012), labeling data from $[\text{U-}^{13}\text{C}]$ glucose and $[\text{U-}^{13}\text{C}]$ xylose experiments were fitted to three models accounting for various dilution effects: i) a base model that did not account for any dilution; ii) an extended model that accounted for the dilution of CO_2 from unlabeled sources (either external or internal); and iii) an extended model that accounted for CO_2 dilution and dilutions resulting from lipid turnover, modeled here as dilutions of intracellular glyceraldehyde 3-phosphate (GAP) and AcCoA. Figure 2.5 shows the determined sum of squares residuals (SSR) values from fitting each model to each set of labeling data. For the aerobic cultures, the only dilution effect that had to be accounted for to get a statistically acceptable fit was CO_2 dilution. For the anaerobic cultures, both CO_2 dilution and dilutions resulting from lipid turnover had to be included in the model to obtain statistically acceptable fits. When carbohydrate and amino acid turnover was included in the models, there was no significant effect on the SSR values (see Figure A.1) which suggests that turnover of proteins, glycogen, and RNA was minimal.

2.3.6 ^{13}C -Metabolic Flux Analysis

Next, we quantified precise metabolic fluxes for all four growth conditions using state-of-the-art techniques in ^{13}C -MFA. Specifically, we performed parallel labeling experiments using the optimal isotopic tracers $[1,2\text{-}^{13}\text{C}]$ glucose, $[1,6\text{-}^{13}\text{C}]$ glucose, $[1,2\text{-}^{13}\text{C}]$ xylose and $[5\text{-}^{13}\text{C}]$ xylose, which were identified using the approaches described in (Antoniewicz, 2013; Crown and Antoniewicz, 2012; Crown et al., 2016b, 2012), and measured isotopic labeling of biomass amino acids, biomass glycogen and RNA, and external succinate (anaerobic cultures only). The measured

mass isotopomer distributions together with the measured external rates (Table 2.1) were then fitted to the validated metabolic network models that were updated with

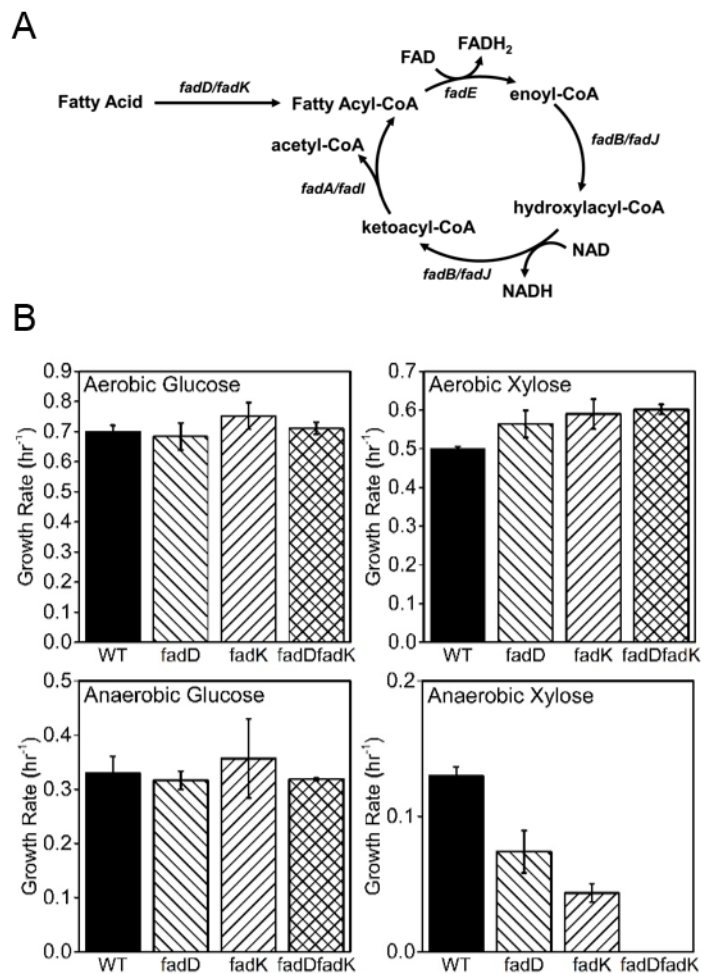


Figure 2.4 (A) β -oxidation pathway with genes encoding each reaction. (B) Growth rates of wild-type *E. coli* and knockout strains $\Delta fadD$, $\Delta fadK$, $\Delta fadD\Delta fadK$ grown aerobically and anaerobically on glucose and xylose as substrates. The double-knockout strains $\Delta fadD\Delta fadK$ did not grow on xylose under anaerobic conditions

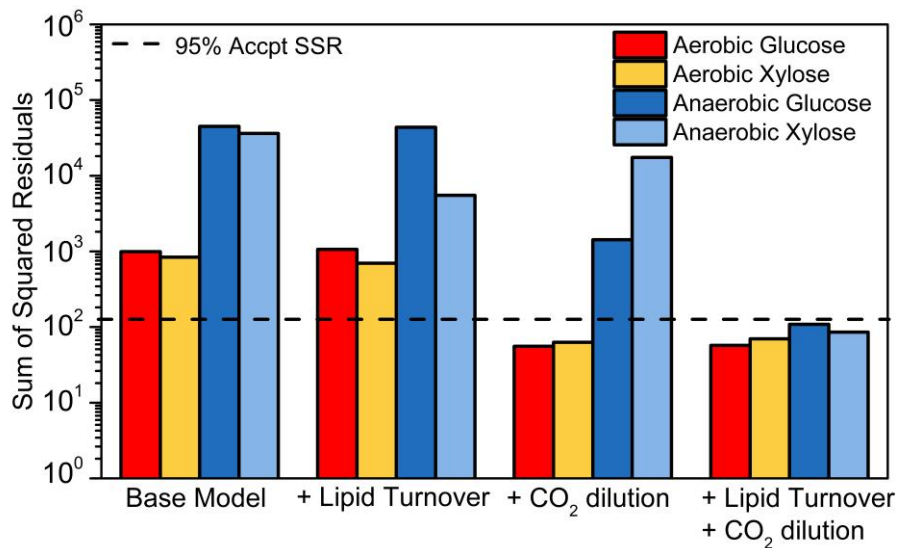


Figure 2.5 Validation of metabolic network models for ¹³C-MFA. Sum of squared residual (SSR) values are shown for models containing various dilution reactions. For the aerobic cultures, inclusion of CO₂ dilution was necessary to obtain an acceptable SSR value (below the dotted line). For the anaerobic cultures, CO₂ and lipid dilution were necessary to achieve an acceptable SSR value.

condition-specific growth stoichiometries based on the measured biomass compositions. Statistically acceptable fits were obtained in all cases. The minimized SSR values were lower than the maximum statistically acceptable SSR values at 95% confidence level, assuming a constant measurement error of 0.4 mol% for all GC-MS measurements (Antoniewicz et al., 2007a). The estimated metabolic fluxes and 95% confidence intervals are provided in Supplemental Materials.

Figure 2.6 shows the estimated flux maps for the four growth conditions. During aerobic growth on glucose and xylose, the classical central metabolic pathways

were active, including glycolysis, pentose phosphate pathway (PPP), and TCA cycle (Fig 6A and 6B). The results for glucose matched well with previous studies (Chen et al., 2011; Scott B Crown et al., 2015). About 24% of glucose was metabolized via the oxidative PPP (oxPPP) and the remaining 76% was metabolized via glycolysis. The Entner–Doudoroff pathway, glyoxylate shunt and malic enzyme were all inactive during growth on glucose, consistent with previous reports. During growth on xylose, about 24% of fructose 6-phosphate (F6P) that was produced from xylose via non-oxidative PPP was metabolized via oxPPP and the remaining 76% via glycolysis. The Entner–Doudoroff pathway and glyoxylate shunt were inactive; however, in contrast to growth on glucose, malic enzyme was active during growth on xylose. For both substrates, phosphoenolpyruvate carboxylase was the only active anaplerotic reaction. The TCA cycle fluxes were notably higher during growth on xylose compared to growth on glucose. For example, during growth on xylose the citrate synthase flux corresponded to 35% of xylose uptake rate (or 3.3 ± 0.2 mmol/gDW.h), while during growth on glucose the citrate synthase flux was 26% of glucose uptake rate (or 2.3 ± 0.1 mmol/gDW.h)

The anaerobic flux maps were strikingly different from the aerobic flux maps (Fig 2.6C and 2.6D). Most notably, the flux through oxPPP was significantly reduced and the TCA cycle became bifurcated. Under the anaerobic conditions, only 8% of glucose was metabolized via oxPPP, and oxPPP was inactive during anaerobic growth on xylose. For both substrates, the TCA cycle was disconnected between α -ketoglutarate (AKG) and succinyl-CoA. The oxidative branch of the TCA cycle served to supply AKG, a precursor for several amino acids, while the reductive branch of the TCA cycle produced the by-product succinate. Similar to aerobic cultures, the

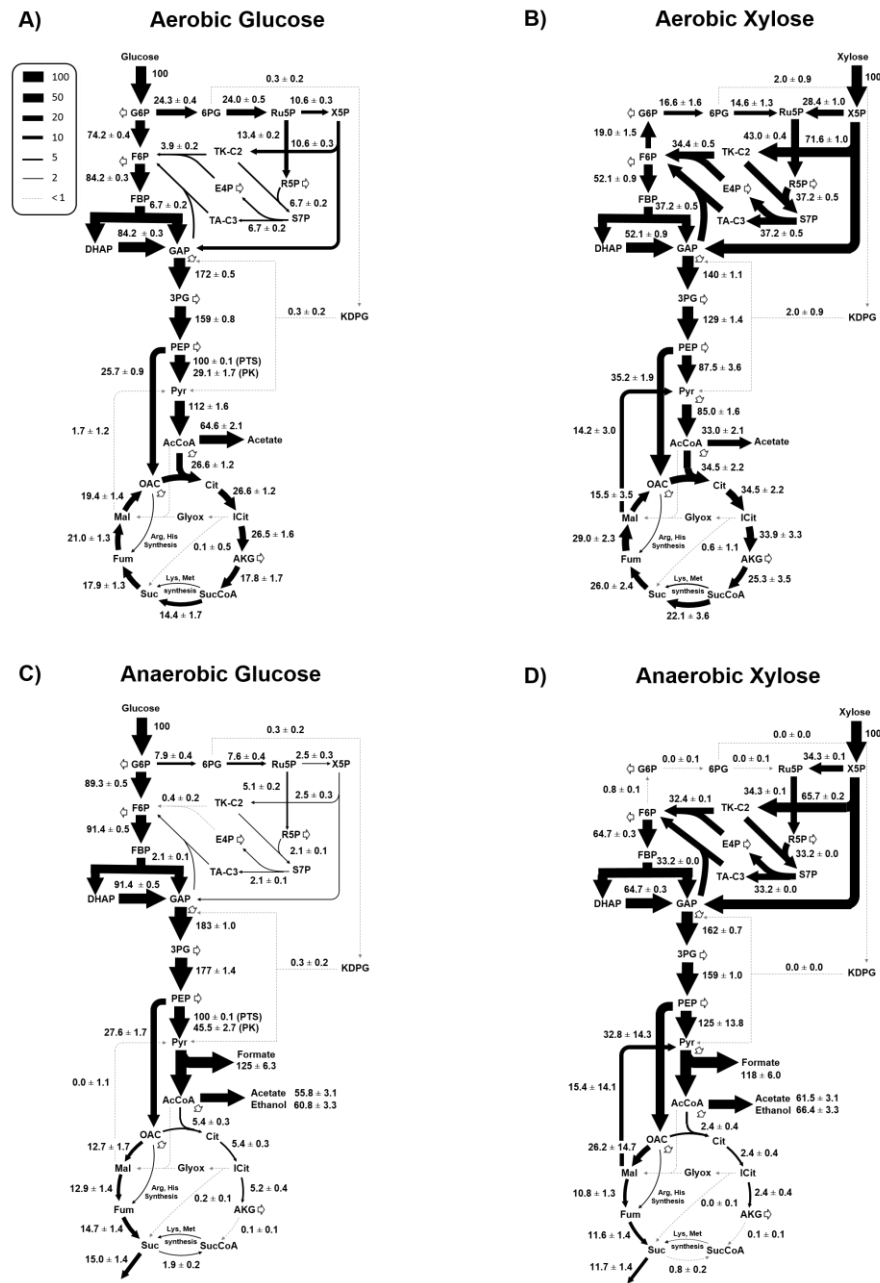


Figure 2.6 Metabolic flux maps for *E. coli* grown in batch culture at four growth conditions: aerobic and anaerobic growth on glucose and xylose, respectively. Fluxes were determined using integrate ^{13}C -MFA by simultaneously fitting labeling data from two tracers for each substrate. For glucose, $[1,2\text{-}^{13}\text{C}]$ glucose and $[1,6\text{-}^{13}\text{C}]$ glucose tracers were used. For xylose, $[1,2\text{-}^{13}\text{C}]$ xylose and $[5\text{-}^{13}\text{C}]$ xylose tracers were used. Complete flux results are provided in Tables A.7 and A.8.

Entner–Doudoroff pathway and glyoxylate shunt were inactive for both substrates, and malic enzyme was only active during growth on xylose. Similar results have been previously reported regarding the low flux of the TCA cycle under anaerobic conditions (Chen et al., 2011). However, fermentation product profiles vary from our results. This difference is most likely due to experimental setup (i.e. pH control vs. no pH control).

During aerobic growth on both substrates, sufficient CO₂ was produced in central carbon metabolism (via oxPPP, glycolysis, and TCA cycle) to support anaplerosis via phosphoenolpyruvate carboxylase (PEP + CO₂ → oxaloacetate). However, during anaerobic growth, the amount of CO₂ produced was dramatically reduced due to lower oxPPP and TCA cycle fluxes. Moreover, pyruvate formate lyase was mainly used to convert pyruvate to AcCoA under anaerobic conditions (which does not generate CO₂), compared to pyruvate dehydrogenase during aerobic growth (which does generate CO₂). For example, for the anaerobic glucose culture, the net CO₂ production rate via oxPPP and TCA cycle was reduced to 0.13 mmol/gDW.h, which was lower than 0.28 mmol/gDW.h of CO₂ needed for anaplerosis. For xylose, the net CO₂ production via oxPPP and TCA cycle was only 0.04 mmol/gDW.h, much less than 0.18 mmol/gDW.h of CO₂ needed for anaplerosis. Thus, for both substrates additional CO₂ must have been generated via other pathways. This result is in agreement with our findings described in previous sections, where we concluded that a large fraction of CO₂ during anaerobic growth must originate from biomass turnover.

2.3.7 Quantitative analysis of co-factor balances

To provide additional insights into the physiology of *E. coli* grown aerobically and anaerobically on glucose and xylose, we calculated for each condition the

production and consumption rates of key co-factors in metabolism NADH/FADH₂, NADPH, and ATP, using the ¹³C-MFA estimated fluxes. The results are summarized in Fig. 2.7.

For the aerobic cultures, the production and consumption rates of NADH/FADH₂ and NADPH were very similar during growth on glucose (32.0 mmol/gDW.h for NADH/FADH₂, and 10.9 mmol/gDW.h for NADPH) and growth on xylose (29.8 mmol/gDW.h for NADH/FADH₂, and 10.9 mmol/gDW.h for NADPH). The co-factors NADH/FADH₂ were produced about equally via glycolysis (~50% contribution) and the TCA cycle (~50% contribution) for both substrates. The vast majority of NADH/FADH₂ was oxidized to generate ATP via oxidative phosphorylation. Based on our flux results, we estimated that the oxygen consumption rates were 13.8 and 13.2 mmol/gDW.h for growth on glucose and xylose, respectively. During growth on glucose, NADPH was produced mainly via oxPPP (39%) and transhydrogenase (39%), and to a lesser extent in the TCA cycle (21%). During growth on xylose, NADPH was produced about equally via transhydrogenase (31%), the TCA cycle (30%), and oxPPP (27%), and to a lesser extent by malic enzyme (12%).

For the anaerobic cultures, the total production and consumption rates of NADH and NADPH were significantly reduced, especially during growth on xylose. For the anaerobic glucose culture, the production rates of NADH and NADPH were 25.6 mmol/gDW.h and 9.5 mmol/gDW.h, respectively; and for the anaerobic xylose culture, the production rates of NADH and NADPH were 18.0 mmol/gDW.h and 3.4 mmol/gDW.h, respectively. For both substrates, nearly all NADH was produced in glycolysis (>95%), and the majority of the generated NADH was used for ethanol

production. During growth on glucose, NADPH was mainly produced via transhydrogenase (72%), and to a lesser extent via oxPPP (21%). During growth on xylose, NADPH was produced about equally by malic enzyme (50%) and transhydrogenase (41%). The TCA cycle did not contribute significantly to NADPH production.

Biological energy (in the form of ATP) is needed for three key cellular processes: i) transport of substrates and nutrients into the cells, ii) cell growth (anabolism), and iii) maintenance. During aerobic growth, ATP is mainly produced via respiration and substrate-level phosphorylation, and to a lesser extent from acetate production. For example, our flux analysis results suggest that the majority of ATP was produced via oxidative phosphorylation (68% for glucose and 70% for xylose); here, we assumed a value of 2.0 for the P/O ratio. Even if we assume a more conservative value for the P/O ratio of 1.5 (Noguchi et al., 2004; Taymaz-Nikerel et al., 2010), oxidative phosphorylation is still the major contributor to ATP production during aerobic growth on glucose (61%) and xylose (63%). The total ATP production rate was slightly higher during growth on glucose (79.7 mmol/gDW.h) compared to growth on xylose (72.0 mmol/gDW.h). During growth on glucose, 11% of ATP was used for glucose transport (8.8 mmol/gDW.h), 34% for cell growth (26.9 mmol/gDW.h), and 55% for maintenance (43.9 mmol/gDW.h). We define maintenance cost to be the difference between the total rate of ATP production and ATP consumption for substrate uptake and cell growth. If we assume $P/O = 1.5$, the estimated ATP maintenance cost is reduced to 30.1 mmol/gDW.h. For glucose transport, we equate the donated phosphate via PTS transport with one ATP equivalent. During growth on xylose, a relatively larger fraction of ATP was used for

substrate transport and phosphorylation (26%, or 19.0 mmol/gDW.h), 38% for cell growth (27.4 mmol/gDW.h), and 35% for maintenance (25.5 mmol/gDW.h). Assuming $P/O = 1.5$, the estimated ATP maintenance cost is reduced to 12.3 mmol/gDW.h.

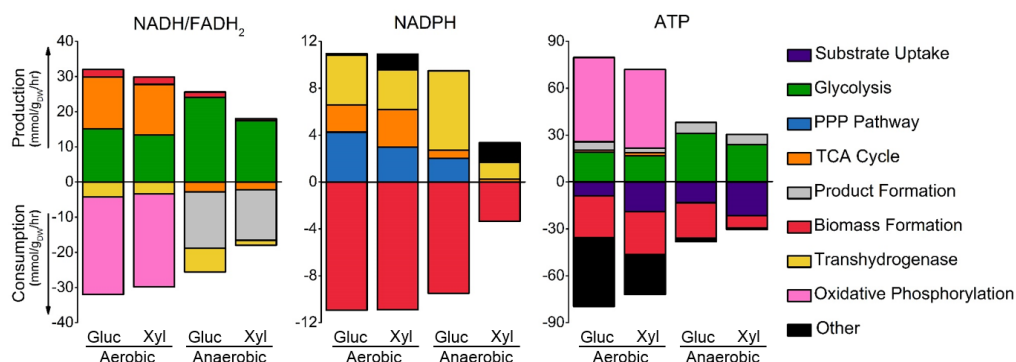


Figure 2.7 Production and consumption of key co-factors in metabolism NADH/FADH₂, NADPH, and ATP, during aerobic and anaerobic growth on glucose (Gluc) or xylose (Xyl). “Other” in NADPH panel represents the contribution of malic enzyme to NADPH production. “Other” in ATP panel represents the estimated ATP maintenance cost (here, assuming P/O ratio = 2.0)

During anaerobic growth, the total ATP production rate was reduced for both substrates. We estimated that ATP production rate was higher during anaerobic growth on glucose (38.1 mmol/gDW.h) compared to anaerobic growth on xylose (30.5 mmol/gDW.h). For both substrates, ATP was mainly produced via substrate-level phosphorylation in glycolysis (~80% for both substrates), with acetate production contributing the remaining ~20%. During growth on glucose, 34% of ATP was used for glucose transport (13.1 mmol/gDW.h), 59% for cell growth (22.5 mmol/gDW.h), and 6% for maintenance (2.2 mmol/gDW.h). During growth on xylose, 71% of ATP was used for xylose transport (21.6 mmol/gDW.h), 26% for cell growth (7.8

mmol/gDW.h), and 3% for maintenance (1.0 mmol/gDW.h). These results suggest that the higher ATP cost for xylose transport and phosphorylation (2 ATP equivalents), compared to glucose (1 ATP equivalent), significantly affects cell growth and biomass yield on xylose. Taken together, these results illustrate that key differences exist between glucose and xylose metabolism at the level of co-factor production and utilization, and that these differences could play a role in determining cell physiology of *E. coli*.

2.4 Conclusion

E. coli is the most widely used microorganism in industry and academia. Previous studies on *E. coli* metabolism have been limited mainly to aerobic growth on glucose. Only a few studies have focused on elucidating fermentative metabolism, and no ¹³C-MFA studies exist on xylose metabolism in *E. coli*. To address this critical gap in current understanding, here, we have applied state-of-the-art methods in ¹³C-MFA to determine precise metabolic fluxes for wild-type *E. coli* grown aerobically and anaerobically on glucose and xylose. We measured condition-specific changes in biomass composition, quantified biomass turnover, and determined that β -oxidation was strictly required for anaerobic growth on xylose. By analyzing co-factor balances, we identified important differences in pathway utilization for the production and consumption of energy and redox cofactors. These validated flux maps can now be used as references for COBRA predictions. In particular, the elucidation of biomass turnover under various conditions will further improve these predictive tools. If biomass turnover is not included, it is likely that predictions will be incorrect. Taken together, this study provides a wealth of new information on aerobic and anaerobic

metabolism in *E. coli* that can be used in future metabolic engineering studies to improve predictive strategies for new strain designs.

Acknowledgements

In this study, Christopher P. Long measured the condition-dependent biomass composition.

Chapter 3

CHARACTERIZATION OF GLUCOSE AND XYLOSE CO-CONSUMING STRAINS AID IN IDENTIFICATION OF IDEAL DESIGN FOR SUGAR CO-UTILIZATION

3.1 Introduction

Lignocellulosic biomass as a feedstock for bioprocesses is desirable as it is a renewable source that can be hydrolyzed into sugars, an attractive substrate for bioconversion. When hydrolyzed, this feedstock becomes a mixture of C5 and C6 sugars such as glucose, xylose, mannose, and galactose (Gírio et al., 2010). Ideally, this mixture could be fed to an organism that is capable of using all sugar monomers simultaneously. However, regulatory mechanisms, such as carbon catabolite repression, and the lack of transport mechanisms often prevent efficient utilization of lignocellulosic hydrolysate (Jeffries, 2006; Liang et al., 2015). To address these issues, regulatory bottlenecks have been alleviated through adaptive evolution and elimination of key genes in the regulatory pathway (Gawand et al., 2013; Kim et al., 2015). Transport machinery has also been expressed in organisms to widen their substrate capabilities (Gonçalves et al., 2014; Grotkjær et al., 2005).

The model organism, *Escherichia coli*, has been the subject of many of these efforts. In particular, components of the phosphotransferase system (PTS) have been removed to allow simultaneous consumption of sugars (Liang et al., 2015; Christopher P Long et al., 2017a). This system also plays a major role in carbon catabolite repression, in which glucose is preferentially used over other sugars. However, few works have provided a detailed characterization of these PTS knockouts and how efficiently they would utilize sugar mixtures.

Apart from targeting the PTS system, several *E. coli* strains have been specifically engineered for co-utilization of sugars. GX50, a strain designed by Kim et al (Kim et al., 2015), was adaptively evolved to use glucose and xylose after elimination of the arabinose transcriptional regulator which represses the xylose transcriptional activator. LMSE2, a strain designed by Gawand et al (Gawand et al., 2013), was designed to require glucose and xylose after deletion of the central carbon metabolism genes, *pgi*, *edd*, and *rpe*. In doing so, this strain is limited stoichiometrically and therefore, cannot grow unless both sugars are used. These two strains are the most successfully engineered strains to date for co-utilization of glucose and xylose.

In this work, we examine the co-utilization capability of all the PTS knockouts with various feed compositions. We use ^{13}C -tracers to evaluate how each sugar is allocated towards biomass components. The two engineered strains described above are also characterized using high resolution ^{13}C -metabolic flux analysis. Their uptake profile based on feed composition is also quantified which provides insights into the “ideal” co-utilizing strain.

3.2 Materials and Methods

3.2.1 Materials

Media and chemicals were purchased from Sigma-Aldrich (St. Louis, MO). Tracers were purchased from Cambridge Isotope Laboratories: [1,2- ^{13}C]glucose (99.9 atom% ^{13}C), [1,6- ^{13}C]glucose (99.6%), [U- ^{13}C]glucose (99.3%), [1,2- ^{13}C]xylose (99.3%), [5- ^{13}C]xylose (99.6%), and [U- ^{13}C]xylose (99.3%). M9 minimal medium was used for all experiments.

3.2.2 Strains and growth conditions

The PTS knockouts and wild-type *E. coli* BW21135 were obtained from the Keio collection. The engineered strains, GX50 and LMSE2, were given to us by (Kim et al., 2015) and (Gawand et al., 2013), respectively. For experiments involving the PTS knockouts, a culture was grown overnight at 37°C in M9 minimal medium containing 6 g/L glucose and 6 g/L xylose in a shaker flask. The pre-culture was then washed and re-suspended in fresh M9 medium containing different ratios of glucose to xylose (0:4, 1:3, 2:2, 1:3, 4:0) where 2:2 is 6 g/L glucose and 6 g/L xylose. For labeling experiments, [U-¹³C]glucose replaced unlabeled glucose at the same concentration. For experiments involving WT, GX50, and LMSE2, a culture was grown overnight at 37°C in M9 minimal medium containing 3 g/L glucose and 3 g/L xylose in a shaker flask. The pre-culture was then washed and re-suspended in fresh M9 medium containing different ratios of glucose to xylose (0:1, 0:2, 1:1, 1:2, 2:1, 2:2, 0:2, 0:1), where 2:2 is 6 g/L glucose and 6 g/L xylose. The following tracers were used for ¹³C-MFA: [1, 2-¹³C]glucose and [1, 2-¹³C]xylose, [1, 6-¹³C]glucose and [5-¹³C]xylose. The initial OD₆₀₀ of inoculated cultures was approximately 0.05. Cells were grown at 37°C in parallel mini-bioreactors with a working volume of 10 mL, as described previously. Air was sparged into the liquid at a rate of 12 mL/min to provide oxygen and to ensure sufficient mixing of the culture by the rising gas bubbles.

3.2.3 Analytical methods

Samples were collected at multiple times during the exponential growth phase to monitor cell growth, substrate uptake, and production formation. Cell pellets and supernatants for isotopic labeling analysis were collected at an OD₆₀₀ of approximately 0.5. Cell growth was monitored by measuring the optical density at 600nm (OD₆₀₀)

using a spectrophotometer (Eppendorf BioPhotometer). After centrifugation of the samples, the supernatant was separated from the biomass pellet. Glucose, xylose and acetate concentrations were determined using an Agilent 1200 Series HPLC (Whitaker et al., 2017).

3.2.4 Gas chromatography-mass spectrometry

GC-MS analysis was performed on an Agilent 7890B GC system equipped with a DB-5MS capillary column (30 m, 0.25 mm i.d., 0.25 μ m-phase thickness; Agilent J&W Scientific), connected to an Agilent 5977A Mass Spectrometer operating under ionization by electron impact (EI) at 70 eV. Helium flow was maintained at 1 mL/min. The source temperature was maintained at 230°C, the MS quad temperature at 150°C, the interface temperature at 280°C, and the inlet temperature at 250°C. GC-MS analysis of *tert*-butyldimethylsilyl (TBDMS) derivatized proteinogenic amino acids was performed as described in (Antoniewicz et al., 2007a). Labeling of glucose (derived from glycogen) and ribose (derived from RNA) were determined as described in (Long et al., 2016a; McConnell and Antoniewicz, 2016). In all cases, mass isotopomer distributions were obtained by integration (Antoniewicz et al., 2007a) and corrected for natural isotope abundances (Fernandez et al., 1996).

3.2.5 Tracer simulations

Tracer simulations were performed as described in (Crown and Antoniewicz, 2012). Briefly, simulated data was generated using a random set of fluxes. ^{13}C -MFA was then used to estimate these fluxes and confidence intervals for different tracer schemes (using both single and parallel tracer experiments), defining the observability

of each flux given the tracers used. This analysis was performed for models containing different relative uptake rates of glucose and xylose.

3.2.6 Metabolic network model and ^{13}C -metabolic flux analysis

The metabolic network model used for ^{13}C -MFA is provided in Supplemental Materials. The model are based on the *E. coli* model described in (Gonzalez et al., 2017) and include all major metabolic pathways of central carbon metabolism, lumped amino acid biosynthesis reactions, and a lumped biomass formation reaction.

All ^{13}C -MFA calculations were performed using the Metran software which is based on the elementary metabolite units (EMU) framework (Antoniewicz et al., 2007b). Fluxes were estimated by minimizing the variance-weighted sum of squared residuals (SSR) between the experimentally measured and model predicted external rates and mass isotopomer distributions of biomass amino acids, glucose derived from glycogen, and ribose derived from RNA using non-linear least-squares regression (Antoniewicz et al., 2006). All measured mass isotopomers are provided in Supplemental Materials. For integrated analysis of parallel labeling experiments, the data sets were fitted simultaneously to a single flux model as described previously (Leighty and Antoniewicz, 2012). Flux estimation was repeated 10 times starting with random initial values for all fluxes to find a global solution. At convergence, accurate 95% confidence intervals were computed for all estimated fluxes by evaluating the sensitivity of the minimized SSR to flux variations. Precision of estimated fluxes was determined as follows (Antoniewicz et al., 2006)

$$\text{Flux precision (stdev)} = [(\text{flux}_{\text{upper bound 95\%}}) - (\text{flux}_{\text{lower bound 95\%}})] / 4 \quad (7)$$

To describe fractional labeling of metabolites, G-value parameters were included in ^{13}C -MFA. As described previously (Antoniewicz et al., 2007c), the G-value represents the fraction of a metabolite pool that is produced during the labeling experiment, while 1-G represents the fraction that is naturally labeled, i.e. from the inoculum. By default, one G-value parameter was included for each measured metabolite in each data set. Reversible reactions were modeled as separate forward and backward fluxes. Net and exchange fluxes were determined as follows: $v_{\text{net}} = v_f - v_b$; $v_{\text{exch}} = \min(v_f, v_b)$.

3.2.7 Goodness-of-fit analysis

To determine the goodness-of-fit, ^{13}C -MFA fitting results were subjected to a χ^2 -statistical test. In short, assuming that the model is correct and data are without gross measurement errors, the minimized SSR is a stochastic variable with a χ^2 -distribution (Antoniewicz et al., 2006). The number of degrees of freedom is equal to the number of fitted measurements n minus the number of estimated independent parameters p . The acceptable range of SSR values is between $\chi^2_{\alpha/2}(n-p)$ and $\chi^2_{1-\alpha/2}(n-p)$, where α is a certain chosen threshold value, for example 0.05 for 95% confidence interval.

3.3 Results and Discussion

3.3.1 Knockouts of PTS respond to feed composition

The PTS is composed of four components, encoded by the genes *ptsG*, *ptsH*, *ptsI*, and *crr* (Long et al., 2017a). We characterized four *E. coli* strains, each lacking one of these genes, during growth on different sugar mixtures (Figure 3.1). When comparing growth rates, most knockouts ($\Delta ptsG$, $\Delta ptsH$, and $\Delta ptsI$) have a slower

growth rate on glucose than on xylose, contrary to what is observed for wild-type *E. coli* (Figure 3.1A). This effect is most noticeable for $\Delta ptsI$, in which the growth rate on xylose (0.66 h^{-1}) is 4.3 times faster than the growth rate on glucose (0.15 h^{-1}). $\Delta ptsH$ and $\Delta ptsI$ appear to be the only knockouts that show a strong dependence of growth rate on the feed composition, where increasing the glucose concentration relative to the xylose concentration results in a slower growth rate.

To determine the contribution of each sugar to the synthesis of biomass components as well as the effect of the feed composition on this contribution, [U- ^{13}C] glucose was used in place of unlabeled glucose. The ^{13}C -labeling of proteinogenic amino acids and carbohydrates (glycogen, RNA) were measured (Figure 3.1B-D). The labeling of alanine provides insight into the relative uptake of each sugar where 50% ^{13}C -labeling of alanine would indicate that the sugars are consumed at the same rate. Based on the ^{13}C -labeling of alanine, $\Delta ptsG$, $\Delta ptsH$, and $\Delta ptsI$ all show a clear preference for xylose over glucose (<50% labeling) while Δcrr prefers glucose (>50% labeling). Additionally, $\Delta ptsG$, $\Delta ptsH$, and $\Delta ptsI$, have similar % ^{13}C -labeling of alanine and therefore, have similar relative uptake rates of the two sugars. For all strains, increasing the glucose concentration relative to xylose leads to a higher relative glucose uptake rate, indicated by the higher labeling of each component as the ratio of glucose to xylose increases.

The ^{13}C -labeling of RNA and glycogen reveals the labeling of the intermediates ribose 5-phosphate (R5P) and glucose 6-phosphate (G6P), respectively. The source of glycogen, either glucose or xylose, appears to be most sensitive in $\Delta ptsI$ where the difference in glycogen labeling between the 1:3 and 3:1 cases is 53%, compared to the other strains, in which the difference ranges between 12% and 28%.

Additionally, while glucose is phosphorylated directly to form G6P, the precursor to glycogen, $\Delta ptsG$, $\Delta ptsH$, and $\Delta ptsI$ generally have $<50\%$ ^{13}C -labeling of glycogen, indicating that the majority of glycogen is derived from xylose. The opposite conclusion can be made for RNA, in which the labeling in $\Delta ptsG$, $\Delta ptsH$, and $\Delta ptsI$ is low, indicating that the main source of RNA is xylose. Δcrr exhibits a clear preference for glucose with high ^{13}C -labeling of both glycogen and RNA ($> 50\%$).

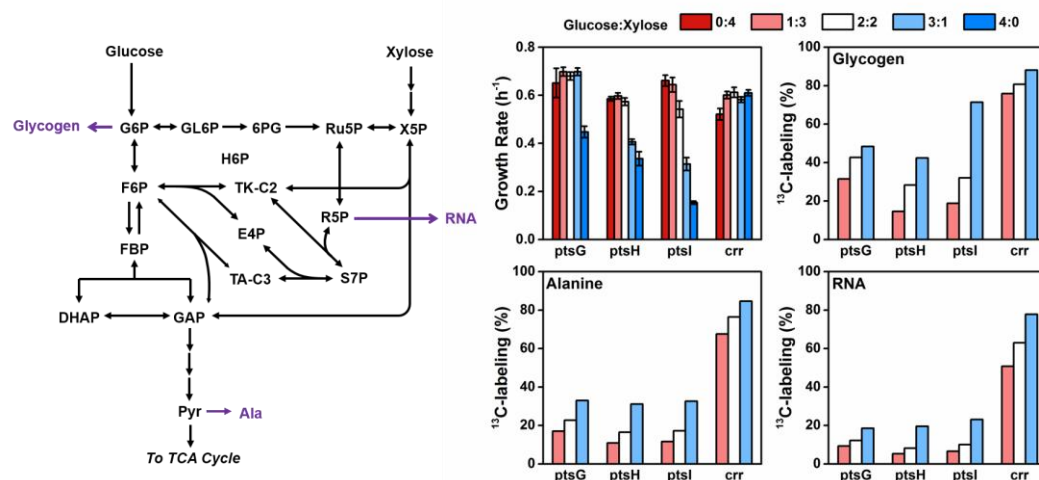


Figure 3.1 Characterization of growth and sugar allocation in PTS knockouts. The growth rate and ^{13}C -labeling of glycogen, RNA, and alanine were measured for each PTS knockout at different ratios of glucose to xylose, as indicated by the color. For the ^{13}C -labeling experiment, [U- ^{13}C]glucose and unlabeled xylose were used as tracers. The growth rates of both $\Delta ptsH$ and $\Delta ptsI$ vary depending on the ratio of glucose to xylose. As the ratio of glucose to xylose increases, the relative uptake of glucose also increases. Based on the ^{13}C -labeling of alanine, $\Delta ptsG$, $\Delta ptsH$, and $\Delta ptsI$ all prefer xylose over glucose ($<50\%$ labeling in alanine) while Δcrr prefers glucose ($>50\%$ labeling in alanine). Error bars indicate standard error ($n=3$).

3.3.2 Engineered strains for co-utilization exhibit various uptake profiles

We next characterized two engineered glucose and xylose co-utilizing strains, GX50 and LMSE2, and compared them to wild-type *E. coli*. For each strain, the initial sugar uptake rates were measured (Figure 3.2). The fraction of the initial total uptake used for xylose was then plotted versus the initial fraction of xylose in the media to obtain an uptake profile that is a function of the %xylose concentration. Using this profile, we were able to simulate the glucose and xylose concentrations measured in our experiments over the entire duration of the culture. For WT *E. coli*, providing both glucose and xylose leads to diauxic growth (Figure 3.2A-C) where xylose starts to be consumed only after all glucose has been exhausted. This translates to an uptake profile in which the % xylose uptake is zero at any % xylose concentration value that is less than 100% (only xylose). The initial uptake rate of glucose does not seem to be affected by the presence of xylose.

For LMSE2, no growth was observed when only one sugar was provided, due to the stoichiometric limitations of the strain (Figure 3.2D-F). When both sugars were present, the absolute sugar uptake rate was constant at approximately 5.6 mmol/g_{DW}/hr, regardless of the feed composition. Therefore, the uptake profile is constant at approximately 60% xylose uptake, or approximately 3.5 mmol/g_{DW}/hr, at all % xylose concentrations. When both sugars are present in approximately equal amounts, they are both used completely. However, the design of the strain prevents complete utilization of both sugars when they are present in unequal amounts. Once one sugar is completely consumed, growth ceases preventing further uptake of the residual sugar.

Unlike LMSE2, the uptake profile of GX50 responds to the extracellular sugar concentration (Figure 3.2G-I); the uptake rate of glucose increases as the

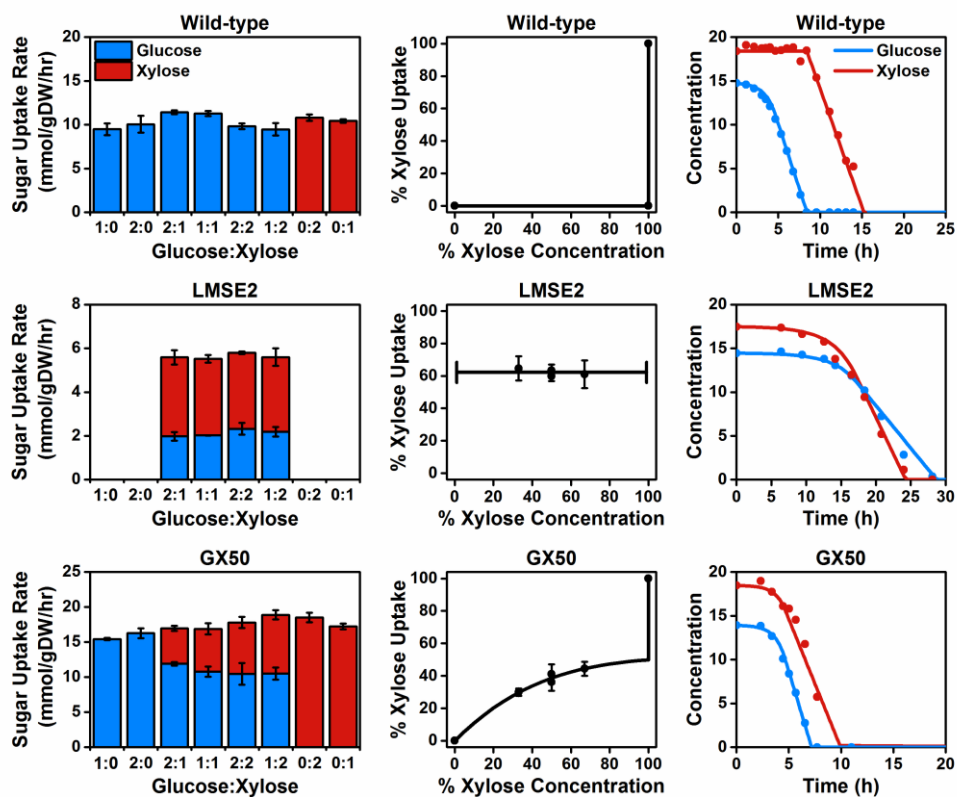


Figure 3.2 Comparison of two co-utilizing strains and WT *E. coli*. For each strain, the initial uptake rates of glucose and xylose were measured. The ratio of these rates (% Xylose Uptake) was plotted versus initial fraction of xylose in the culture (% Xylose Concentration). Additionally, using these uptake profiles, we were able to simulate the glucose and xylose concentrations and compare this simulation to the measured concentrations. In WT, diauxic growth was observed, as expected, with the uptake rate of glucose being unaffected by the presence of xylose. The ratio of uptake rates for LMSE2 remained constant at 60% xylose uptake and no growth was observed when glucose or xylose were the sole substrate. The uptake rates in GX50 varied, depending on the initial concentrations of the two sugars, with a general preference for xylose. Error bars indicate standard error (n=3).

concentration of glucose increases relative to xylose. In general, this strain prefers glucose over xylose as seen by the % xylose uptake being < 50% at all % xylose concentrations tested. This strain grows approximately four times faster than LMSE2 and will exhaust both sugars, regardless of the relative concentrations.

3.3.3 Comprehensive analysis of engineered strains for co-utilization

High resolution ^{13}C -metabolic flux analysis was now used to quantify intracellular fluxes for both engineered strains. However, before performing the tracer experiments, the optimal tracer scheme must be identified. This process is not trivial, especially as you increase the number of substrates. Therefore, we used simulations to determine the precision of using various tracer schemes in both single and parallel labeling experiments (Figure 3.3). Low precision was observed when only one labeling experiment was performed. Additionally, labeling only one substrate severely impacts precision when the unlabeled substrate is the main carbon source. For example, using any xylose tracer when 75% of the total uptake is allocated for glucose results in low precision. Therefore, we were able to identify the optimal tracer scheme as performing two parallel labeling experiments, one using [1,6- ^{13}C]glucose and [5- ^{13}C]xylose and the other using [1,2- ^{13}C]glucose and [1,2- ^{13}C]xylose as tracers. This choice of tracer resulted in high precision regardless of the relative uptake of the sugars.

Figure 3.4 shows the flux maps for LMSE2 and GX50 during growth on a 1:1 mixture of glucose and xylose. The fluxes shown are normalized to the total substrate uptake rate. LMSE2 has a higher relative flux through the pentose phosphate pathway since all flux from glucose is routed through the oxidative PP pathway. GX50 exhibits a higher relative flux through the TCA cycle and secretes less acetate. Flux analysis

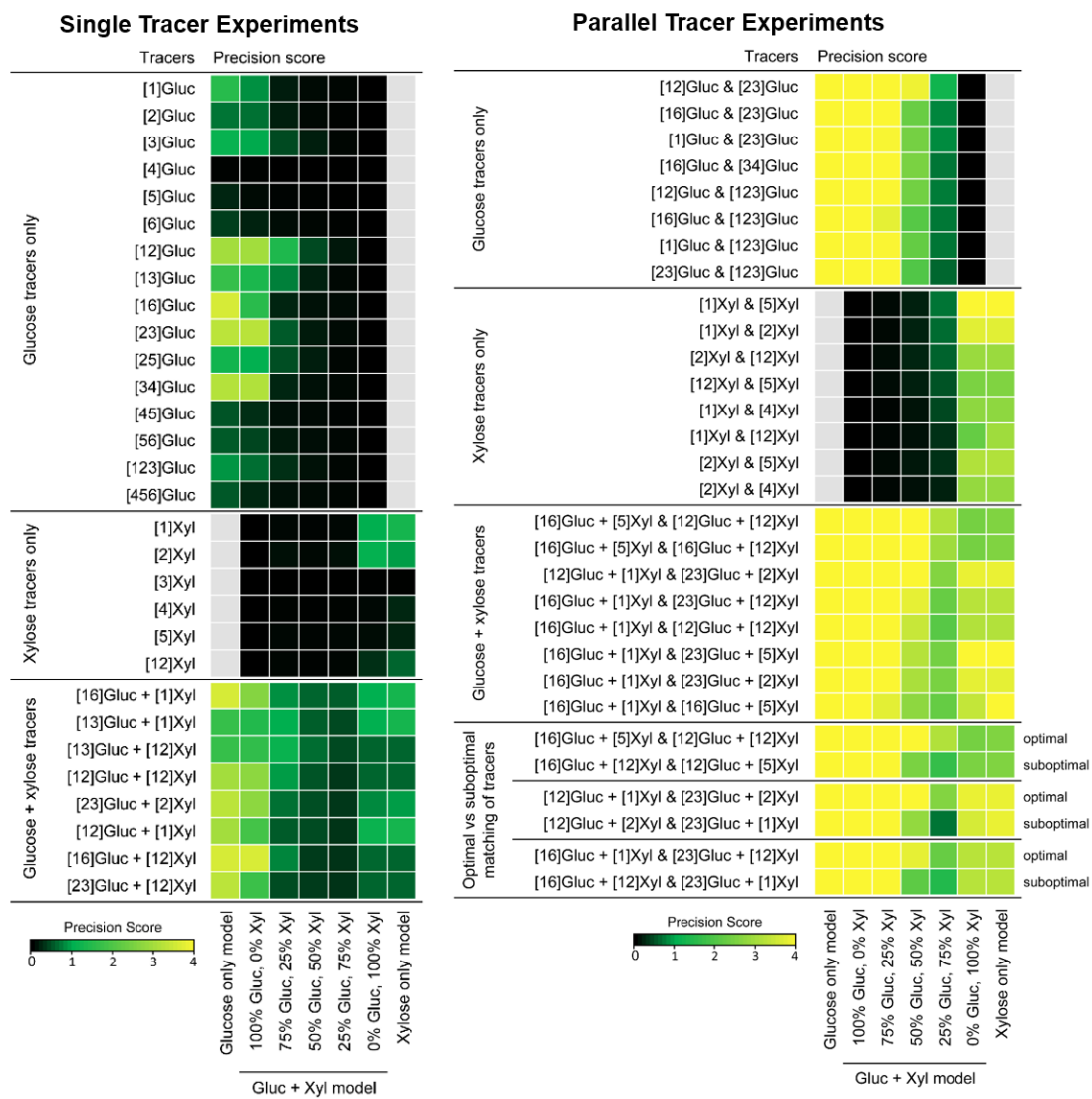


Figure 3.3 Precision of estimated fluxes for various tracer schemes. Improved precision is observed using parallel labeling experiments with each sugar isotopically labeled. Poor precision is observed in single labeling experiments or when only one substrate is isotopically labeled.

was also able to correctly identify that the fluxes through *pgi*, *edd*, and *rpe*, in LMSE2 were zero. Overall, the absolute fluxes of LMSE2 are lower than those of GX50 as the sugar uptake rates in LMSE2 are significantly slower.

¹³C-MFA can also be used to compare intracellular fluxes for each strain as the sugar composition changes. Figure 3.5 shows the relative changes in fluxes compared to the 1:1 mixture. For LMSE2, the sugar composition does not affect the fluxes in upper central carbon metabolism. This is expected because the relative uptake of the sugars is restricted by the gene knockouts. However, higher glucose concentrations (2:1) lead to > 15% increase in TCA cycle fluxes. When the xylose concentration is greater than the glucose concentration (1:2), there is a > 15% decrease in TCA cycle fluxes. For GX50, a lower ratio of glucose to xylose (1:2) leads to an increase in PPP flux while the opposite is seen for a higher ratio of glucose to xylose (2:1). Equal amounts of glucose and xylose (1:1, 2:2) result in similar intracellular fluxes for both strains. Since GX50 can grow on each sugar by itself, ¹³C-MFA was also performed for growth on glucose only and xylose only. Doubling the concentration of either sugar did not affect intracellular fluxes (Figure B.4).

Using the fluxes estimated by ¹³C-MFA, we can examine the production and consumption of the key cofactors in metabolism NADH/FADH₂, NADPH, and ATP for each strain and condition (Figure 3.6). For LMSE2, the transhydrogenase is not a major sink of NADH while in GX50, it accounts for, on average, 0.6 mol NADH/ mol substrate consumed (~45% of the total NADH consumed). More than 0.49 mol NADPH/mol substrate (~75% of the total NADPH produced) is produced via the oxidative pentose phosphate pathway in LMSE2. While this pathway is also a source of NADPH in GX50, it accounts for almost half of the total NADPH while the remainder is produced by the transhydrogenase. For GX50, the cofactor balances are similar when both substrates are present and when there is only glucose. A difference is only seen when xylose is the only substrate in which

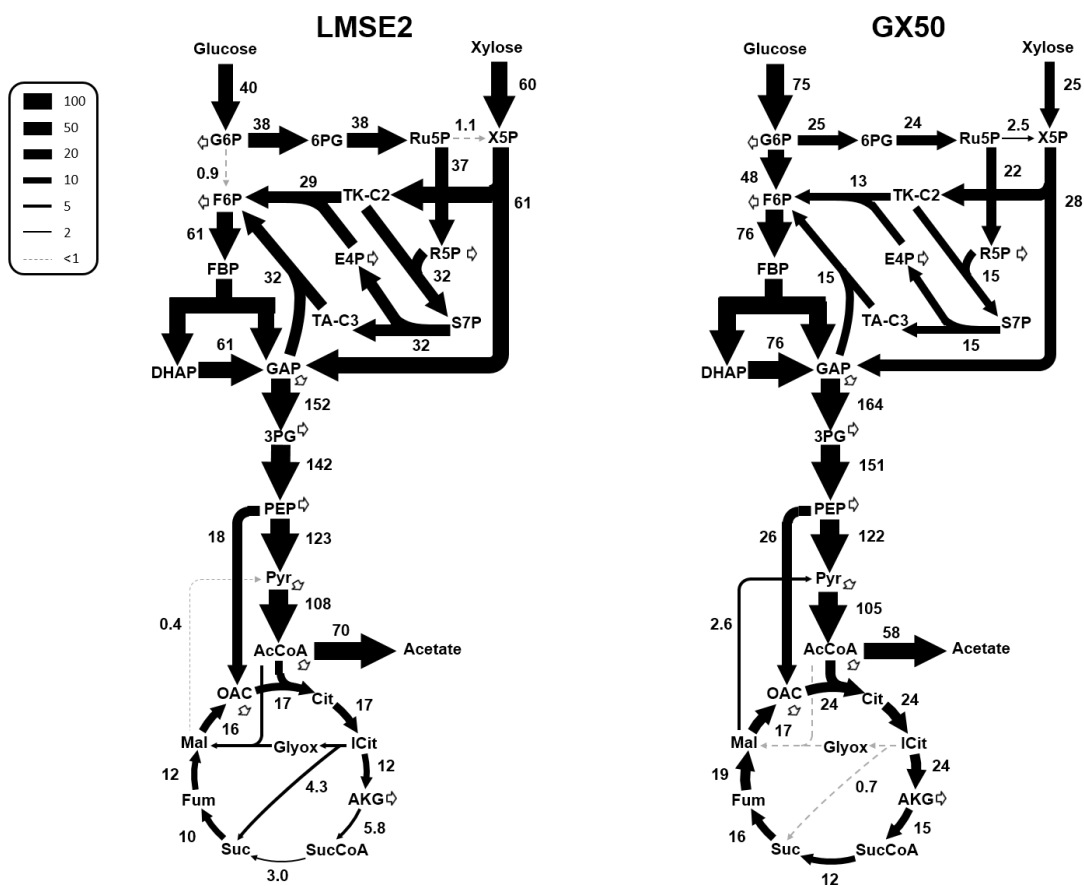


Figure 3.4 Metabolic flux map for strains LMSE2 and GX50 grown in a 1:1 ratio of glucose to xylose. Fluxes were estimated using ^{13}C -MFA, including measurements from parallel labeling experiments using $[1,2-^{13}\text{C}]$ glucose + $[1,2-^{13}\text{C}]$ xylose and $[1,6-^{13}\text{C}]$ glucose and $[5-^{13}\text{C}]$ xylose as tracers.

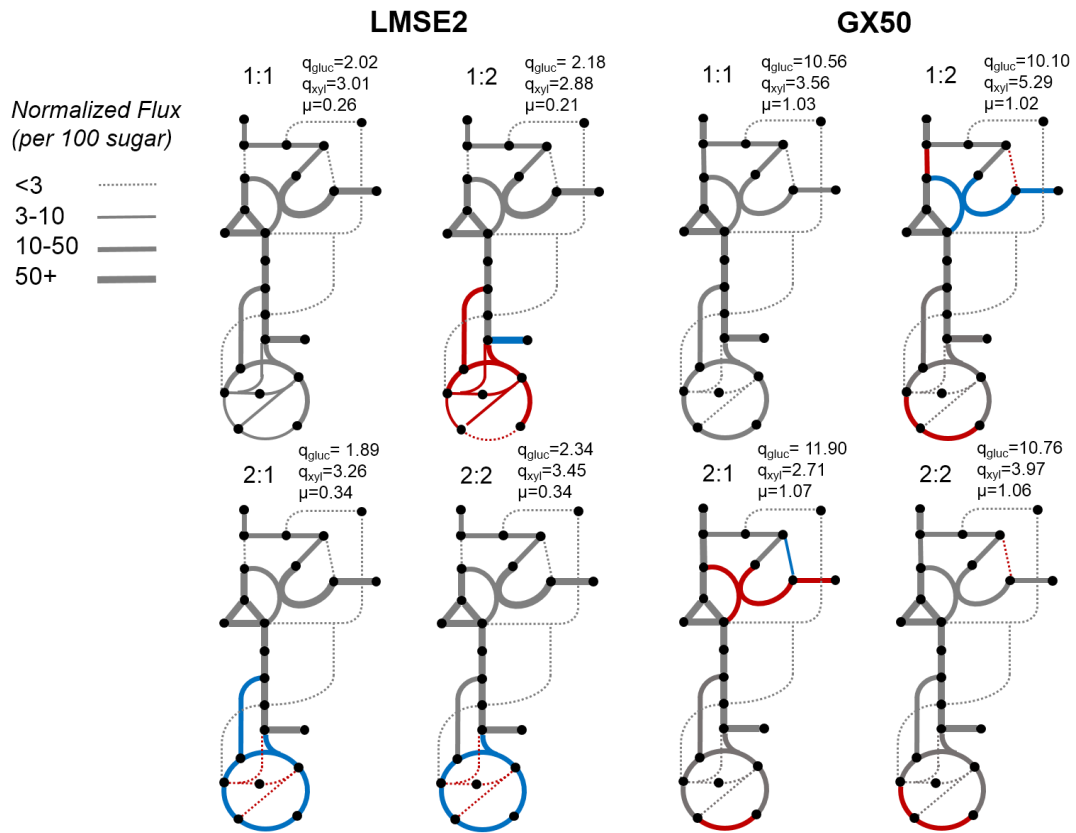


Figure 3.5 Comparison of estimate fluxes for various glucose/xylose mixtures. Highlighted changes indicate at least a 15% relative increase (blue) or decrease (red) compared to the fluxes estimate for a 1:1 glucose/xylose mixture. Changes in the TCA cycle fluxes are observed for LMSE2 while changes in the PPP fluxes are observed for GX50.

anaplerosis is more active in the production of NADPH, the transhydrogenase is less active, and the PPP is no longer a main source of NADPH. While the consumption and production of reducing equivalents is quite different between the two strains, the breakdown of ATP usage is strikingly similar for all conditions. Additionally, the sugar composition doesn't appear to impact the cofactor distribution.

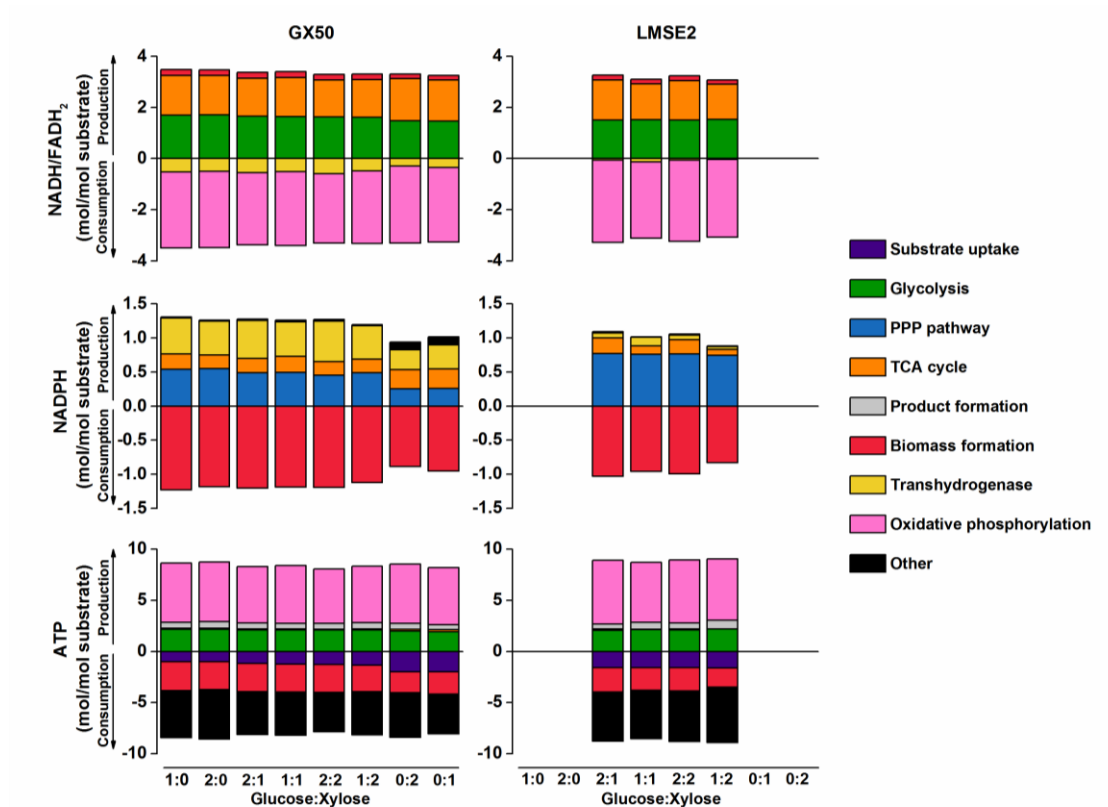


Figure 3.6 Production and consumption of key co-factors in metabolism. Using fluxes estimated by ^{13}C -MFA, utilization of NADH/FADH_2 , NADPH , and ATP was quantified for each strain. GX50 and LMSE2 differ in the consumption of NADH and production of NADPH by the transhydrogenase as well as the production of NADPH by the PP pathway. ATP allocation remains relatively constant for both strains.

3.3.4 Ideal co-utilizing strain demands linear uptake profile

We have presented a detailed characterization of several strains that can co-utilize glucose and xylose. Some were rationally engineered to have this ability while others were constructed by removing the regulatory mechanism that prevents co-utilization natively. Most strains tested were responsive to the extracellular sugar concentration, although it is possible to limit this response as seen in the case of LMSE2. Based on these results, we can make some conclusions regarding the ideal

co-utilizing strain. The ideal strain should not experience CCR and it should be sensitive to extracellular concentrations and use all available sugar.

Figure 3.7 shows hypothetical uptake profiles and how each of these strains would use various sugar mixtures. One extreme that is undesirable is a strain that experiences carbon catabolite repression (case A), such as WT *E. coli*, in which diauxic growth is observed and there is never a period in which both sugars are consumed. The other extreme is a strain that is not sensitive to the sugar composition, and therefore, stops growth once one sugar is exhausted, leaving residual sugar (case D). The two intermediate cases (B and C) have a parabolic uptake profile or a linear uptake profile, respectively. In the parabolic case, the strain still shows a preference for one sugar, such as here where the strain prefers glucose unless greater than 90% of the available sugar is xylose. This hypothetical strain is similar to case A, in which there is a point in the fermentation that glucose reaches a concentration of zero before xylose is completely consumed. In the linear case, the relative uptake rate of each sugar is directly correlated with the relative extracellular concentration and therefore, the sugars are completely utilized at the same time.

While the simulated concentrations shown are representative of batch fermentations, the implications are even more severe in the case of fed-batch fermentations, which are most commonly used for industrial processes. For case A and B, since one sugar is completely consumed before the other, there will be an accumulation of one sugar over time. If the sugars are present in equal amounts, case D will result in an efficient process. However, any deviation from that composition will lead to wasted carbon. Therefore, the ideal uptake profile is clearly one that is

linear in which, regardless of the feed composition, both sugars will be used up at the same time, leading to the most efficient fermentation.

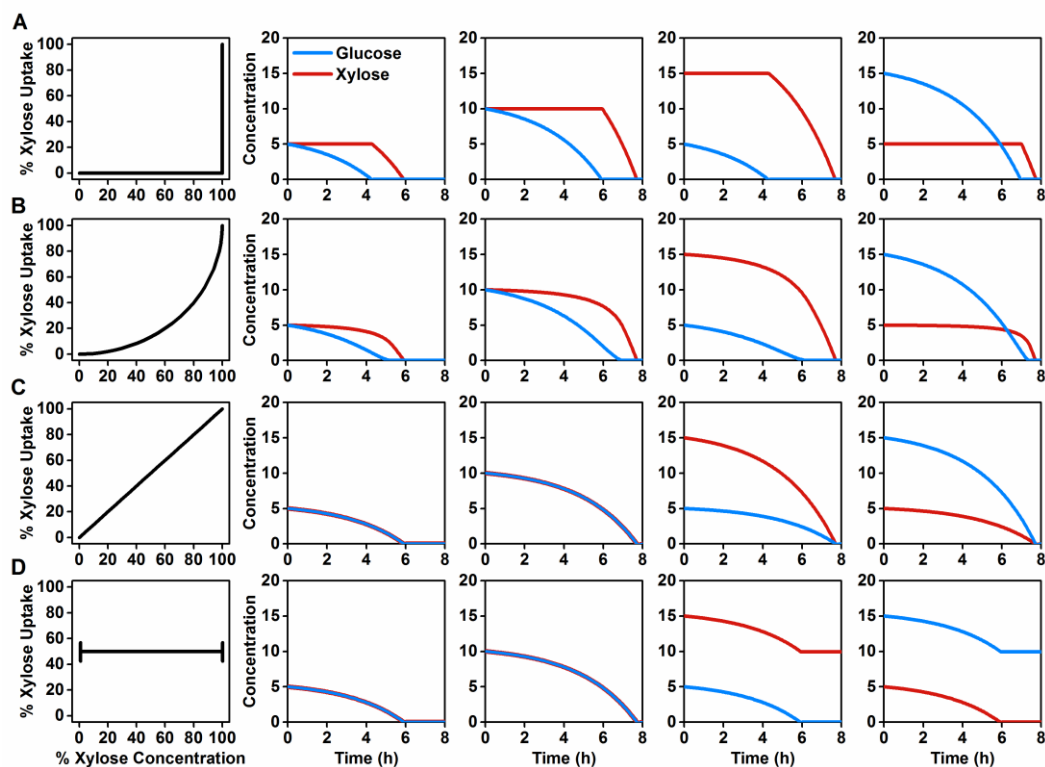


Figure 3.7 Simulation of theoretical uptake profiles. The uptake profiles examined were diauxic (A), parabolic (B), linear (C), and constant (D). Each profile was used to simulate the consumption of glucose and xylose for different starting concentrations in batch culture. It is clear that the only profile resulting in an efficient process is the linear profile, with simultaneous consumption and no residual sugar.

3.4 Conclusion

In this work, we examined various approaches to solving the issue of inefficient utilization of sugar mixtures derived from lignocellulosic biomass. *E. coli* has been the focus of many of these approaches. Here, we first studied several knockouts of the PTS and found that all can co-utilize glucose and xylose.

Additionally, the metabolism of each strain, as identified by ^{13}C -labeling of biomass components, was altered depending on the relative extracellular concentrations of the two sugars. This response was also examined in two engineered strains, GX50 and LMSE2. While the uptake rates of the sugars varied depending on the ratio of the sugars in GX50, this effect was not observed in LMSE2, in which the uptake rates are limited by stoichiometry. For the engineered strains, a detailed analysis of intracellular metabolism was performed using ^{13}C -MFA. Various changes in metabolism were observed as the ratio of glucose to xylose was altered. Specifically, the TCA cycle was affected in LMSE2 while fluxes through the PPP changed in GX50. When comparing the two strains to each other, there were clear differences in intracellular fluxes and cofactor utilization. GX50 utilized the transhydrogenase while LMSE2 used the oxidative PPP as their main sources of NADPH. Flux through the TCA cycle was relatively higher in GX50 compared to LMSE2 while the opposite was observed for PPP fluxes. Interestingly, ATP allocation was similar for both strains.

After analysis of existing strains, we presented various hypothetical strains and examined how these strains could co-utilize a glucose and xylose mixture. The uptake profile that resulted in the most efficient utilization of sugars was one that is linear, where the relative uptake rates of the sugars is directly correlated to the relative concentrations of the sugars. Realizing this design would require identification of an unbiased, universal transport system, one that demonstrates no preference for a specific substrate, and therefore, must have the same affinity for each substrate. With advances in protein engineering, it will be possible to design novel transport systems or reprogram existing ones to achieve a linear uptake profile (Nijland et al., 2014;

Young et al., 2014). These systems can then be expressed in various organisms to generate efficient and sustainable biofactories for production of valuable chemicals.

METHANOL ASSIMILATION IN *Escherichia coli* IS IMPROVED BY CO-UTILIZATION OF THREONINE AND DELETION OF LEUCINE-RESPONSIVE REGULATORY PROTEIN

4.1 Introduction

The production of chemicals and fuels through biological conversion of inexpensive and abundant feedstocks, such as natural gas, offers advantages over traditional fermentation processes (Fei et al., 2014). The main component of natural gas, methane, can be used as a substrate in fermentations either directly or after conversion to methanol. Methanol is an attractive feedstock due to its high electron and energy content (Fei et al., 2014; Olah, 2005). In the past few years, efforts to engineer improved (or entirely new) methylotrophic organisms that efficiently consume methanol and produce value-added chemicals have intensified (Leßmeier et al., 2015; Liao et al., 2016; Whitaker et al., 2015)

Native methylotrophs, such as *Methylobacterium extorquens* AM1 and *Bacillus methanolicus*, use one of several pathways for methanol fixation including the serine cycle and the ribulose monophosphate pathway (RuMP) (Schrader et al., 2009). In these pathways, methanol is first converted to formaldehyde by a methanol dehydrogenase (MDH), which gives the cell access to several one-carbon assimilation pathways. The prospect of using native methylotrophs for bioconversion processes, however, is still problematic because, among other issues (Whitaker et al., 2015), genetic tools are not well established for many of these organisms. Methylotrophic yeasts have been studied extensively and are easily genetically modified, however, their methanol assimilation mechanism requires oxygen, ultimately limiting product yields. As an alternative, genetically tractable and industrially relevant organisms such

as *Escherichia coli* and *Corynebacterium glutamicum* are being engineered to utilize methanol and produce chemicals (Leßmeier et al., 2015; Müller et al., 2015; Whitaker et al., 2017; Witthoff et al., 2015). The RuMP pathway is the preferred pathway for engineering methylotrophy in non-native organisms since it is the only known energy-yielding one-carbon assimilation pathway and does not require oxygen (Whitaker et al., 2015). The two main enzymes in the RuMP pathway are 3-hexulose-6-phosphate synthase (hps) and 6-phospho-3-hexuloisomerase (phi). Together, these enzymes fix formaldehyde to ribulose 5-phosphate (Ru5P) and convert the product, hexulose 6-phosphate, to fructose 6-phosphate (F6P), an intermediate of central carbon metabolism (Figure 1).

In previous work, we successfully engineered a methylotrophic *E. coli* strain that contains an MDH from *Bacillus stearothermophilus* and the RuMP pathway from *Bacillus methanolicus* (Whitaker et al., 2017). We demonstrated that the strain can incorporate abundant amounts of methanol into biomass and secreted products. This was an advancement over previous efforts (Müller et al., 2015); however, our strain was still unable to utilize methanol as the sole carbon source. To maximize methanol incorporation, yeast extract was required as a co-substrate.

To gain a better understanding of methylotrophy in the engineered *E. coli* and elucidate the mechanism by which yeast extract improves methanol utilization, in this study, we performed experiments using ¹³C-tracers to examine the metabolism of methanol assimilation. We evaluated 25 potential co-substrates. Co-consumption of specific amino acids correlated with improved methanol utilization, which led us to hypothesize a new metabolic engineering target to improve methanol utilization that was tested and successfully implemented in our strain, ultimately enhancing the

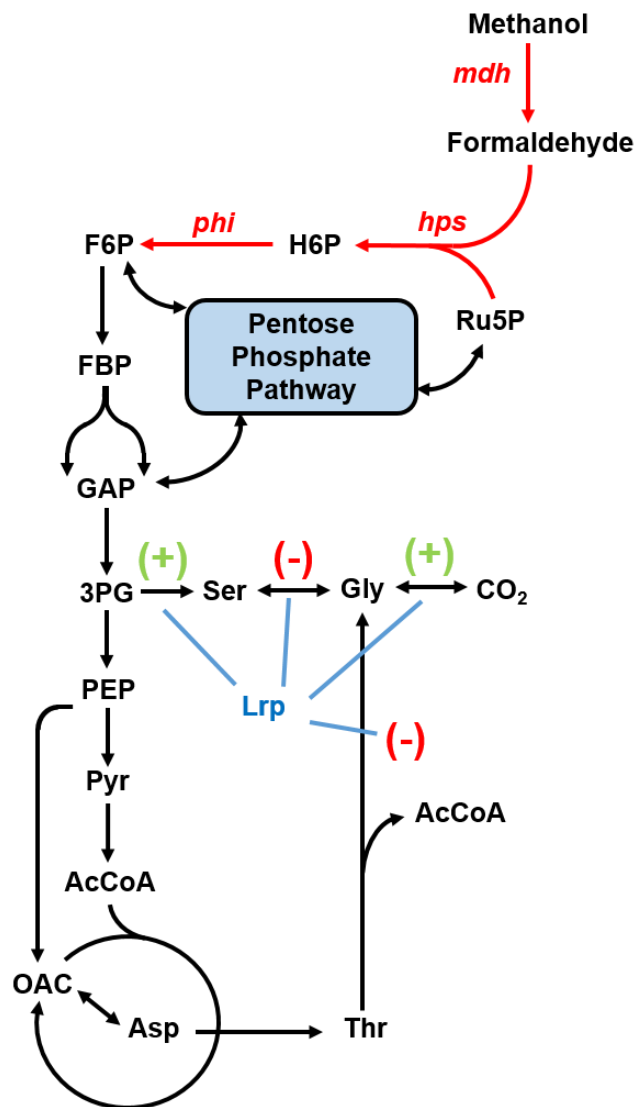


Figure 4.1 Synthetic methylotrophy in *E. coli* and its relation to the global regulator Lrp. To achieve a methylotrophic phenotype in *E. coli*, three heterologous genes were expressed: methanol dehydrogenase (*mdh*), 3-hexulose-6-phosphate synthase (*hps*), and 6-phospho-3-hexuloisomerase (*phi*). Methanol enters the pentose phosphate pathway and through various rearrangement reactions, Ru5P is generated for another round of formaldehyde fixation. In this work, we demonstrate that increased methanol assimilation is associated with increased flux from threonine (Thr) to glycine (Gly) and serine (Ser). To improve incorporation of methanol, the leucine-responsive protein (Lrp), which negatively regulates reactions denoted with (-) and positively regulates reactions denoted (+), was deleted.

methylo-trophic ability of our strain. Overall, this study represents a rational engineering approach for studying substrate utilization and improving synthetic methylo-trophy and provides an illustrative example of the design-build-test-learn cycle in metabolic engineering (Nielsen and Keasling, 2016).

4.2 Materials and Methods

4.2.1 Materials

Media and chemicals were purchased from Sigma-Aldrich (St. Louis, MO). ¹³C-Methanol (99% ¹³C) was purchased from Isotec (St. Louis, MO). M9 minimal medium was used for all experiments.

4.2.2 Strains and growth conditions

The base methylo-trophic *E. coli* strain used here was described in detail in Whitaker et al., 2016. Briefly, *E. coli* BW25113 Δ *frmA* was obtained from the Keio collection and used for further genetic manipulations (Baba et al., 2006). Deletion of *lrp* was performed as described upon removal of the kanamycin cassette from the *frmA* locus via pCP20 (Datsenko and Wanner, 2000). Methanol assimilation genes were cloned into pETM6 (Xu et al., 2012) for episomal expression. Briefly, an operon composed of the *mdh* from *B. stearo-thermophilus* and *hps* and *phi* from *B. methanolicus* was constructed. The heterologous genes were synthesized as gBlocks (IDT, Coralville, IA) with synthetic ribosomal binding sites designed using the RBS Calculator v2.0 (Borujeni et al., 2014; Salis et al., 2009), and the operon consisted of a synthetic promoter (P_{trc}) and terminator. The respective fragments were then Gibson assembled into pETM6 digested with AvrII and NheI.

For experiments involving glucose, yeast extract, casamino acids, or tryptone as substrates, a culture was grown overnight from frozen stock in Luria Broth (LB) medium at 37 °C in a shaker flask. The pre-culture was then re-suspended in fresh M9 medium containing 1.5 g/L of the substrate. For cultures containing methanol, ¹³C-labeled methanol was added at 60 mM initial concentration. The initial OD₆₀₀ of the inoculated cultures was approximately 0.05. Cells were grown at 37°C in shaker flasks with a working volume of 25 mL. Samples were collected at 24 and 48 hours for GC-MS analysis.

For experiments involving amino acids as substrates, a culture was grown overnight from frozen stock in LB medium. The pre-culture was then re-suspended in fresh medium containing 5 mM of a specific amino acid. For cultures containing methanol, ¹³C-labeled methanol was added at 60 mM. The initial OD₆₀₀ of inoculated cultures was approximately 0.05. Cells were grown at 37°C in shaker flasks with a working volume of 25 mL. Samples were collected at 72 hours for GC-MS analysis.

For studies comparing the base strain and the Δlrp strain, a culture was grown overnight from frozen stock in LB medium at 37 °C in a shaker flask. The pre-culture was then re-suspended in fresh M9 medium containing 1.5 g/L yeast extract. For cultures containing methanol, ¹³C-methanol was added at 60 mM. For cultures containing threonine, threonine was added at 5 mM. The initial OD₆₀₀ of inoculated cultures was approximately 0.05. Cells were grown at 37°C in shaker flasks with a working volume of 25 mL. Samples were collected at 24, 48, and 72 hours for GC-MS analysis.

4.2.3 Analytical methods

Samples were collected at regular intervals to monitor cell growth and measure isotopic labeling of biomass components, including RNA, glycogen and amino acids (Long et al., 2016a). Optical density at 600 nm (OD_{600}) was measured using a spectrophotometer (Eppendorf BioPhotometer). The OD_{600} values were converted to cell dry weight concentrations using a pre-determined OD_{600} -dry cell weight relationship ($1.0 OD_{600} = 0.32 \text{ g}_{\text{DW}}/\text{L}$) (Long et al., 2016b). The percent increase in biomass as a result of methanol being co-utilized was calculated as follows:

$$\frac{OD_{600} \text{ of culture with methanol} - OD_{600} \text{ of culture without methanol}}{OD_{600} \text{ of culture without methanol} - \text{initial } OD_{600} \text{ of culture}} \times 100\% \quad (4.1)$$

4.2.4 Amino acid quantification

To quantify the amino acid content of yeast extract, casamino acids, and tryptone, two 100 μL samples of a 1.5 g/L solution of these substrates were used for isotope ratio analysis, using fully labeled [$U\text{-}^{13}\text{C}$]algal amino acids as internal standards. Two samples were prepared. One sample was immediately derivatized with TBDMS to measure free amino acids. The second sample was hydrolyzed overnight at 110°C in 6N HCl, and then derivatized to measure peptides + free amino acids. The analysis was performed four times for each substrate.

4.2.5 RNA and glycogen quantification

The amount of RNA and glycogen (% of cell dry weight), and isotopic labeling of these macromolecules was determined as described in (Christopher P. Long and Antoniewicz, 2014). Briefly, biomass samples were hydrolyzed with HCl resulting in the release of ribose (from RNA) and glucose (from glycogen). The sugars were then derivatized and analyzed by GC-MS (McConnell and Antoniewicz, 2016). For

quantification of RNA and glycogen, isotope ratio analysis was performed using fully ^{13}C -labeled *E. coli* as the internal standard. Fully labeled *E. coli* was generated by growing *E. coli* on $[\text{U-}^{13}\text{C}]$ glucose, washing the cells twice with glucose-free medium, and aliquoting identical (1 mL of an $\text{OD}_{600}=1.0$, or 0.32 mg of dry weight) samples, to be used as internal standards.

4.2.6 Gas chromatography-mass spectrometry

GC-MS analysis of isotopic labeling of sugars (i.e. ribose and glucose from RNA and glycogen, respectively) was performed as described in (Long et al., 2016a). The measured GC-MS fragments contained the first four carbons of ribose (m/z 284 fragment), and the first five carbons of glucose (m/z 370 fragment). GC-MS analysis of fructose-6-phosphate was performed as described in (Ahn et al., 2016). GC-MS analysis of *tert*-butyldimethylsilyl (TBDMS) derivatized proteinogenic amino acids was performed as described in (Gonzalez et al., 2017). All GC-MS analyses were performed on an Agilent 7890B GC system equipped with a DB-5MS capillary column (30 m, 0.25 mm i.d., 0.25 μm -phase thickness; Agilent J&W Scientific), connected to an Agilent 5977A Mass Spectrometer operating under ionization by electron impact (EI) at 70 eV. Mass isotopomer distributions were obtained by integration (Antoniewicz et al., 2007a) and corrected for natural isotope abundances (Fernandez et al., 1996). Average carbon labeling was calculated using the following formula:

$$\text{Average Carbon Labeling (\%)} = \text{sum}(M_i * i) / n \quad (4.2)$$

where n is the number of carbons, M_i is the corrected abundance of the i^{th} mass isotopomer.

4.3 Results

4.3.1 ¹³C-labeling demonstrates that yeast extract is a superior co-substrate compared to glucose in enhancing methanol assimilation

Previously, we successfully engineered a synthetic methylotrophic *E. coli* that is able to utilize methanol for cell growth when yeast extract is provided as a co-substrate (Whitaker et al., 2017). Here, we compared methanol utilization of this strain with yeast extract versus glucose as co-substrates. Experiments were performed either with 60 mM of ¹³C-methanol or without methanol. Glucose and yeast extract were each present at 1.5 g/L. Figure 4.2A shows the increase in biomass concentration when methanol was co-utilized with either of the two substrates, i.e. relative to experiments without methanol. Co-utilization of yeast extract and methanol resulted in 33% higher final biomass concentration compared to the experiment without methanol (i.e. yeast extract alone), while a higher final OD₆₀₀ was achieved with glucose (Figure C1). However, when glucose and methanol were co-utilized, the final biomass concentration was only ~1% higher compared to glucose alone. Improvement in methanol assimilation when co-utilizing yeast extract was also reflected in the ¹³C-labeling of major biomass components such as proteins, RNA, and glycogen (Figure 4.2B). When yeast extract and ¹³C-methanol were co-utilized, significant labeling was detected in biomass components (e.g. 17% labeling in glycogen) and intracellular metabolites (e.g. 30% labeling in F6P, Figure C2), whereas when glucose and ¹³C-methanol were co-utilized, low ¹³C-labeling was observed (less than 3% labeling). Thus, based on ¹³C-labeling and growth data, yeast extract appears to be a better co-substrate compared to glucose for methanol assimilation. One possible explanation is that carbon catabolite repression prevents efficient methanol co-utilization in the presence of glucose. However, we also observed the same effect with other sugars and

organics acids as co-substrates (Figure 4.3). While high labeling was detected in biomass components, certain amino acids, notably leucine, valine, and phenylalanine (Table C.3), were not labeled by ^{13}C -methanol. Given that amino acids are the main components of yeast extracts (Figure C.3), these data suggest that a possible regulatory mechanism activated in the presence of yeast extract leads to the observed ^{13}C -labeling patterns. In addition to yeast extract, casamino acids and tryptone were also tested as co-substrates (Figures C.4, C.5). The ^{13}C -labeling patterns and growth improvements were similar to those observed with yeast extract as the co-substrate, thus further supporting the hypothesis that amino acids are responsible for improved methylotrophy.

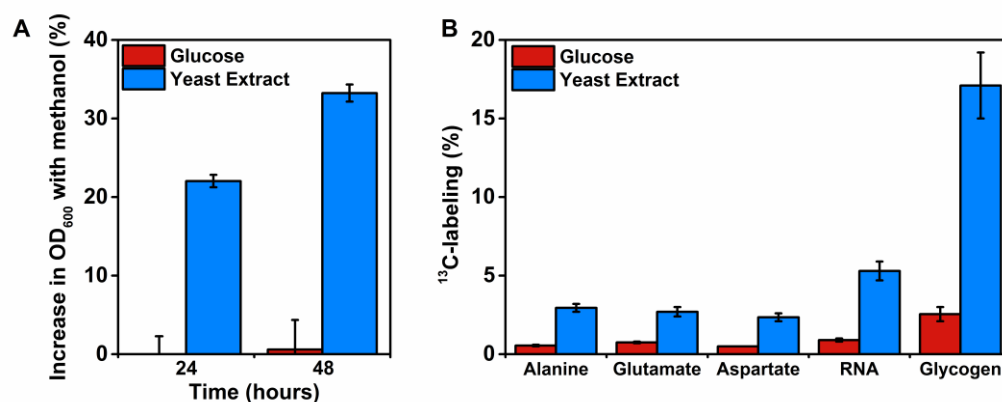


Figure 4.2 Yeast extract is a better co-substrate for methanol assimilation than glucose. (A) The increase in OD₆₀₀ in the presence of methanol compared to the absence of methanol was determined for growth with the co-substrates glucose (red bars) and yeast extract (blue bars). (B) ^{13}C -labeling in biomass components (amino acids, RNA, and glycogen) from ^{13}C -methanol was measured for both co-substrates after 48 hours. Overall, yeast extract was the superior co-substrate for methanol assimilation as indicated by higher labeling and improved growth in the presence of methanol. Error bars indicate standard error (n=2).

4.3.2 Threonine as a co-substrate leads to high ¹³C-labeling and enhanced growth

In an effort to explain why yeast extract was a superior co-substrate for methanol assimilation, we performed a series of experiments where we systematically evaluated each amino acid individually as a potential co-substrate for methanol utilization. We hypothesized that the presence of certain amino acids may trigger a cellular response that results in the high methanol assimilation phenotype observed with yeast extract. For comparative analysis, we also evaluated five non-amino acid carbon sources: acetate, pyruvate, succinate, xylose, and glucose. Experiments were performed as described in the previous section, where two cultures were performed in parallel, one with 60 mM ¹³C-methanol and one without methanol. The initial concentration of each co-substrate was 5 mM.

In total, twenty-five co-substrates were thus evaluated, which we classified into three groups: 1) amino acids for which no degradation pathways are known in *E. coli* (Link et al., 2015) and therefore, *E. coli* cannot use these substrates for growth alone: Histidine (His), Tyrosine (Tyr), Valine (Val), Methionine (Met), Isoleucine (Ile), Leucine (Leu), Phenylalanine (Phe), Lysine (Lys); 2) amino acids for which degradation pathways are known to exist in *E. coli*: Arginine (Arg), Cysteine (Cys), Tryptophan (Trp), Proline (Pro), Glycine (Gly), Serine (Ser), Glutamate (Glu), Asparagine (Asn), Threonine (Thr), Glutamine (Gln), Alanine (Ala), Aspartate (Asp); and 3) other substrates (i.e. non-amino acids): Acetate (Ac), Pyruvate (Pyr), Succinate (Suc), Xylose (Xyl), Glucose (Gluc). Cell growth was monitored for three days in all experiments. Figure 4.3 shows representative growth profiles for leucine, threonine, acetate, and glucose as co-substrates.

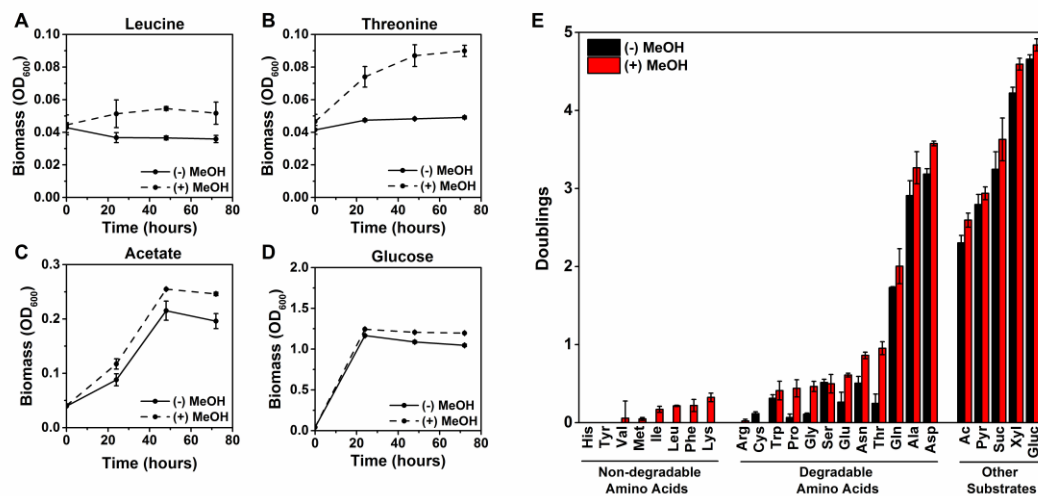


Figure 4.3 Growth is improved in the presence of methanol for several co-substrates. Growth profiles for *E. coli* on leucine (A), threonine (B), acetate (C), and glucose (D) as co-substrates in the presence (dashed line) or absence (solid line) of methanol. The number of cell doublings in both the presence and absence of methanol was determined for each co-substrate (E). In the presence of methanol, growth was improved for many co-substrates, however, the extent of improvement varied, generally decreasing with increased growth. Error bars indicate standard error (n = 2).

As expected, no growth was observed on the non-degradable amino acids as sole carbon sources. Figure 4.3A shows the biomass concentration during growth on leucine, which is representative of the group of non-degradable amino acids. In the presence of ¹³C-methanol, the final biomass concentration was slightly higher compared to leucine alone. Similar results were obtained for the other non-degradable amino acids. Figure 4.3E also shows the number of cell doublings observed for each condition. In a few cases, slight net growth was observed in the presence of ¹³C-methanol (<0.4 doublings), but no net growth was observed without methanol.

For the second group of amino acids (i.e. the degradable amino acids), significant growth was observed in many cases, with the number of doublings ranging between 0 and 3.6 (Fig 4.3E). For several amino acid co-substrates (proline, glycine, glutamate, asparagine, and threonine), there was a pronounced improvement in the number of doublings in the presence of ^{13}C -methanol compared to the control experiments without methanol, e.g. 0.95 for threonine (Fig 4.3E). Overall, amino acids that generated better growth as sole substrates resulted in smaller improvements in the number of doublings in the presence of methanol. For example, in the case of alanine, aspartate, and glutamate, there was <16% increase in the number of doublings between the condition with methanol and the condition without methanol.

For the third set of co-substrates (i.e. sugars and organic acids), significant growth was observed in all cases, with the number of doublings ranging from 2.3 to 4.8. However, the improvement in cell growth as a result of ^{13}C -methanol co-utilization was small in all cases (<13%, Fig 4.3E), following the same trend as observed for the degradable amino acids.

In addition to quantifying growth profiles, we also measured isotopic labeling of biomass components (specifically, glycogen, RNA, and proteinogenic amino acids) for all experiments where ^{13}C -methanol was used as a co-substrate (all data are provided in Supplemental Materials). Figures 4.4A and 4.4B show the measured mass isotopomer distributions (MID) of glycogen and RNA, after correction for natural isotope abundances, where M+0, M+1, M+2, etc represent the mass isotopomers with no carbons labeled, one carbon labeled, two carbons labeled, etc, respectively. We observed high labeling of RNA (up to 29%, 1-M+0) and glycogen (up to 84%, 1-M+0) for all amino acid co-substrates, and especially for non-degradable amino acids as co-

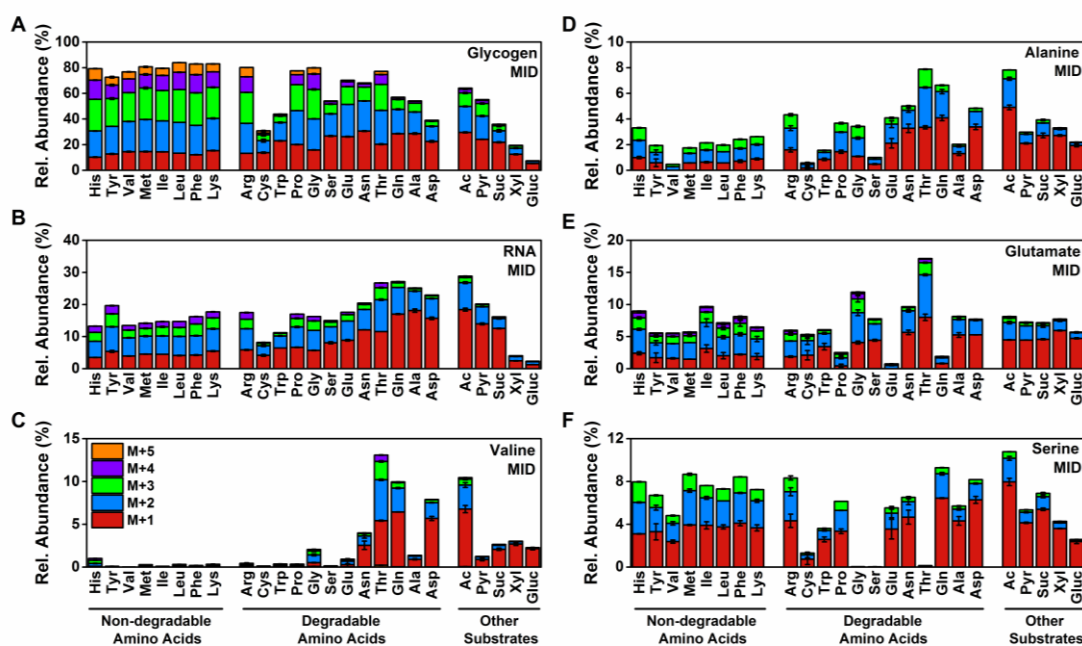


Figure 4.4 Threonine as a co-substrate leads to high ^{13}C -methanol incorporation in biomass components. Isotopic labeling from ^{13}C -methanol was measured for 25 co-substrates. Here, mass isotopomer distributions (MID) of glycogen (A), RNA (B), valine (C), alanine (D), glutamate (E), and serine (F) are shown. Relative abundances are the measured mass isotopomer distributions that have been corrected for natural isotope abundances. High labeling in biomass components was observed when threonine was the co-substrate. Error bars indicate standard error ($n = 2$).

substrates. Since little or no growth was observed in these cultures, the observed high labeling must be the result of turnover of glycogen and RNA. In many cases, we observed up to M+5 labeled glycogen and up to M+4 labeled RNA, indicating that ^{13}C -methanol carbon efficiently cycled through the pentose phosphate pathway, resulting in multiple carbons being labeled in biomass components. For the degradable amino acids, labeling of glycogen and RNA was generally lower compared to the non-degradable amino acids as co-substrates. A notable exception was threonine, for which

we observed high ^{13}C -labeling in both glycogen (77%, 1-M+0) and RNA (27%, 1-M+0). For the other substrates, the labeling of glycogen and RNA was much lower, especially for substrates that produced high growth rates such as glucose and xylose (~5% labeling in RNA, and <20% labeling in glycogen). Thus, there was an inverse correlation between cell growth rate and ^{13}C -labeling of RNA and glycogen for these co-substrates.

Figures 4.4C-4.4F show the mass isotopomer distributions of four representative proteinogenic amino acids (valine, alanine, glutamate, and serine) from the experiments with ^{13}C -methanol. For the non-degradable amino acids as co-substrates, significant labeling was observed in alanine, serine and glutamate (up to M+3), but no labeling was observed in valine and most other amino acids (Tables C.3, C.4). Again, since little or no growth was observed for these co-substrates, it is likely that the labeling was due to protein and amino acid turnover (i.e. similar to glycogen and RNA turnover). For the degradable amino acids as co-substrates, significant labeling was observed in alanine, serine and glutamate (up to M+3), and for a few co-substrates, significant labeling was also observed in amino acids such as valine that typically were not labeled in the presence of yeast extract (Fig 4.4C). Most notably, threonine as a co-substrate produced high ^{13}C -labeling of valine (up to M+4) and other amino acids (Table C.4). For the third set of co-substrates (i.e. sugars and organic acids), the amount of labeling in biomass amino acids was significantly lower and mainly M+1 labeling was observed.

Based on these results, threonine was identified as the most promising co-substrate for methanol assimilation, since it produced high labeling in RNA, glycogen and biomass proteins and improved cell growth. Interestingly, no labeling from ^{13}C -

methanol was detected in glycine and serine when threonine was the co-substrate (Fig. 4.4, and Table C.4). This suggests that glycine and serine were produced directly from threonine, likely via threonine dehydrogenase, which converts threonine to glycine and acetyl-CoA (Thr → Gly + AcCoA), and serine hydroxymethyltransferase, which combines glycine and methylenetetrahydrofolate to produce serine (Gly + MEETHF → Ser).

4.3.3 A potential role for the leucine-responsive protein (Lrp) in methylotrophy

After observing high labeling and increased growth with threonine as the co-substrate, we hypothesized that improved methanol utilization correlates with threonine degradation, via its conversion to glycine and serine. During growth on glucose and other carbon sources, such as xylose, threonine degradation does not occur (Gonzalez et al., 2017; Long et al., 2017). As such, under these growth conditions, threonine is not converted to glycine and the net flux is from serine to glycine, instead of glycine to serine. Our results thus suggest that rewiring amino acid metabolism at the threonine/glycine/serine node may be a potential metabolic engineering target to improve methanol utilization. Metabolic fluxes at this node are regulated by the leucine-responsive regulatory protein (Lrp) (Calvo and Matthews, 1994; Wang et al., 1994) (Figure 4.1), which is generally associated with the “feast and famine” response in *E. coli*. During growth in rich media, i.e. ‘feast’, Lrp levels are low while during nutrient limitation, i.e. ‘famine,’ Lrp levels are high. As such, Lrp regulates biosynthetic pathways depending upon the nutritional state of the cell. Lrp levels also increase when cells enter the stationary phase (Traxler et al., 2011). As illustrated in Figure 1, Lrp represses the conversion of threonine to glycine and the conversion of glycine to serine. We thus hypothesized that by knocking out Lrp, we

may be able to increase the flux through these pathways and, indirectly, improve methanol assimilation.

4.3.4 Deletion of the Lrp gene enhances methanol assimilation

We generated the Δlrp strain by deleting the *lrp* gene from our base methylotrophic *E. coli* strain. Growth characteristics of the base strain and the Δlrp strain were then compared in medium containing 1.5 g/L yeast extract, with and without 60 mM ^{13}C -methanol (Figure 4.5). For both strains, stationary phase was reached after ~10 hrs. Co-utilization of methanol and yeast extract resulted in significantly higher biomass concentrations for both strains compared to cultures without methanol. At 72 hr, the biomass concentration of the base strain was 37% higher with methanol compared to no methanol, and the biomass concentration of the Δlrp strain was 34% higher with methanol compared to no methanol. Overall, the biomass concentration of the Δlrp strain was consistently higher compared to the base strain. Mutations in *lrp* are known to result in improved cell performance during stationary phase, a phenotype known as GASP, Growth Advantage in Stationary Phase (Finkel, 2006). It has been hypothesized that this mutation may increase the ability of the cells to combat the native starvation response in *E. coli*.

Labeling of glycogen and RNA was also measured for experiments with ^{13}C -methanol (Figure 4.6A-D). High labeling in these metabolites serves as an indicator of efficient methanol assimilation and of efficient cycling of the pentose phosphate pathway. Glycogen labeling in the Δlrp strain was significantly higher than glycogen labeling in the base strain in terms of both 1-M+0 and average carbon labeling. In the Δlrp strain, glycogen labeling reached 72% (1-M+0), while glycogen labeling in the base strain only reached 45% (1-M+0). A similar trend was

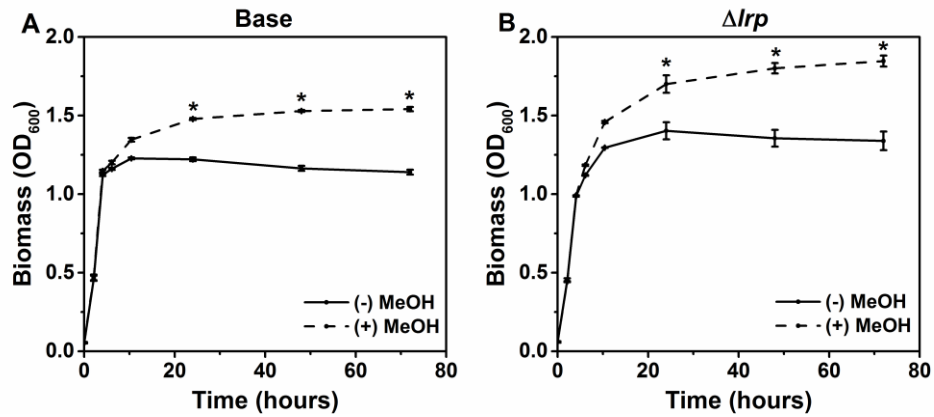


Figure 4.5 Deletion of *lrp* increases biomass concentration in both the absence and presence of methanol. The base (A) and Δlrp (B) strains were grown in 1.5 g/L yeast extract with (dashed line) and without (solid line) 60 mM ¹³C-methanol. Both strains reached a higher OD₆₀₀ in the presence of methanol. The OD₆₀₀ of the Δlrp strain was consistently higher than that of the base strain. Error bars indicate standard error (n = 3). An asterisk indicates a statistically significant difference (p < 0.05) between the conditions with and without methanol for each strain.

observed for RNA labeling, with the Δlrp strain reaching higher RNA labeling (24%, 1-M+0) compared to the base strain (14%, 1-M+0). Additionally, labeling of RNA and glycogen was measured with threonine supplementation to yeast extract (Figure C6). When threonine was supplemented to the base strain, the labeling was similar to the labeling observed in the Δlrp strain without threonine supplementation. This result suggests that deletion of Lrp captures the positive effects of threonine supplementation. Interestingly, addition of threonine to the Δlrp strain further improved labeling incorporation from ¹³C-methanol (Figure C6), suggesting that there is still room for further improvement of methanol utilization in our strain.

The absolute amounts of ¹³C-glycogen and ¹³C-RNA, as a fraction of dry weight, were also measured for both strains grown in yeast extract and ¹³C-methanol

(Figure 4.6E-F). The amount of ^{13}C -labeled RNA remained relatively constant for the base strain during stationary phase, while it increased slightly for the Δlrp strain. The amount of ^{13}C -labeled glycogen remained low in the base strain (between 0.1% and 0.3% DW) during the stationary phase. In contrast, for the Δlrp strain, the amount of ^{13}C -glycogen was much higher (0.8% DW) at the early timepoints and then reached similar levels as the base strain.

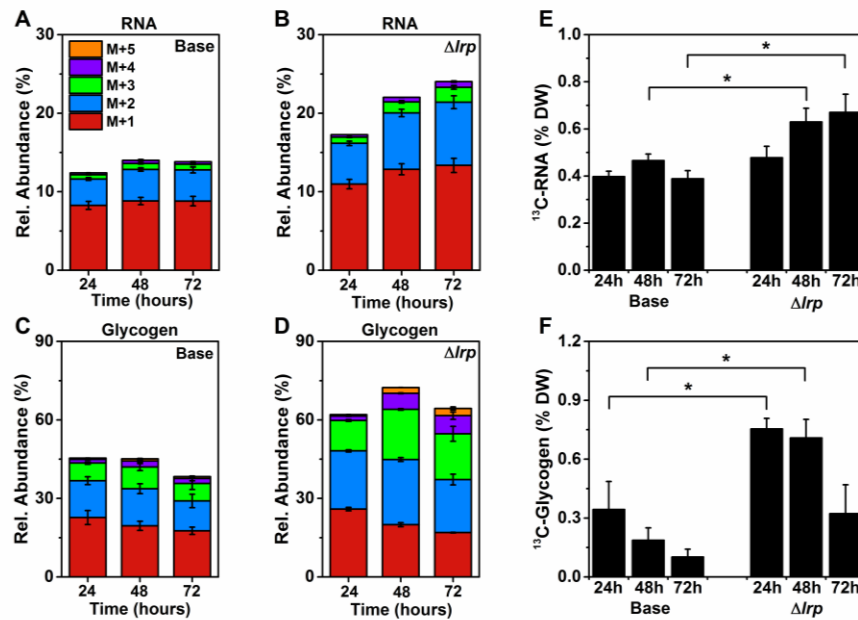


Figure 4.6 ^{13}C -labeling in RNA and glycogen from ^{13}C -methanol are significantly enhances when *lrp* is deleted. Isotopic labeling of RNA (A, B) and glycogen (C, D) from ^{13}C -methanol was measured for both the base strain and the Δlrp strain. Relative abundances are the measured mass isotopomer distributions that have been corrected for natural isotope abundances. Absolute amounts of ^{13}C -RNA (E) and ^{13}C -glycogen (F) were also measured and are represented here as % dry weight (DW). ^{13}C -labeling of glycogen and RNA in the Δlrp strain was significantly higher than that of the base strain at each respective timepoint ($p < 0.05$). While the total amount of ^{13}C -RNA was similar for both strains, the amount of ^{13}C -glycogen was significantly higher in the Δlrp strain. Error bars indicate standard error ($n = 3$). An asterisk indicates a statistically significant difference ($p < 0.05$).

4.4 Discussion and Conclusions

Methanol is an abundant and attractive substrate for bioprocesses given its high electron and energy content. In this study, we have applied a rational engineering approach based on ^{13}C -labeling studies to gain a better understanding of the mechanisms leading to improved methylotrophy in *E. coli*. Through our investigations, we identified a correlation between net flux through pathways normally repressed by the leucine-responsive regulatory protein and increased methanol assimilation. Based on this finding, we hypothesized that by knocking out Lrp we could improve methanol utilization. We tested this hypothesis and demonstrated significant improvements in methanol utilization in our synthetic methylotrophic *E. coli*.

From the results in Figure 4.3, it is clear that regulation of metabolic pathways plays an important role in how methanol is metabolized. The contrast observed in ^{13}C -labeling and yield when comparing glucose and yeast extract as co-substrates suggests that pathways upregulated/downregulated when sugars are present are not conducive to methanol assimilation. However, when yeast extract is present, one or more of its components appears to induce regulation that increases methanol incorporation. Additionally, when examining the labeling of amino acids, it was observed that some amino acids were highly labeled while others remained completely unlabeled with yeast extract as the co-substrate, which further supports the hypothesis that a unique regulatory mechanism is responsible for the observed phenotype.

Therefore, to probe this mechanism, a systematic analysis of various co-substrates (amino acids, sugars, and organic acids) was performed. Each co-substrate was evaluated in terms of growth enhancement and incorporation of ^{13}C -methanol into biomass components. Several amino acids showed high labeling and growth in the

presence of ^{13}C -methanol and it is possible that synergistic interactions between several co-substrates may further improve these phenotypes. However, based on our results, threonine appeared to be the best single co-substrate for methanol assimilation out of the 25 co-substrates examined. When threonine and methanol were co-utilized, we observed a substantial increase in the number of cell doublings, and enhanced labeling was observed in biomass components from ^{13}C -methanol. Interestingly, extensive labeling of amino acids that were typically not labeled was observed, e.g. up to M+4 labeling was observed in valine, which no other co-substrate achieved. In *E. coli*, threonine is first broken down to acetyl-CoA and glycine and then further metabolized to serine. Compared to growth on other substrates, flux through this pathway must be significantly higher during growth on threonine and it correlated with increased methanol incorporation. Therefore, we hypothesized that increasing flux through these reactions would increase methanol assimilation.

To improve flux through the threonine degradation pathway, the regulator Lrp, which specifically represses this pathway, was therefore removed (Figure 4.1). After deletion of this gene, methanol assimilation increased as was demonstrated by higher ^{13}C -labeling in glycogen and RNA as well as higher total amount of ^{13}C -glycogen and ^{13}C -RNA (Figure 4.6). Lrp is generally believed to respond to starvation, i.e. it is downregulated in rich media and upregulated during nutrient limitation. Many pathways are controlled by Lrp, and generally, anabolic genes are enhanced while catabolic ones are repressed when Lrp expression is high. Given that Lrp is a global regulator targeting hundreds of genes (Cho et al., 2011, 2008; Tani et al., 2002), the exact mechanism that resulted in improved methanol utilization in our strain remains unclear and may even be an indirect effect. A thorough investigation should be

performed in the future to examine the expression levels of various genes in the two strains under various conditions. This could better elucidate the mechanism by which Lrp impacts methylotrophy. Additionally, further analysis into the starvation response as well as other global regulators involved in this response could be a strategy for improvement of our strain.

Based on the results in this study, it is clear that regulation plays an important role in methylotrophy. Typically, strain engineering consists of studying metabolic reactions and manipulating the overall stoichiometry to achieve the desired output. However, when engineering strains to consume a new substrate, it may be necessary to delve more into studying how microbes respond to the new substrate on a global level rather than simply adding heterologous genes. Additionally, this analysis requires a rational approach such as the one taken in this work where growth conditions were analyzed and probed extensively. In the case of synthetic methylotrophy, while *E. coli* has all the necessary machinery for methanol consumption, it still cannot use methanol as the only substrate for growth. It is clear that when *E. coli* encounters methanol it does not respond in the same way as other substrates, such as glucose or acetate, where specific pathways are upregulated to optimize the consumption of these substrate. Therefore, manipulating global responses to new substrates is key in achieving improved organisms with novel substrate capabilities. Overall, our results suggest that modulating global regulators of metabolism can be a successful strategy to improve methanol utilization in *E. coli*.

Acknowledgements

In this study, R. Kyle Bennett generated all genetically engineered *E. coli* strains.

METABOLIC MODEL VALIDATION AND ¹³C-METABOLIC FLUX ANALYSIS OF THE METHANOGENIC ARCHAEON *Methanosarcina acetivorans*

5.1 Introduction

Methanogenesis is a unique pathway that produces methane from several substrates, primarily one carbon (C1) compounds. It is an essential component of the global carbon cycle in which biomass is oxidized to carbon dioxide (CO₂) and then converted to methane (CH₄) by anaerobic microorganisms. CH₄ can then be oxidized back to CO₂ by aerobic methanotrophic bacteria (Mcanulty, 2013). Methanogens are the anaerobic archaea that carry out methanogenesis, which include microorganisms from the *Methanosarcina*, *Methanobacteriales*, and *Methanococcales* genera (Ferry, 2010). The *Methanosarcina* species is the most versatile in its substrate capabilities. It has been shown to utilize acetate and several C1 compounds, such as methanol, carbon dioxide, and carbon monoxide, for methane production (Rother and Metcalf, 2004; Welander and Metcalf, 2005). These organisms have gained much attention over recent years, not only because they play a crucial role in the global carbon cycle, but they could contribute to the development of alternative fuels. Natural gas, which is primarily composed of methane, is a major energy source typically used for heating and electricity. However, methane has the potential to be converted to liquid fuels (Fei et al., 2014). Engineering efforts have already led to the generation of methane-utilizing organisms that convert methane to products such as organic acids (Kalyuzhnaya et al., 2013; Soo et al., 2016). However, these processes have low yields and require further optimization before industrial implementation. Therefore, it is of

interest to further explore these organisms for chemical production and better understand their underlying metabolism.

Several pathways contribute to methane production in methanogens. In the CO₂ reduction pathway, CO₂ is reduced to CH₄ using electrons from hydrogen (H₂). In the acetoclastic pathway, the carbonyl carbon from acetate is oxidized to CO₂ while the methyl carbon is reduced to CH₄. In the methylotrophic pathway, methanol is converted to both carbon dioxide and methane, with the oxidative branch providing electrons for methane production. Lastly, in the methyl reduction pathway, methanol is reduced to CH₄ with electrons provided by H₂ (Ferry, 2010; Welander and Metcalf, 2005).

There have been several studies investigating the growth capabilities of the *Methanosarcina* genus. When these pathways were first being elucidated, radioactive tracers were used to determine how carbons were allocated when multiple substrates were available for growth (Ferguson and Mah, 1983; Smith and Mah, 1978). More recently, with the development of genetic tools for this species, studies using mutants of the methanogenesis pathway have revealed new pathways and demonstrated the ability of these mutants to grow on various substrates (Welander and Metcalf, 2008, 2005). One organism in particular, *Methanosarcina acetivorans* (*M. acetivorans*), has been shown to grow on carbon monoxide (Rother and Metcalf, 2004) and perform trace methane oxidation (Moran et al., 2005). It has also been genetically engineered to utilize methyl esters to produce methane (Lessner et al., 2010).

While the growth of *M. acetivorans* and underlying biochemistry of the methanogenesis pathway have been widely studied, the intracellular dynamics of this organism have yet to be established. Two genome-scale models (Gonnerman et al.,

2013; Kumar et al., 2011) have been constructed and used to predict growth on substrates and the lethality of knockouts. However, these models were unable to accurately simulate uptake rates and growth yields during growth on methanol, acetate, and CO₂. A more recent model was improved to correctly predict these parameters (Nazem-Bokaei et al., 2016). While these models are useful for preliminary analysis, for genetic engineering purposes, it is necessary to have a reliable model that can provide information about the metabolic state of an organism, as defined by intracellular fluxes. ¹³C- metabolic flux analysis (¹³C-MFA) is a high-resolution technique for measuring intracellular fluxes (Antoniewicz, 2013; Crown and Antoniewicz, 2013b). With the use of ¹³C-labeled substrates, or tracers, unique labeling patterns in metabolites can be measured and used in a least squares regression analysis to estimate fluxes. It has been applied to several non-model organisms such as *Geobacillus* LC300, *Clostridium acetobutylicum*, and *Vibrio natriegens* (Au et al., 2014; Cordova and Antoniewicz, 2015; Long et al., 2017b).

In this work, detailed characterization of growth on methanol was performed for *M. acetivorans*. Analysis of the gases in the headspace indicated that methane is exclusively derived from methanol while carbon dioxide is also produced from methanol, which is then incorporated into biomass. We established a network model for *M. acetivorans* consisting of reactions from central carbon metabolism, amino acid biosynthetic pathways, and methanogenesis. ¹³C-MFA was used to validate the proposed network model and generate the first flux map for *M. acetivorans*. It was found that the majority of the methanol consumed was used for methane and carbon dioxide production while the flux through gluconeogenesis was only the amount necessary for biomass production. Additionally, an incomplete TCA cycle was

confirmed for this organism. This is one of the few applications of ^{13}C -MFA to organisms that grow on C1 substrates. The validated network model can now be used as a base model for other methanogens as well as for future engineering of these organisms.

5.2 Materials and Methods

5.2.1 Materials

Media and chemicals were purchased from Sigma-Aldrich (St. Louis, MO). ^{13}C -methanol (99% ^{13}C), [1,4- ^{13}C]aspartate, and [U- ^{13}C]glutamate were purchased from Cambridge Isotope Laboratories (Andover, MA). [U- ^{13}C]Acetic acid (99% ^{13}C) was purchased from Isotec (St. Louis, MO). The defined growth medium contained per liter of medium: 3.0 g Na_2CO_3 , 0.6 g Na_2HPO_4 , 0.5 g NH_4Cl , 10.17 g $\text{MgCl}_2 \cdot 6\text{H}_2\text{O}$, 0.17 g $\text{CaCl}_2 \cdot 2\text{H}_2\text{O}$, 0.76 g KCl , 23.38 g NaCl , 0.25 g Cysteine-HCl $\cdot\text{H}_2\text{O}$, 0.25 g $\text{Na}_2\text{S} \cdot 9\text{H}_2\text{O}$, 0.001 g resazurin, 10 mL of vitamins solution (100x), 10 mL of trace elements solution (100x), and 5 mL of methanol.

5.2.2 Strain and growth conditions

M. acetivorans C2A was grown anaerobically under a headspace containing 19% CO_2 and 81% N_2 (25 psig) at 37°C in an anaerobic chamber (Forma, Thermo Scientific). For small scale tracer experiments, cultures were grown in 12 mL glass vials with 7 mL of headspace. For large scale tracer experiments, cultures were grown in 160 mL glass bottles with 130 mL of headspace. All bottles were capped with rubber stoppers and crimped. In addition to the tracer, methanol and CO_2 also served as carbon sources. All tracers were added immediately before inoculation at the following concentrations: 125 mM ^{13}C -methanol, 1mM [1,4- ^{13}C]aspartate, 1mM [U-

^{13}C]glutamate. Cells were inoculated at an OD_{600} of approximately 0.1 and allowed to grow for 46 hours, after which an OD_{600} of approximately 0.80 – 1.00 was reached. Samples were then collected for GC-MS and HPLC analysis.

5.2.3 Analytical methods

Medium samples were collected at multiple time points during the culture to monitor cell growth, methanol consumption and product accumulation. Optical density at 600 nm (OD_{600}) was measured using a spectrophotometer (Eppendorf BioPhotometer). The OD_{600} values were converted to cell dry weight concentrations using a pre-determined OD_{600} -dry cell weight relationship ($1.0 \text{ OD}_{600} = 0.25 \text{ g}_{\text{DW}}/\text{L}$; molecular weight of dry biomass = $24.6 \text{ g}_{\text{DW}}/\text{C-mol}$). After centrifugation, the supernatant was separated from the biomass pellet and acetate and formate concentrations in the supernatant were determined using an Agilent 1200 Series HPLC (Au et al., 2014).

5.2.4 Gas analysis by mass spectrometer

Molar percentages of nitrogen (m/z 28), carbon dioxide (CO_2 , m/z 44), ^{13}C -labeled carbon dioxide ($^{13}\text{CO}_2$, m/z 45), methane (m/z 16), ^{13}C -labeled methane (m/z 17), argon (m/z 40), hydrogen (m/z 2), and oxygen (m/z 32) in gas samples were measured by a process mass spectrometer (Ametek Proline, Berwyn, PA).

5.2.5 Gas chromatography-mass spectrometry

GC-MS analysis of ^{13}C -labeling of *tert*-butyldimethylsilyl (TBDMS) derivatized proteinogenic amino acids was performed as described by (Leighty and Antoniewicz, 2012). GC-MS analysis was performed on an Agilent 7890B GC system equipped with a DB-5MS capillary column (30 m, 0.25 mm i.d., 0.25 μm -phase

thickness; Agilent J&W Scientific), connected to an Agilent 5977A Mass Spectrometer operating under ionization by electron impact (EI) at 70 eV. Helium flow was maintained at 1 mL/min. The source temperature was maintained at 230°C, the MS quad temperature at 150°C, the interface temperature at 280°C, and the inlet temperature at 250°C. 1 µL was injected at 1:40 split ratio. The column was started at 80°C for 2 min, increased to 280°C at 7°C/min, and held for 20 min. Mass isotopomer distributions were obtained by integration (Antoniewicz et al., 2007a) and corrected for natural isotope abundances (Fernandez et al., 1996).

5.2.6 Metabolic network model

A metabolic network model of *M. acetivorans* metabolism was constructed for ¹³C-MFA based on available genome scale models (Gonnerman et al., 2013; Kumar et al., 2011) and KEGG and PathwayTools metabolic pathway databases (Caspi et al., 2012; Kanehisa and Goto, 2000; Kanehisa et al., 2012). The model includes all major metabolic pathways of central carbon metabolism, a set of lumped amino acid biosynthesis reactions and a lumped biomass formation reaction. The model is provided in Table D.1.

5.2.7 ¹³C-Metabolic flux analysis

¹³C-MFA was performed using the Metran software (Crown and Antoniewicz, 2013a; Yoo et al., 2008), which is based on the elementary metabolite units (EMU) framework (Antoniewicz et al., 2007b; Young et al., 2008). Fluxes were estimated by minimizing the variance-weighted sum of squared residuals (SSR) between the experimentally measured and model predicted mass isotopomer distributions of amino acids using non-linear least-squares regression (Antoniewicz et al., 2006). Flux

estimation was repeated 10 times starting with random initial values for all fluxes to find a global solution. At convergence, accurate 95% confidence intervals were computed for all estimated fluxes by evaluating the sensitivity of the minimized SSR to flux variations (Antoniewicz et al., 2006). Precision of estimated fluxes was determined as follows (Antoniewicz et al., 2006):

$$\text{Flux precision (stdev)} = [(\text{flux}_{\text{upper bound 95\%}}) - (\text{flux}_{\text{lower bound 95\%}})] / 4 \quad (7)$$

To describe the fractional labeling of biomass amino acids, G-value parameters were included in ^{13}C -MFA. One G-value parameter was included for each measured amino acid, as described previously (Antoniewicz et al., 2007c; Leighty and Antoniewicz, 2012). Reversible reactions were modeled as separate forward and backward fluxes. Net and exchange fluxes were determined as follows: $v_{\text{net}} = v_f - v_b$; $v_{\text{exch}} = \min(v_f, v_b)$.

5.2.8 Goodness-of-fit analysis

To determine the goodness-of-fit, ^{13}C -MFA fitting results were subjected to a χ^2 -statistical test. In short, assuming that the model is correct and data are without gross measurement errors, the minimized SSR is a stochastic variable with a χ^2 -distribution (Antoniewicz et al., 2006). The number of degrees of freedom is equal to the number of fitted measurements n minus the number of estimated independent parameters p . The acceptable range of SSR values is between $\chi^2_{\alpha/2}(n-p)$ and $\chi^2_{1-\alpha/2}(n-p)$, where α is a certain chosen threshold value, for example 0.05 for 95% confidence interval.

5.3 Results and Discussion

5.3.1 Characterization of growth on ^{13}C -methanol

Growth on ^{13}C -methanol under a N_2/CO_2 headspace was characterized. The growth curve is shown in Figure 5.1A, where growth ceases after all methanol is consumed. The measured growth rate was $0.06 \pm 0.01 \text{ hr}^{-1}$. During growth on methanol, both methane and carbon dioxide are produced because carbon dioxide evolution provides the reducing equivalents required for the formation of methane. Therefore, if cells were cultured with ^{13}C -methanol, it's expected that $^{13}\text{CH}_4$ and $^{13}\text{CO}_2$ would be detected in the headspace. Figure 5.1B shows the gas composition as a function of time. As expected, $^{13}\text{CH}_4$ and $^{13}\text{CO}_2$ were observed. The majority of the carbon dioxide produced is ^{13}C -labeled. Additionally, all the methane produced is labeled, confirming no additional production of methane from an alternative carbon source, such as CO_2 . The carbon and electron balances are shown in Figure 5.2. The majority of the carbon (~60%) and electrons (~80%) from methanol are used for methane production while only ~22% of the carbon and ~16% of the electrons are used for biomass production, leaving ~11% of the carbon to be converted to CO_2 .

Additionally, the biomass composition of *M. acetivorans* was measured and compared to *E. coli* (Figure 5.3). Similar trends were observed in how the cell dry weight is allocated for each biomass component for both organisms. Protein was the most abundant fraction at 62 wt% while RNA and glycogen composed 13 wt% and 8 wt%, respectively, of the cell dry weight. During analysis of the biomass composition, it was found that the cell membrane of *M. acetivorans* is composed of isoprene units, rather than fatty acids, which are found in membranes of prokaryotes. Therefore, the

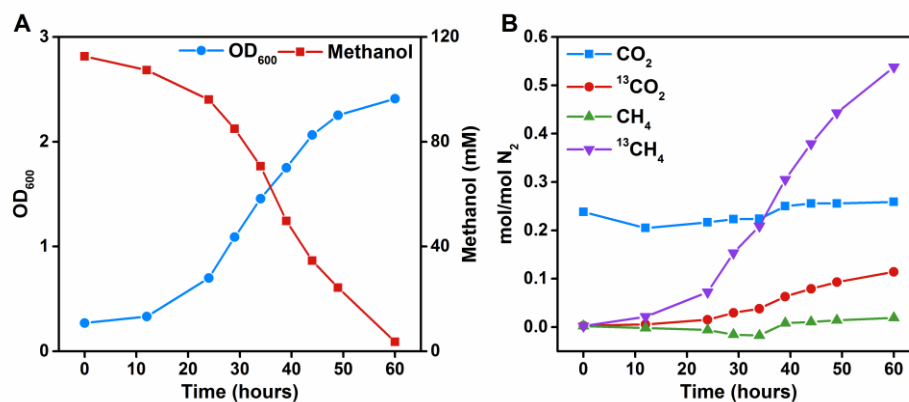


Figure 5.1 Physiological characterization of *M. acetivorans* during growth on ¹³C-methanol. (A) Growth and methanol consumption were monitored until all methanol was consumed. (B) CO₂, ¹³CO₂, CH₄, and ¹³CH₄ were also monitored over the course of the culture, normalized to the N₂ in the headspace.

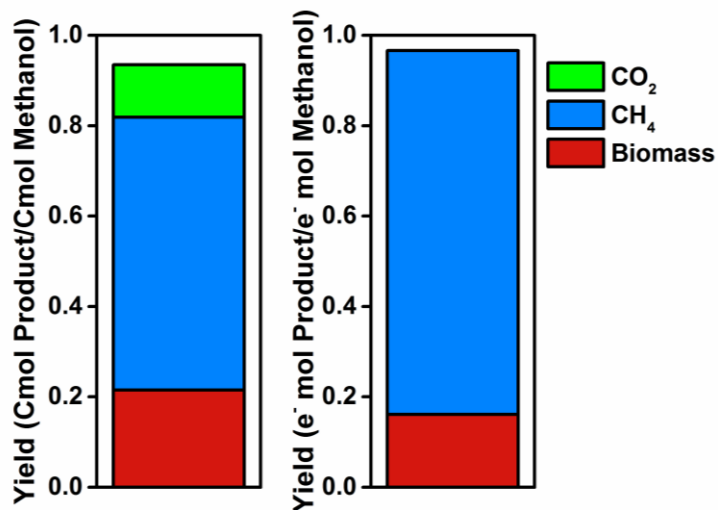


Figure 5.2 Carbon and electron balances. The majority of carbon and electrons from methanol are used for production of methane. Both balances close (> 90%).

remaining fraction of the dry weight is likely allocated to isoprene. The amino acid profile for *M. acetivorans* is similar to the profile found in *E. coli* with the exception of glutamate; the amount of glutamate is higher in *M. acetivorans* than *E. coli*.

5.3.2 Network model validation

The network model for *M. acetivorans* is presented in Figure 5.4, with the exception of amino acid biosynthesis pathways and one-carbon metabolism. The ribulose 1,5 bisphosphate carboxylase/oxygenase reaction (Rubisco) was hypothesized to be active in this organism (Finn et al, 2004) so it was included in the model. In methanogenesis, the methyl carbon of acetyl-CoA is derived from methanol while the carbonyl carbon originates from carbon dioxide. A CO₂ fixation step with acetyl-CoA to form pyruvate initiates gluconeogenesis (Mukhopadhyay et al., 2001) while the TCA cycle begins with an additional CO₂ fixation reaction with pyruvate to produce oxaloacetate. Figure 5.5 shows the relative abundance of each labeled mass isotopomer for several amino acids measured during growth on ¹³C-methanol. These labeling patterns confirm the presence of an incomplete TCA cycle. If the cycle were complete, labeling of aspartate, which is derived from oxaloacetate, should be similar to that of glutamate, which originates from α -ketoglutarate. Examining the abundances of the mass isotopomers (i.e. M+1 for one carbon labeled, M+2 for two carbons labeled), it can be seen that there is a high abundance of the M+2 mass isotopomer of glutamate but essentially no M+2 mass isotopomer of aspartate. A complete TCA cycle would result in similar labeling in both of these amino acids. Addition of small amounts of [1,4-¹³C]aspartate and [U-¹³C]glutamate tracers, during growth on methanol, were used to further verify the incomplete cycle. If there were an incomplete cycle, labeling

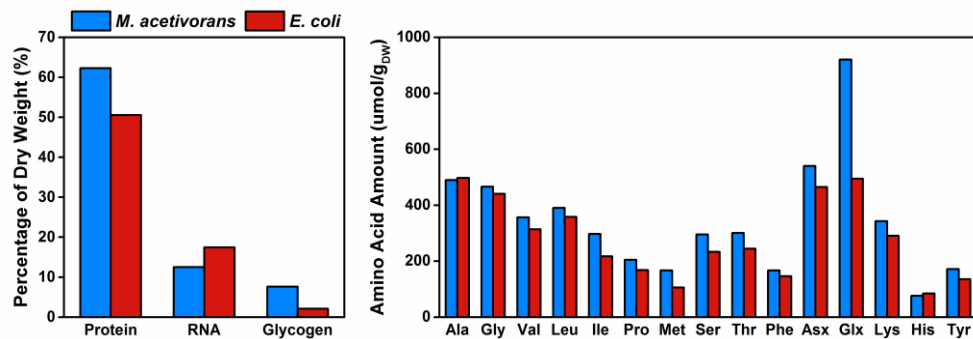


Figure 5.3 Biomass composition analysis of *M. acetivorans* compared to *E. coli*.

from aspartate should be present in glutamate but labeling in glutamate should not appear in aspartate. Figure 5.6A shows the relative abundance of labeling measured in glutamate and aspartate for both tracers. Both amino acids were labeled from their respective tracers, as expected. However, there is no labeling of aspartate from the glutamate tracer, but labeling is present in glutamate from the aspartate tracer, confirming the presence of an incomplete TCA cycle.

The [1,4-¹³C]aspartate tracer also revealed the presence of an additional set of reactions, not included in our original model. Figure 5.6B shows the labeling (1 – M+0) of glycine, serine, threonine, and aspartate when cells were grown with [1,4-¹³C]aspartate. Labeling was detected in the Gly246 fragment, containing both carbons in glycine, but not in the Gly218 fragment; therefore, the first carbon of glycine must be labeled by aspartate. Threonine aldolase catalyzes the reaction that converts threonine, derived from aspartate, to acetaldehyde and glycine, which must be the mechanism that led to the observed labeling. Therefore, the threonine aldolase reaction

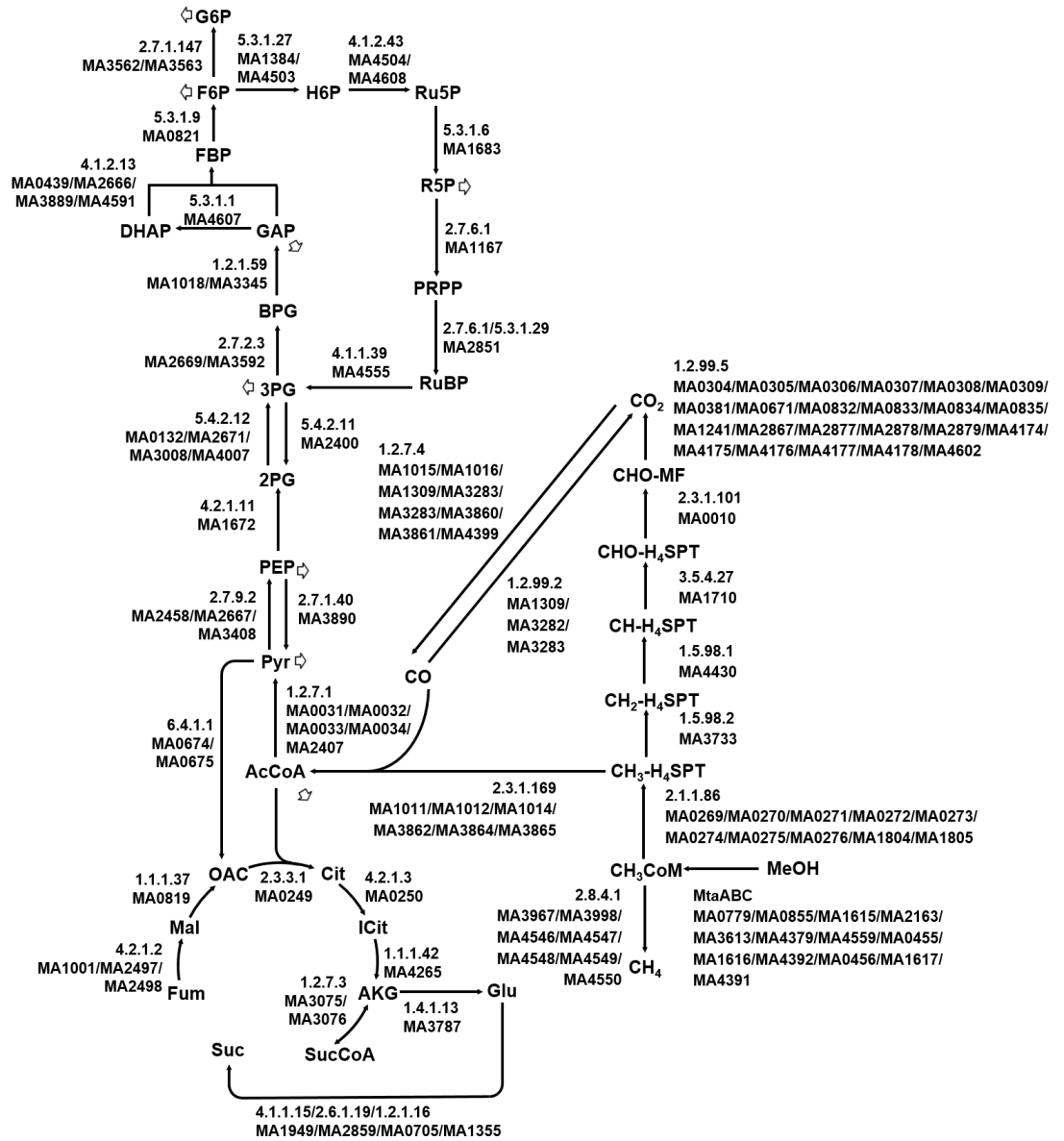


Figure 5.4 Network model for *M. acetivorans* and annotated genes based on KEGG and Biocyc databases and genome-scale models.

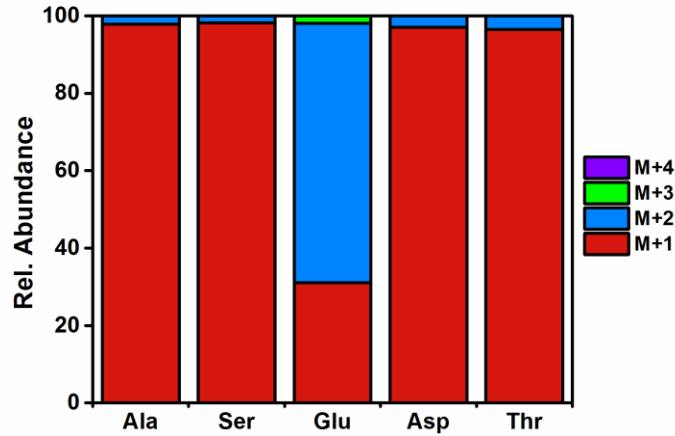


Figure 5.5 Mass isotopomer distributions for the amino acids alanine (Ala), serine (Ser), glutamate (Glu), aspartate (Asp), and threonine (Thr) during growth on ^{13}C -methanol. The difference in labeling between glutamate and aspartate indicate the presence of an incomplete TCA cycle.

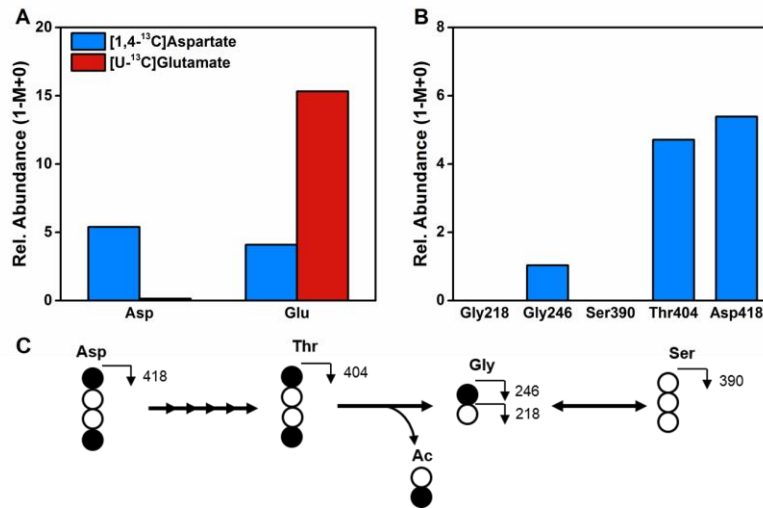


Figure 5.6 ^{13}C -labeling from [1,4- ^{13}C]aspartate and [U- ^{13}C]glutamate tracer experiments reveal presence of incomplete TCA cycle (A) and threonine aldolase (B). (C) If threonine aldolase is active, a [1,4- ^{13}C]aspartate tracer will result in labeling of the 246 m/z fragment of glycine but not the 216 m/z fragment of glycine, which is indeed observed in (B).

was added to the existing model. No labeling was detected in serine suggesting the net flux between serine and glycine is towards glycine.

The presence of an incomplete cycle is not surprising as this is the case found in most anaerobic organisms. In aerobes, the TCA cycle is used for amino acid precursor synthesis as well as a source of significant amounts of reducing power. Under aerobic conditions, NAD^+ can be regenerated by transferring electrons to oxygen, the final electron acceptor. However, anaerobic environments do not have access to an effective electron acceptor like oxygen. This results in a decreased flux through the TCA cycle and removal of certain reducing power-producing reactions. The effect of oxygen on the TCA cycle was studied in *E. coli* (Gray et al. 1966). It was found that removal of oxygen results in decreased expression of TCA cycle enzymes, which supports the idea that the energy-producing role of the cycle declines without an effective electron acceptor. ^{13}C -MFA has been applied in *E. coli* under anaerobic conditions and has shown that indeed, flux through the TCA cycle decreases when oxygen is absent. A similar analysis was also applied to an anaerobic bacterium, *Clostridium acetobutylicum* (*C. acetobutylicum*) (Au et al., 2014). The results reveal that the TCA cycle is characterized by small fluxes and is incomplete in multiple locations. Unlike in *C. acetobutylicum*, where the TCA cycle operates in the oxidative direction, our results suggest that, in *M. acetivorans*, the cycle bifurcates with citrate synthase, aconitase, isocitrate dehydrogenase, and α -ketoglutarate dehydrogenase operating in the oxidative direction while malate dehydrogenase and fumarase operate in the reductive direction.

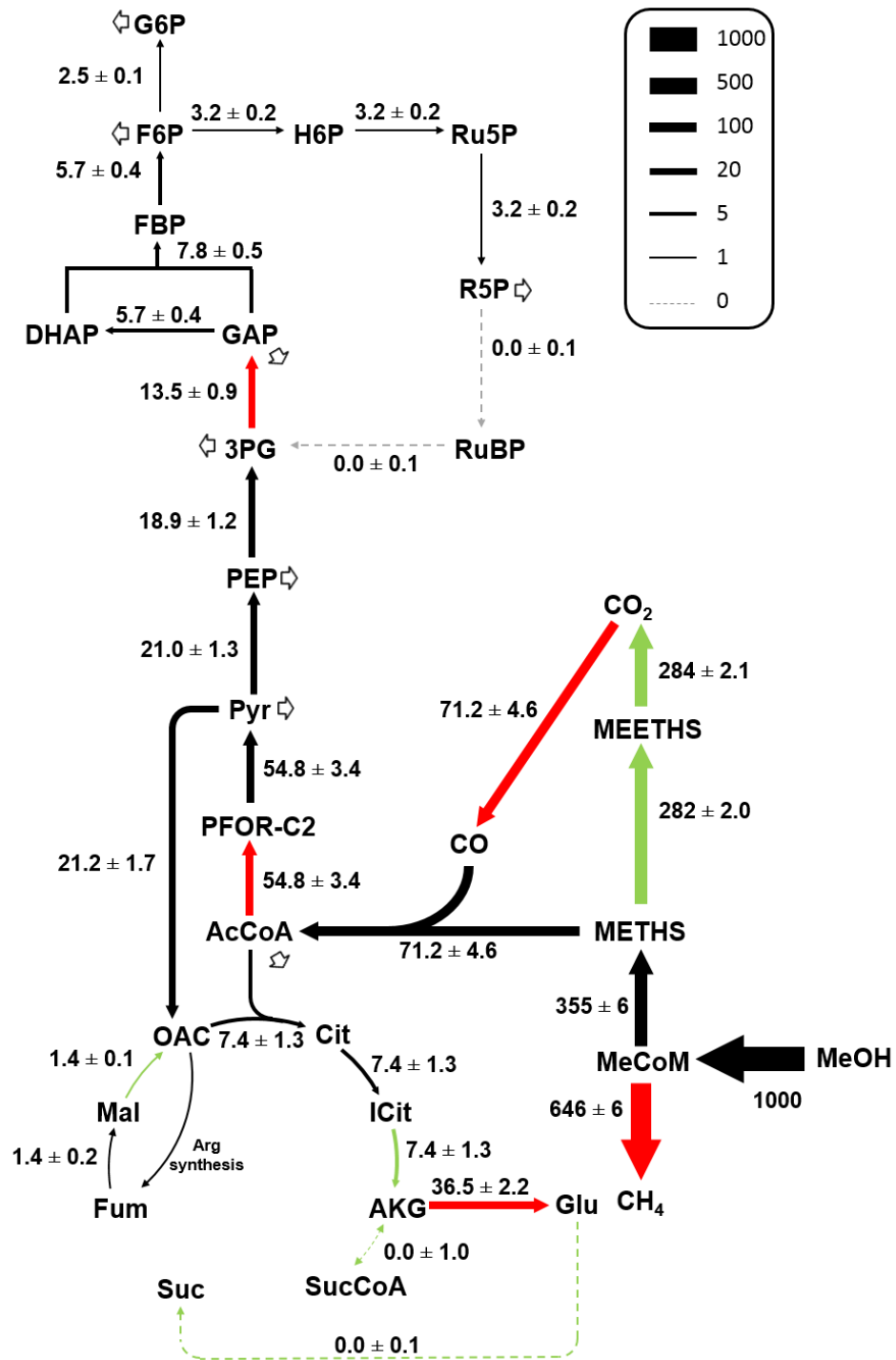


Figure 5.7 Metabolic flux map for *M. acetivorans* during growth on ^{13}C -methanol. Fluxes were determined using ^{13}C -MFA.

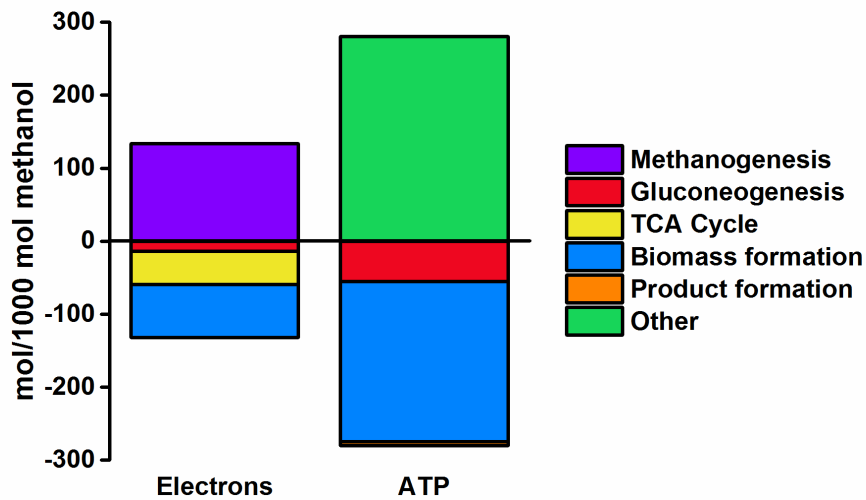


Figure 5.8 Allocation of electrons and ATP across different pathways during growth on methanol.

5.3.3 ^{13}C -Metabolic flux analysis

^{13}C -MFA has been applied to various organisms utilizing a wide range of substrates. However, applying this technique to study an organism that uses one carbon substrates generally requires more advanced computational approaches as the assumptions made for ^{13}C -MFA no longer apply. For these organisms, using a ^{13}C -tracer of the one carbon substrate will prevent metabolism from reaching an isotopic steady state; all measured metabolites will become fully labeled and therefore, the labeling patterns of these metabolites are no longer dependent on the fluxes. In this case, to resolve fluxes, non-stationary ^{13}C -flux analysis can be used; however, this requires samples to be taken at multiple time points, precise quenching of metabolism, and more advanced computational methods. Instead, a properly designed tracer experiment can allow for the use of ^{13}C -MFA for estimating fluxes during metabolism

of a one carbon substrate, greatly decreasing the complexity of the experimental design and data analysis. For this method, one can take advantage of natural dilutions occurring during growth, from turnover of macromolecules or external carbon sources, or can make use of metabolite exchanges that do not impact metabolism. In the case of *M. acetivorans* growing on ^{13}C -methanol, it was found that when unlabeled carbon dioxide is present in the headspace, it will be used in the conversion of CO_2 to CO , resulting in an AcCoA pool that is ~100% M+1 labeled, where the labeled methyl carbon comes from ^{13}C -methanol. In Figure 5.5, it can be seen that most amino acids are essentially M+1 labeled as all of these are derived from AcCoA produced from methanogenesis. Glutamate is M+2 labeled because it is formed after condensation of OAC and AcCoA, both containing one labeled carbon. This experimental design allows for isotopic steady state to be reached. All measured metabolites will now be partially labeled and these labeling patterns can be used to resolve intracellular fluxes. Additionally, one can take advantage of the acetate exchange occurring when methanol is present, where there is no net consumption or accumulation of acetate. Therefore, we performed parallel labeling experiments using methanol + [U- ^{13}C]acetate and ^{13}C -methanol + acetate and applied ^{13}C -MFA. The results are shown in Tables D.2 and D.3 and Figure D.1.

^{13}C -MFA was performed using the model described in Figure 4 using ^{13}C -methanol as the tracer. Biomass amino acid measurements were fit to the network model and an acceptable fit was achieved with a sum of squared residuals value of 88.7 at a 95% confidence level (acceptable range between 79.4 and 136.4). Figure 5.6 shows the resulting flux map. It can be seen that the flux through methanogenesis is significantly higher than the flux through gluconeogenesis. The flux through the TCA

cycle is even smaller, with certain reactions predicted to have no flux. It is likely that the flux is too small for the model to predict a value, but labeling data shows that there is a non-zero flux through those reactions. Additionally, it was hypothesized that Rubisco was active in this organism. However, the flux through this pathway is calculated to be zero. Therefore, under these conditions, this enzyme seems to be inactive. The flux through the ribulose monophosphate pathway is solely used to produce the necessary ribose moieties of RNA and DNA and to synthesize aromatic amino acids, which is typically accomplished through the pentose phosphate pathway in prokaryotes.

In an anaerobic environment, ATP and electrons are vital resources that are not as easily managed as under aerobic conditions. Therefore, it's imperative to develop an understanding of how these are allocated, especially if the goal is to engineer an organism to produce chemicals. This would most likely require re-allocation of cellular resources and therefore, adjustment of intracellular fluxes. In addition to fluxes, Figure 5.6 shows which reactions result in the production of electrons, shown in green, and which result in the consumption of electrons, shown in red. It's clear that the main source of electrons is through the production of carbon dioxide, while a major source of electron depletion is conversion of CO_2 to CO and methane production. Figure 5.7 shows a more global allocation of electrons. There is net production of electrons by methanogenesis which are then used for biomass production and the TCA cycle, specifically, conversion of AcCoA to pyruvate. Essentially all ATP required for biomass production and gluconeogenesis comes from ion transport and ATP synthase activity.

5.4 Conclusion

This is the first study to present a complete characterization of extra- and intracellular metabolism in a one-carbon substrate utilizing organism using high resolution ^{13}C -MFA. Specifically, the network model for *M. acetivorans* was constructed and validated using ^{13}C -methanol. Uptake of CO_2 allowed for dilution of labeling, enabling the use of conventional ^{13}C -MFA in place of more complex approaches. This method can also be applied to other one-carbon substrate utilizing organisms.

Future work will consist of calculating fluxes, using this model, during growth on other substrates such as acetate. While most substrates are consumed in the methanogenesis pathway, it will be interesting to see how fluxes differ and how effectively this organism will utilize certain substrates over others. The resulting flux profiles can be then used to create kinetic models to better understand the metabolism of *M. acetivorans*. Additionally, with the validation of this model, it will be straightforward to extend it to other organisms of the *Methanosarcina* species as well as other methanogens.

Acknowledgements

In this study, Christopher P. Long measured the biomass composition for *E. coli* and *M. acetivorans*.

APPLICATION AND EVALUATION OF METABOLIC FLUX ANALYSIS METHODS FOR METABOLIC AND ISOTOPIC NON-STEADY STATE

6.1 Introduction

Metabolic flux analysis (MFA) has become an invaluable tool for studying metabolism and guiding metabolic engineering (Antoniewicz, 2015; Iwatani et al., 2008). Its ability to precisely quantify intracellular fluxes makes it the optimal method for characterizing *in vivo* metabolism. Because of this, it has been applied to a wide range of organisms (i.e. *E. coli*, *S. cerevisiae*, *C. acetobutylicum*, *V. natrigens*, cyanobacteria) (Au et al., 2014; Gonzalez et al., 2017; Long et al., 2017b; Young et al., 2011) for various purposes such as identifying targets for improvement of product yields and studying how extracellular conditions affect metabolism.

MFA allows for the determination of fluxes by balancing fluxes in a stoichiometric model, assuming no accumulation of intermediates. Extracellular rates are included to further constrain the system. However, the limited amount of data required for MFA prevents complete observability of all fluxes. Therefore, ^{13}C -MFA has emerged as the superior method due to incorporation of ^{13}C -labeling data. Including metabolite labeling patterns provides additional constraints on the fluxes, resulting in more precise estimation of fluxes (Antoniewicz, 2015). While this method is more computationally intensive, there have been several attempts at decreasing this complexity, such as the introduction of elementary metabolite unit (EMU) balancing, where the minimal amount of information is used to determine fluxes, significantly decreasing the mathematical operations required (Antoniewicz et al., 2007b).

To apply ^{13}C -MFA, it is assumed that the system being interrogated is at metabolic steady state and isotopic steady state, where fluxes and isotopic labeling

remain constant over time. This assumption limits the extension of ^{13}C -MFA to systems where these assumptions do not hold. For systems that are close to isotopic steady state, a G parameter can be used to account for the dilution of metabolites (Antoniewicz et al., 2007c). However, a more advanced technique must be used for systems where isotopic steady state will never be reached. For example, any system in which the substrate contains only one carbon will never reach isotopic steady state. Therefore, a new method was developed, called ^{13}C -nonstationary MFA (^{13}C -NMFA), where time-dependent labeling data and pool sizes are measured at various time points. This data can then be used to resolve fluxes (Young et al., 2008). For systems with time-dependent fluxes (metabolic non-steady state), dynamic MFA (DMFA) can be used to quantify these fluxes using concentration and rate data from multiple time points (Leighty and Antoniewicz, 2011). This method will now be further extended to include isotopic labeling measurements (^{13}C -DMFA).

Here, we apply each of these methods (^{13}C -MFA, ^{13}C -NMFA, ^{13}C -DMFA) to a simple model under various conditions, including metabolic non-steady state and isotopic non-steady state. First, we present a framework for ^{13}C -DMFA, an extension of previous methods to include isotopic labeling and time-dependent fluxes. We then compare these MFA methods and present the appropriate method for specific systems.

6.2 Methods

6.2.1 Metabolic Network Model

For studying each method, we will use the simple network model shown in Figure 6.1. This model was previously used to demonstrate the EMU decomposition method (Antoniewicz et al., 2007b). Therefore all atom transitions and EMU balances

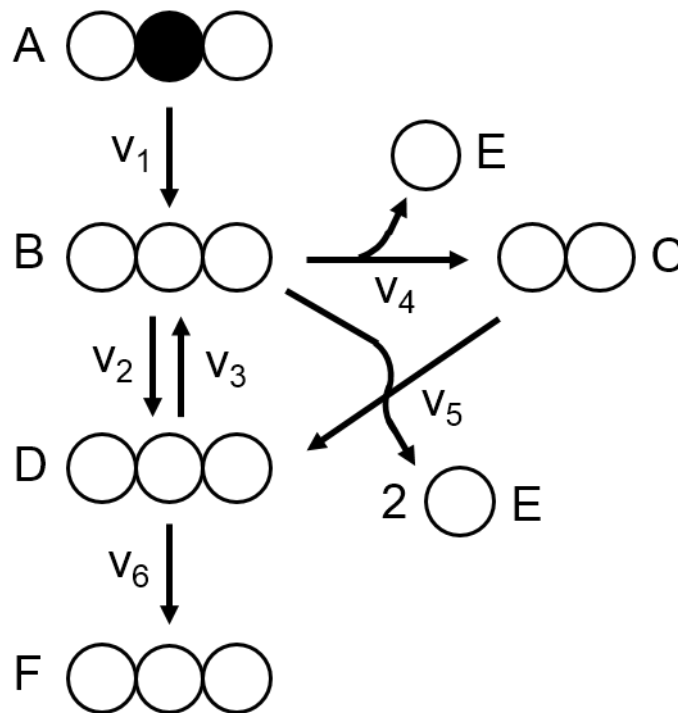


Figure 6.1 Simple metabolic network model that will be used for evaluating metabolic flux analysis methods.

are presented in that paper and will not be repeated here. In this network model, there are three free fluxes: v_1 , v_3 , and v_4 . For the remaining analysis, v_1 will be set to 100. Additionally, the concentrations of B, C, and D will be estimated when using ^{13}C -NMFA and ^{13}C -DMFA.

6.2.2 Simulation of labeling using EMU balances

For a general network model, we can set up a mass balance equation for each

EMU network:

$$\frac{d(MX)}{dt} = AX + BY \tag{6.1}$$

M is the concentration matrix, containing the metabolite concentrations on the diagonal. X contains the mass isotopomer distributions (MIDs) of metabolites in that EMU network. Y contains MIDs from previously calculated EMUs or MIDS from extracellular metabolites. A and B contain fluxes from each mass balance equation.

For ^{13}C -MFA, it is assumed that the system is at isotopic steady state.

Therefore, Equation 6.1 simplifies to

$$AX = -BY \quad (6.2)$$

$$X = A^{-1}BY \quad (6.3)$$

X can be found for each EMU network, where each row of X gives the MID of the selected metabolite.

For systems that are close to isotopic steady state, we can apply ^{13}C -MFA and include G-values (^{13}C -MFAg), or dilution parameters, to account for transients in labeling. Each simulated MID can be represented by the following equation:

$$x_i^{sim} = g_i * x_i^{iss} + (1 - g_i) * x^{natural} \quad (6.4)$$

x_i^{sim} is the simulated MID of metabolite i, g_i is the g-value for that metabolite, x_i^{iss} is the MID of metabolite i at isotopic steady state (iss), and $x^{natural}$ is a vector representing natural abundance. The MID at isotopic steady state can be calculated using ^{13}C -MFA.

For systems that are not at isotopic steady state, we must use ^{13}C -NMFA. Here, the MIDs, X, are now a function of time. We can expand equation 6.1, assuming that the concentrations of metabolites remain constant. The resulting ordinary differential equation (6.5) can be integrated to achieve the labeling of metabolites in X over time.

$$\frac{dX}{dt} = M^{-1}(AX + BY) \quad (6.5)$$

For systems that are not at metabolic steady state, we must use ^{13}C -DMFA. Again, the MIDs are still a function of time (6.5) but now, so are the fluxes, v_j . Here, we will assume that fluxes are a linear function of time, where constants v_{jb} and v_{je} represent the fluxes at time t_b and t_e , respectively.

$$v_j = v_{jb} + (v_{je} - v_{jb}) * \left(\frac{t - t_b}{t_e - t_b} \right) \quad (6.6)$$

6.2.3 Calculation of parameter sensitivities

To calculate confidence intervals for parameter estimates, we also need to derive equations for the sensitivities of the measurements with respect to the parameters (i.e. fluxes, concentrations, g-values), in the form of first order derivatives (Antoniewicz et al., 2006). As shown in (Antoniewicz et al., 2007b) for ^{13}C -MFA, the first order derivatives with respect to each flux, v_j , can be calculated using the following equation for each size EMU network:

$$\frac{dX}{dv_j} = A^{-1} \left(\frac{\partial B}{\partial v_j} Y + B \frac{\partial Y}{\partial v_j} - \frac{\partial A}{\partial v_j} X \right) \quad (6.7)$$

When using g-values, we are including additional parameters that must be estimated. Similarly, we need to calculate first order derivatives with respect to each g-value, in addition to the fluxes. For each metabolite i , we can calculate the following derivatives for g_i and v_j . Here, the derivative of x_i^{iss} with respect to the fluxes can be determined using equation 6.7.

$$\frac{\partial x_i^{sim}}{\partial v_j} = g_i * \frac{\partial x_i^{iss}}{\partial v_j} \quad (6.8)$$

$$\frac{\partial x_i^{sim}}{\partial g_i} = x_i^{iss} - x_i^{natural} \quad (6.9)$$

For ^{13}C -NMFA, we can also estimate pool sizes. Equations 6.10 and 6.11 can be used to calculate the sensitivities with respect to the fluxes, v_j , and the pool sizes, c_i , as a function of time. Again, these can be integrated over time to determine the sensitivities as a function of time.

$$\frac{d}{dt} \frac{\partial X}{\partial v_j} = M^{-1} \left(\frac{\partial A}{\partial v_j} X + A \frac{\partial X}{\partial v_j} + \frac{\partial B}{\partial v_j} Y + B \frac{\partial Y}{\partial v_j} \right) \quad (6.10)$$

$$\frac{d}{dt} \frac{\partial X}{\partial c_i} = M^{-1} \left(A \frac{\partial X}{\partial c_i} + B \frac{\partial Y}{\partial c_i} - \frac{\partial M}{\partial c_i} \frac{dX}{dt} \right) \quad (6.11)$$

For ^{13}C -DMFA, we have included two more parameters and now have four parameters to represent the transient fluxes. Again, we must calculate first order derivatives, with respect to all parameters, which are now the pool sizes and the beginning and end fluxes for each free flux. Here are the first order derivatives with respect to the additional parameters.

$$\frac{d}{dt} \frac{\partial X}{\partial v_{jb}} = M^{-1} \left(\frac{\partial A}{\partial v_j} \frac{\partial v_j}{\partial v_{jb}} X + A \frac{\partial X}{\partial v_{jb}} + \frac{\partial B}{\partial v_j} \frac{\partial v_j}{\partial v_{jb}} Y + B \frac{\partial Y}{\partial v_j} \frac{\partial v_j}{\partial v_{jb}} \right) \quad (6.12)$$

$$\frac{d}{dt} \frac{\partial X}{\partial v_{je}} = M^{-1} \left(\frac{\partial A}{\partial v_j} \frac{\partial v_j}{\partial v_{je}} X + A \frac{\partial X}{\partial v_{je}} + \frac{\partial B}{\partial v_j} \frac{\partial v_j}{\partial v_{je}} Y + B \frac{\partial Y}{\partial v_j} \frac{\partial v_j}{\partial v_{je}} \right) \quad (6.13)$$

Each flux, v_j , can be differentiated with respect to each parameter, v_{jb} and v_{je} . We can then substitute these into equations 6.12 and 6.13 to obtain first order derivatives with respect to the beginning and end fluxes (equations 6.17 and 6.18).

$$\frac{\partial v_j}{\partial v_{jb}} = 1 - \left(\frac{t - t_b}{t_e - t_b} \right) \quad (6.14)$$

$$\frac{\partial v_j}{\partial v_{je}} = \left(\frac{t - t_b}{t_e - t_b} \right) \quad (6.15)$$

$$m = \left(\frac{t - t_b}{t_e - t_b} \right) \quad (6.16)$$

$$\frac{d}{dt} \frac{\partial X}{\partial v_{jb}} = M^{-1} \left(\frac{\partial A}{\partial v_j} X * (1 - m) + A \frac{\partial X}{\partial v_{jb}} + \frac{\partial B}{\partial v_j} Y * (1 - m) + B \frac{\partial Y}{\partial v_j} * (1 - m) \right) \quad (6.17)$$

$$\frac{d}{dt} \frac{\partial X}{\partial v_{je}} = M^{-1} \left(\frac{\partial A}{\partial v_j} X * m + A \frac{\partial X}{\partial v_{je}} + \frac{\partial B}{\partial v_j} Y * m + B \frac{\partial Y}{\partial v_j} * m \right) \quad (6.18)$$

6.2.4 Extension of EMU balances to include metabolite C

The EMU balances presented in Antoniewicz et al (Antoniewicz et al., 2007b) were extended to include labeling of metabolite C to simulate the effect of include the labeling measurement of C on the precision and accuracy of estimated parameters. The following matrices can be used as EMU balances and include the labeling of C_{12} . Each

equation is in the form $AX = -BY$, where each of these matrices is described above and can be used in all previously defined differential equations.

$$\begin{bmatrix} -v_4 & v_4 & 0 & 0 & 0 \\ 0 & -v_1-v_3 & v_3 & 0 & 0 \\ 0 & v_2 & -v_2-v_5 & v_5 & 0 \\ 0 & 0 & 0 & -v_1-v_3 & v_3 \\ v_5 & 0 & 0 & v_2 & -v_2-v_5 \end{bmatrix} \begin{bmatrix} C_1 \\ B_2 \\ D_2 \\ B_3 \\ D_3 \end{bmatrix} = \begin{bmatrix} 0 & 0 \\ -v_1 & 0 \\ 0 & 0 \\ 0 & -v_1 \\ 0 & 0 \end{bmatrix} \begin{bmatrix} A_2 \\ A_3 \end{bmatrix} \quad (6.19)$$

$$\begin{bmatrix} -v_5-v_2 & v_2 & 0 \\ v_3 & -v_1-v_3 & 0 \\ 0 & v_4 & -v_4 \end{bmatrix} \begin{bmatrix} D_{23} \\ B_{23} \\ C_{12} \end{bmatrix} = \begin{bmatrix} -v_5 & 0 \\ 0 & -v_1 \\ 0 & 0 \end{bmatrix} \begin{bmatrix} B_3 \times C_1 \\ A_{23} \end{bmatrix} \quad (6.20)$$

$$\begin{bmatrix} -v_6 & v_6 & 0 \\ 0 & -v_5-v_2 & v_2 \\ 0 & v_3 & -v_1-v_3 \end{bmatrix} \begin{bmatrix} F_{123} \\ D_{123} \\ B_{123} \end{bmatrix} = \begin{bmatrix} 0 & 0 \\ -v_5 & 0 \\ 0 & -v_1 \end{bmatrix} \begin{bmatrix} B_{23} \times C_1 \\ A_{123} \end{bmatrix} \quad (6.21)$$

6.2.5 Estimation of parameters

Parameters were estimated by first generating a random set of parameters, u_k . This set of parameters was used to simulate MIDs, X^{sim} , for the measured metabolites. These simulated patterns and the associated sensitivities (dX/du , where u is each parameter, see section 6.2.3) were used to calculate the Jacobian (J) and Hessian (H) matrices (Antoniewicz et al., 2006):

$$H = \frac{dX}{du} * D^{-1} * \frac{dX}{du} \quad (6.22)$$

$$J = \frac{dX}{du} * D^{-1} * (X^{sim} - X^{obs}) \quad (6.23)$$

D is a diagonal matrix containing the measurement error on the diagonal. Here, we assume a labeling measurement error of 0.003. X^{obs} contains the measured MIDs.

These matrices can be used to determine the set of parameters used in the next iteration to simulate a new set of MIDs. The step size (Δu) between the current (k) set

of parameters and the next (k+1) set can be calculated using the Hessian and Jacobian matrices.

$$\Delta u = -H^{-1} * J \quad (6.24)$$

$$u_{k+1} = u_k + \Delta u \quad (6.25)$$

This iteration process continues until Δu reaches a specified value and represents the optimal solution (u_{opt}).

For ^{13}C -NMFA and ^{13}C -DMFA, we also examined the effect of including measurements of pool sizes on the accuracy and precision of each method. To do this, an additional term was added to the Hessian matrix equation that accounted for the sensitivity of the pool sizes with respect to the parameters. We assume that the pool sizes are not a function of the fluxes i.e. $dB/dv_j = 0$ and that the pool sizes of each metabolite are independent i.e. $dB/dC = 0$. Therefore, the new Hessian matrix can be generated using the following equation:

$$H = \frac{dX}{du} * D^{-1} * \frac{dX}{du} + \frac{dM}{du} * D_M^{-1} * \frac{dM}{du} \quad (6.26)$$

dM/du contains the sensitivities of the pool sizes with respect to each parameter and D_M is a diagonal matrix containing the pool size measurement error on the diagonal.

The new Jacobian matrix can be generated using the following equation:

$$J = \frac{dX}{du} * D^{-1} * (X^{sim} - X^{obs}) + \frac{dM}{du} * D_M^{-1} * (Met^{sim} - Met^{obs}) \quad (6.27)$$

Met^{sim} contains the simulated pool sizes and Met^{obs} contains the measured (actual) pool sizes.

6.2.6 Statistical Analysis

For each method, we calculate the sum of squared residuals as well as the uncertainty and accuracy of the estimated parameters (Antoniewicz et al., 2006). The sum of squared residuals can be calculated using the following equation:

$$SSR = (X^{sim} - X^{obs}) * D^{-1} * (X^{sim} - X^{obs}) \quad (6.28)$$

When including pool sizes, the equation for SSR must also be extended.

$$SSR = (X^{sim} - X^{obs}) * D^{-1} * (X^{sim} - X^{obs}) + (Met^{sim} - Met^{obs}) * D_M^{-1} * (Met^{sim} - Met^{obs}) \quad (6.29)$$

With the sensitivities calculated above from first order derivatives, we can calculate the uncertainty of the estimated parameters using the following equation:

$$SD u_{opt} = \sqrt{H^{-1}} \quad (6.30)$$

To calculate the accuracy, the absolute value of the difference between the estimated parameters and actual parameters was used. For ¹³C-MFA and ¹³C-MFAG, the largest accuracy and uncertainty observed out of all time points was used. For ¹³C-NMFA, since one value for the fluxes was determined to represent all data points, the maximum difference between the estimated value and the actual flux value at each time point was used.

6.3 Results and Discussion

6.3.1 Simulation of labeling patterns

Using the network model in Figure 6.1, we can calculate MIDs for various pool sizes and fluxes. There are three free fluxes, v_1 , v_3 , and v_4 . We set v_1 to remain constant at 100. At time = 0, $v_3 = 50$ and $v_4 = 20$. To interrogate systems at metabolic non-steady state, v_3 will decrease and v_4 will increase by a certain percentage (0%, 5%, 10%, 15%, 20% and 25%) of the initial value over the course of the experiment. Figure 6.2 shows example of how v_3 and v_4 change over time. The pool sizes tested are 0.5, 2, 4, 6, 8, and 10 for each metabolite. Changing the pool sizes varies the time it takes to reach isotopic steady state. Smaller pool sizes reach isotopic steady state

more quickly than large pool sizes. Thus, larger pool sizes will test the ability of these MFA methods to capture non-isotopic steady state. Figure 6.3A shows labeling of metabolite D for different pool sizes with constant fluxes. When the pool size is large, the labeling of these metabolites require a longer time to reach isotopic steady state. Figure 6.3B shows the labeling of metabolite D for various flux changes with a pool size of 10. For flux changes less than 25%, the labeling of D does not change significantly. As will be seen in the next section, even with these small flux changes, some methods can no longer correctly estimate fluxes.

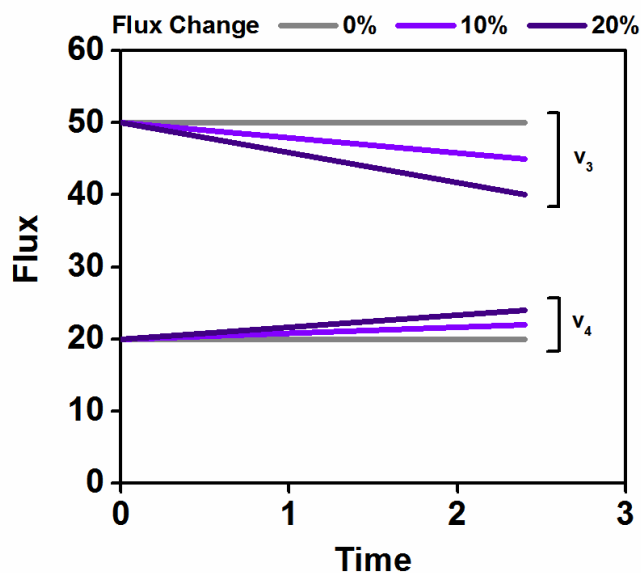


Figure 6.2 Changes in fluxes v_3 and v_4 . Shown here are changes of 0%, 10%, and 20%. Additionally 5%, 15%, and 25% changes were also tested. Flux v_3 decreases over time and flux v_4 increases over time.

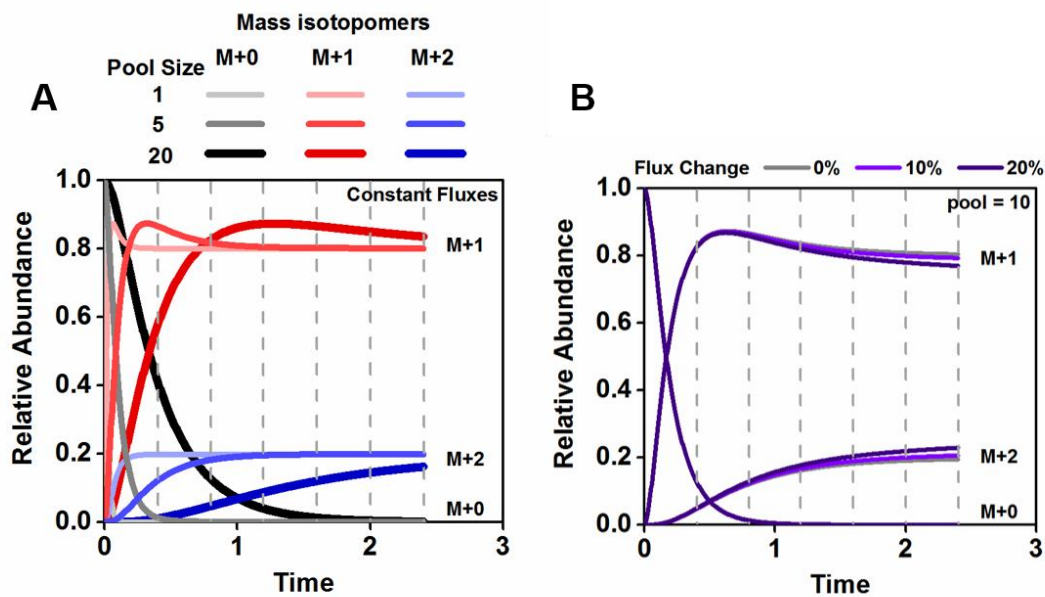


Figure 6.3 Simulated MIDs of metabolite D. (A) shows the MIDs when the fluxes are constant over time for pool sizes 1, 5, and 20. (B) shows the MIDs when the fluxes change by 0%, 10%, and 20% for a pool size of 10. The grey dashed lines indicate the timepoints used to estimate parameters.

6.3.2 Application of metabolic flux analysis methods to a simple model

We can simulate an experiment in which six data points are taken at equidistant intervals and the labeling patterns of metabolites B and D are measured (Figure 6.3). Using these labeling patterns, we can apply the various MFA methods to estimate a set of parameters. Table 6.1 shows the four methods that will be tested and their associated parameters. For each method, the sum of squared residuals, uncertainty in the flux estimates, and accuracy of the flux estimates are calculated and compared in Figure 6.5.

Method	Estimated parameters
^{13}C -MFA	v_3, v_4
^{13}C -MFAg	v_3, v_4, g_B, g_D
^{13}C -NMFA	$v_3, v_4, [B], [C], [D]$
^{13}C -DMFA	$v_{3b}, v_{3e}, v_{4b}, v_{4e}, [B], [C], [D]$

Table 6.1 ^{13}C -Metabolic flux analysis methods and the parameters estimated in each method.

Figure 6.4 compares how each method performs in flux estimation for the case with the largest pool size (10) and the largest flux change (25%) and demonstrates how each method was used to estimate fluxes over time. ^{13}C -MFA and ^{13}C -MFAg are applied at each time point to obtain an estimate of v_3 and v_4 at the time at which each sample was taken. ^{13}C -MFA performs rather poorly, especially when estimating fluxes at early timepoints, likely due to the changes in labeling early in the experiment. For ^{13}C -NMFA and ^{13}C -DMFA, all labeling data from all time points are fit simultaneously to achieve one set of estimates for the parameters. ^{13}C -NMFA only estimates one flux for the entire duration of the experiment, with the confidence interval not overlapping with the correct values in some cases (v_4). ^{13}C -DMFA is the only method that captures the entire flux change within the confidence interval.

Figure 6.5 summarizes how each method performs for all flux changes and pool sizes tested. ^{13}C -MFA appears to estimate parameters well for cases in which there are small pool sizes (<2), even in the presence of transient fluxes. This method can correctly estimate fluxes at each time point, if the labeling has reached isotopic steady state. Once the pool sizes becomes larger than 2, the SSR value increases

substantially, indicating that the simulated labeling patterns are not in agreement with the measured labeling patterns. For these pool sizes, we also observe low accuracy and precision. Even at metabolic steady state, this method cannot estimate fluxes for large pool sizes because the assumption of isotopic steady state no longer holds in the time frame considered here.

^{13}C -MFAg seems to improve upon ^{13}C -MFA. In all cases, this method can simulate labeling patterns that are in agreement with the measured labeling patterns as indicated by the low SSR values. However, the uncertainty and accuracy of the flux estimates are similar to those calculated for ^{13}C -MFA. This indicates that there are too many parameters and the model is being overfitted. Therefore, this method should

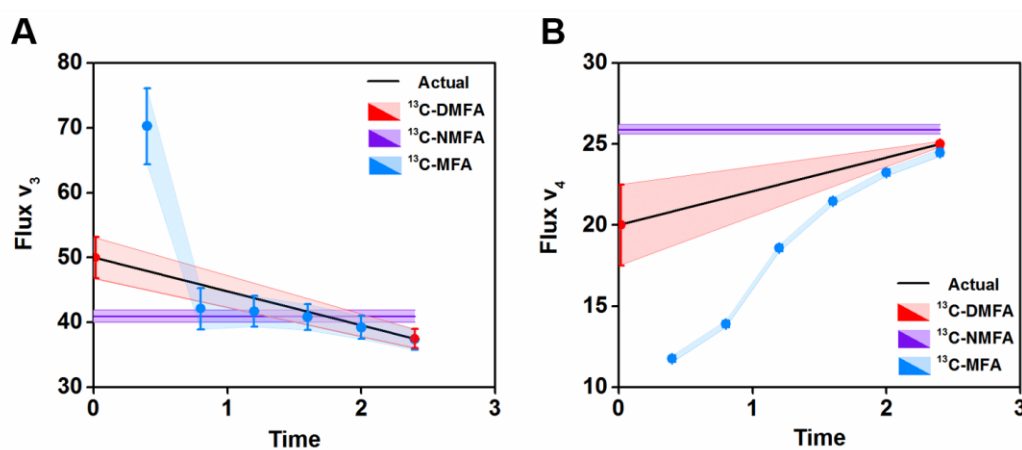


Figure 6.4 Comparison of flux estimation for each MFA method using a pool size of 10 and a flux change of 25%. The estimated parameters as well as the uncertainties of those estimates are shown for both v_3 (A) and v_4 (B). The shaded regions indicate the uncertainty. ^{13}C -MFA was used to estimate fluxes at each of the six timepoints. ^{13}C -NMFA estimated one flux value for the entire duration of the experiment. ^{13}C -DMFA estimated the initial and final flux values.

only be applied to cases in which isotopic steady state is reached. Fortunately, both cases can capture transient fluxes accurately for systems at isotopic steady state.

As stated earlier, ^{13}C -NMFA is typically used when there is a possibility of non-isotopic steady state in a system that is at metabolic steady state. Figure 6.4 clearly shows why this is the case. Regardless of the pool size, this method can accurately and precisely estimate fluxes at metabolic steady state. However, as the system moves away from metabolite steady state, it becomes more difficult for this method to estimate fluxes, even when the effect of the fluxes on the labeling is quite minimal (Figure 6.3B). This is likely due to the fact that we are trying to estimate one v_3 and v_4 value for the entire duration of the experiment, although those values are changing with time. Indeed, as the changes in fluxes become more drastic, the accuracy of the flux estimates decreases and the SSR increases.

^{13}C -DMFA can be used for transient systems, ones that are both at isotopic and metabolic non-steady state. Indeed, we see that this method can precisely and accurately determine fluxes when pool sizes are large and when fluxes are time-dependent. Additionally, low SSR values are achieved using this method for all cases. However, in some cases, there are higher uncertainties in the fluxes. Therefore, we will examine the effect of including additional measurements on accuracy and precision.

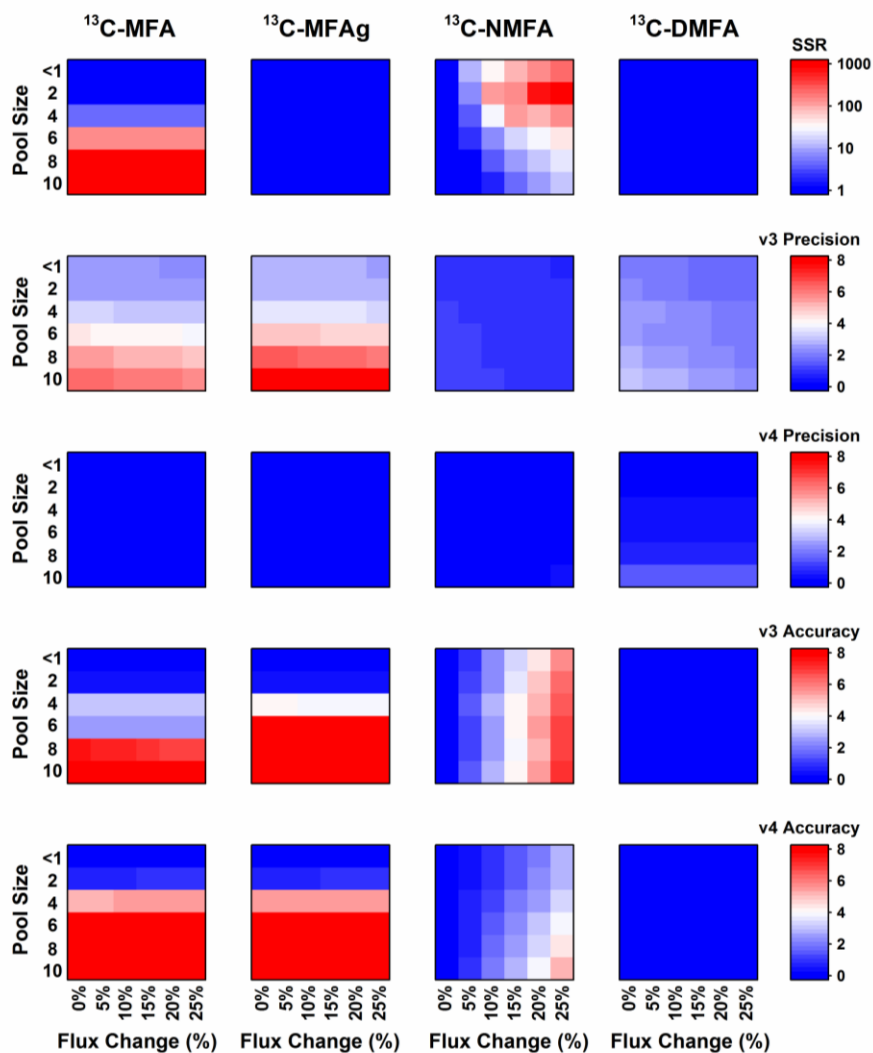


Figure 6.5 Comparison of MFA methods using labeling measurements of metabolites B and D. Each heat map corresponds to a different statistical value for each method: SSR, precision, or accuracy. Precision and accuracy are determined with respect to the estimated values of the fluxes v_3 and v_4 .

6.3.3 Effect of including additional measurements

When applying ^{13}C -MFA techniques, one must decide what measurements to use and therefore, what data needs to be collected in the lab. This represents a tradeoff where more measurements will lead to higher precision and accuracy but this may also require more analysis or sampling during the experiment. Here, we examine the effect of measuring the labeling of an additional metabolite, metabolite C, on the precision and accuracy of each method. Additionally, for ^{13}C -NMFA and ^{13}C -DMFA, we examine the effect of measuring metabolite pools.

After including the labeling of C, we observe several changes (Figure 6.5). For ^{13}C -MFA, including additional data results in worse fits and estimation compared to Figure 6.4, where less data was used for estimation. This also holds true for ^{13}C -NMFA. Including additional data further constrains these methods, resulting in worse fits, but highlights the scenarios in which these methods should be used: ^{13}C -MFA should only be used for small pool sizes and ^{13}C -NMFA should only be used for constant fluxes. For ^{13}C -DMFA, we actually observe an improvement in precision of flux estimates with the additional measurements. This can be clearly observed for the uncertainty in v_4 for the largest pool size. In Figure 6.4, the uncertainty in v_4 is around 2 for some cases but the uncertainty decreases closer to 0 when the labeling of C is included.

Both ^{13}C -NMFA and ^{13}C -DMFA estimate pool sizes in addition to fluxes. Therefore, we can interrogate the effect of including pool size measurements on the precision and accuracy of flux estimates. Figure 6.7 shows the results of including measurements of pool sizes for metabolites B, C, and D with an uncertainty of 5%, 20%, and 100% in the measurement itself. For ^{13}C -NMFA, including pool size measurements has a similar effect as including an additional labeling measurement;

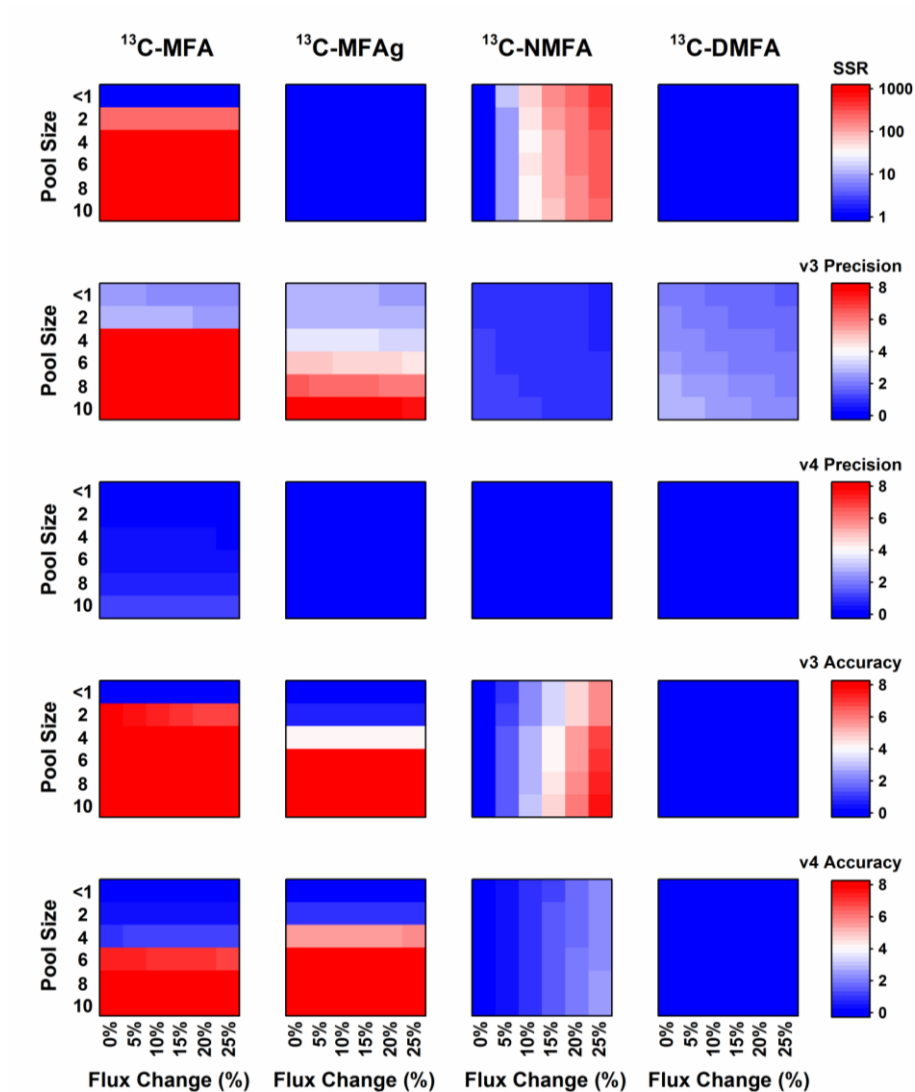


Figure 6.6 Comparison of MFA methods using labeling measurements of metabolites B, C, and D. Each heat map corresponds to a different statistical value for each method: SSR, precision, or accuracy. Precision and accuracy are determined with respect to the estimated values of the fluxes v_3 and v_4 .

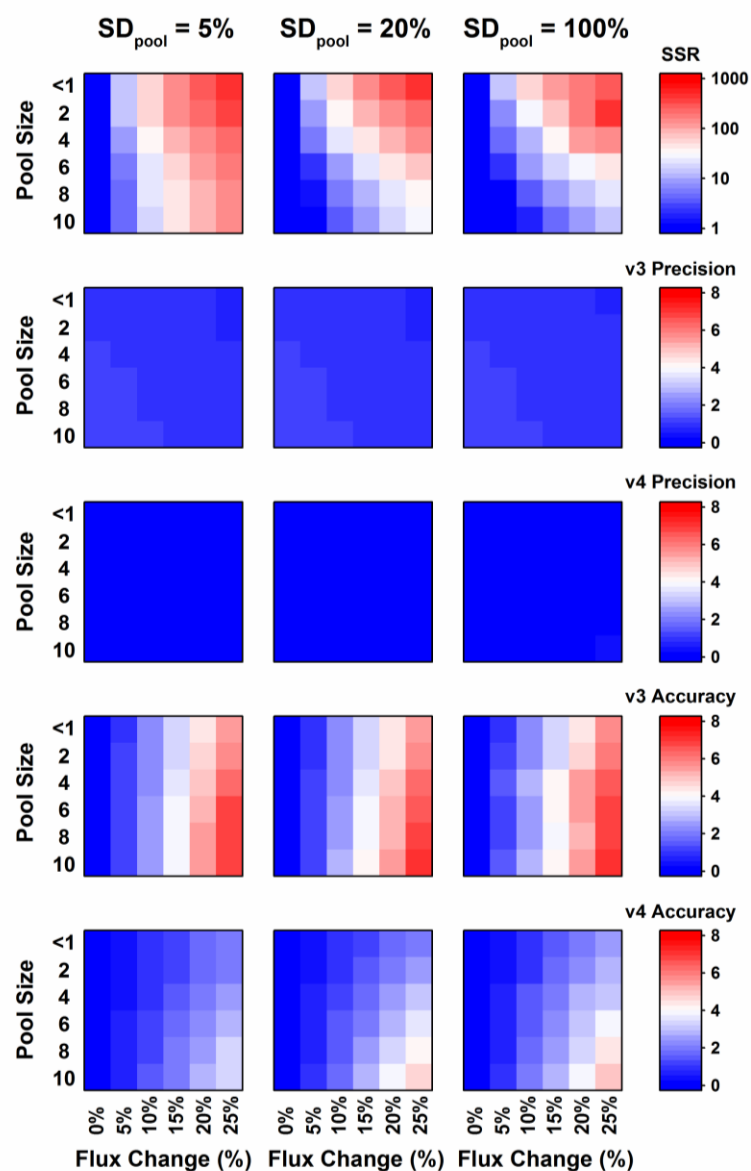


Figure 6.7 Comparison of flux estimation using ^{13}C -NMFA after including labeling measurements of metabolites B and D as well as pool size measurements of metabolites B, C, and D with different uncertainties in the measurement (5%, 20%, 100%). Each heat map corresponds to a different statistical value for each method: SSR, precision, or accuracy. Precision and accuracy are determined with respect to the estimated values of the fluxes v_3 and v_4 .

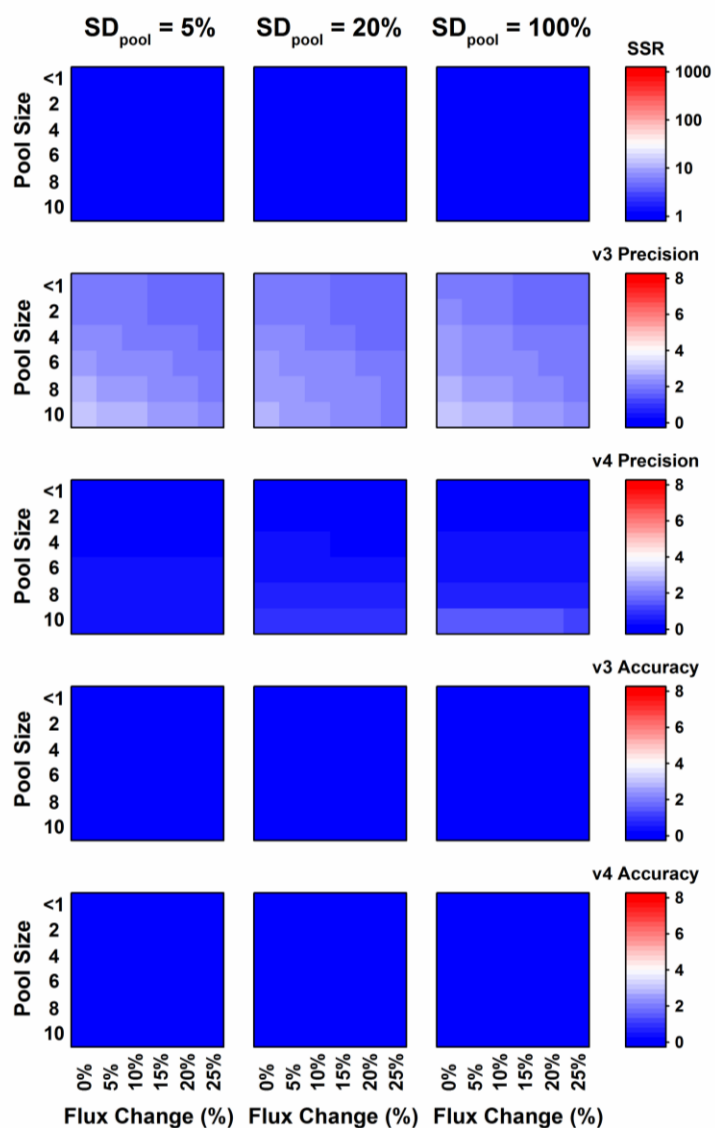


Figure 6.8 Comparison of flux estimation using ^{13}C -DMFA after including labeling measurements of metabolites B and D as well as pool size measurements of metabolites B, C, and D with different uncertainties in the measurement (5%, 20%, 100%). Each heat map corresponds to a different statistical value for each method: SSR, precision, or accuracy. Precision and accuracy are determined with respect to the estimated values of the fluxes v_3 and v_4 .

the SSR increases compared to without the additional measurement. However, the additional measurement seems to improve the overall accuracy. While ^{13}C -DMFA performs well even without additional measurements, we still observe improvements in precision when including pool size measurements. For both methods, as we increase the uncertainty in the measurement itself, we see a decrease in accuracy and precision but an increase in the overall fit (for ^{13}C -NMFA). If the uncertainty in the measurement is high, that increases the parameter space for the pool size estimates, giving the method more freedom to choose an estimate that results in a better fit, whether or not that estimate is close to the actual value.

6.3.4 Testing the limits of ^{13}C -DMFA

From the previous analysis, it appears that ^{13}C -DMFA can be applied to almost any system. Here we wanted to identify conditions in which ^{13}C -DMFA is no longer effective. Therefore, we tested larger pool sizes (i.e. very long times needed to reach isotopic steady state) and more significant changes in fluxes over time. Here we tested pool sizes of 10, 50, 100, 150, and 200 and flux changes of 0%, 20%, 40%, 60%, 80%, and 100%. Figure 6.9A shows the labeling of metabolite D for constant fluxes at pool sizes of 10, 100, and 200. There are clear differences in the labeling at each time point for these three cases. For a pool size of 10, we can observe some M+2 labeling but there is no significant M+2 labeling for pool sizes of 100 and 200 in the time frame examined. We can also examine the effect of the flux changes on the labeling of metabolite D for different pool size. For a pool size of 100 (Figure 6.9B), the changes in flux do not significantly impact the labeling of D. However for smaller pool sizes (Figure 6.9C), the changes in fluxes have a more significant effect on the labeling of

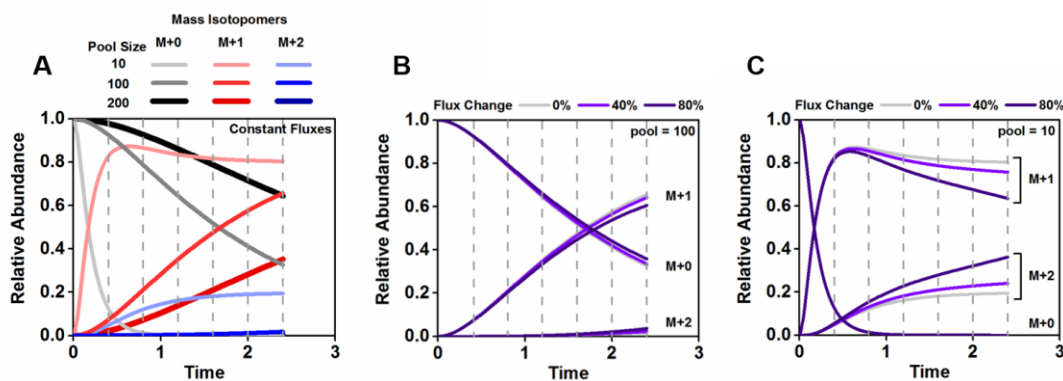


Figure 6.9 Simulated MID curves of metabolite D. (A) shows the MID curves when the fluxes are constant over time for pool sizes 10, 100, and 200. (B) shows the MID curves when the fluxes change by 0%, 40%, and 80% for a pool size of 100. (C) shows the MID curves when the fluxes change by 0%, 40%, and 80% for a pool size of 10. The grey dashed lines indicate what timepoints were used to estimate parameters.

D. Because the turnover over rate for the larger pools is much slower, and therefore takes longer time, the flux changes that occur very quickly do not significantly impact the labeling of these metabolites.

Again, we simulated labeling patterns for these extreme scenarios and used ^{13}C -DMFA to estimate fluxes and pool sizes. We again compared the SSR, precision and accuracy for each scenario (Figure 6.10). When only measuring the labeling of B and D, ^{13}C -DMFA cannot estimate fluxes with high precision for pool sizes larger than 10. We even observe decreased accuracy for larger pool sizes. If additional measurements are included, such as the labeling of C or pool size measurements, there is improved accuracy and precision. However, it's clear that at large pool sizes (>100), ^{13}C -DMFA should be applied with caution. For these systems, other methods are needed to study intracellular fluxes and metabolism.

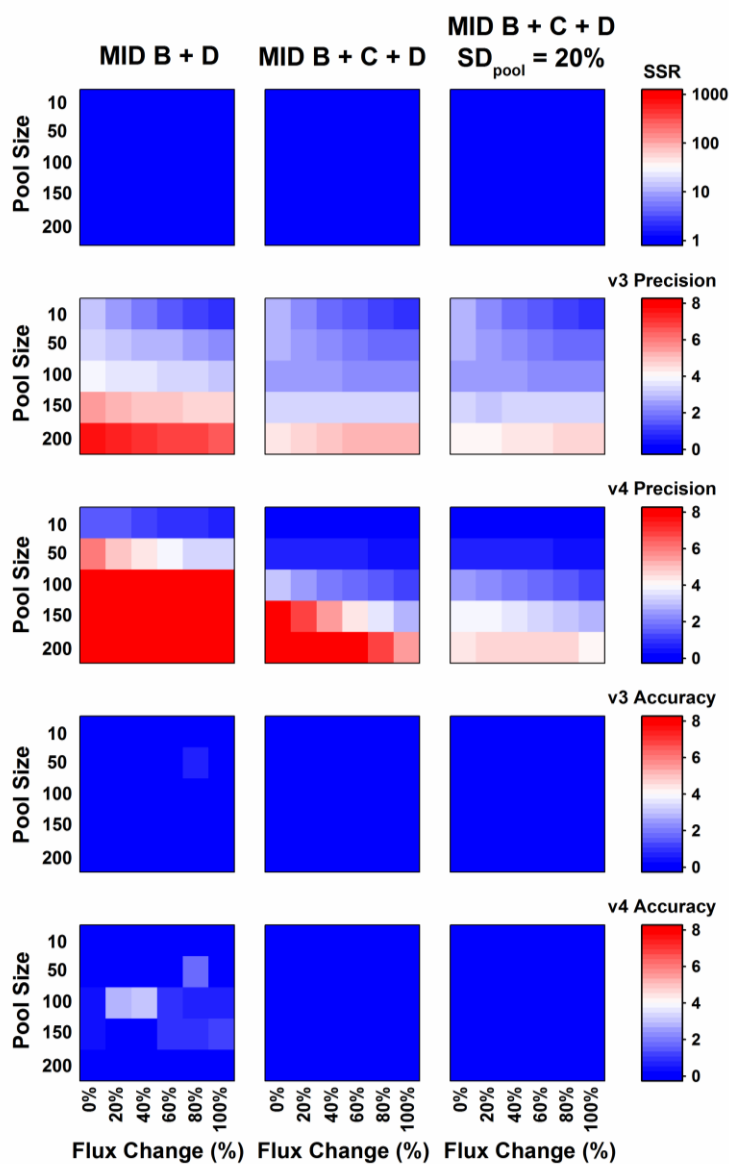


Figure 6.10 Comparison of flux estimation using ^{13}C -DMFA after including labeling measurements of metabolites B and D, measurements of B, C, D, and measurements of B, C, D and pool sizes (uncertainty in measurement is 20%). Each heat map corresponds to a different statistical value for each method: SSR, precision, or accuracy. Precision and accuracy are determined with respect to the estimated values of the fluxes v_3 and v_4 .

6.4 Conclusions

In summary, we have applied various MFA methods to a simple network model and have shown in which cases each of these methods should be used. Figure 6.11 summarizes these results. For small pool sizes or in cases in which isotopic steady state can be achieved, ^{13}C -MFA (or ^{13}C -MFAg), the simplest methods presented here, can be applied. For larger pool sizes (non-isotopic steady state) and systems at metabolic steady state, ^{13}C -NMFA must be used. However, this method can also be applied for systems at isotopic steady state, although ^{13}C -MFA would be a simpler approach. Lastly, systems that are not at metabolic steady state and cannot be evaluated using ^{13}C -MFA must be interrogated with ^{13}C -DMFA. While ^{13}C -DMFA can be applied to most systems, this method does have its limits and therefore should be applied with caution at systems that are from isotopic steady state. Additionally, including measurements of pool sizes and additional metabolites will improve parameter estimation.

		Flux Changes		
		None	Small	Large
Pool Sizes	Small	^{13}C -MFAg	^{13}C -MFAg	^{13}C -MFAg
	↓	^{13}C -NMFA	^{13}C -DMFA	^{13}C -DMFA
	Large	^{13}C -NMFA	^{13}C -DMFA	^{13}C -DMFA

Figure 6.8 Summary of MFA methods and when to apply them. When choosing a method, one must consider if the system is at metabolic or isotopic steady state. ^{13}C -MFA and ^{13}C -MFAg can be used for isotopic steady state. ^{13}C -NMFA can be used for isotopic non-steady state. ^{13}C -DMFA can be used for metabolic and isotopic non-steady state.

This work represents the first extension of DMFA to include isotopic labeling to achieve ^{13}C -DMFA. Now, there are sufficient methods for determining accurate fluxes in almost any system. Future work will require further extension and evaluation of this method to a larger network model, representative of the metabolism of an organism.

CONCLUSIONS AND FUTURE WORK

7.1 Summary of Conclusions

In this work, we aimed to show the potential and wide-spread applications of ^{13}C -tracers, from elucidating intracellular fluxes using ^{13}C -MFA to validating and improving an engineered organism. Beyond demonstrating the various uses of ^{13}C -tracers, we have further extended the methodology of flux analysis to include the estimation of time-dependent fluxes using ^{13}C -DMFA, allowing almost any system to be studied using metabolic flux analysis.

Towards the goal of this dissertation, we first applied ^{13}C -MFA to study the metabolism of glucose and xylose in *E. coli* under both aerobic and anaerobic conditions. There have been several studies of aerobic glucose metabolism, but apart from this condition, there is limited data for other growth conditions for *E. coli*. To fill this gap in knowledge, fluxes were determined for each condition using an optimal set of tracers. From the flux data, we were able to examine co-factor allocation among the various pathways. Biomass composition was found to vary depending on the condition. Additionally, biomass turnover was confirmed using fully labeled tracers. Lipid turnover was shown to be a significant process under during anaerobic growth on xylose, where blocking lipid turnover prevented growth. This information can now be used to improve predictive modeling approaches. For future studies, biomass composition should be measured as it appears to be affected by environmental conditions. Additionally, biomass turnover must be considered when modeling metabolism as it can be a significant process. Without including these changes in future models, the predictions are likely to be incorrect.

The work in chapter 1 motivated the investigation of *E. coli* strains that can co-utilize glucose and xylose, the two most abundant sugars produced from the hydrolysis of lignocellulosic biomass. *E. coli* has been a major target of engineering for co-utilization of sugars. Strategies include eliminating carbon catabolite repression by targeting the PTS as well as manipulating pathway stoichiometry. Here, we used ^{13}C -tracers to study how the four PTS knockouts respond to various glucose and xylose mixtures. The growth rates of $\Delta ptsH$ and $\Delta ptsI$ are severely impacted by the glucose:xylose ratio, where increasing the relative glucose concentration results in a decrease in growth rate. Additionally, all knockouts responded to changes in the ratio of the sugars, where increasing the relative glucose concentration led to an increase in the relative glucose uptake rate. We also studied two *E. coli* strains, GX50 and LMSE2, which had been previously engineered for co-utilization of glucose and xylose. ^{13}C -MFA was used to quantify fluxes in these two strains at various glucose:xylose ratios. Clear differences were observed in terms of pathway utilization and cofactor allocation between the two strains. We also quantified their ability to respond to various glucose and xylose mixtures by measuring the relative xylose uptake rate as a function of the relative xylose concentration. LMSE2 exhibited a constant profile where the relative xylose uptake rate remained the same, regardless of the relative xylose concentration. Conversely, for GX50, the relative xylose uptake rate increased as the relative xylose concentration increased. Based on these results, we were able to make conclusions about the “ideal” co-utilizing strain. For this strain, the relative xylose uptake rate would be linearly dependent on the relative xylose concentration. This will allow for complete consumption of sugars and a more efficient process.

Beyond sugars, methane and its derivatives have been evaluated as attractive feedstocks for chemical production. Previously, an *E. coli* strain was engineered to use methanol for biomass and chemical production. Here, we aimed to improve this synthetic methylotrophic strain. It was observed that methanol incorporation was significantly higher when yeast extract was used as a co-substrate compared to glucose. This led to the hypothesis that the amino acids present in yeast extract triggered a regulatory response that led to increased methanol assimilation. To investigate this further, 25 different co-substrates were tested for increased growth and methanol assimilation. It was found that co-utilization of threonine led to significant labeling from ^{13}C -methanol and that the regulator Lrp, represses pathways that are activated during growth on threonine. This regulator was removed, resulting in improved ^{13}C -methanol incorporation. This study clearly showed the importance of regulation in methylotrophy, and substrate metabolism in general. When engineering organisms to use new substrates, manipulating global responses to substrates, rather than simply adding heterologous genes and manipulating pathway stoichiometry, is necessary to successfully achieve organisms with new substrate capabilities.

Using methane as a carbon source has received increased attention recently due to its low cost and high electron content. It is also a major metabolite in the global carbon cycle, in which it is produced by organisms called methanogens and metabolized to CO_2 by methanotrophs. Methanogens are organisms that perform methanogenesis, producing methane primarily from one carbon compounds. These organisms have started to receive more attention, not only because of their role in the global carbon cycle, but also as a possible host for alternative fuel production from methane. However, a detailed understanding of their metabolism is lacking. Here, we

aimed to better elucidate the metabolism of the model methanogen *M. acetivorans* during growth on methanol. A detailed characterization of growth on methanol was performed. It was observed that all methane was derived from methanol while carbon dioxide was first produced through methanogenesis and then incorporated into biomass through CO₂ fixing reactions in central carbon metabolism. A network model was constructed and then validated using ¹³C-MFA, generating the first flux map for *M. acetivorans*. Typically, for autotrophic organisms, ¹³C-NMFA is required to obtain estimates for fluxes. However, we were able to design the experiment in a specific way that allowed for application of classical ¹³C-MFA, significantly decreasing the complexity of the experimental and computational framework. As far as we know, this is the only application of classical ¹³C-MFA to an autotrophic organism.

So far, we have seen various applications of ¹³C-tracers and ¹³C-MFA to different systems. As discussed in chapter 6, there are cases where traditional ¹³C-MFA cannot be applied, demonstrating the limitations of ¹³C-MFA. Here, we also present different approaches for estimating fluxes for atypical systems, ones not at metabolic or isotopic steady state. Specifically, we present the first application of ¹³C-dynamic metabolic flux analysis, which can be used for systems in which fluxes are changing with time. The inclusion of ¹³C-labeling measurements allows for precise and accurate estimation of concentrations and fluxes. Additionally, we evaluate the four established methods of flux analysis for different experimental conditions and discuss the strengths and limitations of each method.

7.2 Future work

Future work for studying sugar metabolism

This work emphasized the need for more experimental data from studies of sugar metabolism. We studied the metabolism of glucose and xylose, a PTS and a non-PTS sugar. It would be interesting to examine if there are any differences between the metabolisms of glucose vs galactose or between arabinose vs xylose. This would better highlight the effect on metabolism of the substrate itself rather than the pathways used for metabolism of that substrate. In this work, it was clear that the metabolism of glucose and xylose would be different as they enter at different points of metabolism. However, the differences in glucose and galactose metabolism are not as apparent.

While *E.coli* has been the model organism for these studies, these experiments should be extended to other organisms, including non-model ones that have been identified as promising hosts for chemical production. Additionally, novel sugar pathways (such as those shown in Figure 1.1) should be implemented and compared to the traditional sugar catabolic pathways. This would provide a clear answer as to whether these pathways do in fact improve metabolism of these sugars, in terms of decreased CO₂ loss and increased product yield. To this end, it would also be interesting to identify a “minimal” sugar catabolic pathway. A direct path from glucose (or xylose) to product can be identified and implemented in such a way that all other pathways are removed, preventing carbon from being used, and wasted, for other biological resources.

Future work for improving synthetic methylotrophy

Regulation appears to play a major role in methylotrophy. An extension of this work would be to perform a thorough transcriptomic analysis of our strain during growth on yeast extract and methanol (a high methanol incorporation condition) and

during growth on glucose and methanol (a low methanol incorporation condition). Comparing these two conditions could provide insight into which genes/pathways are favorable for methylotrophy. This could also provide more information on the specific pathways in the Δlrp strain that led to the observed phenotype. It would also be interesting to test combinations of amino acids as co-substrates. It's possible that combining threonine with another amino acid would also result in an improved methylotrophic phenotype.

This section would have greatly benefited from a metabolic analysis of native methylotrophs. So far, there have been no studies applying ^{13}C -metabolic flux analysis to RuMP-utilizing methylotrophs. It's likely that the complexity of ^{13}C -NMFA has limited its application to methylotrophic organisms. However, since methanol is increasingly being used as a feedstock for bioconversion, these studies would be very useful. Specifically, it would be valuable to compare the fluxome and transcriptome of native methylotrophs to *E. coli* during "growth" on methanol. This will give insight into how the two organisms respond to methanol and provide targets for manipulating regulation.

While our engineered *E. coli* strain has the necessary genes to use methanol, it cannot use methanol as the sole carbon source for growth. This is likely due to the unbalanced pathway kinetics and fluxes in the pentose phosphate pathway, preventing an effective autocatalytic cycle (Barenholz et al., 2017). Unlike *E. coli*, native methylotrophs have evolved to achieve this pathway balancing. Hypothetically, each enzyme in the pentose phosphate pathway can be expressed at different levels to achieve that cycle. However, it would be easier to let our *E. coli* strain identify this balance through adaptive evolution. This would require a strain that links methanol

consumption to growth and allows evolution towards a fully methylotrophic phenotype. A set of knockouts can be identified, using flux balance analysis, that allow for growth on a particular substrate only in the presence of methanol (Antonovsky et al., 2016; Gawand et al., 2013). Two designs that we have identified seem promising. The first design is a strain containing the following knockouts: $\Delta frmA \Delta gpmAM \Delta fbp \Delta glpx \Delta mgsA$. This strain cannot grow on glucose or xylose alone but will be able to use either sugar in the presence of methanol. The second design is a strain containing the following knockouts: $\Delta frmA \Delta fbp \Delta glpx$. This strain cannot grow on gluconeogenic substrates (i.e. acetate, succinate, pyruvate) alone but can use these substrates in the presence of methanol. The important trait of these designs is that the required knockouts do not prevent methanol-only growth which allows for adaptive evolution towards a complete methylotrophic strain.

Future work on methanogen metabolism

Studies of methanogens have been increasing due to their important roles in nature and their potential as biofactories. Therefore, obtaining a systems-wide understanding of these organisms is imperative if these organisms are to be engineered. Therefore, the validated network model can be used to study growth on other substrates, such as acetate. Growth on acetate can also be used to simulate interactions in the microbiome, in which sugars are converted to acids and then converted to methane by methanogens in the gut.

M. acetivorans is a model methanogen and, therefore, is a good host for studying the reversal of methanogenesis, a possible route to anaerobic methanotrophy. The key to reverse methanogenesis is identification of a suitable electron acceptor.

¹³C-tracers would be invaluable for these studies, in which different electron acceptors

can be tested and the extent of ^{13}C -methane conversion can be measured. Additionally, the reversibility of each step in methanogenesis can be studied by feeding labeled metabolic intermediates of the methanogenesis pathway.

Future work on metabolic flux analysis methods

^{13}C -MFA is now the state-of-the-art method for estimating fluxes. However, this method has its limitations, as described in chapter 6. We presented a framework for a new method, ^{13}C -DMFA, and evaluated when the various flux analysis methods (^{13}C -MFA, ^{13}C -NMFA, ^{13}C -DMFA) should be applied. All of these methods were applied to a simple model, containing a few reactions. Ideally, these methods would be tested with a larger metabolic network model and used to estimate fluxes for any system, even with more complex flux changes. This method can better elucidate pathways that were, until now, thought to be unobservable. These include, cyclic and parallel pathways, as well as reversible reactions. Only with incorporation of ^{13}C -labeling measurements can these fluxes be estimated.

REFERENCES

If you want to number your bibliographic entries, change the style of the items to *Bib Entry - numbered*.

Abubackar, H.N., Veiga, M.C., Kennes, C., 2015. Carbon monoxide fermentation to ethanol by *Clostridium autoethanogenum* in a bioreactor with no accumulation of acetic acid. *Bioresour. Technol.* 186, 122–127.

Ahn, W.S., Antoniewicz, M.R., 2013. Parallel labeling experiments with [1,2-(13)C]glucose and [U-(13)C]glutamine provide new insights into CHO cell metabolism. *Metab. Eng.* 15, 34–47.

Ahn, W.S., Crown, S.B., Antoniewicz, M.R., 2016. Evidence for transketolase-like TKTL1 flux in CHO cells based on parallel labeling experiments and 13C-metabolic flux analysis. *Metab. Eng.* 37, 72–78.

Antoniewicz, M.R., 2015. Methods and advances in metabolic flux analysis : a mini - review.

Antoniewicz, M.R., 2015. Parallel labeling experiments for pathway elucidation and 13C metabolic flux analysis. *Curr. Opin. Biotechnol.* 36, 91–97.

Antoniewicz, M.R., 2013. (13)C metabolic flux analysis: optimal design of isotopic labeling experiments. *Curr. Opin. Biotechnol.* 24, 1116–21.

Antoniewicz, M.R., Kelleher, J.K., Stephanopoulos, G., 2011. Measuring deuterium enrichment of glucose hydrogen atoms by gas chromatography/mass spectrometry. *Anal. Chem.* 83, 3211–3216.

Antoniewicz, M.R., Kelleher, J.K., Stephanopoulos, G., 2007a. Accurate assessment of amino acid mass isotopomer distributions for metabolic flux analysis. *Anal. Chem.* 79, 7554–9.

Antoniewicz, M.R., Kelleher, J.K., Stephanopoulos, G., 2007b. Elementary metabolite units (EMU): a novel framework for modeling isotopic distributions. *Metab. Eng.* 9, 68–86.

Antoniewicz, M.R., Kelleher, J.K., Stephanopoulos, G., 2006. Determination of confidence intervals of metabolic fluxes estimated from stable isotope measurements. *Metab. Eng.* 8, 324–37.

- Antoniewicz, M.R., Kraynie, D.F., Laffend, L. a, González-Lergier, J., Kelleher, J.K., Stephanopoulos, G., 2007c. Metabolic flux analysis in a nonstationary system: fed-batch fermentation of a high yielding strain of *E. coli* producing 1,3-propanediol. *Metab. Eng.* 9, 277–92.
- Antoniewicz, M.R., Stephanopoulos, G., Kelleher, J.K., 2006. Evaluation of regression models in metabolic physiology: predicting fluxes from isotopic data without knowledge of the pathway. *Metabolomics* 2, 41–52.
- Antonovsky, N., Gleizer, S., Noor, E., Zohar, Y., Herz, E., Barenholz, U., Zelcbuch, L., Amram, S., Wides, A., Tepper, N., Davidi, D., Bar-On, Y., Bareia, T., Wernick, D.G., Shani, I., Malitsky, S., Jona, G., Bar-Even, A., Milo, R., 2016. Sugar Synthesis from CO₂ in *Escherichia coli*. *Cell* 166, 115–125.
- Aristilde, L., Lewis, I. a., Park, J.O., Rabinowitz, J.D., 2015. Hierarchy in pentose sugar metabolism in *Clostridium acetobutylicum*. *Appl. Environ. Microbiol.* 81, 1452–1462.
- Au, J., Choi, J., Jones, S.W., Venkataramanan, K.P., Antoniewicz, M.R., 2014. Parallel labeling experiments validate *Clostridium acetobutylicum* metabolic network model for ¹³C metabolic flux analysis. *Metab. Eng.* 26, 23–33.
- Baba, T., Ara, T., Hasegawa, M., Takai, Y., Okumura, Y., Baba, M., Datsenko, K. a, Tomita, M., Wanner, B.L., Mori, H., 2006. Construction of *Escherichia coli* K-12 in-frame, single-gene knockout mutants: the Keio collection. *Mol. Syst. Biol.* 2, 1–11.
- Balderas-Hernández, V.E., Hernández-Montalvo, V., Bolívar, F., Gosset, G., Martínez, A., 2011. Adaptive evolution of *Escherichia coli* inactivated in the phosphotransferase system operon improves co-utilization of xylose and glucose under anaerobic conditions. *Appl. Biochem. Biotechnol.* 163, 485–96.
- Barenholz, U., Davidi, D., Reznik, E., Bar-On, Y., Antonovsky, N., Noor, E., Milo, R., 2017. Design principles of autocatalytic cycles constrain enzyme kinetics and force low substrate saturation at flux branch points. *Elife* 6, 1–32.
- Becker, J., Boles, E., 2003. A modified *Saccharomyces cerevisiae* strain that consumes L -arabinose and produces ethanol. *Society* 69, 4144–4150.
- Becker, S.A., Feist, A.M., Mo, M.L., Hannum, G., Palsson, B.O., Herrgard, M.J., 2011. Quantitative prediction of cellular metabolism with constraint-based models: the COBRA Toolbox v2.0. *Nat. Protoc.* 6, 1290–1307.

- Bennett, R.K., Steinberg, L.M., Chen, W., Papoutsakis, E.T., 2018. Engineering the bioconversion of methane and methanol to fuels and chemicals in native and synthetic methylotrophs. *Curr. Opin. Biotechnol.* 50, 81–93.
- Berg, I. a, Kockelkorn, D., Ramos-Vera, W.H., Say, R.F., Zarzycki, J., Hügler, M., Alber, B.E., Fuchs, G., 2010. Autotrophic carbon fixation in archaea. *Nat. Rev. Microbiol.* 8, 447–60.
- Borujeni, A., Channarasappa, A.S., Salis, H.M., 2014. Translation rate is controlled by coupled trade-offs between site accessibility, selective RNA unfolding and sliding at upstream standby sites. *Nucleic Acids Res.* 42, 2646–2659.
- Burgard, A.P., Pharkya, P., Maranas, C.D., 2003. OptKnock: A Bilevel Programming Framework for Identifying Gene Knockout Strategies for Microbial Strain Optimization. *Biotechnol. Bioeng.* 84, 647–657.
- Calvo, J.M., Matthews, R.G., 1994. The leucine-responsive regulatory protein, a global regulator of metabolism in *Escherichia coli*. *Microbiol. Rev.* 58, 466–490.
- Campbell, J.W., Morgan-Kiss, R.M., Cronan, J.E., 2003. A new *Escherichia coli* metabolic competency: Growth on fatty acids by a novel anaerobic β -oxidation pathway. *Mol. Microbiol.* 47, 793–805.
- Chen, X., Alonso, A.P., Allen, D.K., Reed, J.L., Shachar-Hill, Y., 2011. Synergy between $(13)\text{C}$ -metabolic flux analysis and flux balance analysis for understanding metabolic adaptation to anaerobiosis in *E. coli*. *Metab. Eng.* 13, 38–48.
- Cho, B.-K., Barrett, C.L., Knight, E.M., Park, Y.S., Palsson, B.O., 2008. Genome-scale reconstruction of the Lrp regulatory network in *Escherichia coli*. *Proc. Natl. Acad. Sci.* 105, 19462–19467.
- Cho, B.-K., Federowicz, S., Park, Y.-S., Zengler, K., Palsson, B.Ø., 2011. Deciphering the transcriptional regulatory logic of amino acid metabolism. *Nat. Chem. Biol.* 8, 65–71.
- Choi, S., Song, C.W., Shin, J.H., Lee, S.Y., 2015. Biorefineries for the production of top building block chemicals and their derivatives. *Metab. Eng.* 28, 223–239.
- Choudhary, M.K., Yoon, J.M., Gonzalez, R., Shanks, J. V., 2011. Re-examination of Metabolic Fluxes in *Escherichia coli* during Anaerobic Fermentation of Glucose Using 13C Labeling Experiments and 2-dimensional Nuclear Magnetic Resonance (NMR) Spectroscopy. *Biotechnol. Bioprocess Eng.* 16, 419–437.

- Cordova, L.T., Antoniewicz, M.R., 2015. (¹³C) metabolic flux analysis of the extremely thermophilic, fast growing, xylose-utilizing *Geobacillus* strain LC300. *Metab. Eng.* 1–10.
- Cordova, L.T., Long, C.P., Venkataramanan, K.P., Antoniewicz, M.R., 2015. Complete genome sequence, metabolic model construction and phenotypic characterization of *Geobacillus* LC300, an extremely thermophilic, fast growing, xylose-utilizing bacterium. *Metab. Eng.* 32, 74–81.
- Cordova, L.T., Lu, J., Cipolla, R.M., Sandoval, N.R., Long, C.P., Antoniewicz, M.R., 2016. Co-utilization of glucose and xylose by evolved *Thermus thermophilus* LC113 strain elucidated by ¹³C metabolic flux analysis and whole genome sequencing. *Metab. Eng.* 37, 63–71.
- Crown, S.B., Ahn, W.S., Antoniewicz, M.R., 2012. Rational design of ¹³C-labeling experiments for metabolic flux analysis in mammalian cells. *BMC Syst. Biol.* 6, 43.
- Crown, S.B., Antoniewicz, M.R., 2013a. Publishing (¹³C) metabolic flux analysis studies: A review and future perspectives. *Metab. Eng.* 20, 42–8.
- Crown, S.B., Antoniewicz, M.R., 2013b. Parallel labeling experiments and metabolic flux analysis: Past, present and future methodologies. *Metab. Eng.* 16, 21–32.
- Crown, S.B., Antoniewicz, M.R., 2012. Selection of tracers for ¹³C-metabolic flux analysis using elementary metabolite units (EMU) basis vector methodology. *Metab. Eng.* 14, 150–61.
- Crown, S.B., Kelleher, J.K., Rouf, R., Muoio, D.M., Antoniewicz, M.R., 2016a. Comprehensive metabolic modeling of multiple ¹³C-isotopomer data sets to study metabolism in perfused working hearts. *Am. J. Physiol. - Hear. Circ. Physiol.* 311, H881–H891.
- Crown, S.B., Long, C.P., Antoniewicz, M.R., 2016b. Optimal tracers for parallel labeling experiments and ¹³C metabolic flux analysis: A new precision and synergy scoring system. *Metab. Eng.* 38, 10–18.
- Crown, S.B., Long, C.P., Antoniewicz, M.R., 2015. Integrated ¹³C-metabolic flux analysis of 14 parallel labeling experiments in *Escherichia coli*. *Metab. Eng.* 28, 151–8.

- Crown, S.B., Marze, N., Antoniewicz, M.R., 2015. Catabolism of branched chain amino acids contributes significantly to synthesis of odd-chain and even-chain fatty acids in 3T3-L1 adipocytes. *PLoS One* 10, 1–22.
- Datsenko, K. a, Wanner, B.L., 2000. One-step inactivation of chromosomal genes in *Escherichia coli* K-12 using PCR products. *Proc. Natl. Acad. Sci.* 97, 6640–5.
- David, H., Krogh, A.M., Roca, C., Åkesson, M., Nielsen, J., 2005. CreA influences the metabolic fluxes of *Aspergillus nidulas* during growth on glucose and xylose. *Microbiology* 151, 2209–2221.
- Ducat, D.C., Way, J.C., Silver, P. a., 2011. Engineering cyanobacteria to generate high-value products. *Trends Biotechnol.* 29, 95–103.
- Edwards, J.S., Ramakrishna, R., Palsson, B.O., 2002. Characterizing the metabolic phenotype: A phenotype phase plane analysis. *Biotechnol. Bioeng.* 77, 27–36.
- Elkins, J.G., Raman, B., Keller, M., 2010. Engineered microbial systems for enhanced conversion of lignocellulosic biomass. *Curr. Opin. Biotechnol.* 21, 657–662.
- Fast, A.G., Papoutsakis, E.T., 2012. Stoichiometric and energetic analyses of non-photosynthetic CO₂-fixation pathways to support synthetic biology strategies for production of fuels and chemicals. *Curr. Opin. Chem. Eng.* 1, 380–395.
- Fast, A.G., Schmidt, E.D., Jones, S.W., Tracy, B.P., 2015. Acetogenic mixotrophy: novel options for yield improvement in biofuels and biochemicals production. *Curr. Opin. Biotechnol.* 33, 60–72.
- Fei, Q., Guarnieri, M.T., Tao, L., Laurens, L.M.L., Dowe, N., Pienkos, P.T., 2014. Bioconversion of natural gas to liquid fuel: opportunities and challenges. *Biotechnol. Adv.* 32, 596–614.
- Fendt, S.-M., Sauer, U., 2010. Transcriptional regulation of respiration in yeast metabolizing differently repressive carbon substrates. *BMC Syst. Biol.* 4, 12.
- Feng, X., Zhao, H., 2013. Investigating xylose metabolism in recombinant *Saccharomyces cerevisiae* via ¹³C metabolic flux analysis 1–12.
- Ferguson, T.J., Mah, R.A., 1983. Methanogenesis from Acetate or Methanol in *Methanosarcina* spp Effect of H₂-CO₂ on Methanogenesis from Acetate. *Appl. Environ. Microbiol.*

- Fernandez, C., Des Rosiers, C., Previs, S., David, F., Brunengraber, H., 1996. Correction of ^{13}C mass isotopomer distributions for natural stable isotope abundance. *J. Mass Spectrom.* 31, 255–262.
- Ferry, J.G., 2010. How to make a living by exhaling methane. *Annu. Rev. Microbiol.* 64, 453–73.
- Finkel, S.E., 2006. Long-term survival during stationary phase: evolution and the GASP phenotype. *Nat.Rev.Microbiol.* 4, 113–120.
- Finn, M., Tabita, F.R., 2004. Modified Pathway To Synthesize Ribulose Modified Pathway To Synthesize Ribulose 1, 5-Bisphosphate in Methanogenic Archaea 186.
- Fonseca, C., Neves, A.R., Antunes, A.M.M., Noronha, J.P., Hahn-H??gerdal, B., Santos, H., Spencer-Martins, I., 2008. Use of in vivo ^{13}C nuclear magnetic resonance spectroscopy to elucidate L-arabinose metabolism in yeasts. *Appl. Environ. Microbiol.* 74, 1845–1855.
- Fu, N., Peiris, P., Markham, J., Bavor, J., 2009. A novel co-culture process with *Zymomonas mobilis* and *Pichia stipitis* for efficient ethanol production on glucose/xylose mixtures. *Enzyme Microb. Technol.* 45, 210–217.
- Gawand, P., Hyland, P., Ekins, A., Martin, V.J.J., Mahadevan, R., 2013. Novel approach to engineer strains for simultaneous sugar utilization. *Metab. Eng.* 20, 63–72.
- Gebreselassie, N. a, Antoniewicz, M.R., 2015. (^{13}C)-metabolic flux analysis of co-cultures: A novel approach. *Metab. Eng.* 31, 132–139.
- Gírio, F.M., Fonseca, C., Carvalheiro, F., Duarte, L.C., Marques, S., Bogel-Łukasik, R., 2010. Hemicelluloses for fuel ethanol: A review. *Bioresour. Technol.* 101, 4775–800.
- Gonçalves, D.L., Matsushika, A., de Sales, B.B., Goshima, T., Bon, E.P.S., Stambuk, B.U., 2014. Xylose and xylose/glucose co-fermentation by recombinant *Saccharomyces cerevisiae* strains expressing individual hexose transporters. *Enzyme Microb. Technol.* 63, 13–20.
- Gong, F., Liu, G., Zhai, X., Zhou, J., Cai, Z., Li, Y., 2015. Quantitative analysis of an engineered CO_2 -fixing *Escherichia coli* reveals great potential of heterotrophic CO_2 fixation. *Biotechnol. Biofuels* 8, 86.

- Gonnerman, M.C., Benedict, M.N., Feist, A.M., Metcalf, W.W., Price, N.D., 2013. Genomically and biochemically accurate metabolic reconstruction of *Methanosarcina barkeri* Fusaro, iMG746. *Biotechnol. J.* 8, 1070–9.
- Gonzalez, J.E., Long, C.P., Antoniewicz, M.R., 2017. Comprehensive analysis of glucose and xylose metabolism in *Escherichia coli* under aerobic and anaerobic conditions by ¹³C metabolic flux analysis. *Metab. Eng.* 39, 9–18.
- Gray, C.T., Wimpenny, J.W.T., Mossman, M.R., 1966. Regulation of Metabolism in Facultative Bacteria 7, 33–41.
- Grimmler, C., Held, C., Liebl, W., Ehrenreich, A., 2010. Transcriptional analysis of catabolite repression in *Clostridium acetobutylicum* growing on mixtures of d-glucose and d-xylose. *J. Biotechnol.* 150, 315–323.
- Grotkjær, T., Christakopoulos, P., Nielsen, J., Olsson, L., 2005. Comparative metabolic network analysis of two xylose fermenting recombinant *Saccharomyces cerevisiae* strains. *Metab. Eng.* 7, 437–444.
- Guadalupe-Medina, V., Wisselink, H.W., Luttik, M.A., De Hulster, E., Daran, J.M., Pronk, J.T., Van Maris, A.J. a., 2013. Carbon dioxide fixation by Calvin-Cycle enzymes improves ethanol yield in yeast. *Biotechnol. Biofuels* 6.
- Hasona, A., Kim, Y., Healy, F.G., Ingram, L.O., Shanmugam, K.T., 2004. Pyruvate formate lyase and acetate kinase are essential for anaerobic growth of *Escherichia coli* on xylose. *J. Bacteriol.* 186, 7593–600.
- Haynes, C. a, Gonzalez, R., 2014. Rethinking biological activation of methane and conversion to liquid fuels. *Nat. Chem. Biol.* 10, 331–9.
- He, M., Wu, B., Qin, H., Ruan, Z., Tan, F., Wang, J., Shui, Z., Dai, L., Zhu, Q., Pan, K., Tang, X., Wang, W., Hu, Q., 2014. *Zymomonas mobilis*: a novel platform for future biorefineries. *Biotechnol. Biofuels* 7, 101.
- Herz, E., Antonovsky, N., Bar-On, Y., Davidi, D., Gleizer, S., Prywes, N., Noda-Garcia, L., Lyn Frisch, K., Zohar, Y., Wernick, D.G., Savidor, A., Barenholz, U., Milo, R., 2017. The genetic basis for the adaptation of *E. coli* to sugar synthesis from CO₂. *Nat. Commun.* 8.
- Himmel, M.E., Bayer, E. a., 2009. Lignocellulose conversion to biofuels: current challenges, global perspectives. *Curr. Opin. Biotechnol.* 20, 316–317.

- Hu, P., Chakraborty, S., Kumar, A., Woolston, B., Liu, H., Emerson, D., Stephanopoulos, G., 2016. Integrated bioprocess for conversion of gaseous substrates to liquids. *Proc. Natl. Acad. Sci.* 113, 3773–3778.
- Iwatani, S., Van Dien, S., Shimbo, K., Kubota, K., Kageyama, N., Iwahata, D., Miyano, H., Hirayama, K., Usuda, Y., Shimizu, K., Matsui, K., 2007. Determination of metabolic flux changes during fed-batch cultivation from measurements of intracellular amino acids by LC-MS/MS. *J. Biotechnol.* 128, 93–111.
- Iwatani, S., Yamada, Y., Usuda, Y., 2008. Metabolic flux analysis in biotechnology processes. *Biotechnol. Lett.* 30, 791–9.
- Jeffries, T.W., 2006. Engineering yeasts for xylose metabolism. *Curr. Opin. Biotechnol.* 17, 320–326.
- Jones, S.W., Fast, A.G., Carlson, E.D., Wiedel, C. a., Au, J., Antoniewicz, M.R., Papoutsakis, E.T., Tracy, B.P., 2016. CO₂ fixation by anaerobic non-photosynthetic mixotrophy for improved carbon conversion. *Nat. Commun.* 7, 1–9.
- Jordà, J., Jouhten, P., Cámara, E., Maaheimo, H., Albiol, J., Ferrer, P., 2012. Metabolic flux profiling of recombinant protein secreting *Pichia pastoris* growing on glucose:methanol mixtures. *Microb. Cell Fact.* 11, 57.
- Jung, I.Y., Lee, J.W., Min, W.K., Park, Y.C., Seo, J.H., 2015. Simultaneous conversion of glucose and xylose to 3-hydroxypropionic acid in engineered *Escherichia coli* by modulation of sugar transport and glycerol synthesis. *Bioresour. Technol.* 198, 709–716.
- Kalyuzhnaya, M.G., Yang, S., Rozova, O.N., Smalley, N.E., Clubb, J., Lamb, a., Gowda, G. a N., Raftery, D., Fu, Y., Bringel, F., Vuilleumier, S., Beck, D. a C., Trotsenko, Y. a, Khmelenina, V.N., Lidstrom, M.E., 2013. Highly efficient methane biocatalysis revealed in a methanotrophic bacterium. *Nat. Commun.* 4, 2785. d
- Khodayari, A., Zomorodi, A.R., Liao, J.C., Maranas, C.D., 2014. A kinetic model of *Escherichia coli* core metabolism satisfying multiple sets of mutant flux data. *Metab. Eng.* 25, 50–62.
- Kim, J., Reed, J.L., 2012. RELATCH: relative optimality in metabolic networks explains robust metabolic and regulatory responses to perturbations. *Genome Biol.* 13, R78.

- Kim, S.M., Choi, B.Y., Ryu, Y.S., Jung, S.H., Park, J.M., Kim, G.-H., Lee, S.K., 2015. Simultaneous utilization of glucose and xylose via novel mechanisms in engineered *Escherichia coli*. *Metab. Eng.* 30, 141–148.
- King, Z. a., Lloyd, C.J., Feist, A.M., Palsson, B.O., 2015. Next-generation genome-scale models for metabolic engineering. *Curr. Opin. Biotechnol.* 35, 23–29.
- Kopke, M., Held, C., Hujer, S., Liesegang, H., Wiezer, A., Wollherr, A., Ehrenreich, A., Liebl, W., Gottschalk, G., Durre, P., 2010. *Clostridium ljungdahlii* represents a microbial production platform based on syngas. *Proc. Natl. Acad. Sci.* 107, 13087–13092.
- Leighty, R.W., Antoniewicz, M.R., 2013. COMPLETE-MFA: Complementary parallel labeling experiments technique for metabolic flux analysis. *Metab. Eng.* 20, 49–55.
- Leighty, R.W., Antoniewicz, M.R., 2012. Parallel labeling experiments with [U-¹³C]glucose validate *E. coli* metabolic network model for ¹³C metabolic flux analysis. *Metab. Eng.* 14, 533–41.
- Leighty, R.W., Antoniewicz, M.R., 2011. Dynamic metabolic flux analysis (DMFA): A framework for determining fluxes at metabolic non-steady state. *Metab. Eng.* 13, 745–755.
- Leßmeier, L., Pfeifenschneider, J., Carnicer, M., Heux, S., Portais, J.-C., Wendisch, V.F., 2015. Production of carbon-13-labeled cadaverine by engineered *Corynebacterium glutamicum* using carbon-13-labeled methanol as co-substrate. *Appl. Microbiol. Biotechnol.* 99, 10163–10176.
- Lessner, D.J., Lhu, L., Wahal, C.S., Ferry, J.G., 2010. An Engineered Methanogenic Pathway Derived from the Domains Bacteria and Archaea.
- Li, Y.H., Ou-Yang, F.Y., Yang, C.H., Li, S.Y., 2015. The coupling of glycolysis and the Rubisco-based pathway through the non-oxidative pentose phosphate pathway to achieve low carbon dioxide emission fermentation. *Bioresour* 187, 189–197.
- Liang, Q., Zhang, F., Li, Y., Zhang, X., Li, J., Yang, P., Qi, Q., 2015. Comparison of individual component deletions in a glucose-specific phosphotransferase system revealed their different applications. *Sci. Rep.* 5, 13200.

- Liao, J.C., Mi, L., Pontrelli, S., Luo, S., 2016. Fuelling the future: microbial engineering for the production of sustainable biofuels. *Nat. Rev. Microbiol.* 14, 288–304.
- Lin, C.W., Wu, C.H., Tran, D.T., Shih, M.C., Li, W.H., Wu, C.F., 2011. Mixed culture fermentation from lignocellulosic materials using thermophilic lignocellulose-degrading anaerobes. *Process Biochem.* 46, 489–493.
- Link, H., Fuhrer, T., Gerosa, L., Zamboni, N., Sauer, U., 2015. Real-time metabolome profiling of the metabolic switch between starvation and growth. *Nat. Methods* 12, 1091–1097.
- Liu, L., Zhang, L., Tang, W., Gu, Y., Hua, Q., Yang, S., Jiang, W., Yang, C., 2012. Phosphoketolase pathway for xylose catabolism in *Clostridium acetobutylicum* revealed by ¹³C metabolic flux analysis. *J. Bacteriol.* 194, 5413–22.
- Liu, R., Liang, L., Chen, K., Ma, J., Jiang, M., Wei, P., Ouyang, P., 2012. Fermentation of xylose to succinate by enhancement of ATP supply in metabolically engineered *Escherichia coli*. *Appl. Microbiol. Biotechnol.* 94, 959–68.
- Long, C.P., Antoniewicz, M.R., 2014. Metabolic flux analysis of *Escherichia coli* knockouts: lessons from the Keio collection and future outlook. *Curr. Opin. Biotechnol.* 28, 127–133.
- Long, C.P., Antoniewicz, M.R., 2014. Quantifying Biomass Composition by Gas Chromatography/Mass Spectrometry. *Anal. Chem.* 86, 9423–9427.
- Long, C.P., Au, J., Gonzalez, J.E., Antoniewicz, M.R., 2016a. ¹³C metabolic flux analysis of microbial and mammalian systems is enhanced with GC–MS measurements of glycogen and RNA labeling. *Metab. Eng.* 38, 65–72.
- Long, C.P., Au, J., Sandoval, N.R., Gebreselassie, N. a, Antoniewicz, M.R., 2017a. Enzyme I facilitates reverse flux from pyruvate to phosphoenolpyruvate in *Escherichia coli*. *Nat. Commun.* 8, 14316.
- Long, C.P., Gonzalez, J.E., Cipolla, R.M., Antoniewicz, M.R., 2017b. Metabolism of the fast-growing bacterium *Vibrio natriegens* elucidated by ¹³C- metabolic flux analysis. *Metab. Eng.* 44, 191–197.
- Long, C.P., Gonzalez, J.E., Feist, A.M., Palsson, B.O., Antoniewicz, M.R., 2017. Fast growth phenotype of *E. coli* K-12 from adaptive laboratory evolution does not require intracellular flux rewiring. *Metab. Eng.* 44, 100–107.

- Long, C.P., Gonzalez, J.E., Sandoval, N.R., Antoniewicz, M.R., 2016b. Characterization of physiological responses to 22 gene knockouts in *Escherichia coli* central carbon metabolism. *Metab. Eng.* 37, 102–113.
- Matheron, C., Delort, A.M., Gaudet, G., Forano, E., 1998. In vivo ¹³C NMR study of glucose and cellobiose metabolism by four cellulolytic strains of the genus *Fibrobacter*. *Biodegradation* 9, 451–461.
- Mcanulty, M.J., 2013. *Biofuels : Microbially Generated Methane and Hydrogen*. eLS.
- McConnell, B.O., Antoniewicz, M.R., 2016. Measuring the Composition and Stable-Isotope Labeling of Algal Biomass Carbohydrates via Gas Chromatography/Mass Spectrometry. *Anal. Chem.* 88, 4624–4628.
- Moran, J.J., House, C.H., Freeman, K.H., Ferry, J.G., 2005. Trace methane oxidation studied in several Euryarchaeota under diverse conditions. *Archaea* 1, 303–9.
- Mukhopadhyay, B., Purwantini, E., Cynthia, L., Wolfe, R.S., 2001. Oxaloacetate Synthesis in the Methanarchaeon *Methanosarcina barkeri* : Pyruvate Carboxylase Genes and a Putative *Escherichia coli* -Type Bifunctional Biotin Protein Ligase Gene (*bpl* / *birA*) Exhibit a Unique Organization Oxaloacetate Synthesis in the Metha.
- Müller, J.E., Meyer, F., Litsanov, B., Kiefer, P., Potthoff, E., Heux, S., Quax, W.J., Wendisch, V.F., Brautaset, T., Portais, J.-C., Vorholt, J. a., 2015. Engineering *Escherichia coli* for methanol conversion. *Metab. Eng.* 28, 190–201.
- Munasinghe, P.C., Khanal, S.K., 2010. Biomass-derived syngas fermentation into biofuels. *Bioresour. Technol.* 101, 5013–5022.
- Nazem-Bokaei, H., Gopalakrishnan, S., Ferry, J.G., Wood, T.K., Maranas, C.D., 2016. Assessing methanotrophy and carbon fixation for biofuel production by *Methanosarcina acetivorans*. *Microb. Cell Fact.* 15, 10.
- Neidhardt, F.C., 1987. *Escherichia Coli and Salmonella Typhimurium*. ASM Press, Washington, D.C.
- Nielsen, J., Keasling, J.D., 2016. *Engineering Cellular Metabolism*. Cell 164, 1185–1197.
- Nijland, J.G., Shin, H.Y., De Jong, R.M., De Waal, P.P., Klaassen, P., Driessen, A.J.M., 2014. Engineering of an endogenous hexose transporter into a specific D-

- xylose transporter facilitates glucose-xylose co-consumption in *Saccharomyces cerevisiae*. *Biotechnol. Biofuels* 7, 1–11.
- Noguchi, Y., Nakai, Y., Shimba, N., Toyosaki, H., Kawahara, Y., Sugimoto, S., Suzuki, E.I., 2004. The energetic conversion competence of *Escherichia coli* during aerobic respiration studied by ^{31}P NMR using a circulating fermentation system. *J. Biochem.* 136, 509–515.
- Olah, G., 2005. Beyond oil and gas: the methanol economy. *Angew. Chemie (International ed.)* 44, 2636–9.
- Papoutsakis, E.T., 2015. Reassessing the Progress in the Production of Advanced Biofuels in the Current Competitive Environment and Beyond: What Are the Successes and Where Progress Eludes Us and Why. *Ind. Eng. Chem. Res.* 54, 10170–10182.
- Perrenoud, A., Sauer, U., 2005. Impact of global transcriptional regulation by ArcA, ArcB, Cra, Crp, Cya, Fnr, and Mlc on glucose catabolism in *Escherichia coli*. *J. Bacteriol.* 187, 3171–9.
- Pluschkell, S.B., Flickinger, M.C., 2002. Dissimilation of $[(^{13}\text{C})]$ methanol by continuous cultures of *Bacillus methanolicus* MGA3 at 50 degrees C studied by (^{13}C) NMR and isotope-ratio mass spectrometry. *Microbiology* 148, 3223–33.
- Ren, C., Gu, Y., Hu, S., Wu, Y., Wang, P., Yang, Y., Yang, C., Yang, S., Jiang, W., 2010. Identification and inactivation of pleiotropic regulator CcpA to eliminate glucose repression of xylose utilization in *Clostridium acetobutylicum*. *Metab. Eng.* 12, 446–454.
- Rother, M., Metcalf, W.W., 2004. Anaerobic growth of *Methanosarcina acetivorans* C2A on carbon monoxide: an unusual way of life for a methanogenic archaeon. *Proc. Natl. Acad. Sci. U. S. A.* 101, 16929–34.
- Salis, H.M., Mirsky, E. a, Voigt, C. a, 2009. Automated design of synthetic ribosome binding sites to control protein expression. *Nat. Biotechnol.* 27, 946–50.
- Sandberg, T.E., Long, C.P., Gonzalez, J.E., Feist, A.M., Antoniewicz, M.R., Palsson, B.O., 2016. Evolution of *E. coli* on $[\text{U-}^{13}\text{C}]$ glucose reveals a negligible isotopic influence on metabolism and physiology. *PLoS One* 11, 1–14.
- Satish Kumar, V., Ferry, J.G., Maranas, C.D., 2011. Metabolic reconstruction of the archaeon methanogen *Methanosarcina acetivorans*. *BMC Syst. Biol.* 5, 28.

- Schmidt, A., Kochanowski, K., Vedelaar, S., Ahrné, E., Volkmer, B., Callipo, L., Knoop, K., Bauer, M., Aebersold, R., Heinemann, M., 2016. The quantitative and condition-dependent *Escherichia coli* proteome. *Nat. Biotechnol.* 34, 104–110.
- Schrader, J., Schilling, M., Holtmann, D., Sell, D., Filho, M.V., Marx, A., Vorholt, J., 2009. Methanol-based industrial biotechnology: current status and future perspectives of methylotrophic bacteria. *Trends Biotechnol.* 27, 107–15.
- Segre, D., Vitkup, D., Church, G.M., 2002. Analysis of optimality in natural and perturbed.
- Shlomi, T., Berkman, O., Ruppin, E., 2005. Regulatory on/off minimization of metabolic flux. *PNAS.* 102, 7695–7700.
- Smith, M.R., Mah, R.A., 1978. Growth and Methanogenesis by *Methanosarcina* Strain 227 on Acetate and Methanol. *Appl. Environ. Microbiol.* 36.
- Soo, V.W.C., Tripathi, A., Mcanulty, M.J., Zhu, F., Zhang, L., Smith, P.B., Agrawal, S., Salis, H.M., Patterson, A.D., Wood, T.K., 2016. Reversing Methanogenesis to Capture Methane for Liquid Biofuels. *Microb. Cell Fact.* 1–14.
- Sund, C.J., Liu, S., Germane, K.L., Servinsky, M.D., Gerlach, E.S., Hurley, M.M., 2015. Phosphoketolase flux in *Clostridium acetobutylicum* during growth on L-arabinose. *Microbiology* 161, 430–440.
- Tani, H.T., Khodursky, A., Blumenthal, R.M., Brown, P.O., Matthews, R.G., 2002. Adaptation to famine: A family of stationary-phase genes revealed by microarray analysis. *Proc. Natl. Acad. Sci.* 99, 13471–13476.
- Tao, H.A.N., Gonzalez, R., Martinez, A., Rodriguez, M., Ingram, L.O., Preston, J.F., Shanmugam, K.T., Ackerlind, J.B., 2001. Engineering a Homo-Ethanol Pathway in *Escherichia coli*: Increased Glycolytic Flux and Levels of Expression of Glycolytic Genes during Xylose Fermentation 183, 2979–2988.
- Taymaz-Nikerel, H., Borujeni, A.E., Verheijen, P.J.T., Heijnen, J.J., van Gulik, W.M., 2010. Genome-derived minimal metabolic models for *Escherichia coli* MG1655 with estimated in vivo respiratory ATP stoichiometry. *Biotechnol. Bioeng.* 107, 369–81.
- Toya, Y., Nakahigashi, K., Tomita, M., Shimizu, K., 2012. Metabolic regulation analysis of wild-type and *arcA* mutant *Escherichia coli* under nitrate conditions using different levels of omics data. *Mol. Biosyst.* 8, 2593–604.

- Traxler, M.F., Zacharia, V.M., Marquardt, S., Summers, S.M., Nguyen, H.T., Stark, S.E., Conway, T., 2011. Discretely calibrated regulatory loops controlled by ppGpp partition gene induction across the “feast to famine” gradient in *Escherichia coli*. *Mol. Microbiol.* 79, 830–845.
- Wang, Q., Wu, J., Friedberg, D., Plakto, J., Calvo, J.M., 1994. Regulation of the *Escherichia coli* *lrp* gene. *J. Bacteriol.* 176, 1831–1839.
- Wasylenko, T.M., Stephanopoulos, G., 2015. Metabolomic and (13)C-metabolic flux analysis of a xylose-consuming *Saccharomyces cerevisiae* strain expressing xylose isomerase. *Biotechnol. Bioeng.* 112, 470–83.
- Welander, P. V, Metcalf, W.W., 2008. Mutagenesis of the C1 oxidation pathway in *Methanosarcina barkeri*: new insights into the Mtr/Mer bypass pathway. *J. Bacteriol.* 190, 1928–36.
- Welander, P. V, Metcalf, W.W., 2005. Loss of the *mtr* operon in *Methanosarcina* blocks growth on methanol, but not methanogenesis, and reveals an unknown methanogenic pathway. *Proc. Natl. Acad. Sci. U. S. A.* 102, 10664–10669.
- Whitaker, W.B., Jones, J.A., Bennett, K., Gonzalez, J., Vernacchio, V.R., Collins, S.M., Palmer, M. a., Schmidt, S., Antoniewicz, M.R., Koffas, M. a., Papoutsakis, E.T., 2017. Engineering the Biological Conversion of Methanol to Specialty Chemicals in *Escherichia coli*. *Metab. Eng.* 39, 49–59.
- Whitaker, W.B., Sandoval, N.R., Bennett, R.K., Fast, A.G., Papoutsakis, E.T., 2015. Synthetic methylotrophy: engineering the production of biofuels and chemicals based on the biology of aerobic methanol utilization. *Curr. Opin. Biotechnol.* 33, 165–175.
- Witthoff, S., Schmitz, K., Niedenführ, S., Nöh, K., Noack, S., Bott, M., Marienhagen, J., 2015. Metabolic Engineering of *Corynebacterium glutamicum* for the Metabolization of Methanol. *Appl. Environ. Microbiol.* 81, 2215–2225.
- Woolston, B.M., Edgar, S., Stephanopoulos, G., 2013. Metabolic Engineering: Past and Future. *Annu. Rev. Chem. Biomol. Eng.* 4, 259–288.
- Xu, P., Vansiri, A., Bhan, N., Koffas, M. a G., 2012. EPathBrick: A synthetic biology platform for engineering metabolic pathways in *E. coli*. *ACS Synth. Biol.* 1, 256–266.

- Yishai, O., Goldbach, L., Tenenboim, H., Lindner, S.N., Bar-Even, A., 2017. Engineered assimilation of exogenous and endogenous formate in *Escherichia coli*. ACS Synth. Biol. 6(9) 1722-1731
- Yoo, H., Stephanopoulos, G., Kelleher, J.K., 2004. Quantifying carbon sources for de novo lipogenesis in wild-type and IRS-1 knockout brown adipocytes. J. Lipid Res. 45, 1324–1332.
- Young, E.M., Tong, a., Bui, H., Spofford, C., Alper, H.S., 2014. Rewiring yeast sugar transporter preference through modifying a conserved protein motif. Proc. Natl. Acad. Sci. 111, 131–136.
- Young, J.D., Shastri, A. a, Stephanopoulos, G., Morgan, J. a, 2011. Mapping photoautotrophic metabolism with isotopically nonstationary (13)C flux analysis. Metab. Eng. 13, 656–65.
- Young, J.D., Walther, J.L., Antoniewicz, M.R., Yoo, H., 2008. An Elementary Metabolite Unit (EMU) Based Method of Isotopically Nonstationary Flux Analysis 99, 686–699.

Appendix A

SUPPLEMENTARY DATA FOR CHAPTER 2

Table A.1 Biomass composition (% Dry Weight) of *E. coli* grown on glucose or xylose under aerobic and anaerobic conditions.

	Aerobic Glucose	Aerobic Xylose	Anaerobic Glucose	Anaerobic Xylose
Protein (%DW)	50.5	61.4	51.6	56.5
RNA (%DW)	17.5	18.1	11.4	9.2
Lipid (%DW)	6.2	6.1	6.4	6.1
Glycogen (%DW)	2.1	5.0	8.7	5.4

Table A.2 Fatty acid composition (umol/gFA) of *E. coli* grown on glucose or xylose under aerobic and anaerobic conditions.

umol/gFA	Aerobic Glucose	Aerobic Xylose	Anaerobic Glucose	Anaerobic Xylose
C14:0	341	346	409	588
C16:1	1225	1101	891	1337
C16:0	1096	1173	1386	1292
C18:1	850	916	754	357
C18:0	135	107	212	146

Table A.3 Amino acid composition (umol/gProtein) of *E. coli* grown on glucose or xylose under aerobic and anaerobic conditions.

umol/gProtein	Aerobic Glucose	Aerobic Xylose	Anaerobic Glucose	Anaerobic Xylose
Ala	984	992	1040	928
Gly	872	860	839	824
Val	621	612	615	612
Leu	709	706	712	734
Ile	430	423	429	435
Pro	332	326	331	332
Met	209	209	213	223
Ser	462	457	473	474
Thr	484	480	495	501
Phe	289	290	287	300
Asx	921	939	938	946
Glx	979	1009	969	993
Lys	575	569	580	567
His	166	164	160	157
Tyr	268	271	271	282
Arg	567	559	546	536
Cys	176	173	169	166
Trp	109	107	105	103

Table A.4 Metabolic network models for ¹³C-metabolic flux analysis of *E. coli* grown on glucose or xylose under aerobic and anaerobic conditions.

AG = Aerobic Glucose Model
 AX = Aerobic Xylose Model
 NG = Anaerobic Glucose Model
 NX = Anaerobic Xylose Model

Glycolysis

(1) [AG NG] Gluc.ext (abcdef) + PEP (ghi) -> G6P (abcdef) +
 Pyr(ghi)

(2) [AG AX NG NX] G6P (abcdef) \rightleftharpoons F6P (abcdef)
 (3) [AG AX NG NX] F6P (abcdef) + ATP \rightleftharpoons FBP (abcdef)
 (4) [AG AX NG NX] FBP (abcdef) \rightleftharpoons DHAP (cba) + GAP (def)
 (5) [AG AX NG NX] DHAP (abc) \rightleftharpoons GAP (abc)
 (6) [AG AX NG NX] GAP (abc) \rightleftharpoons 3PG (abc) + ATP + NADH
 (7) [AG AX NG NX] 3PG (abc) \rightleftharpoons PEP (abc)
 (8) [AG AX NG NX] PEP (abc) \rightleftharpoons Pyr (abc) + ATP

Pentose Phosphate Pathway

(9) [AG AX NG NX] G6P (abcdef) \rightarrow 6PG (abcdef) + NADPH
 (10) [AG AX NG NX] 6PG (abcdef) \rightarrow Ru5P (bcdef) + CO₂ (a) + NADPH
 (11) [AG AX NG NX] Ru5P (abcde) \rightleftharpoons X5P (abcde)
 (12) [AG AX NG NX] Ru5P (abcde) \rightleftharpoons R5P (abcde)
 (13) [AG AX NG NX] X5P (abcde) \rightleftharpoons TK-C2 (ab) + GAP (cde)
 (14) [AG AX NG NX] F6P (abcdef) \rightleftharpoons TK-C2 (ab) + E4P (cdef)
 (15) [AG AX NG NX] S7P (abcdefg) \rightleftharpoons TK-C2 (ab) + R5P (cdefg)
 (16) [AG AX NG NX] F6P (abcdef) \rightleftharpoons TA-C3 (abc) + GAP (def)
 (17) [AG AX NG NX] S7P (abcdefg) \rightleftharpoons TA-C3 (abc) + E4P (defg)

Entner-Doudoroff Pathway

(18) [AG AX NG NX] 6PG (abcdef) \rightarrow KDPG (abcdef)
 (19) [AG AX NG NX] KDPG (abcdef) \rightarrow Pyr (abc) + GAP (def)

Xylose Metabolism

(20) [AX NX] Xyl (abcde) \rightarrow Xylu (abcde)
 (21) [AX NX] Xylu (abcde) + ATP \rightarrow X5P (abcde)

TCA Cycle

(22) [AG AX NG NX] Pyr (abc) \rightarrow AcCoA (bc) + CO₂ (a) + NADH
 (23) [AG AX NG NX] OAC (abcd) + AcCoA (ef) \rightarrow Cit (dcbfca)
 (24) [AG AX NG NX] Cit (abcdef) \rightleftharpoons ICit (abcdef)
 (25) [AG AX NG NX] ICit (abcdef) \rightarrow AKG (abcde) + CO₂ (f) + NADPH
 (26) [AG AX NG NX] AKG (abcde) \rightarrow SucCoA (bcde) + CO₂ (a) + NADH
 (27) [AG AX NG NX] SucCoA (abcd) \rightleftharpoons Suc ($\frac{1}{2}$ abcd + $\frac{1}{2}$ dcba) + ATP
 (28) [AG AX NG NX] Suc ($\frac{1}{2}$ abcd + $\frac{1}{2}$ dcba) \rightleftharpoons Fum ($\frac{1}{2}$ abcd + $\frac{1}{2}$ dcba) + FADH₂
 (29) [AG AX NG NX] Fum ($\frac{1}{2}$ abcd + $\frac{1}{2}$ dcba) \rightleftharpoons Mal (abcd)
 (30) [AG AX NG NX] Mal (abcd) \rightleftharpoons OAC (abcd) + NADH

Glyoxylate Shunt

(31) [AG AX NG NX] ICit (abcdef) \rightleftharpoons Glyox (ab) + Suc ($\frac{1}{2}$ edcf + $\frac{1}{2}$ fcde)
 (32) [AG AX NG NX] Glyox (ab) + AcCoA (cd) \rightarrow Mal (abcd)

Amphibolic Reactions

- (33) [AG AX NG NX] Mal (abcd) -> Pyr (abc) + CO₂ (d) + NADPH
(34) [AG AX NG NX] PEP (abc) + CO₂ (d) -> OAC (abcd)
(35) [AG AX] OAC (abcd) + ATP -> PEP (abc) + CO₂ (d)

Fermentation Reactions

- (36) [AG AX NG NX] AcCoA (ab) <=> Ac (ab) + ATP
(37) [NG NX] AcCoA (ab) + NADH <=> Acetal (ab)
(38) [NG NX] Acetal (ab) + NADH <=> EtOH (ab)
(39) [NG NX] Form (a) -> CO₂ (a) + H₂
(40) [NG NX] Pyr (abc) <=> AcCoA (bc) + Form (a)

Amino Acid Biosynthesis

- (41) [AG AX NG NX] AKG (abcde) + NADPH + NH₃ -> Glu (abcde)
(42) [AG AX NG NX] Glu (abcde) + ATP + NH₃ -> Gln (abcde)
(43) [AG AX NG NX] Glu (abcde) + ATP + 2 NADPH -> Pro (abcde)
(44) [AG AX NG NX] Glu (abcde) + CO₂ (f) + Gln (ghijk) + Asp (lmno) + AcCoA (pq) + 5 ATP + NADPH -> Arg (abcdef) + AKG (ghijk) + Fum (lmno) + Ac (pq)
(45) [AG AX NG NX] OAC (abcd) + Glu (efghi) -> Asp (abcd) + AKG (efghi)
(46) [AG AX NG NX] Asp (abcd) + 2 ATP + NH₃ -> Asn (abcd)
(47) [AG AX NG NX] Pyr (abc) + Glu (defgh) -> Ala (abc) + AKG (defgh)
(48) [AG AX NG NX] 3PG (abc) + Glu (defgh) -> Ser (abc) + AKG (defgh) + NADH
(49) [AG AX NG NX] Ser (abc) <=> Gly (ab) + MEETHF (c)
(50) [AG AX NG NX] Gly (ab) <=> CO₂ (a) + MEETHF (b) + NADH + NH₃
(51) [AG AX NG NX] Thr (abcd) -> Gly (ab) + AcCoA (cd) + NADH
(52) [AG AX NG NX] Ser (abc) + AcCoA (de) + 3 ATP + 4 NADPH + SO₄ -> Cys (abc) + Ac (de)
(53) [AG AX NG NX] Asp (abcd) + Pyr (efg) + Glu (hijkl) + SucCoA (mnop) + ATP + 2 NADPH -> LL-DAP (½ abcdgfe + ½ efgdcba) + AKG (hijkl) + Suc (½ mnop + ½ ponm)
(54) [AG AX NG NX] LL-DAP (½ abcdefg + ½ gfedcba) -> Lys (abcdef) + CO₂ (g)
(55) [AG AX NG NX] Asp (abcd) + 2 ATP + 2 NADPH -> Thr (abcd)
(56) [AG AX NG NX] Asp (abcd) + METHF (e) + Cys (fgh) + SucCoA (ijkl) + ATP + 2 NADPH -> Met (abcde) + Pyr (fgh) + Suc (½ ijkl + ½ lkji) + NH₃
(57) [AG AX NG NX] Pyr (abc) + Pyr (def) + Glu (ghijk) + NADPH -> Val (abcef) + CO₂ (d) + AKG (ghijk)
(58) [AG AX NG NX] AcCoA (ab) + Pyr (cde) + Pyr (fgh) + Glu (ijklm) + NADPH -> Leu (abdghe) + CO₂ (c) + CO₂ (f) + AKG (ijklm) + NADH

- (59) [AG AX NG NX] Thr (abcd) + Pyr (efg) + Glu (hijkl) + NADPH -> Ile (abfcgd) + CO₂ (e) + AKG (hijkl) + NH₃
- (60) [AG AX NG NX] PEP (abc) + PEP (def) + E4P (ghij) + Glu (klmno) + ATP + NADPH -> Phe (abcefghij) + CO₂ (d) + AKG (klmno)
- (61) [AG AX NG NX] PEP (abc) + PEP (def) + E4P (ghij) + Glu (klmno) + ATP + NADPH -> Tyr (abcefghij) + CO₂ (d) + AKG (klmno) + NADH
- (62) [AG AX NG NX] Ser (abc) + R5P (defgh) + PEP (ijk) + E4P (lmno) + PEP (pqr) + Gln (stuvw) + 3 ATP + NADPH -> Trp (abcdklmnoj) + CO₂ (i) + GAP (fgh) + Pyr (pqr) + Glu (stuvw)
- (63) [AG AX NG NX] R5P (abcde) + FTTHF (f) + Gln (ghijk) + Asp (lmno) + 5 ATP -> His (edcbaf) + AKG (ghijk) + Fum (lmno) + 2 NADH

One-carbon Metabolism

- (64) [AG AX NG NX] MEETHF (a) + NADH -> METHF (a)
- (65) [AG AX NG NX] MEETHF (a) -> FTTHF (a) + NADPH
- (66) [NG NX] Form (a) + ATP -> FTTHF (a)

Oxidation Phosphorylation

- (67) [AG AX] NADH + 1/2 O₂ -> 2 ATP
- (68) [AG AX] FADH₂ + 1/2 O₂ -> 1 ATP

Transhydrogenation

- (69) [AG AX NG NX] NADH <=> NADPH
- (70) [NG NX] FADH₂ <=> NADH

ATP Hydrolysis

- (71) [AG AX NG NX] ATP -> ATP.ext

Transport

- (72) [AX NX] Xyl.ext (abcde) + ATP -> Xyl (abcde)
- (73) [AG AX NG NX] Ac (ab) -> Ac.ext (ab)
- (74) [NG NX] Form (a) -> Form.ext (a)
- (75) [NG NX] EtOH (ab) -> EtOH.ext (ab)
- (76) [NG NX] Suc (abcd) -> Suc.ext (abcd)
- (77) [AG AX NG NX] CO₂ (a) -> CO₂.ext (a)
- (78) [NG NX] H₂ -> H₂.ext
- (79) [AG AX] O₂.ext -> O₂
- (80) [AG AX NG NX] NH₃.ext -> NH₃
- (81) [AG AX NG NX] SO₄.ext -> SO₄

Biomass Formation

(82) [AG]

0.49731 Ala + 0.28651 Arg + 0.2326 Asn + 0.2326 Asp
+ 0.088707 Cys + 0.24738 Glu + 0.24738 Gln +
0.44054 Gly + 0.08398 His + 0.21739 Ile + 0.35853 Leu
+ 0.29077 Lys + 0.10557 Met + 0.14618 Phe + 0.16797
Pro + 0.23355 Ser + 0.24446 Thr + 0.13526 Tyr +
0.31392 Val + 0.18148 G6P + 0.0709 F6P + 0.10233
GAP + 0.53768 3PG + 0.0828 Pyr + 2.0826 AcCoA +
0.0869 AKG + 0.30055 OAC + 0.05506 Trp + 0.65979
R5P + 0.0511 PEP + 30.7648 ATP + 4.5162 NADPH +
0.38804 MEETHF + 1.2644 NAD -> 1.2644 NADH +
30.7648 ADP + 30.7648 Pi + 4.5162 NADP + 0.38804
THF + 35.476 Biomass

(82) [AX]

0.60876 Ala + 0.34319 Arg + 0.28805 Asn + 0.28805
Asp + 0.10625 Cys + 0.30972 Glu + 0.30972 Gln +
0.52767 Gly + 0.10059 His + 0.25947 Ile + 0.43365 Leu
+ 0.34911 Lys + 0.12817 Met + 0.17808 Phe + 0.2003
Pro + 0.28028 Ser + 0.29473 Thr + 0.16619 Tyr +
0.37585 Val + 0.35965 G6P + 0.0709 F6P + 0.099809
GAP + 0.54618 3PG + 0.0828 Pyr + 2.0431 AcCoA +
0.0869 AKG + 0.30839 OAC + 0.06595 Trp + 0.67866
R5P + 0.0511 PEP + 35.5766 ATP + 4.4615 NADPH +
0.39907 MEETHF + 1.2949 NAD -> 1.2949 NADH +
35.5766 ADP + 35.5766 Pi + 4.4615 NADP + 0.39907
THF + 41.3527 Biomass

(82) [NG]

0.53667 Ala + 0.28153 Arg + 0.24198 Asn + 0.24198
Asp + 0.087164 Cys + 0.25003 Glu + 0.25003 Gln +
0.43287 Gly + 0.082519 His + 0.22129 Ile + 0.36735
Leu + 0.29899 Lys + 0.10968 Met + 0.14783 Phe +
0.17097 Pro + 0.24423 Ser + 0.25532 Thr + 0.14 Tyr +
0.31718 Val + 0.58985 G6P + 0.0709 F6P + 0.10388
GAP + 0.4299 3PG + 0.0828 Pyr + 2.1082 AcCoA +
0.0869 AKG + 0.22277 OAC + 0.054102 Trp + 0.47269
R5P + 0.0511 PEP + 29.6686 ATP + 4.4607 NADPH +
0.27872 MEETHF + 0.93793 NAD -> 0.93793 NADH
+ 29.6686 ADP + 29.6686 Pi + 4.4607 NADP +
0.27872 THF + 36.7639 Biomass

(82) [NX]

0.52453 Ala + 0.30305 Arg + 0.26737 Asn + 0.26737
Asp + 0.093827 Cys + 0.28068 Glu + 0.28068 Gln +

0.46596 Gly + 0.088826 His + 0.24595 Ile + 0.4146 Leu
+ 0.32059 Lys + 0.12617 Met + 0.16943 Phe + 0.18784
Pro + 0.26816 Ser + 0.28294 Thr + 0.15956 Tyr + 0.346
Val + 0.38483 G6P + 0.0709 F6P + 0.095676 GAP +
0.3828 3PG + 0.0828 Pyr + 1.9457 AcCoA + 0.0869
AKG + 0.1951 OAC + 0.058237 Trp + 0.40613 R5P +
0.0511 PEP + 30.0681 ATP + 4.1089 NADPH +
0.23982 MEETHF + 0.81305 NAD -> 0.81305 NADH
+ 30.0681 ADP + 30.0681 Pi + 4.1089 NADP +
0.23982 THF + 36.7571 Biomass

Labeling dilution from lipid turnover and external acetate

(83) [AG AX NG NX] AcCoA.unlabeled (ab) + AcCoA (cd) -> AcCoA (ab) +
AcCoA.out (cd)
(84) [NG NX] GAP.unlabeled (abc) + GAP (def) -> GAP (abc) +
GAP.out (def)

Table A.5 Mass isotopomer distributions from parallel labeling experiments with *E. coli* grown on glucose under aerobic and anaerobic conditions.

Condition	Aerobic Glucose			Anaerobic Glucose		
	[U- ¹³ C]	[1,2- ¹³ C]	[1,6- ¹³ C]	[U- ¹³ C]	[1,2- ¹³ C]	[1,6- ¹³ C]
Ala232 (M0)	11.8	47.0	19.1	11.4	45.4	16.7
Ala232 (M1)	3.7	14.5	61.0	3.7	11.6	63.4
Ala232 (M2)	65.8	30.3	13.9	66.1	34.0	13.8
Ala232 (M3)	13.1	5.9	5.3	13.2	6.4	5.4
Ala232 (M4)	5.6	2.3	0.7	5.6	2.6	0.7
Ala260 (M0)	11.6	46.3	18.6	10.9	44.6	16.4
Ala260 (M1)	3.0	13.1	60.3	3.1	11.7	62.6
Ala260 (M2)	2.8	30.8	14.5	3.1	33.4	14.4
Ala260 (M3)	64.2	6.8	5.6	64.3	7.1	5.6
Ala260 (M4)	12.8	2.6	0.9	12.9	2.8	0.8
Ala260 (M5)	5.6	0.4	0.2	5.7	0.4	0.1
Gly218 (M0)	12.7	51.4	75.6	18.3	48.9	76.3
Gly218 (M1)	67.7	36.3	16.7	63.1	38.4	16.0
Gly218 (M2)	13.9	9.5	6.8	13.3	9.8	6.8
Gly218 (M3)	5.7	2.8	1.0	5.3	3.0	0.9

Gly246 (M0)	11.9	49.0	73.8	17.5	47.8	74.8
Gly246 (M1)	4.2	36.6	17.5	5.9	38.1	16.8
Gly246 (M2)	65.4	10.7	7.3	59.6	10.4	7.1
Gly246 (M3)	12.9	3.2	1.2	11.8	3.2	1.1
Gly246 (M4)	5.7	0.5	0.2	5.2	0.5	0.2
Val260 (M0)	11.9	32.1	15.1	11.7	30.1	15.1
Val260 (M1)	3.0	12.1	13.2	2.9	8.8	9.6
Val260 (M2)	1.5	30.2	53.3	2.0	32.6	56.7
Val260 (M3)	2.2	9.7	12.8	2.4	8.3	12.7
Val260 (M4)	63.0	12.5	4.8	62.6	16.0	5.0
Val260 (M5)	13.0	2.4	0.7	12.9	3.0	0.7
Val260 (M6)	5.5	0.9	0.1	5.4	1.2	0.1
Val288 (M0)	11.9	31.8	15.0	11.7	29.7	15.0
Val288 (M1)	3.1	11.3	12.9	3.0	8.8	9.5
Val288 (M2)	1.3	30.3	52.9	1.3	32.1	56.2
Val288 (M3)	0.4	9.6	13.1	1.0	8.5	13.0
Val288 (M4)	2.5	13.0	5.1	3.0	15.9	5.2
Val288 (M5)	62.8	2.9	0.8	62.3	3.3	0.8
Val288 (M6)	12.5	1.1	0.2	12.4	1.5	0.3
Val288 (M7)	5.5	0.2	0.0	5.4	0.2	0.0
Leu274 (M0)	12.1	24.6	15.0	11.8	22.7	15.2
Leu274 (M1)	3.1	16.2	5.6	3.1	14.1	4.7
Leu274 (M2)	1.2	21.4	16.3	1.2	20.6	11.5
Leu274 (M3)	0.5	17.9	46.7	1.0	18.9	51.7
Leu274 (M4)	2.9	11.1	11.3	4.3	12.2	11.5
Leu274 (M5)	62.4	6.7	4.2	61.0	8.9	4.6
Leu274 (M6)	12.5	1.5	0.6	12.3	2.0	0.6
Leu274 (M7)	5.3	0.4	0.1	5.2	0.6	0.1
Pro258 (M0)	12.0	35.5	21.9	12.3	46.8	38.8
Pro258 (M1)	3.0	17.5	16.9	3.2	12.3	14.0
Pro258 (M2)	2.1	24.6	38.1	3.3	22.9	36.0
Pro258 (M3)	2.7	11.3	16.8	2.8	5.6	7.8
Pro258 (M4)	62.4	8.7	4.9	61.0	9.8	2.9
Pro258 (M5)	12.4	1.9	1.2	12.1	2.0	0.5
Pro258 (M6)	5.3	0.6	0.2	5.2	0.7	0.1
Ser390 (M0)	10.9	36.3	17.5	10.5	32.8	14.6
Ser390 (M1)	4.1	22.2	53.3	5.5	23.7	55.4

Ser390 (M2)	3.3	27.9	18.8	4.1	29.2	19.2
Ser390 (M3)	55.9	9.2	8.2	54.7	9.7	8.5
Ser390 (M4)	17.4	3.6	1.8	17.1	3.8	1.9
Ser390 (M5)	8.3	0.8	0.4	8.1	0.8	0.4
Thr376 (M0)	10.7	36.9	21.1	10.1	35.1	16.2
Thr376 (M1)	4.2	22.1	37.0	4.4	17.6	50.2
Thr376 (M2)	6.9	23.9	26.1	33.9	28.0	21.7
Thr376 (M3)	53.3	11.7	11.1	34.5	13.0	8.9
Thr376 (M4)	16.9	4.2	3.6	12.4	4.9	2.3
Thr376 (M5)	7.9	1.3	1.0	4.7	1.5	0.7
Phe302 (M0)	12.9	48.1	71.7	12.8	45.4	72.2
Phe302 (M1)	4.6	37.0	19.4	4.6	39.3	19.1
Phe302 (M2)	66.6	11.6	7.6	66.7	11.7	7.4
Phe302 (M3)	16.0	3.4	1.3	16.0	3.6	1.3
Phe308 (M0)	14.3	25.7	14.3	14.3	24.2	14.8
Phe308 (M1)	4.1	11.2	5.2	4.0	9.2	5.1
Phe308 (M2)	1.5	24.6	12.0	1.5	25.9	7.6
Phe308 (M3)	0.3	11.6	49.3	0.3	10.3	52.7
Phe308 (M4)	0.1	15.2	13.4	0.1	17.2	13.7
Phe308 (M5)	0.1	6.2	4.8	0.1	6.7	5.1
Phe308 (M6)	0.3	3.7	0.8	0.4	4.3	0.9
Phe308 (M7)	4.4	1.3	0.1	4.6	1.7	0.1
Phe308 (M8)	75.0	0.4	0.0	74.8	0.4	0.0
Phe336 (M0)	13.9	25.2	14.1	13.8	24.1	14.4
Phe336 (M1)	4.1	10.6	5.2	4.1	8.8	4.8
Phe336 (M2)	1.5	24.7	11.8	1.5	25.8	7.6
Phe336 (M3)	0.3	11.6	48.9	0.3	10.5	52.6
Phe336 (M4)	0.1	15.4	13.8	0.1	17.2	14.1
Phe336 (M5)	0.0	6.5	5.1	0.0	7.0	5.3
Phe336 (M6)	0.1	3.9	0.9	0.1	4.3	0.9
Phe336 (M7)	0.5	1.5	0.2	0.6	1.8	0.2
Phe336 (M8)	5.0	0.4	0.0	5.2	0.5	0.0
Phe336 (M9)	74.5	0.1	0.0	74.3	0.1	0.0
Asp390 (M0)	11.1	36.6	20.5	10.7	35.0	15.9
Asp390 (M1)	4.2	22.0	37.2	4.3	17.5	50.5
Asp390 (M2)	6.9	24.1	26.3	33.2	28.1	21.7
Asp390 (M3)	53.1	11.8	11.3	34.6	13.0	9.0
Asp390 (M4)	16.8	4.2	3.7	12.4	5.0	2.4

Asp390 (M5)	7.9	1.2	1.0	4.7	1.4	0.5
Asp418 (M0)	10.9	34.7	19.9	10.2	34.3	15.8
Asp418 (M1)	3.9	19.1	32.3	4.0	17.7	49.5
Asp418 (M2)	2.6	24.5	28.0	3.0	27.6	22.3
Asp418 (M3)	7.7	12.3	13.5	35.2	13.4	9.3
Asp418 (M4)	50.9	6.7	4.7	31.4	5.2	2.5
Asp418 (M5)	16.3	2.1	1.3	11.8	1.5	0.6
Asp418 (M6)	7.7	0.6	0.3	4.3	0.3	0.1
Glu330 (M0)	11.1	32.2	19.1	11.2	43.1	35.3
Glu330 (M1)	3.2	17.9	16.5	3.3	13.4	14.6
Glu330 (M2)	2.1	25.0	38.1	3.3	23.6	36.4
Glu330 (M3)	2.6	12.4	18.5	2.9	6.6	9.4
Glu330 (M4)	60.5	9.3	5.8	59.2	10.2	3.5
Glu330 (M5)	14.6	2.4	1.5	14.3	2.4	0.7
Glu330 (M6)	5.9	0.8	0.3	5.8	0.9	0.1
Glu432 (M0)	10.1	27.3	16.9	10.1	36.5	31.2
Glu432 (M1)	3.7	16.3	14.8	3.7	15.9	15.3
Glu432 (M2)	1.9	23.5	31.3	2.7	21.0	32.5
Glu432 (M3)	1.1	14.4	22.3	2.5	10.2	13.5
Glu432 (M4)	6.1	11.0	10.1	31.5	10.0	5.6
Glu432 (M5)	52.5	5.2	3.4	32.9	4.4	1.5
Glu432 (M6)	16.7	1.8	0.9	12.0	1.6	0.3
Glu432 (M7)	7.9	0.5	0.2	4.6	0.4	0.1
Tyr302 (M0)	13.5	47.8	71.6	13.1	44.9	n/a
Tyr302 (M1)	4.8	37.1	19.4	4.7	39.2	n/a
Tyr302 (M2)	66.0	11.7	7.6	66.3	12.1	n/a
Tyr302 (M3)	15.7	3.4	1.4	15.9	3.7	n/a
RNA_Rib173 (M0)	17.9	66.9	19.6	21.7	60.4	21.9
RNA_Rib173 (M1)	3.4	8.9	73.1	3.8	6.9	71.3
RNA_Rib173 (M2)	73.5	22.6	6.4	69.5	30.6	6.0
RNA_Rib173 (M3)	5.1	1.6	0.9	5.0	2.1	0.9
RNA_Rib284 (M0)	15.7	16.0	73.6	19.4	17.8	65.4

RNA_Rib284 (M1)	2.4	46.8	21.1	3.0	33.2	28.7
RNA_Rib284 (M2)	0.6	27.3	3.8	0.9	32.3	4.5
RNA_Rib284 (M3)	2.2	8.3	1.0	2.3	14.2	1.0
RNA_Rib284 (M4)	71.6	1.2	0.3	67.2	2.0	0.3
RNA_Rib284 (M5)	7.5	0.3	0.1	7.1	0.4	0.1
Glycogen_Gluc1 73 (M0)	23.5	86.8	52.7	6.2	87.9	31.3
Glycogen_Gluc1 73 (M1)	4.1	8.5	43.0	3.0	8.2	62.8
Glycogen_Gluc1 73 (M2)	67.6	4.4	3.8	84.8	3.6	5.2
Glycogen_Gluc1 73 (M3)	4.8	0.4	0.5	6.0	0.3	0.7
Glycogen_Gluc3 70 (M0)	20.6	26.6	48.8	4.7	28.8	28.9
Glycogen_Gluc3 70 (M1)	4.1	6.5	41.0	1.0	6.4	57.8
Glycogen_Gluc3 70 (M2)	0.9	52.6	8.2	0.2	51.4	10.8
Glycogen_Gluc3 70 (M3)	0.4	11.5	1.5	0.2	10.7	1.9
Glycogen_Gluc3 70 (M4)	2.3	2.3	0.3	2.9	2.1	0.3
Glycogen_Gluc3 70 (M5)	61.6	0.4	0.1	78.3	0.4	0.1
Glycogen_Gluc3 70 (M6)	8.5	0.1	0.0	10.7	0.1	0.0
Glycogen_Gluc3 70 (M7)	1.6	0.0	0.0	2.0	0.0	0.0
Suc289.ext (M0)					34.8	10.1
Suc289.ext (M1)					15.5	60.1
Suc289.ext (M2)					31.3	20.7
Suc289.ext (M3)					13.1	7.3
Suc289.ext (M4)					4.1	1.5
Suc289.ext (M5)					1.0	0.3

Suc289.ext (M6)		0.2	0.0
C16:0 (M0)	16.0		13.9
C16:0 (M1)	3.0		2.6
C16:0 (M2)	0.4		0.3
C16:0 (M3)	0.0		0.0
C16:0 (M4)	0.0		0.0
C16:0 (M5)	0.0		0.0
C16:0 (M6)	0.0		0.0
C16:0 (M7)	0.0		0.0
C16:0 (M8)	0.0		0.0
C16:0 (M9)	0.0		0.0
C16:0 (M10)	0.0		0.1
C16:0 (M11)	0.1		0.1
C16:0 (M12)	0.2		1.1
C16:0 (M13)	0.4		1.4
C16:0 (M14)	3.5		12.0
C16:0 (M15)	8.1		8.0
C16:0 (M16)	66.9		59.1
C16:0 (M17)	1.1		1.0
C16:0 (M18)	0.3		0.3
Pyr174 (M0)	0.1		0.4
Pyr174 (M1)	0.1		0.3
Pyr174 (M2)	2.4		2.5
Pyr174 (M3)	84.9		85.3
Pyr174 (M4)	8.5		7.8
Pyr174 (M5)	4.0		3.6
PEP453 (M0)	0.2		0.3
PEP453 (M1)	0.5		0.5
PEP453 (M2)	1.7		2.0
PEP453 (M3)	66.5		66.1
PEP453 (M4)	20.7		20.6
PEP453 (M5)	10.4		10.5
3PG585 (M0)	0.3		0.6
3PG585 (M1)	0.2		0.4
3PG585 (M2)	1.5		1.7
3PG585 (M3)	59.3		58.8
3PG585 (M4)	25.1		25.0
3PG585 (M5)	13.6		13.5

Table A.6 Mass isotopomer distributions from parallel labeling experiments with *E. coli* grown on xylose under aerobic and anaerobic conditions.

Condition	Aerobic Xylose			Anaerobic Xylose		
	[U- ¹³ C]	[1,2- ¹³ C]	[5- ¹³ C]	[U- ¹³ C]	[1,2- ¹³ C]	[5- ¹³ C]
Ala232 (M0)	11.3	51.8	36.2	11.9	50.0	38.4
Ala232 (M1)	4.1	13.5	47.2	4.2	11.5	46.2
Ala232 (M2)	65.9	27.5	11.9	65.4	30.4	11.1
Ala232 (M3)	13.1	5.2	4.0	12.9	5.8	3.8
Ala232 (M4)	5.6	2.0	0.6	5.6	2.3	0.5
Ala260 (M0)	11.1	50.5	35.5	9.8	41.4	37.8
Ala260 (M1)	2.9	13.4	46.6	4.6	17.9	45.9
Ala260 (M2)	3.6	7.2	12.6	4.6	14.3	11.5
Ala260 (M3)	64.1	22.5	4.4	63.0	20.5	4.0
Ala260 (M4)	12.7	4.4	0.7	12.5	4.4	0.6
Ala260 (M5)	5.6	1.9	0.1	5.5	1.6	0.1
Gly218 (M0)	12.8	54.1	75.3	15.7	52.2	76.3
Gly218 (M1)	67.7	34.2	16.7	65.3	35.5	15.9
Gly218 (M2)	13.8	9.2	7.0	13.4	9.5	6.9
Gly218 (M3)	5.7	2.6	1.0	5.5	2.8	0.9
Gly246 (M0)	11.7	52.7	73.7	14.6	50.4	75.2
Gly246 (M1)	4.6	13.0	17.4	5.3	13.0	16.4
Gly246 (M2)	65.2	27.2	7.4	62.5	28.8	7.1
Gly246 (M3)	12.8	5.1	1.2	12.2	5.4	1.0
Gly246 (M4)	5.7	2.1	0.3	5.5	2.4	0.3
Val260 (M0)	1.6	36.9	21.5	9.9	34.2	22.0
Val260 (M1)	2.9	11.5	33.1	2.6	8.9	37.1
Val260 (M2)	1.5	30.6	33.0	6.8	33.5	30.3
Val260 (M3)	3.1	8.1	9.1	4.1	7.6	7.9
Val260 (M4)	62.6	10.3	2.8	59.3	12.5	2.4
Val260 (M5)	12.9	2.0	0.5	12.2	2.4	0.4
Val260 (M6)	5.4	0.7	0.1	5.1	0.9	0.1
Val288 (M0)	11.6	36.4	21.1	9.8	29.0	21.7
Val288 (M1)	3.0	11.3	32.4	2.7	12.4	36.5
Val288 (M2)	1.2	18.2	32.6	2.2	20.9	30.0
Val288 (M3)	0.5	17.3	9.5	5.3	18.0	8.0
Val288 (M4)	3.7	5.6	3.2	5.3	8.2	2.7

Val288 (M5)	62.2	8.8	0.6	58.2	8.6	0.4
Val288 (M6)	12.3	1.8	0.5	11.6	2.1	0.6
Val288 (M7)	5.4	0.7	0.1	5.0	0.7	0.1
Leu274 (M0)	11.7	28.4	16.9	9.9	25.5	15.8
Leu274 (M1)	3.0	17.1	20.0	2.9	15.5	24.8
Leu274 (M2)	1.2	22.9	31.6	1.9	23.2	32.7
Leu274 (M3)	0.5	15.8	22.7	5.9	17.1	19.5
Leu274 (M4)	3.9	9.4	6.4	10.2	10.5	5.1
Leu274 (M5)	61.9	5.0	2.1	53.7	6.4	1.7
Leu274 (M6)	12.4	1.2	0.3	11.0	1.4	0.2
Leu274 (M7)	5.3	0.3	0.1	4.5	0.4	0.1
Pro258 (M0)	11.7	33.9	21.1	11.1	35.3	23.4
Pro258 (M1)	2.9	17.1	30.5	3.0	9.4	37.0
Pro258 (M2)	2.1	26.9	32.3	9.5	32.6	29.3
Pro258 (M3)	3.6	10.9	11.8	4.7	7.4	7.6
Pro258 (M4)	62.1	8.7	3.4	55.9	12.1	2.3
Pro258 (M5)	12.3	1.8	0.8	11.0	2.3	0.4
Pro258 (M6)	5.3	0.6	0.1	4.7	0.9	0.1
Ser390 (M0)	10.5	42.1	31.7	9.3	37.1	33.1
Ser390 (M1)	4.0	17.9	43.8	5.2	18.9	43.0
Ser390 (M2)	3.8	11.4	16.3	5.0	14.0	15.9
Ser390 (M3)	55.8	19.7	6.4	55.1	20.7	6.2
Ser390 (M4)	17.5	6.2	1.5	17.3	6.5	1.4
Ser390 (M5)	8.3	2.7	0.3	8.2	2.7	0.3
Thr376 (M0)	10.3	34.9	26.9	8.8	36.4	32.3
Thr376 (M1)	4.1	23.4	39.3	4.9	19.1	43.7
Thr376 (M2)	6.9	19.7	21.8	17.5	25.2	16.0
Thr376 (M3)	53.8	15.1	8.7	46.8	13.1	6.2
Thr376 (M4)	17.0	5.0	2.6	15.4	4.7	1.4
Thr376 (M5)	7.9	1.8	0.7	6.7	1.5	0.3
Phe302 (M0)	12.4	52.3	71.0	12.2	48.7	72.4
Phe302 (M1)	5.0	14.6	20.0	5.3	15.3	18.9
Phe302 (M2)	66.6	26.9	7.7	66.5	29.2	7.4
Phe302 (M3)	16.0	6.1	1.4	16.0	6.7	1.3
Phe308 (M0)	13.8	13.5	14.6	12.0	11.1	11.9
Phe308 (M1)	3.9	22.9	15.9	3.3	22.6	18.9
Phe308 (M2)	1.4	8.0	30.7	1.3	7.0	33.5

Phe308 (M3)	0.3	24.2	27.9	0.3	26.5	25.8
Phe308 (M4)	0.1	10.8	8.0	0.2	10.3	7.3
Phe308 (M5)	0.1	9.9	2.5	1.2	11.3	2.2
Phe308 (M6)	0.4	6.9	0.4	5.1	7.1	0.4
Phe308 (M7)	6.3	1.9	0.1	7.0	2.0	0.1
Phe308 (M8)	73.8	1.9	0.0	69.5	2.0	0.0
Phe336 (M0)	13.4	13.2	14.4	11.1	10.9	11.8
Phe336 (M1)	4.0	22.6	15.3	3.3	21.3	18.1
Phe336 (M2)	1.5	7.8	30.7	1.2	7.2	33.6
Phe336 (M3)	0.3	13.8	27.9	0.3	15.0	26.1
Phe336 (M4)	0.1	18.4	8.4	0.2	19.3	7.6
Phe336 (M5)	0.0	5.9	2.6	0.3	6.1	2.3
Phe336 (M6)	0.1	10.4	0.5	3.0	11.8	0.4
Phe336 (M7)	0.6	4.7	0.1	3.9	4.9	0.1
Phe336 (M8)	7.1	1.6	0.0	7.6	1.6	0.0
Phe336 (M9)	72.9	1.7	0.0	69.1	1.8	0.0
Asp390 (M0)	10.6	34.9	26.8	9.0	36.6	32.2
Asp390 (M1)	4.0	23.3	39.2	4.9	19.2	43.6
Asp390 (M2)	6.8	19.8	21.9	17.3	24.9	16.1
Asp390 (M3)	53.6	15.1	8.8	46.7	13.1	6.3
Asp390 (M4)	16.9	5.0	2.7	15.3	4.7	1.4
Asp390 (M5)	8.0	1.8	0.7	6.7	1.5	0.3
Asp418 (M0)	10.5	31.5	24.7	8.7	34.9	32.0
Asp418 (M1)	3.8	21.4	36.9	4.4	19.7	43.3
Asp418 (M2)	2.6	17.1	23.7	3.3	9.7	16.3
Asp418 (M3)	7.7	14.7	10.3	17.5	20.0	6.5
Asp418 (M4)	51.2	10.5	3.4	44.7	10.4	1.5
Asp418 (M5)	16.4	3.6	0.9	14.9	4.1	0.3
Asp418 (M6)	7.8	1.3	0.2	6.6	1.2	0.1
Glu330 (M0)	10.6	31.4	19.5	9.4	33.3	21.5
Glu330 (M1)	3.1	17.6	30.0	3.0	10.1	36.5
Glu330 (M2)	2.0	27.0	32.6	9.4	32.2	30.0
Glu330 (M3)	3.4	11.9	12.9	5.0	8.6	8.7
Glu330 (M4)	60.4	9.1	4.0	54.8	12.1	2.7
Glu330 (M5)	14.6	2.2	0.9	13.1	2.7	0.5
Glu330 (M6)	5.9	0.7	0.2	5.3	1.0	0.1
Glu432 (M0)	9.7	24.7	16.5	8.3	25.7	19.1
Glu432 (M1)	3.6	16.8	26.0	3.2	13.7	34.1

Glu432 (M2)	1.8	21.9	31.4	3.7	26.1	30.3
Glu432 (M3)	1.1	17.1	16.7	7.0	14.4	11.3
Glu432 (M4)	6.4	10.1	6.8	16.7	11.9	4.1
Glu432 (M5)	52.6	6.5	2.0	41.4	5.7	0.9
Glu432 (M6)	16.8	2.0	0.5	13.6	2.0	0.2
Glu432 (M7)	8.0	0.7	0.1	6.1	0.6	0.0
Tyr302 (M0)	12.8	52.1	70.8	12.3	48.4	72.3
Tyr302 (M1)	5.1	14.7	19.9	5.4	15.2	18.9
Tyr302 (M2)	66.2	27.1	7.8	66.4	29.5	7.5
Tyr302 (M3)	15.9	6.2	1.4	15.9	6.8	1.3
RNA_Rib173 (M0)	17.2	77.1	26.6	19.5	77.6	27.2
RNA_Rib173 (M1)	3.7	7.8	67.1	3.9	8.5	66.6
RNA_Rib173 (M2)	74.1	13.9	5.5	71.7	12.9	5.4
RNA_Rib173 (M3)	5.0	1.2	0.8	5.0	1.0	0.8
RNA_Rib284 (M0)	14.7	13.2	84.0	16.3	15.2	83.7
RNA_Rib284 (M1)	2.3	3.2	12.9	2.6	3.8	13.1
RNA_Rib284 (M2)	0.6	60.2	2.3	1.6	58.7	2.1
RNA_Rib284 (M3)	3.1	8.3	0.7	3.2	8.3	0.8
RNA_Rib284 (M4)	71.9	13.6	0.1	69.1	12.6	0.3
RNA_Rib284 (M5)	7.4	1.4	0.1	7.2	1.4	0.1
Glycogen_Gluc1 73 (M0)	12.4	69.0	42.3	13.0	67.5	36.9
Glycogen_Gluc1 73 (M1)	3.9	7.2	52.7	4.1	7.7	57.6
Glycogen_Gluc1 73 (M2)	78.2	22.2	4.4	77.4	23.1	4.7
Glycogen_Gluc1 73 (M3)	5.5	1.6	0.6	5.5	1.7	0.8

Glycogen_Gluc3 70 (M0)	10.5	19.1	79.0	9.3	11.0	79.2
Glycogen_Gluc3 70 (M1)	2.0	4.2	17.2	1.9	3.1	16.6
Glycogen_Gluc3 70 (M2)	0.4	2.8	3.1	0.6	2.4	3.1
Glycogen_Gluc3 70 (M3)	0.3	43.3	0.5	2.0	50.3	0.6
Glycogen_Gluc3 70 (M4)	3.9	8.0	0.1	4.5	9.0	0.1
Glycogen_Gluc3 70 (M5)	71.3	19.5	0.0	70.2	20.8	0.3
Glycogen_Gluc3 70 (M6)	9.8	2.7	0.0	9.7	2.9	0.1
Glycogen_Gluc3 70 (M7)	1.8	0.5	0.0	1.8	0.5	0.1
Suc289.ext (M0)					34.8	31.6
Suc289.ext (M1)					17.8	49.6
Suc289.ext (M2)					7.8	13.1
Suc289.ext (M3)					24.8	4.8
Suc289.ext (M4)					10.7	0.8
Suc289.ext (M5)					3.3	0.1
Suc289.ext (M6)					0.8	0.0
C16:0 (M0)	14.2			10.3		
C16:0 (M1)	2.7			2.0		
C16:0 (M2)	0.3			0.2		
C16:0 (M3)	0.0			0.0		
C16:0 (M4)	0.0			0.0		
C16:0 (M5)	0.0			0.0		
C16:0 (M6)	0.0			0.0		
C16:0 (M7)	0.0			0.0		
C16:0 (M8)	0.0			0.4		
C16:0 (M9)	0.0			0.3		
C16:0 (M10)	0.0			2.6		
C16:0 (M11)	0.1			1.7		
C16:0 (M12)	0.2			11.2		
C16:0 (M13)	0.5			5.0		
C16:0 (M14)	3.4			27.9		
C16:0 (M15)	11.6			6.6		
C16:0 (M16)	65.5			31.0		
C16:0 (M17)	1.2			0.6		

C16:0 (M18)	0.3	0.1
Pyr174 (M0)	0.2	3.8
Pyr174 (M1)	0.1	2.0
Pyr174 (M2)	3.2	4.0
Pyr174 (M3)	84.9	79.8
Pyr174 (M4)	7.9	7.1
Pyr174 (M5)	3.7	3.3
PEP453 (M0)	0.2	3.1
PEP453 (M1)	0.1	2.2
PEP453 (M2)	2.3	3.6
PEP453 (M3)	66.3	61.9
PEP453 (M4)	20.7	19.3
PEP453 (M5)	10.4	9.8
3PG585 (M0)	0.2	4.2
3PG585 (M1)	0.2	2.9
3PG585 (M2)	2.1	3.7
3PG585 (M3)	58.8	54.2
3PG585 (M4)	25.1	22.7
3PG585 (M5)	13.6	12.2

Table A.7 Results of ^{13}C -MFA for *E. coli* grown on glucose under aerobic and anaerobic conditions. The reaction numbers correspond to the reactions listed in Table A.4. The fluxes are normalized to a substrate uptake rate of 100. 95% confidence intervals of fluxes (LB95 = lower bound, UB95 = upper bound) were determined by evaluating the sensitivity of the minimized SSR to flux variations.

Condition	Aerobic Glucose			Anaerobic Glucose		
SSR	173			33		
Net Fluxes						
Reaction No.	Best Fit	LB95	UB95	Best Fit	LB95	UB95
(1)	100.0	99.9	100.1	100.0	99.9	100.1
(2)	74.2	73.3	75.1	89.3	88.4	90.2
(3)	84.2	83.5	84.8	91.4	90.5	92.6
(4)	84.2	83.5	84.8	91.4	90.5	92.6
(5)	84.2	83.5	84.8	91.4	90.5	92.6

(6)	172.1	171.0	173.1	183.3	181.8	185.6
(7)	159.2	157.7	160.7	176.7	174.5	180.0
(8)	29.1	25.3	31.8	45.5	40.4	51.1
(9)	24.3	23.4	25.1	7.9	7.1	8.5
(10)	24.0	23.1	24.9	7.6	6.7	8.3
(11)	10.6	10.0	11.2	2.5	1.9	3.0
(12)	13.4	13.0	13.8	5.1	4.5	5.5
(13)	10.6	10.0	11.2	2.5	1.9	3.0
(14)	-3.9	-4.2	-3.5	-0.4	-0.7	-0.1
(15)	-6.7	-7.0	-6.4	-2.1	-2.3	-1.8
(16)	-6.7	-7.0	-6.4	-2.1	-2.3	-1.8
(17)	6.7	6.4	7.0	2.1	1.8	2.3
(18)	0.3	0.0	0.9	0.3	0.0	0.9
(19)	0.3	0.0	0.9	0.3	0.0	0.9
(20)	Not in the model			Not in the model		
(21)	Not in the model			Not in the model		
(22)	111.9	108.8	115.0	5.6	0.0	15.1
(23)	26.6	24.1	28.9	5.4	4.6	6.0
(24)	26.6	24.1	28.9	5.4	4.6	6.0
(25)	26.5	22.6	28.9	5.2	4.4	5.8
(26)	17.8	13.7	20.2	0.1	0.0	0.4
(27)	14.4	10.3	17.0	-1.9	-2.2	-1.5
(28)	17.9	15.2	20.2	-14.7	-17.4	-12.0
(29)	21.0	18.4	23.3	-12.9	-15.7	-10.1
(30)	19.4	16.3	21.7	-12.7	-16.5	-9.9
(31)	0.1	0.0	1.8	0.2	0.0	0.5
(32)	0.1	0.0	1.8	0.2	0.0	0.5
(33)	1.7	0.0	4.6	0.0	0.0	4.3
(34)	25.7	23.7	27.4	27.6	24.7	31.4
(35)	1.6	0.0	3.2	Not in the model		
(36)	60.6	56.3	64.8	53.5	47.7	60.6
(37)	Not in the model			Not in the model		
(38)	Not in the model			Not in the model		
(39)	Not in the model			Not in the model		
(40)	Not in the model			Not in the model		
(41)	50.3	48.4	52.4	29.3	24.9	32.0
(42)	5.7	5.5	5.9	3.3	2.8	3.5
(43)	1.4	1.4	1.5	0.8	0.7	0.9
(44)	2.4	2.3	2.5	1.4	1.2	1.5
(45)	14.4	13.7	15.0	8.5	7.2	9.4
(46)	2.0	1.9	2.0	1.2	1.0	1.3
(47)	4.2	4.0	4.4	2.6	2.2	2.8
(48)	8.3	8.0	8.7	4.5	3.8	5.0

(49)	4.2	4.1	4.5	2.1	1.7	2.4
(50)	0.6	0.6	0.6	0.0	0.0	0.3
(51)	0.1	0.0	0.2	0.0	0.0	0.5
(52)	1.6	1.6	1.7	1.0	0.8	1.0
(53)	2.5	2.4	2.6	1.5	1.2	1.6
(54)	2.5	2.4	2.6	1.5	1.2	1.6
(55)	4.0	3.7	4.2	2.3	2.0	2.7
(56)	0.9	0.9	0.9	0.5	0.5	0.6
(57)	2.6	2.5	2.8	1.5	1.3	1.7
(58)	3.0	2.9	3.1	1.8	1.5	1.9
(59)	1.8	1.8	1.9	1.1	0.9	1.2
(60)	1.2	1.2	1.3	0.7	0.6	0.8
(61)	1.1	1.1	1.2	0.7	0.6	0.7
(62)	0.5	0.4	0.5	0.3	0.2	0.3
(63)	0.7	0.7	0.7	0.4	0.3	0.4
(64)	0.9	0.9	0.9	0.5	0.5	0.6
(65)	0.7	0.7	0.7	0.3	0.0	0.4
(66)	Not in the model			Not in the model		
(67)	297.6	284.3	308.9	Not in the model		
(68)	17.9	15.2	20.2	Not in the model		
(69)	47.9	40.8	55.8	51.8	42.0	58.1
(70)	Not in the model			Not in the model		
(71)	497.8	450.8	538.4	17.0	0.0	55.4
(72)	Not in the model			Not in the model		
(73)	64.6	60.5	68.8	55.8	50.2	62.7
(74)	Not in the model			Not in the model		
(75)	Not in the model			Not in the model		
(76)	Not in the model			Not in the model		
(77)	171.8	163.4	178.4	2.4	0.0	17.2
(78)	Not in the model			Not in the model		
(79)	157.8	149.9	164.4	Not in the model		
(80)	54.6	52.5	56.8	32.1	27.2	34.9
(81)	1.6	1.6	1.7	1.0	0.8	1.0
(82)	8.4	8.1	8.8	4.9	4.1	5.3
(83)	11.8	10.2	13.5	6.5	5.2	7.7
(84)	Not in the model			Not in the model		
Exchange Fluxes						
(2)	87.7	54.5	145.3	64.3	43.0	109.4
(3)	73.1	14.6	Inf	34.5	0.3	Inf
(4)	73.4	14.6	Inf	33.5	0.3	Inf
(5)	18.3	0.0	66.4	247.3	10.1	Inf
(6)	Inf	0.0	Inf	17.2	0.0	Inf
(7)	>1000	0.0	Inf	9.6	0.0	Inf

(8)	0.0	0.0	287.5	0.0	0.0	97.0
(11)	97.8	38.8	Inf	83.7	35.9	Inf
(12)	0.0	0.0	Inf	0.0	0.0	Inf
(13)	93.9	38.8	Inf	83.7	35.9	Inf
(14)	6.4	5.8	7.1	3.8	3.3	4.2
(15)	2.3	0.0	Inf	0.3	0.0	Inf
(16)	0.0	0.0	28.5	18.7	0.1	31.2
(17)	78.3	0.0	Inf	3.7	0.0	Inf
(24)	28.2	0.0	Inf	4.2	0.0	Inf
(27)	19.0	0.0	Inf	10.9	0.0	Inf
(28)	>1000	17.1	Inf	0.0	0.0	Inf
(29)	854.7	160.5	Inf	200.1	3.3	Inf
(30)	448.8	154.5	Inf	4.7	0.4	Inf
(31)	2.7	1.1	4.2	0.1	0.0	0.2
(36)	56.9	0.0	Inf	0.5	0.0	Inf
(37)		Not in the model		2.8	0.0	Inf
(38)		Not in the model		6.1	0.0	Inf
(40)		Not in the model		32.2	14.8	57.5
(49)	3.8	3.5	4.2	3.5	2.9	4.1
(50)	0.0	0.0	0.2	0.0	0.0	0.0
(69)	30.7	0.0	Inf	2.9	0.0	Inf
(70)		Not in the model		14.5	0.0	Inf

Table A.8 Results of ^{13}C -MFA for *E. coli* grown on xylose under aerobic and anaerobic conditions. The reaction numbers correspond to the reactions listed in Table A.4. The fluxes are normalized to a substrate uptake rate of 100. 95% confidence intervals of fluxes (LB95 = lower bound, UB95 = upper bound) were determined by evaluating the sensitivity of the minimized SSR to flux variations.

Condition	Aerobic Xylose			Anaerobic Xylose		
SSR	33			175		
Net Fluxes						
Reaction No.	Best Fit	LB95	UB95	Best Fit	LB95	UB95
(1)	Not in the model			Not in the model		
(2)	-19.0	-21.6	-15.7	-0.8	-1.1	-0.5
(3)	52.1	50.5	54.0	64.7	64.3	65.4
(4)	52.1	50.5	54.0	64.7	64.3	65.4
(5)	52.1	50.5	54.0	64.7	64.3	65.4

(6)	140.3	138.4	142.5	161.9	160.7	163.4
(7)	128.7	126.1	131.3	159.1	157.3	161.4
(8)	87.5	83.0	97.6	124.6	88.6	142.5
(9)	16.6	13.1	19.2	0.0	0.0	0.3
(10)	14.6	11.9	17.1	0.0	0.0	0.3
(11)	-28.4	-30.4	-26.6	-34.3	-34.6	-34.0
(12)	43.0	42.2	43.7	34.3	34.0	34.6
(13)	71.6	69.6	73.4	65.7	65.4	66.0
(14)	-34.4	-35.4	-33.3	-32.4	-32.7	-32.2
(15)	-37.2	-38.1	-36.3	-33.2	-33.3	-33.2
(16)	-37.2	-38.1	-36.3	-33.2	-33.3	-33.2
(17)	37.2	36.3	38.1	33.2	33.2	33.3
(18)	2.0	0.2	3.6	0.0	0.0	0.2
(19)	2.0	0.2	3.6	0.0	0.0	0.2
(20)		100.0			99.9	
(21)		100.0			99.9	
(22)	85.0	81.8	88.3	17.0	7.0	26.4
(23)	34.5	28.7	37.4	2.4	1.7	3.0
(24)	34.5	28.7	37.4	2.4	1.7	3.0
(25)	33.9	24.4	37.4	2.4	1.7	3.0
(26)	25.3	15.3	29.0	0.1	0.0	0.3
(27)	22.1	11.9	25.8	-0.8	-1.1	-0.4
(28)	26.0	19.6	29.0	-11.6	-14.3	-8.9
(29)	29.0	22.8	32.0	-10.8	-13.6	-8.0
(30)	15.5	10.7	24.3	-26.2	-66.8	-9.6
(31)	0.6	0.0	4.5	0.0	0.0	0.3
(32)	0.6	0.0	4.5	0.0	0.0	0.3
(33)	14.2	6.1	17.8	15.4	0.0	55.3
(34)	35.2	31.6	39.3	32.8	16.0	71.6
(35)	0.0	0.0	8.9		Not in the model	
(36)	29.1	24.8	33.4	60.4	54.1	67.0
(37)		Not in the model			Not in the model	
(38)		Not in the model			Not in the model	
(39)		Not in the model			Not in the model	
(40)		Not in the model			Not in the model	
(41)	49.2	46.5	52.9	13.1	9.0	16.1
(42)	5.6	5.3	6.0	1.5	1.0	1.8
(43)	1.4	1.3	1.5	0.4	0.3	0.5
(44)	2.3	2.2	2.5	0.6	0.4	0.7
(45)	14.1	13.3	15.4	3.8	2.6	5.1
(46)	2.0	1.9	2.1	0.5	0.4	0.7
(47)	4.2	3.9	4.5	1.1	0.7	1.3
(48)	7.9	7.4	8.5	2.0	1.3	2.5

(49)	3.9	3.6	4.3	0.9	0.5	1.1
(50)	0.4	0.3	0.4	0.0	0.0	0.4
(51)	0.0	0.0	0.6	0.0	0.0	0.8
(52)	1.6	1.5	1.7	0.4	0.3	0.5
(53)	2.4	2.3	2.6	0.6	0.4	0.8
(54)	2.4	2.3	2.6	0.6	0.4	0.8
(55)	3.8	3.6	4.5	1.1	0.7	2.0
(56)	0.9	0.8	0.9	0.3	0.2	0.3
(57)	2.6	2.4	2.8	0.7	0.5	0.9
(58)	3.0	2.8	3.2	0.8	0.6	1.0
(59)	1.8	1.7	1.9	0.5	0.3	0.6
(60)	1.2	1.2	1.3	0.3	0.2	0.4
(61)	1.1	1.1	1.2	0.3	0.2	0.4
(62)	0.5	0.4	0.5	0.1	0.1	0.1
(63)	0.7	0.7	0.7	0.2	0.1	0.2
(64)	0.9	0.8	0.9	0.3	0.2	0.3
(65)	0.7	0.7	0.7	0.2	0.0	0.2
(66)	Not in the model			Not in the model		
(67)	252.4	219.6	269.2	Not in the model		
(68)	26.0	19.6	29.0	Not in the model		
(69)	35.5	22.9	62.7	13.2	-35.2	32.6
(70)	Not in the model			Not in the model		
(71)	268.9	164.4	327.1	9.0	0.0	51.9
(72)	100.0			99.9		
(73)	33.0	28.9	37.1	61.5	55.3	67.9
(74)	Not in the model			Not in the model		
(75)	Not in the model			Not in the model		
(76)	Not in the model			Not in the model		
(77)	151.3	130.3	162.4	23.8	-0.4	70.1
(78)	Not in the model			Not in the model		
(79)	139.2	119.8	148.7	Not in the model		
(80)	53.7	50.9	57.8	14.4	9.7	17.7
(81)	1.6	1.5	1.7	0.4	0.3	0.5
(82)	6.8	6.5	7.4	2.0	1.4	2.5
(83)	0.7	0.0	1.9	7.0	4.9	9.3
(84)	Not in the model			Not in the model		
Exchange Fluxes						
(2)	8.7	0.0	Inf	1.8	0.0	Inf
(3)	40.3	1.9	Inf	16.5	2.1	Inf
(4)	31.1	2.2	Inf	19.6	2.1	Inf
(5)	22.5	2.6	Inf	218.5	4.7	Inf
(6)	>1000	16.2	Inf	0.0	0.0	97.9
(7)	137.8	0.0	Inf	348.6	0.0	Inf

(8)	74.0	0.0	118.3	21.0	16.6	25.8
(11)	>1000	0.0	Inf	81.8	0.0	Inf
(12)	>1000	0.0	Inf	79.0	0.0	Inf
(13)	79.7	58.7	86.7	49.9	21.7	69.6
(14)	7.4	1.6	37.6	21.7	9.4	48.3
(15)	65.1	0.0	Inf	561.0	77.4	Inf
(16)	42.0	0.0	77.9	23.4	0.0	52.5
(17)	64.7	0.0	Inf	559.9	78.4	Inf
(24)	22.0	0.0	Inf	8.1	0.0	Inf
(27)	10.2	0.0	Inf	19.9	0.0	Inf
(28)	0.0	0.0	Inf	0.0	0.0	Inf
(29)	357.4	106.7	Inf	21.5	3.5	Inf
(30)	240.4	108.4	Inf	12.3	2.0	Inf
(31)	0.5	0.0	2.1	0.0	0.0	0.1
(36)	23.8	0.0	Inf	24.9	0.0	Inf
(37)	Not in the model			Not in the model		
(38)	Not in the model			Not in the model		
(40)	Not in the model			Not in the model		
(49)	2.3	1.9	2.7	1.2	0.8	1.6
(50)	0.1	0.0	0.2	0.0	0.0	0.0
(69)	12.7	0.0	Inf	20.1	0.0	Inf
(70)	Not in the model			Not in the model		

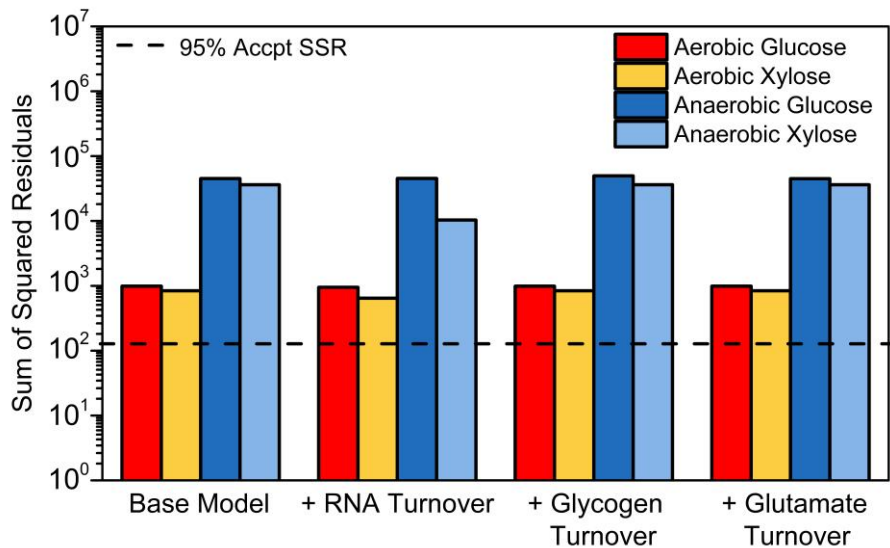


Figure A.1 Analysis of ^{13}C -MFA goodness-of-fit for various metabolic network models. Sum of squared residual values are shown here for models containing different dilution reactions in the model. Overall, including dilution reactions that account for RNA turnover, glycogen turnover, and amino acid turnover (here, glutamate turnover) did not improve the goodness-of-fit.

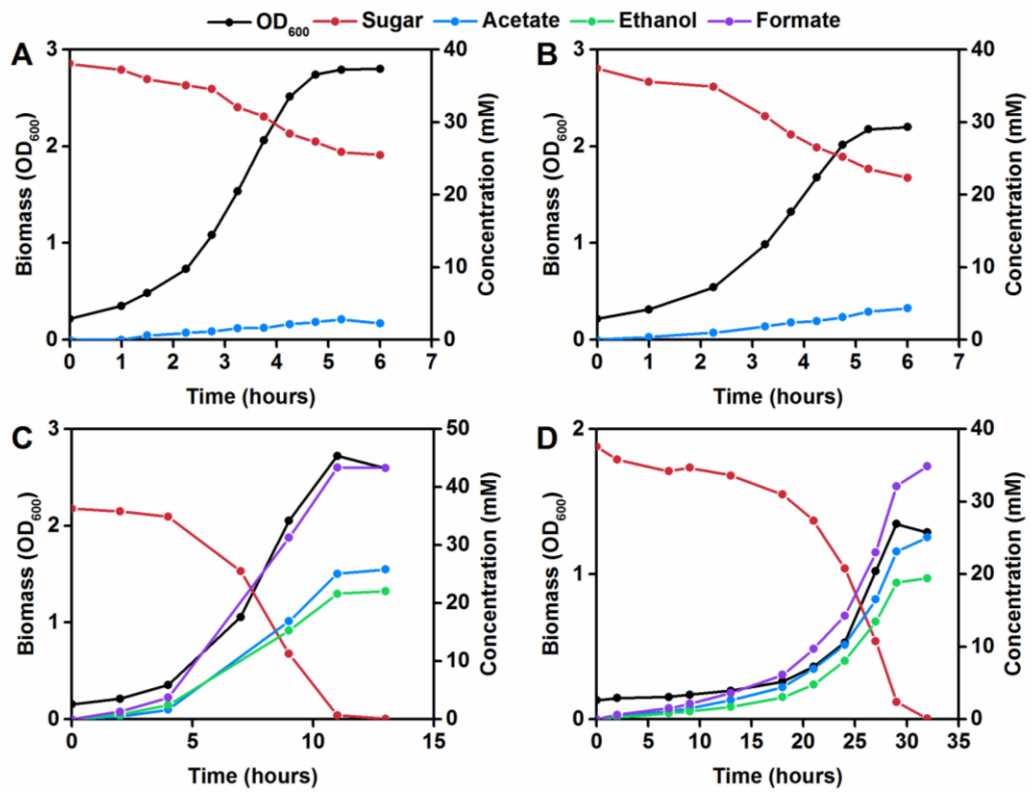


Figure A.2 Representative growth curves for each condition: Aerobic Glucose (A), Aerobic Xylose (B), Anaerobic Glucose (C), Anaerobic Xylose (D).

Appendix B

SUPPLEMENTARY DATA FOR CHAPTER 3

Table B.1 ^{13}C -labeling (in %) of proteinogenic amino acids and carbohydrates for Δcrr , ΔptsG , ΔptsH , and ΔptsI knockouts during growth on [U- ^{13}C]glucose and unlabeled xylose. The condition indicates the ratio of glucose to xylose. “Avg” indicates the average carbon labeling.

Strain	Δcrr			ΔptsG			ΔptsH			ΔptsI		
Condition	1:3	2:2	3:1	1:3	2:2	3:1	1:3	2:2	3:1	1:3	2:2	3:1
Avg	68	76	85	17	20	23	11	14	17	12	14	17
Ala232 (M0)	31	22	14	82	79	76	88	85	82	87	85	82
Ala232 (M1)	3	3	2	2	2	2	2	2	3	2	2	3
Ala232 (M2)	66	75	84	16	19	22	10	13	15	11	13	16
Ala232 (M3)	0	0	0	0	0	0	0	0	0	0	0	0
Ala232 (M4)	0	0	0	0	0	0	0	0	0	0	0	0
Avg	68	76	85	17	20	23	11	14	16	12	14	17
Ala260 (M0)	28	19	13	80	77	73	87	84	80	86	83	79
Ala260 (M1)	5	4	2	3	3	4	2	3	3	3	3	4
Ala260 (M2)	6	5	4	3	3	3	2	2	3	2	2	3
Ala260 (M3)	62	72	81	14	17	19	9	11	13	9	12	14
Ala260 (M4)	0	0	0	0	0	0	0	0	0	0	0	0
Ala260 (M5)	0	0	0	0	0	0	0	0	0	0	0	0
Avg	68	77	85	17	19	22	10	13	15	11	14	17
Gly218 (M0)	33	24	15	83	81	78	90	87	85	89	86	83
Gly218 (M1)	68	77	85	17	19	22	10	13	15	11	14	17
Gly218 (M2)	0	0	0	0	0	0	0	0	0	0	0	0
Gly218 (M3)	0	0	0	0	0	0	0	0	0	0	0	0
Avg	68	76	85	17	19	22	10	13	16	12	14	17
Gly246 (M0)	28	20	13	81	78	75	88	86	83	87	84	81
Gly246 (M1)	9	7	4	4	4	5	2	3	4	3	4	5
Gly246 (M2)	63	73	82	15	17	19	9	12	14	10	12	14
Gly246 (M3)	0	0	0	0	0	0	0	0	0	0	0	0
Gly246 (M4)	0	0	0	0	0	0	0	0	0	0	0	0
Avg	67	76	84	16	19	22	10	13	15	12	14	16

Val260 (M0)	16	12	10	69	65	60	80	75	70	77	73	68
Val260 (M1)	1	1	0	3	3	3	3	4	4	3	3	4
Val260 (M2)	29	20	8	25	27	30	15	18	22	18	21	24
Val260 (M3)	4	4	3	1	1	1	0	1	1	0	1	1
Val260 (M4)	49	63	77	3	4	5	1	2	3	1	2	3
Val260 (M5)	0	0	0	0	0	0	0	0	0	0	0	0
Val260 (M6)	0	0	0	0	0	0	0	0	0	0	0	0
Avg	67	76	85	16	19	22	10	13	15	11	14	16
Val288 (M0)	15	12	10	68	63	59	79	74	69	76	72	67
Val288 (M1)	2	1	0	4	4	4	3	4	5	3	4	5
Val288 (M2)	14	9	3	14	15	17	9	11	13	10	12	14
Val288 (M3)	17	13	5	12	13	14	7	9	10	8	10	11
Val288 (M4)	6	6	5	1	1	1	0	1	1	0	1	1
Val288 (M5)	47	61	76	3	4	5	1	2	3	1	2	3
Val288 (M6)	0	0	0	0	0	0	0	0	0	0	0	0
Val288 (M7)	0	0	0	0	0	0	0	0	0	0	0	0
Avg	67	76	84	16	19	22	10	13	15	11	14	16
Leu274 (M0)	12	10	10	59	54	49	72	66	60	69	64	59
Leu274 (M1)	4	2	0	13	13	14	10	12	14	11	12	13
Leu274 (M2)	9	4	1	20	22	24	14	16	18	16	18	20
Leu274 (M3)	23	18	8	5	7	8	2	3	4	3	4	5
Leu274 (M4)	14	12	8	2	3	4	1	2	2	1	2	2
Leu274 (M5)	38	54	73	1	1	1	0	1	1	0	0	1
Leu274 (M6)	0	0	0	0	0	0	0	0	0	0	0	0
Leu274 (M7)	0	0	0	0	0	0	0	0	0	0	0	0
Avg	65	74	82	16	19	21	10	13	16	11	14	16
Ile200 (M0)	13	11	10	62	57	51	73	67	61	70	65	59
Ile200 (M1)	3	1	0	10	11	12	10	11	13	11	12	13
Ile200 (M2)	13	7	3	19	21	23	13	15	18	15	17	19
Ile200 (M3)	19	15	7	6	8	9	3	4	5	4	5	6
Ile200 (M4)	18	18	15	2	3	3	1	1	2	1	1	2
Ile200 (M5)	34	48	64	1	1	2	0	1	1	0	1	1
Ile200 (M6)	0	0	0	0	0	0	0	0	0	0	0	0
Ile200 (M7)	0	0	0	0	0	0	0	0	0	0	0	0
Avg	66	74	82	16	19	21	10	13	15	11	14	16
Ile274 (M0)	13	11	10	62	57	51	73	67	61	70	65	59
Ile274 (M1)	3	1	0	10	11	12	10	12	13	11	12	13
Ile274 (M2)	13	7	3	19	21	23	13	15	18	15	17	19
Ile274 (M3)	19	14	7	6	8	9	3	4	5	4	5	6

Ile274 (M4)	18	18	15	2	3	3	1	1	2	1	1	2
Ile274 (M5)	34	48	65	1	1	2	0	1	1	0	1	1
Ile274 (M6)	0	0	0	0	0	0	0	0	0	0	0	0
Ile274 (M7)	0	0	0	0	0	0	0	0	0	0	0	0
Avg	67	76	84	17	19	22	11	13	16	12	14	17
Pro258 (M0)	15	11	10	64	61	56	75	70	64	72	68	63
Pro258 (M1)	4	2	1	11	10	11	10	12	14	12	13	15
Pro258 (M2)	24	17	8	20	23	25	12	15	17	13	16	18
Pro258 (M3)	12	10	7	3	2	3	1	2	3	2	2	3
Pro258 (M4)	45	59	75	2	3	4	1	2	2	1	1	2
Pro258 (M5)	0	0	0	0	0	0	0	0	0	0	0	0
Pro258 (M6)	0	0	0	0	0	0	0	0	0	0	0	0
Avg	67	76	85	16	19	21	10	13	15	11	14	16
Ser362 (M0)	25	18	13	80	76	72	87	83	80	84	80	76
Ser362 (M1)	17	13	8	8	10	14	7	8	10	10	12	15
Ser362 (M2)	59	70	81	12	14	14	7	8	10	6	8	9
Ser362 (M3)	0	0	0	0	0	0	0	0	0	0	0	0
Avg	68	77	85	17	19	22	10	13	16	12	14	17
Ser390 (M0)	22	16	12	78	75	72	86	82	78	82	78	74
Ser390 (M1)	9	6	3	6	6	7	4	6	7	7	9	10
Ser390 (M2)	12	10	6	5	5	6	4	4	5	5	6	7
Ser390 (M3)	57	69	81	12	14	16	6	8	10	6	7	8
Ser390 (M4)	0	0	-1	0	0	0	0	0	0	0	0	0
Ser390 (M5)	0	0	0	0	0	0	0	0	0	0	0	0
Avg	65	74	82	15	18	21	10	13	15	11	13	16
Thr376 (M0)	20	15	11	74	70	66	82	77	72	80	75	71
Thr376 (M1)	12	8	4	11	12	14	9	12	14	11	12	14
Thr376 (M2)	22	20	15	10	12	13	7	8	10	7	9	10
Thr376 (M3)	46	58	70	5	6	7	2	3	4	3	3	4
Thr376 (M4)	0	0	0	0	0	0	0	0	0	0	0	0
Thr376 (M5)	0	0	0	0	0	0	0	0	0	0	0	0
Avg	64	73	81	15	18	21	10	12	15	11	13	16
Thr404 (M0)	17	13	11	71	66	61	79	74	69	77	72	67
Thr404 (M1)	8	5	2	11	12	13	9	10	12	10	11	13
Thr404 (M2)	13	9	4	8	9	10	7	9	10	8	10	11
Thr404 (M3)	25	24	21	9	10	11	4	6	7	5	6	7
Thr404 (M4)	37	49	63	2	3	4	1	1	2	1	1	2
Thr404 (M5)	0	0	0	0	0	0	0	0	0	0	0	0

Thr404 (M6)	0	0	0	0	0	0	0	0	0	0	0	0
Avg	67	76	84	16	19	21	10	12	15	11	13	16
Phe302 (M0)	29	21	14	82	80	77	89	87	84	88	85	82
Phe302 (M1)	8	7	4	3	4	4	2	2	3	3	4	4
Phe302 (M2)	63	73	82	14	17	19	9	11	13	9	11	13
Phe302 (M3)	0	0	0	0	0	0	0	0	0	0	0	0
Avg	63	73	83	13	15	17	8	10	12	9	11	14
Phe308 (M0)	13	11	11	61	56	51	75	69	63	70	65	59
Phe308 (M1)	1	0	0	3	3	4	3	4	4	4	5	5
Phe308 (M2)	7	3	0	21	23	25	15	17	19	16	18	20
Phe308 (M3)	4	2	0	5	6	7	4	5	5	4	5	6
Phe308 (M4)	13	9	3	5	6	7	2	3	4	3	4	5
Phe308 (M5)	11	7	3	2	3	3	1	1	2	1	2	2
Phe308 (M6)	15	14	8	1	2	2	0	1	1	1	1	1
Phe308 (M7)	12	12	9	0	0	1	0	0	0	0	0	0
Phe308 (M8)	25	41	65	0	0	0	0	1	1	0	0	0
Avg	63	73	83	13	16	18	8	10	13	9	12	14
Phe336 (M0)	12	10	11	60	55	50	74	68	62	69	64	58
Phe336 (M1)	1	0	0	4	4	4	3	4	5	5	6	6
Phe336 (M2)	4	1	0	12	13	14	8	10	11	9	10	12
Phe336 (M3)	6	3	0	14	16	17	10	12	13	11	12	14
Phe336 (M4)	5	3	1	3	4	4	2	2	3	3	4	4
Phe336 (M5)	14	10	3	3	4	5	1	2	3	2	2	3
Phe336 (M6)	13	11	5	2	2	3	1	1	1	1	1	2
Phe336 (M7)	10	10	6	1	1	1	0	0	1	0	1	1
Phe336 (M8)	12	13	10	0	0	1	0	0	0	0	0	0
Phe336 (M9)	23	39	64	0	0	0	0	0	1	0	0	0
Avg	65	73	81	17	19	22	12	15	17	13	15	18
Asp302 (M0)	26	19	13	79	75	72	85	81	78	83	80	77
Asp302 (M1)	17	15	11	9	10	11	6	8	9	7	9	10
Asp302 (M2)	56	66	76	12	14	16	9	11	13	9	11	13
Asp302 (M3)	0	0	0	0	0	0	0	0	0	0	0	0
Avg	65	73	82	15	18	21	10	13	15	11	13	16
Asp390 (M0)	20	15	11	74	70	66	82	77	72	79	76	71
Asp390 (M1)	12	8	4	11	12	14	9	11	13	11	12	14
Asp390 (M2)	22	20	15	10	11	13	7	8	10	7	9	10
Asp390 (M3)	46	57	70	5	6	8	2	3	4	3	3	4
Asp390 (M4)	0	0	0	0	0	0	0	0	0	0	0	0

Asp390 (M5)	0	0	0	0	0	0	0	0	0	0	0	0
Avg	64	72	80	15	18	21	10	13	15	11	13	16
Asp418 (M0)	17	13	11	70	66	61	79	73	68	76	72	67
Asp418 (M1)	9	6	2	11	12	14	9	11	12	10	11	13
Asp418 (M2)	13	10	5	8	9	11	7	9	11	8	10	11
Asp418 (M3)	25	24	21	9	10	11	4	6	7	5	6	7
Asp418 (M4)	36	48	62	2	3	3	1	1	2	1	1	2
Asp418 (M5)	0	0	0	0	0	0	0	0	0	0	0	0
Asp418 (M6)	0	0	0	0	0	0	0	0	0	0	0	0
Avg	67	76	84	16	19	22	11	14	17	12	14	17
Glu330 (M0)	14	11	9	66	62	57	75	69	63	73	68	63
Glu330 (M1)	5	2	1	9	9	10	10	11	13	11	12	14
Glu330 (M2)	25	18	8	21	24	26	13	16	18	14	16	18
Glu330 (M3)	12	11	7	2	2	3	1	2	3	2	2	3
Glu330 (M4)	44	58	75	2	3	4	1	2	2	1	1	2
Glu330 (M5)	0	0	0	0	0	0	0	0	0	0	0	0
Glu330 (M6)	0	0	0	0	0	0	0	0	0	0	0	0
Avg	66	74	83	16	19	21	11	14	17	12	14	17
Glu432 (M0)	12	10	9	61	56	51	71	65	59	69	64	59
Glu432 (M1)	4	2	0	10	11	12	10	11	13	11	12	13
Glu432 (M2)	13	8	3	19	21	23	14	16	19	15	17	19
Glu432 (M3)	20	15	8	6	8	9	3	5	6	4	5	6
Glu432 (M4)	18	18	16	2	3	3	1	2	2	1	2	2
Glu432 (M5)	34	47	65	1	1	2	1	1	1	0	1	1
Glu432 (M6)	0	0	0	0	0	0	0	0	0	0	0	0
Glu432 (M7)	0	0	0	0	0	0	0	0	0	0	0	0
Avg	67	76	84	16	19	21	10	12	15	11	14	16
Tyr302 (M0)	28	21	14	82	79	76	89	86	84	87	85	82
Tyr302 (M1)	8	7	4	3	4	4	2	3	3	3	4	5
Tyr302 (M2)	63	73	83	14	17	19	9	11	13	10	12	14
Tyr302 (M3)	0	0	0	0	0	0	0	0	0	0	0	0
Avg	57	68	79	12	16	23	7	10	23	8	12	26
RNA_Rib173 (M0)	42	31	20	88	84	76	93	90	76	92	88	74
RNA_Rib173 (M1)	2	2	2	0	1	1	0	0	1	0	1	2
RNA_Rib173 (M2)	56	67	78	12	15	23	6	10	23	7	11	25

Avg	51	63	78	9	12	19	5	8	20	7	10	23
RNA_Rib284 (M0)	33	24	16	84	79	70	91	86	68	88	82	62
RNA_Rib284 (M1)	3	2	1	3	3	4	2	3	5	3	4	7
RNA_Rib284 (M2)	23	19	9	9	11	16	6	8	15	6	9	17
RNA_Rib284 (M3)	7	7	6	1	1	2	0	1	2	1	1	4
RNA_Rib284 (M4)	33	48	69	4	5	8	2	3	9	2	4	10
Avg	77	81	87	34	46	51	16	30	44	20	34	71
Glycogen_Gluc 173 (M0)	22	18	11	65	54	48	83	69	55	79	65	27
Glycogen_Gluc 173 (M1)	3	3	3	1	1	2	1	1	2	1	2	3
Glycogen_Gluc 173 (M2)	75	79	86	34	45	50	16	30	43	20	33	70
Avg	76	81	88	32	43	48	15	28	42	19	32	71
Glycogen_Gluc 370 (M0)	13	12	8	60	47	39	78	63	43	70	54	14
Glycogen_Gluc 370 (M1)	2	1	0	3	4	4	2	3	6	5	6	6
Glycogen_Gluc 370 (M2)	7	4	1	8	9	11	6	8	11	9	10	9
Glycogen_Gluc 370 (M3)	10	7	4	3	4	6	3	4	8	4	6	9
Glycogen_Gluc 370 (M4)	7	7	5	1	2	3	1	1	3	1	2	5
Glycogen_Gluc 370 (M5)	62	69	81	25	35	38	10	21	30	11	22	57

Table B.2 Metabolic network models for ^{13}C -metabolic flux analysis of GX50 and LMSE2 strains grown on mixtures of glucose and xylose or on glucose/xylose alone.

L = LMSE2 with glucose + xylose

G = GX50 with glucose + xylose
 GG = GX50 with glucose
 GX = GX50 with xylose

Glycolysis

(1) [L G GG] Gluc.ext (abcdef) + PEP (ghi) -> G6P (abcdef) + Pyr(ghi)
 (2) [L G GG GX] G6P (abcdef) <=> F6P (abcdef)
 (3) [L G GG GX] F6P (abcdef) + ATP <=> FBP (abcdef)
 (4) [L G GG GX] FBP (abcdef) <=> DHAP (cba) + GAP (def)
 (5) [L G GG GX] DHAP (abc) <=> GAP (abc)
 (6) [L G GG GX] GAP (abc) <=> 3PG (abc) + ATP + NADH
 (7) [L G GG GX] 3PG (abc) <=> PEP (abc)
 (8) [L G GG GX] PEP (abc) <=> Pyr (abc) + ATP

Pentose Phosphate Pathway

(9) [L G GG GX] G6P (abcdef) -> 6PG (abcdef) + NADPH
 (10) [L G GG GX] 6PG (abcdef) -> Ru5P (bcdef) + CO₂ (a) + NADPH
 (11) [L G GG GX] Ru5P (abcde) <=> X5P (abcde)
 (12) [L G GG GX] Ru5P (abcde) <=> R5P (abcde)
 (13) [L G GG GX] X5P (abcde) <=> TK-C2 (ab) + GAP (cde)
 (14) [L G GG GX] F6P (abcdef) <=> TK-C2 (ab) + E4P (cdef)
 (15) [L G GG GX] S7P (abcdefg) <=> TK-C2 (ab) + R5P (cdefg)
 (16) [L G GG GX] F6P (abcdef) <=> TA-C3 (abc) + GAP (def)
 (17) [L G GG GX] S7P (abcdefg) <=> TA-C3 (abc) + E4P (defg)

Entner-Doudoroff Pathway

(18) [L G GG GX] 6PG (abcdef) -> KDPG (abcdef)
 (19) [L G GG GX] KDPG (abcdef) -> Pyr (abc) + GAP (def)

Xylose Metabolism

(20) [L G GX] Xyl (abcde) -> Xylu (abcde)
 (21) [L G GX] Xylu (abcde) + ATP -> X5P (abcde)

TCA Cycle

(22) [L G GG GX] Pyr (abc) -> AcCoA (bc) + CO₂ (a) + NADH
 (23) [L G GG GX] OAC (abcd) + AcCoA (ef) -> Cit (dcbfea)
 (24) [L G GG GX] Cit (abcdef) <=> ICit (abcdef)
 (25) [L G GG GX] ICit (abcdef) -> AKG (abcde) + CO₂ (f) + NADPH
 (26) [L G GG GX] AKG (abcde) -> SucCoA (bcde) + CO₂ (a) + NADH
 (27) [L G GG GX] SucCoA (abcd) <=> Suc (½ abcd + ½ dcba) + ATP
 (28) [L G GG GX] Suc (½ abcd + ½ dcba) <=> Fum (½ abcd + ½ dcba) + FADH₂
 (29) [L G GG GX] Fum (½ abcd + ½ dcba) <=> Mal (abcd)
 (30) [L G GG GX] Mal (abcd) <=> OAC (abcd) + NADH

Glyoxylate Shunt

- (31) [L G GG GX] ICit (abcdef) \rightleftharpoons Glyox (ab) + Suc ($\frac{1}{2}$ edcf + $\frac{1}{2}$ fcde)
(32) [L G GG GX] Glyox (ab) + AcCoA (cd) \rightarrow Mal (abdc)

Amphibolic Reactions

- (33) [L G GG GX] Mal (abcd) \rightarrow Pyr (abc) + CO₂ (d) + NADPH
(34) [L G GG GX] PEP (abc) + CO₂ (d) \rightarrow OAC (abcd)
(35) [L G GG GX] OAC (abcd) + ATP \rightarrow PEP (abc) + CO₂ (d)

Fermentation Reactions

- (36) [L G GG GX] AcCoA (ab) \rightleftharpoons Ac (ab) + ATP

Amino Acid Biosynthesis

- (37) [L G GG GX] AKG (abcde) + NADPH + NH₃ \rightarrow Glu (abcde)
(38) [L G GG GX] Glu (abcde) + ATP + NH₃ \rightarrow Gln (abcde)
(39) [L G GG GX] Glu (abcde) + ATP + 2 NADPH \rightarrow Pro (abcde)
(40) [L G GG GX] Glu (abcde) + CO₂ (f) + Gln (ghijk) + Asp (lmno) + AcCoA (pq) + 5 ATP + NADPH \rightarrow Arg (abcdef) + AKG (ghijk) + Fum (lmno) + Ac (pq)
(41) [L G GG GX] OAC (abcd) + Glu (efghi) \rightarrow Asp (abcd) + AKG (efghi)
(42) [L G GG GX] Asp (abcd) + 2 ATP + NH₃ \rightarrow Asn (abcd)
(43) [L G GG GX] Pyr (abc) + Glu (defgh) \rightarrow Ala (abc) + AKG (defgh)
(44) [L G GG GX] 3PG (abc) + Glu (defgh) \rightarrow Ser (abc) + AKG (defgh) + NADH
(45) [L G GG GX] Ser (abc) \rightleftharpoons Gly (ab) + MEETHF (c)
(46) [L G GG GX] Gly (ab) \rightarrow CO₂ (a) + MEETHF (b) + NADH + NH₃
(47) [L G GG GX] CO₂ (a) + MEETHF (b) + NADH + NH₃ \rightarrow Gly(ab)
(48) [L G GG GX] Thr (abcd) \rightarrow Gly (ab) + AcCoA (cd) + NADH
(49) [L G GG GX] Ser (abc) + AcCoA (de) + 3 ATP + 4 NADPH + SO₄ \rightarrow Cys (abc) + Ac (de)
(50) [L G GG GX] Asp (abcd) + Pyr (efg) + Glu (hijkl) + SucCoA (mnop) + ATP + 2 NADPH \rightarrow LL-DAP ($\frac{1}{2}$ abcdgfe + $\frac{1}{2}$ efgdcba) + AKG (hijkl) + Suc ($\frac{1}{2}$ mnop + $\frac{1}{2}$ ponm)
(51) [L G GG GX] LL-DAP ($\frac{1}{2}$ abcdefg + $\frac{1}{2}$ gfedcba) \rightarrow Lys (abcdef) + CO₂ (g)
(52) [L G GG GX] Asp (abcd) + 2 ATP + 2 NADPH \rightarrow Thr (abcd)
(53) [L G GG GX] Asp (abcd) + METHF (e) + Cys (fgh) + SucCoA (ijkl) + ATP + 2 NADPH \rightarrow Met (abcde) + Pyr (fgh) + Suc ($\frac{1}{2}$ ijkl + $\frac{1}{2}$ lkji) + NH₃
(54) [L G GG GX] Pyr (abc) + Pyr (def) + Glu (ghijk) + NADPH \rightarrow Val (abcef) + CO₂ (d) + AKG (ghijk)
(55) [L G GG GX] AcCoA (ab) + Pyr (cde) + Pyr (fgh) + Glu (ijklm) + NADPH \rightarrow Leu (abdghe) + CO₂ (c) + CO₂ (f) + AKG (ijklm) + NADH

- (56) [L G GG GX] Thr (abcd) + Pyr (efg) + Glu (hijkl) + NADPH -> Ile (abfcdg) + CO₂ (e) + AKG (hijkl) + NH₃
- (57) [L G GG GX] PEP (abc) + PEP (def) + E4P (ghij) + Glu (klmno) + ATP + NADPH -> Phe (abcefg hij) + CO₂ (d) + AKG (klmno)
- (58) [L G GG GX] PEP (abc) + PEP (def) + E4P (ghij) + Glu (klmno) + ATP + NADPH -> Tyr (abcefg hij) + CO₂ (d) + AKG (klmno) + NADH
- (59) [L G GG GX] Ser (abc) + R5P (defgh) + PEP (ijk) + E4P (lmno) + PEP (pqr) + Gln (stuvw) + 3 ATP + NADPH -> Trp (abcdklmnoj) + CO₂ (i) + GAP (fgh) + Pyr (pqr) + Glu (stuvw)
- (60) [L G GG GX] R5P (abcde) + FTHF (f) + Gln (ghijk) + Asp (lmno) + 5 ATP -> His (edcbaf) + AKG (ghijk) + Fum (lmno) + 2 NADH

One-carbon Metabolism

- (61) [L G GG GX] MEETHF (a) + NADH -> METHF (a)
- (62) [L G GG GX] MEETHF (a) -> FTHF (a) + NADPH

Oxidation Phosphorylation

- (62) [L G GG GX] NADH + 1/2 O₂ -> 2 ATP
- (63) [L G GG GX] FADH₂ + 1/2 O₂ -> 1 ATP

Transhydrogenation

- (64) [L G GG GX] NADH <=> NADPH

ATP Hydrolysis

- (65) [L G GG GX] ATP -> ATP.ext

Transport

- (66) [L G GX] Xyl.ext (abcde) + ATP -> Xyl (abcde)
- (67) [L G GG GX] Ac (ab) -> Ac.ext (ab)
- (68) [L G GG GX] CO₂ (a) -> CO₂.ext (a)
- (69) [L G GG GX] H₂ -> H₂.ext
- (70) [L G GG GX] O₂.ext -> O₂
- (71) [L G GG GX] NH₃.ext -> NH₃
- (72) [L G GG GX] SO₄.ext -> SO₄

Biomass Formation

- (73) [L G GG GX] **0.49731 Ala + 0.28651 Arg + 0.2326 Asn + 0.2326 Asp + 0.088707 Cys + 0.24738 Glu + 0.24738 Gln + 0.44054 Gly + 0.08398 His + 0.21739 Ile + 0.35853 Leu + 0.29077 Lys + 0.10557 Met + 0.14618 Phe + 0.16797 Pro + 0.23355 Ser + 0.24446 Thr + 0.13526 Tyr + 0.31392 Val + 0.18148 G6P + 0.0709 F6P + 0.10233 GAP + 0.53768 3PG + 0.0828 Pyr + 2.0826 AcCoA + 0.0869 AKG + 0.30055 OAC + 0.05506 Trp**

+ 0.65979 R5P + 0.0511 PEP + 30.7648 ATP + 4.5162 NADPH + 0.38804 MEETHF + 1.2644 NAD -> 1.2644 NADH + 30.7648 ADP + 30.7648 Pi + 4.5162 NADP + 0.38804 THF + 35.476 Biomass

Labeling dilution from external acetate

(74) [L G GG GX] AcCoA.unlabeled (ab) + AcCoA (cd) -> AcCoA (ab) + AcCoA.out (cd)

Table B.3 Results of ¹³C-MFA of LMSE2 grown on glucose and xylose at the specified ratios. The reaction numbers correspond to the reactions listed in Table B.2. The fluxes are normalized to a total substrate uptake rate of 100. 95% confidence intervals of fluxes (LB95 = lower bound, UB95 = upper bound) were determined by evaluating the sensitivity of the minimized SSR to flux variations.

Glucose:Xylose	1:1			2:2		
SSR	158.6			132.8		
Net Fluxes						
Reaction No.	Best Fit	LB95	UB95	Best Fit	LB95	UB95
(1)	40.2	39.6	40.7	40.4	38.3	42.5
(2)	0.9	0.3	1.6	0.8	0.1	1.4
(3)	61.4	59.8	62.9	61.2	58.7	63.5
(4)	61.4	59.8	62.9	61.2	58.7	63.5
(5)	61.4	59.8	62.9	61.2	58.7	63.5
(6)	151.8	147.8	155.6	151.2	145.1	157.0
(7)	141.5	137.3	145.6	140.4	134.4	145.8
(8)	83.2	75.5	87.9	77.9	69.8	83.5
(9)	38.1	37.2	38.8	38.3	36.4	40.3
(10)	38.1	37.0	38.8	38.3	36.4	40.3
(11)	1.1	0.2	1.7	1.2	0.4	1.9
(12)	36.9	36.0	37.8	37.1	35.6	38.7
(13)	61.0	59.1	62.7	60.8	58.4	63.2
(14)	-29.4	-30.3	-28.5	-29.3	-30.4	-28.1
(15)	-31.6	-32.4	-30.6	-31.5	-32.8	-30.3
(16)	-31.6	-32.4	-30.6	-31.5	-32.8	-30.3
(17)	31.6	30.6	32.4	31.5	30.3	32.8
(18)	0.0	0.0	0.7	0.0	0.0	0.5
(19)	0.0	0.0	0.7	0.0	0.0	0.5
(20)	59.8	57.7	61.9	59.6	57.4	61.9

(21)	59.8	57.7	61.9	59.6	57.4	61.9
(22)	108.1	102.6	113.2	103.2	96.2	109.5
(23)	16.5	13.3	19.8	22.9	19.1	27.2
(24)	16.5	13.3	19.8	22.9	19.1	27.2
(25)	2.2	6.5	17.2	21.0	15.3	26.8
(26)	5.8	0.0	10.9	14.3	8.6	20.0
(27)	2.9	-3.0	8.1	11.3	5.6	17.0
(28)	10.1	6.6	13.4	16.2	12.5	20.2
(29)	12.3	8.9	15.6	18.5	14.8	22.6
(30)	16.1	10.6	18.4	19.3	14.2	22.7
(31)	4.3	2.4	6.4	2.0	0.0	4.2
(32)	4.3	2.4	6.4	2.0	0.0	4.2
(33)	0.4	0.0	6.2	1.2	0.0	5.5
(34)	17.5	15.2	19.8	20.0	17.6	22.8
(35)	4.0	0.0	6.5	2.8	0.0	6.0
(36)	66.9	59.9	73.7	57.1	46.4	66.2
(37)	39.2	36.6	41.8	40.7	36.6	45.4
(38)	4.0	3.8	4.3	4.2	3.8	4.7
(39)	1.3	1.2	1.3	1.3	1.2	1.5
(40)	1.7	1.6	1.8	1.7	1.6	2.0
(41)	11.1	10.5	11.9	11.5	10.3	12.7
(42)	1.4	1.3	1.5	1.4	1.3	1.6
(43)	2.9	2.7	3.1	3.0	2.7	3.4
(44)	6.6	6.1	7.0	6.9	6.2	7.7
(45)	3.6	3.4	3.9	3.8	3.5	4.3
(46)	0.4	0.3	0.5	0.4	0.3	0.5
(47)	0.0	0.0	0.1	0.0	0.0	0.1
(48)	0.3	0.1	0.4	0.2	0.0	0.3
(49)	1.4	1.3	1.5	1.4	1.3	1.6
(50)	1.9	1.8	2.1	2.0	1.8	2.3
(51)	1.9	1.8	2.1	2.0	1.8	2.3
(52)	3.4	3.1	3.6	3.4	3.0	3.7
(53)	0.9	0.8	0.9	0.9	0.8	1.0
(54)	2.4	2.2	2.6	2.5	2.2	2.8
(55)	2.6	2.4	2.7	2.7	2.4	3.0
(56)	1.6	1.5	1.8	1.7	1.5	1.9
(57)	1.1	1.0	1.1	1.1	1.0	1.2
(58)	0.8	0.7	0.8	0.8	0.7	0.9
(59)	0.3	0.3	0.3	0.3	0.3	0.4
(60)	0.5	0.5	0.6	0.6	0.5	0.6
(61)	0.9	0.8	0.9	0.9	0.8	1.0
(62)	0.5	0.5	0.6	0.6	0.5	0.6
(63)	288.5	269.6	305.9	301.5	280.0	320.5

(64)	10.1	6.6	13.4	16.2	12.5	20.2
(65)	12.8	2.7	22.7	6.6	-5.2	18.0
(66)	472.6	409.8	529.4	490.1	414.8	551.6
(67)	59.8	57.7	61.9	59.6	57.4	61.9
(68)	70.0	63.2	76.6	60.2	49.8	69.1
(69)	182.3	170.9	193.1	195.0	182.3	207.4
(70)	149.3	138.5	159.3	158.9	146.8	169.7
(71)	41.6	38.9	44.5	43.3	38.9	48.4
(72)	1.4	1.3	1.5	1.4	1.3	1.6
(73)	6.0	5.6	6.4	6.2	5.6	6.9
(74)	1.4	0.1	2.8	1.2	0.0	2.5
Exchange Fluxes						
(2)	0	0	1	0	0	1
(3)	170	0	Inf	0	0	Inf
(4)	777	0	Inf	435	0	Inf
(5)	0	0	5	534	0	Inf
(6)	613	0	Inf	108	0	Inf
(7)	2	0	Inf	0	0	Inf
(8)	0	0	Inf	0	0	Inf
(11)	0	0	0	0	0	1
(12)	Inf	Inf	Inf	Inf	Inf	Inf
(13)	230	0	Inf	Inf	Inf	Inf
(14)	0	0	0	0	0	1
(15)	8	5	Inf	8	5	Inf
(16)	Inf	Inf	Inf	Inf	Inf	Inf
(17)	514	5	Inf	400	5	Inf
(24)	302	0	Inf	245	0	Inf
(27)	10	0	Inf	186	0	Inf
(28)	299	0	Inf	277	0	Inf
(29)	Inf	Inf	Inf	Inf	Inf	Inf
(30)	174	105	372	248	146	677
(31)	0	0	0	0	0	0
(36)	696	0	Inf	46	0	Inf
(45)	2	2	2	2	2	3
(65)	342	0	Inf	230	0	Inf

Glucose:Xylose		1:2			2:1	
SSR		196.6			92.3	
Net Fluxes						
Reaction No.	Best Fit	LB95	UB95	Best Fit	LB95	UB95
(1)	39.6	34.3	44.6	40.1	35.8	44.3
(2)	1.2	0.5	1.9	0.3	-0.4	0.9
(3)	62.2	53.2	70.2	60.8	54.3	67.0

(4)	62.2	53.2	70.2	60.8	54.3	67.0
(5)	62.2	53.2	70.2	60.8	54.3	67.0
(6)	153.9	131.5	173.9	150.4	134.5	166.0
(7)	145.0	123.0	164.3	139.2	124.3	153.8
(8)	89.2	72.4	103.8	75.6	63.7	85.6
(9)	37.3	32.3	42.0	38.5	34.4	42.6
(10)	37.2	32.2	41.9	38.5	34.4	42.6
(11)	1.0	0.1	1.8	1.0	0.3	1.8
(12)	36.2	31.4	40.8	37.4	33.5	41.3
(13)	61.3	52.4	69.3	61.0	54.5	67.4
(14)	-29.7	-33.6	-25.3	-29.3	-32.4	-26.2
(15)	-31.6	-35.6	-27.1	-31.7	-34.9	-28.3
(16)	-31.6	-35.6	-27.1	-31.7	-34.9	-28.3
(17)	31.6	27.1	35.6	31.7	28.3	34.9
(18)	0.1	0.0	0.8	0.0	0.0	0.4
(19)	0.1	0.0	0.8	0.0	0.0	0.4
(20)	60.4	51.5	68.3	59.9	53.6	66.3
(21)	60.4	51.5	68.3	59.9	53.6	66.3
(22)	116.0	95.1	134.1	101.0	89.0	113.2
(23)	12.3	9.8	15.3	25.6	20.3	30.8
(24)	12.3	9.8	15.3	25.6	20.3	30.8
(25)	8.7	5.9	12.1	23.1	16.3	29.9
(26)	3.1	0.5	6.1	16.1	9.6	22.7
(27)	0.7	-2.0	3.5	13.1	6.6	19.5
(28)	6.7	4.8	9.1	18.6	13.8	23.4
(29)	8.6	6.6	11.2	21.0	16.1	26.0
(30)	11.6	7.9	14.7	21.1	14.3	25.5
(31)	3.6	2.4	5.0	2.5	0.4	4.7
(32)	3.6	2.4	5.0	2.5	0.4	4.7
(33)	0.7	0.0	4.6	2.4	0.0	7.9
(34)	14.2	11.3	17.5	22.2	18.4	25.8
(35)	2.1	0.0	5.2	3.6	0.0	7.2
(36)	82.5	61.9	100.4	50.9	39.9	62.2
(37)	33.9	28.3	40.2	42.2	36.4	48.0
(38)	3.5	2.9	4.1	4.4	3.8	5.0
(39)	1.1	0.9	1.3	1.4	1.2	1.5
(40)	1.5	1.2	1.7	1.8	1.6	2.1
(41)	9.7	8.1	11.5	11.9	10.3	13.5
(42)	1.2	1.0	1.4	1.5	1.3	1.7
(43)	2.5	2.1	3.0	3.2	2.7	3.6
(44)	5.7	4.7	6.7	7.2	6.2	8.2
(45)	3.1	2.6	3.7	4.0	3.5	4.5
(46)	0.4	0.3	0.5	0.4	0.3	0.5

(47)	0.0	0.0	0.1	0.0	0.0	0.1
(48)	0.2	0.1	0.3	0.2	0.0	0.4
(49)	1.2	1.0	1.4	1.5	1.3	1.7
(50)	1.7	1.4	2.0	2.1	1.8	2.4
(51)	1.7	1.4	2.0	2.1	1.8	2.4
(52)	2.9	2.4	3.5	3.5	3.0	4.0
(53)	0.8	0.6	0.9	0.9	0.8	1.1
(54)	2.1	1.7	2.5	2.6	2.2	3.0
(55)	2.2	1.8	2.6	2.8	2.4	3.1
(56)	1.4	1.2	1.7	1.8	1.5	2.0
(57)	0.9	0.8	1.1	1.1	1.0	1.3
(58)	0.7	0.6	0.8	0.8	0.7	1.0
(59)	0.3	0.2	0.3	0.3	0.3	0.4
(60)	0.5	0.4	0.6	0.6	0.5	0.7
(61)	0.8	0.6	0.9	0.9	0.8	1.1
(62)	0.5	0.4	0.6	0.6	0.5	0.7
(63)	297.4	246.8	342.0	302.6	263.5	341.0
(64)	6.7	4.8	9.1	18.6	13.8	23.4
(65)	4.1	-7.1	17.1	7.0	-7.1	19.0
(66)	539.7	409.7	656.2	476.6	383.6	566.2
(67)	60.4	51.5	68.3	59.9	53.6	66.3
(68)	85.1	64.7	103.0	54.2	43.3	65.4
(69)	179.6	151.6	204.4	199.5	174.2	224.5
(70)	152.0	126.4	174.7	160.6	139.3	181.6
(71)	36.0	30.1	42.8	45.0	38.7	51.2
(72)	1.2	1.0	1.4	1.5	1.3	1.7
(73)	5.2	4.3	6.1	6.5	5.6	7.3
(74)	1.4	0.0	2.9	0.8	0.0	2.1
Exchange Fluxes						
(2)	0	0	1	0	0	1
(3)	0	0	Inf	0	0	Inf
(4)	17	0	Inf	558	0	Inf
(5)	808	0	Inf	686	0	Inf
(6)	456	0	Inf	113	0	Inf
(7)	0	0	Inf	0	0	Inf
(8)	0	0	Inf	16	0	>1000
(11)	0	0	1	0	0	1
(12)	Inf	Inf	Inf	Inf	Inf	Inf
(13)	Inf	0	Inf	Inf	0	Inf
(14)	0	0	0	0	0	1
(15)	7	4	Inf	16	3	Inf
(16)	Inf	Inf	Inf	Inf	Inf	Inf
(17)	295	4	Inf	40	3	Inf

(24)	564	0	Inf	203	0	Inf
(27)	223	0	Inf	682	0	Inf
(28)	539	0	Inf	0	0	250
(29)	Inf	Inf	Inf	Inf	Inf	Inf
(30)	146	82	301	191	117	378
(31)	0	0	0	0	0	2
(36)	554	0	Inf	84	0	Inf
(45)	2	1	2	3	3	4
(65)	246	0	Inf	370	0	Inf

Table B.4 Results of ^{13}C -MFA for GX50 grown on glucose and xylose at the specified ratios. The reaction numbers correspond to the reactions listed in Table B.2. The fluxes are normalized to a total substrate uptake rate of 100. 95% confidence intervals of fluxes (LB95 = lower bound, UB95 = upper bound) were determined by evaluating the sensitivity of the minimized SSR to flux variations.

Glucose:Xylose		1:1			2:2		
SSR		176.8			154.9		
Net Fluxes							
Reaction No.	Best Fit	LB95	UB95	Best Fit	LB95	UB95	
(1)	74.8	71.0	78.5	73.0	65.0	81.2	
(2)	48.3	45.6	51.0	48.5	42.9	54.2	
(3)	75.5	71.5	79.5	75.3	66.7	84.0	
(4)	75.5	71.5	79.5	75.3	66.7	84.0	
(5)	75.5	71.5	79.5	75.3	66.7	84.0	
(6)	163.5	154.8	172.2	163.2	144.5	182.1	
(7)	150.5	141.8	159.2	150.3	132.2	168.7	
(8)	46.7	40.3	52.2	48.0	38.4	57.9	
(9)	24.9	23.6	26.3	23.0	20.5	25.6	
(10)	24.3	22.9	25.8	22.1	19.6	24.6	
(11)	2.5	1.6	3.3	0.3	-0.6	1.3	
(12)	21.9	21.1	22.7	21.7	19.7	23.8	
(13)	27.7	26.2	29.2	27.3	24.2	30.4	
(14)	-12.5	-13.3	-11.7	-12.3	-13.8	-10.8	
(15)	-15.2	-16.0	-14.4	-15.0	-16.6	-13.4	
(16)	-15.2	-16.0	-14.4	-15.0	-16.6	-13.4	
(17)	15.2	14.4	16.0	15.0	13.4	16.6	
(18)	0.6	0.1	1.2	0.9	0.4	1.5	

(19)	0.6	0.1	1.2	0.9	0.4	1.5
(20)	25.2	24.0	26.5	27.0	24.2	29.7
(21)	25.2	24.0	26.5	27.0	24.2	29.7
(22)	104.9	96.2	113.7	104.9	88.1	122.0
(23)	24.2	22.6	26.0	21.0	18.7	23.4
(24)	24.2	22.6	26.0	21.0	18.7	23.4
(25)	23.5	21.3	25.8	20.0	17.4	22.9
(26)	15.4	13.3	17.8	11.9	9.8	14.5
(27)	11.9	9.8	14.2	8.4	6.4	10.8
(28)	16.2	14.6	17.9	12.9	11.1	14.9
(29)	18.9	17.3	20.7	15.7	13.7	17.8
(30)	17.1	13.4	19.5	13.9	11.1	17.1
(31)	0.7	0.0	1.5	0.9	0.1	1.7
(32)	0.7	0.0	1.5	0.9	0.1	1.7
(33)	2.6	0.1	6.6	2.7	0.0	5.6
(34)	25.7	23.9	28.0	24.8	21.9	27.9
(35)	2.4	0.0	5.5	1.4	0.0	4.7
(36)	54.4	45.7	63.1	57.4	41.3	73.8
(37)	48.8	47.7	49.9	49.0	44.5	53.5
(38)	5.0	4.9	5.1	5.1	4.6	5.5
(39)	1.6	1.5	1.6	1.6	1.4	1.7
(40)	2.1	2.0	2.1	2.1	1.9	2.3
(41)	13.7	13.3	14.2	13.9	12.5	15.2
(42)	1.7	1.7	1.7	1.7	1.6	1.9
(43)	3.6	3.6	3.7	3.7	3.3	4.0
(44)	8.3	8.1	8.6	8.3	7.5	9.1
(45)	4.6	4.4	4.8	4.6	4.1	5.1
(46)	0.7	0.6	0.8	0.6	0.5	0.8
(47)	0.3	0.0	0.4	0.2	0.0	0.4
(48)	0.1	0.0	0.5	0.2	0.0	0.6
(49)	1.7	1.7	1.8	1.7	1.6	1.9
(50)	2.4	2.4	2.5	2.4	2.2	2.7
(51)	2.4	2.4	2.5	2.4	2.2	2.7
(52)	4.0	3.8	4.4	4.1	3.6	4.7
(53)	1.1	1.1	1.1	1.1	1.0	1.2
(54)	3.0	2.9	3.1	3.0	2.7	3.3
(55)	3.2	3.1	3.3	3.2	2.9	3.5
(56)	2.1	2.0	2.1	2.1	1.9	2.3
(57)	1.3	1.3	1.3	1.3	1.2	1.4
(58)	1.0	1.0	1.0	1.0	0.9	1.1
(59)	0.4	0.4	0.4	0.4	0.4	0.4
(60)	0.7	0.7	0.7	0.7	0.6	0.7
(61)	1.1	1.1	1.1	1.1	1.0	1.2

(62)	0.7	0.7	0.7	0.7	0.6	0.7
(63)	274.1	253.3	295.1	259.1	220.0	298.7
(64)	16.2	14.6	17.9	12.9	11.1	14.9
(65)	50.9	45.0	55.9	59.3	50.1	68.3
(66)	420.5	361.9	479.3	384.1	278.9	490.9
(67)	25.2	24.0	26.5	27.0	24.2	29.7
(68)	58.2	49.5	66.9	61.3	45.1	77.7
(69)	190.4	178.8	202.1	180.3	158.4	202.9
(70)	145.2	134.3	156.0	136.0	116.2	156.2
(71)	51.9	50.8	53.1	52.2	47.4	56.9
(72)	1.7	1.7	1.8	1.7	1.6	1.9
(73)	7.5	7.3	7.6	7.5	6.8	8.2
(74)	2.2	1.3	3.0	1.0	0.0	2.1
Exchange Fluxes						
(2)	316	256	403	158	130	192
(3)	0	0	Inf	0	0	Inf
(4)	9	0	Inf	202	0	Inf
(5)	9	0	Inf	247	0	Inf
(6)	12	0	Inf	54	0	Inf
(7)	0	0	424	0	0	Inf
(8)	0	0	216	0	0	123
(11)	308	190	>1000	355	211	>1000
(12)	46	0	Inf	204	0	Inf
(13)	39	35	43	39	34	44
(14)	4	4	5	4	3	4
(15)	2	1	Inf	103	1	Inf
(16)	26	0	31	22	0	28
(17)	166	1	Inf	2	1	Inf
(24)	12	0	Inf	185	0	Inf
(27)	178	0	Inf	262	0	Inf
(28)	326	0	Inf	18	0	Inf
(29)	>1000	82	Inf	189	97	Inf
(30)	122	81	Inf	716	100	Inf
(31)	0	0	1	0	0	1
(36)	140	0	Inf	244	0	Inf
(45)	2	1	2	2	1	2
(65)	164	0	Inf	195	0	Inf

Glucose:Xylose	1:2			2:1		
SSR	184.8			194.1		
Net Fluxes						
Reaction No.	Best Fit	LB95	UB95	Best Fit	LB95	UB95

(1)	65.6	62.2	69.1	81.4	80.6	82.3
(2)	39.5	37.2	41.8	54.9	54.0	55.9
(3)	72.8	68.8	76.7	77.2	76.1	78.4
(4)	72.8	68.8	76.7	77.2	76.1	78.4
(5)	72.8	68.8	76.7	77.2	76.1	78.4
(6)	161.4	152.7	170.2	165.1	162.8	167.5
(7)	149.2	140.8	157.6	152.2	149.5	154.9
(8)	57.0	51.4	62.5	41.6	36.9	46.0
(9)	24.7	23.2	26.2	25.0	24.2	25.7
(10)	23.9	22.4	25.6	23.8	22.9	24.7
(11)	-0.6	-1.4	0.3	4.3	3.5	5.0
(12)	24.5	23.3	25.7	19.5	18.9	20.1
(13)	33.8	31.9	35.7	22.9	22.1	23.5
(14)	-15.6	-16.6	-14.7	-10.1	-10.4	-9.7
(15)	-18.2	-19.2	-17.2	-12.8	-13.1	-12.4
(16)	-18.2	-19.2	-17.2	-12.8	-13.1	-12.4
(17)	18.2	17.2	19.2	12.8	12.4	13.1
(18)	0.8	0.2	1.4	1.1	0.6	1.8
(19)	0.8	0.2	1.4	1.1	0.6	1.8
(20)	34.4	32.6	36.2	18.6	17.8	19.4
(21)	34.4	32.6	36.2	18.6	17.8	19.4
(22)	106.4	98.7	114.1	106.6	101.7	111.5
(23)	21.1	19.2	23.1	22.0	20.2	23.8
(24)	21.1	19.2	23.1	22.0	20.2	23.8
(25)	20.3	18.1	22.9	21.3	19.2	23.5
(26)	12.7	10.6	15.1	13.2	11.3	15.2
(27)	9.4	7.3	11.7	9.6	7.8	11.6
(28)	13.5	11.8	15.3	13.9	12.4	15.5
(29)	16.1	14.4	18.0	16.7	15.1	18.4
(30)	15.3	11.7	17.9	15.1	12.6	18.0
(31)	0.7	0.0	1.5	0.7	0.0	1.4
(32)	0.7	0.0	1.5	0.7	0.0	1.4
(33)	1.6	0.0	5.4	2.3	0.0	4.8
(34)	24.0	21.6	26.6	24.7	22.6	26.8
(35)	2.8	0.0	6.2	1.3	0.0	4.2
(36)	60.3	52.7	68.0	58.2	50.8	65.7
(37)	46.1	43.4	48.8	49.2	46.3	52.2
(38)	4.8	4.5	5.0	5.1	4.8	5.4
(39)	1.5	1.4	1.6	1.6	1.5	1.7
(40)	2.0	1.9	2.1	2.1	2.0	2.2
(41)	12.9	12.1	13.8	14.0	13.1	14.9
(42)	1.6	1.5	1.7	1.7	1.6	1.8
(43)	3.4	3.2	3.6	3.7	3.5	3.9

(44)	7.9	7.4	8.4	8.3	7.8	8.8
(45)	4.4	4.1	4.7	4.6	4.3	4.9
(46)	0.7	0.6	0.8	0.6	0.5	0.7
(47)	0.3	0.1	0.4	0.1	0.0	0.3
(48)	0.1	0.0	0.5	0.3	0.0	0.6
(49)	1.6	1.5	1.7	1.8	1.6	1.9
(50)	2.3	2.2	2.4	2.5	2.3	2.6
(51)	2.3	2.2	2.4	2.5	2.3	2.6
(52)	3.8	3.4	4.2	4.2	3.8	4.6
(53)	1.0	1.0	1.1	1.1	1.0	1.2
(54)	2.8	2.7	3.0	3.0	2.8	3.2
(55)	3.0	2.8	3.2	3.2	3.0	3.4
(56)	1.9	1.8	2.1	2.1	2.0	2.2
(57)	1.2	1.2	1.3	1.3	1.2	1.4
(58)	0.9	0.9	1.0	1.0	0.9	1.0
(59)	0.4	0.4	0.4	0.4	0.4	0.4
(60)	0.6	0.6	0.7	0.7	0.6	0.7
(61)	1.0	1.0	1.1	1.1	1.0	1.2
(62)	0.6	0.6	0.7	0.7	0.6	0.7
(63)	269.8	250.7	289.1	269.2	258.9	279.4
(64)	13.5	11.8	15.3	13.9	12.4	15.5
(65)	48.8	42.1	55.2	55.3	48.1	62.5
(66)	420.7	368.6	473.2	416.4	370.2	462.6
(67)	34.4	32.6	36.2	18.6	17.8	19.4
(68)	63.9	56.3	71.6	62.1	54.8	69.3
(69)	184.1	172.6	196.0	185.7	180.9	190.8
(70)	141.6	131.7	151.8	141.5	136.4	146.7
(71)	49.1	46.3	52.0	52.4	49.3	55.5
(72)	1.6	1.5	1.7	1.8	1.6	1.9
(73)	7.1	6.6	7.5	7.5	7.1	8.0
(74)	3.1	2.2	4.0	0.2	0.0	1.2
Exchange Fluxes						
(2)	283	238	343	188	155	234
(3)	37	0	Inf	3	0	Inf
(4)	0	0	Inf	0	0	Inf
(5)	347	0	Inf	0	0	Inf
(6)	5	0	Inf	118	0	Inf
(7)	0	0	269	0	0	Inf
(8)	0	0	98	0	0	113
(11)	330	181	852	402	229	1424
(12)	0	0	Inf	>1000	>1000	Inf
(13)	39	35	42	39	36	43
(14)	4	4	5	4	3	4

(15)	5	0	Inf	113	0	Inf
(16)	19	9	23	26	0	33
(17)	16	0	Inf	1	0	Inf
(24)	279	0	Inf	224	0	Inf
(27)	131	0	Inf	209	0	Inf
(28)	0	0	Inf	>1000	>1000	Inf
(29)	524	76	Inf	118	77	Inf
(30)	141	77	Inf	>1000	82	Inf
(31)	0	0	1	1	0	2
(36)	194	0	Inf	222	0	Inf
(45)	1	1	2	2	1	2
(65)	341	0	Inf	183	0	Inf

Glucose:Xylose		1:0			2:0	
SSR		157.1			175.9	
Net Fluxes						
Reaction No.	Best Fit	LB95	UB95	Best Fit	LB95	UB95
(1)	100.0	88.0	112.1	100.0	87.9	112.1
(2)	70.9	62.3	79.5	70.5	61.8	79.2
(3)	82.5	72.5	92.5	82.5	72.3	92.7
(4)	82.5	72.5	92.5	82.5	72.3	92.7
(5)	82.5	72.5	92.5	82.5	72.3	92.7
(6)	170.1	149.5	190.7	170.5	149.4	191.5
(7)	156.6	137.3	175.9	157.5	137.6	177.4
(8)	27.5	20.7	34.3	30.1	22.5	37.9
(9)	27.5	24.2	30.9	28.0	24.6	31.4
(10)	26.6	23.3	30.0	26.8	23.5	30.2
(11)	12.2	10.7	13.8	12.5	10.9	14.2
(12)	14.5	12.6	16.3	14.3	12.5	16.1
(13)	12.2	10.7	13.8	12.5	10.9	14.2
(14)	-4.7	-5.4	-4.1	-4.9	-5.6	-4.2
(15)	-7.5	-8.4	-6.6	-7.6	-8.6	-6.7
(16)	-7.5	-8.4	-6.6	-7.6	-8.6	-6.7
(17)	7.5	6.6	8.4	7.6	6.7	8.6
(18)	0.9	0.4	1.3	1.1	0.7	1.6
(19)	0.9	0.4	1.3	1.1	0.7	1.6
(20)		Not in model			Not in model	
(21)		Not in model			Not in model	
(22)	109.4	93.9	124.7	112.9	95.9	129.9
(23)	22.9	19.5	26.6	21.3	18.1	24.7
(24)	22.9	19.5	26.6	21.3	18.1	24.7
(25)	22.5	18.9	26.3	20.3	17.1	23.7

(26)	14.1	11.6	16.9	12.2	10.0	14.7
(27)	10.5	8.4	12.8	8.7	6.9	10.8
(28)	14.6	12.2	17.1	13.3	11.2	15.6
(29)	17.5	14.7	20.4	16.1	13.6	18.7
(30)	16.6	13.7	19.6	15.8	13.2	18.9
(31)	0.5	0.0	1.1	1.1	0.5	1.6
(32)	0.5	0.0	1.1	1.1	0.5	1.6
(33)	1.4	0.0	3.7	1.3	0.0	3.4
(34)	24.2	20.6	28.1	22.9	19.4	26.4
(35)	1.1	0.0	3.3	1.2	0.0	3.6
(36)	59.2	45.3	73.2	64.7	48.7	80.8
(37)	50.6	43.2	58.1	48.7	41.7	56.0
(38)	5.2	4.5	6.0	5.0	4.3	5.8
(39)	1.6	1.4	1.9	1.6	1.3	1.8
(40)	2.2	1.9	2.5	2.1	1.8	2.4
(41)	14.1	12.0	16.2	13.6	11.6	15.6
(42)	1.8	1.5	2.0	1.7	1.5	2.0
(43)	3.8	3.2	4.3	3.6	3.1	4.2
(44)	8.7	7.4	10.0	8.4	7.2	9.6
(45)	4.9	4.2	5.6	4.7	4.0	5.4
(46)	0.6	0.5	0.7	0.6	0.5	0.8
(47)	0.2	0.0	0.3	0.3	0.1	0.4
(48)	0.0	0.0	0.3	0.0	0.0	0.2
(49)	1.8	1.5	2.1	1.7	1.5	2.0
(50)	2.5	2.2	2.9	2.4	2.1	2.8
(51)	2.5	2.2	2.9	2.4	2.1	2.8
(52)	4.0	3.4	4.6	3.9	3.3	4.4
(53)	1.1	1.0	1.3	1.1	0.9	1.3
(54)	3.1	2.7	3.6	3.0	2.6	3.4
(55)	3.3	2.8	3.8	3.2	2.7	3.7
(56)	2.1	1.8	2.5	2.1	1.8	2.4
(57)	1.4	1.2	1.6	1.3	1.1	1.5
(58)	1.0	0.9	1.2	1.0	0.8	1.1
(59)	0.4	0.4	0.5	0.4	0.3	0.5
(60)	0.7	0.6	0.8	0.7	0.6	0.8
(61)	1.1	1.0	1.3	1.1	0.9	1.3
(62)	0.7	0.6	0.8	0.7	0.6	0.8
(63)	282.3	244.9	319.8	285.8	245.8	325.7
(64)	14.6	12.2	17.1	13.3	11.2	15.6
(65)	52.7	42.0	63.8	49.6	38.8	60.7
(66)	459.6	368.7	551.4	483.1	379.6	587.8
(67)		Not in model			Not in model	
(68)	63.2	49.3	77.1	68.5	52.5	84.6

(69)	192.8	169.1	216.9	192.0	167.9	216.3
(70)	148.4	129.1	167.9	149.6	129.1	170.0
(71)	53.9	46.1	62.0	52.0	44.4	59.7
(72)	1.8	1.5	2.1	1.7	1.5	2.0
(73)	7.7	6.6	8.9	7.5	6.4	8.6
(74)	0.0	0.0	0.8	0.5	0.0	1.4
Exchange Fluxes						
(2)	173	131	234	160	122	214
(3)	0	0	Inf	79	0	Inf
(4)	83	0	Inf	0	0	Inf
(5)	85	0	Inf	71	0	Inf
(6)	214	0	Inf	272	0	Inf
(7)	0	0	Inf	0	0	Inf
(8)	0	0	89	0	0	54
(11)	68	27	Inf	70	25	Inf
(12)	115	0	Inf	102	0	Inf
(13)	65	27	Inf	58	25	Inf
(14)	5	5	6	5	5	6
(15)	0	0	Inf	0	0	Inf
(16)	42	34	53	42	0	53
(17)	113	0	Inf	112	0	Inf
(24)	20	0	Inf	34	0	Inf
(27)	83	0	Inf	186	0	Inf
(28)	962	0	Inf	861	0	Inf
(29)	930	66	Inf	>1000	59	Inf
(30)	106	65	Inf	89	57	Inf
(31)	1	0	1	0	0	1
(36)	37	0	Inf	73	0	Inf
(45)	184	0	Inf	78	0	Inf
(65)	2	2	3	2	2	2

Glucose:Xylose	0:1			0:2		
SSR	102.2			108.3		
Net Fluxes						
Reaction No.	Best Fit	LB95	UB95	Best Fit	LB95	UB95
(1)	Not in model			Not in model		
(2)	-14.6	-17.3	-12.0	-14.1	-16.9	-11.9
(3)	55.6	48.7	62.7	56.3	49.4	63.2
(4)	55.6	48.7	62.7	56.3	49.4	63.2
(5)	55.6	48.7	62.7	56.3	49.4	63.2
(6)	146.0	128.3	164.4	147.4	129.5	165.7
(7)	135.8	119.4	152.8	137.9	121.1	155.0

(8)	103.2	88.1	116.8	107.3	91.3	120.4
(9)	13.3	10.9	16.0	13.0	10.8	15.7
(10)	12.3	9.8	14.9	12.2	9.8	14.8
(11)	-29.4	-33.6	-25.4	-29.2	-33.2	-25.2
(12)	41.7	36.5	47.0	41.4	36.2	46.6
(13)	70.6	61.7	79.4	70.8	62.1	79.8
(14)	-34.2	-38.5	-29.9	-34.4	-38.8	-30.2
(15)	-36.4	-40.9	-31.8	-36.4	-41.0	-31.9
(16)	-36.4	-40.9	-31.8	-36.4	-41.0	-31.9
(17)	36.4	31.8	40.9	36.4	31.9	41.0
(18)	1.0	0.0	2.2	0.8	0.0	2.1
(19)	1.0	0.0	2.2	0.8	0.0	2.1
(20)	100.0	87.6	112.5	100.0	87.8	112.5
(21)	100.0	87.6	112.5	100.0	87.8	112.5
(22)	100.1	87.7	113.0	104.8	91.5	118.3
(23)	29.8	24.2	36.2	29.4	23.9	35.5
(24)	29.8	24.2	36.2	29.4	23.9	35.5
(25)	28.7	21.6	36.2	28.4	21.6	35.5
(26)	22.2	15.6	28.9	22.5	16.1	28.8
(27)	19.4	12.9	25.8	19.9	13.6	25.8
(28)	23.3	18.4	28.9	23.4	18.6	28.8
(29)	25.5	20.4	31.4	25.5	20.5	31.1
(30)	15.0	8.4	19.7	15.2	8.2	19.1
(31)	1.1	0.0	3.3	1.0	0.0	3.1
(32)	1.1	0.0	3.3	1.0	0.0	3.1
(33)	11.6	8.7	17.7	11.2	8.9	17.7
(34)	29.9	24.6	36.8	29.0	23.9	35.3
(35)	2.0	0.0	4.9	2.6	0.0	4.6
(36)	49.0	38.9	59.3	55.7	44.6	66.9
(37)	39.1	32.3	45.9	36.2	29.8	42.6
(38)	4.0	3.3	4.7	3.7	3.1	4.4
(39)	1.3	1.0	1.5	1.2	1.0	1.4
(40)	1.7	1.4	2.0	1.6	1.3	1.8
(41)	11.2	9.2	13.1	10.3	8.5	12.2
(42)	1.4	1.1	1.6	1.3	1.0	1.5
(43)	2.9	2.4	3.4	2.7	2.2	3.2
(44)	6.5	5.4	7.7	6.1	5.0	7.1
(45)	3.6	3.0	4.3	3.3	2.7	3.9
(46)	0.4	0.3	0.6	0.4	0.3	0.5
(47)	0.0	0.0	0.1	0.0	0.0	0.1
(48)	0.3	0.0	0.5	0.3	0.0	0.5
(49)	1.4	1.1	1.6	1.3	1.1	1.5
(50)	1.9	1.6	2.3	1.8	1.5	2.1

(51)	1.9	1.6	2.3	1.8	1.5	2.1
(52)	3.4	2.8	4.0	3.1	2.6	3.7
(53)	0.9	0.7	1.0	0.8	0.7	0.9
(54)	2.4	2.0	2.8	2.2	1.8	2.6
(55)	2.6	2.1	3.0	2.4	1.9	2.8
(56)	1.6	1.4	1.9	1.5	1.3	1.8
(57)	1.1	0.9	1.2	1.0	0.8	1.1
(58)	0.8	0.6	0.9	0.7	0.6	0.9
(59)	0.3	0.3	0.4	0.3	0.2	0.4
(60)	0.5	0.4	0.6	0.5	0.4	0.6
(61)	0.9	0.7	1.0	0.8	0.7	0.9
(62)	0.5	0.4	0.6	0.5	0.4	0.6
(63)	267.3	228.5	308.8	278.8	239.4	322.1
(64)	23.3	18.4	28.9	23.4	18.6	28.8
(65)	35.6	16.7	52.9	29.2	10.5	44.5
(66)	383.9	293.0	477.2	435.6	344.5	534.2
(67)	100.0	87.6	112.5	100.0	87.8	112.5
(68)	52.1	42.0	62.2	58.5	47.5	69.6
(69)	190.7	163.7	221.6	194.3	166.9	224.7
(70)	145.3	123.7	168.5	151.1	129.4	175.0
(71)	41.5	34.3	48.8	38.5	31.6	45.2
(72)	1.4	1.1	1.6	1.3	1.1	1.5
(73)	6.0	4.9	7.0	5.5	4.5	6.5
(74)	1.4	0.4	2.6	1.5	0.4	2.7
Exchange Fluxes						
(2)	35	0	Inf	52	0	Inf
(3)	4	1	Inf	33	1	Inf
(4)	173	1	Inf	127	1	Inf
(5)	130	2	Inf	10	4	Inf
(6)	Inf	0	Inf	89	0	Inf
(7)	47	0	Inf	0	0	Inf
(8)	3	0	49	0	0	44
(11)	Inf	Inf	Inf	>1000	31	Inf
(12)	622	0	Inf	21	0	Inf
(13)	51	27	58	47	29	54
(14)	2	0	21	1	0	12
(15)	17	0	Inf	10	0	Inf
(16)	21	0	35	0	0	25
(17)	197	0	Inf	83	0	Inf
(24)	37	0	Inf	78	0	Inf
(27)	37	0	Inf	21	0	Inf
(28)	0	0	Inf	0	0	Inf
(29)	553	111	Inf	571	105	Inf

(30)	207	111	Inf	188	105	Inf
(31)	1	0	2	1	0	2
(36)	161	0	Inf	89	0	Inf
(45)	19	0	Inf	31	0	Inf
(65)	2	1	2	2	1	2

Table B.5 Mass isotopomer distributions from parallel labeling experiments with LMSE2 grown on glucose and xylose at the specified ratio.

Tracer: A) [1,2-¹³C]glucose + [1,2-¹³C]xylose

B) [1,6-¹³C]glucose + [5-¹³C]xylose

Ratio	1:1		2:2		1:2		2:1	
Tracer	A	B	A	B	A	B	A	B
Ala232 (M0)	48.4	33.1	48.1	32.9	48.3	33.1	47.6	32.9
Ala232 (M1)	12.1	50.0	12.1	50.1	12.0	50.1	12.3	50.1
Ala232 (M2)	31.3	12.1	31.4	12.2	31.5	12.0	31.7	12.2
Ala232 (M3)	5.9	4.2	5.9	4.2	5.9	4.2	6.0	4.2
Ala232 (M4)	2.4	0.6	2.4	0.6	2.4	0.6	2.4	0.6
Ala260 (M0)	47.5	32.5	47.3	32.3	47.5	32.6	46.7	32.3
Ala260 (M1)	12.0	49.6	12.0	49.7	11.9	49.7	12.0	49.5
Ala260 (M2)	17.8	12.6	17.9	12.7	17.9	12.5	18.1	12.8
Ala260 (M3)	17.4	4.4	17.5	4.5	17.4	4.4	17.8	4.5
Ala260 (M4)	4.0	0.7	4.0	0.7	4.0	0.7	4.0	0.7
Ala260 (M5)	1.4	0.1	1.4	0.1	1.4	0.1	1.4	0.1
Gly218 (M0)	49.9	75.0	49.8	75.5	49.7	75.0	49.2	75.6
Gly218 (M1)	37.6	17.2	37.7	16.8	37.8	17.2	38.2	16.6
Gly218 (M2)	9.6	6.8	9.6	6.8	9.6	6.8	9.7	6.7
Gly218 (M3)	2.9	1.0	2.9	1.0	2.9	1.0	2.9	1.0
Gly246 (M0)	48.7	73.4	48.7	73.9	48.5	73.4	48.1	74.1
Gly246 (M1)	23.8	17.9	23.7	17.5	23.9	18.0	23.9	17.4
Gly246 (M2)	21.4	7.3	21.5	7.2	21.5	7.3	21.8	7.2
Gly246 (M3)	4.6	1.2	4.6	1.1	4.6	1.2	4.7	1.1
Gly246 (M4)	1.5	0.2	1.5	0.2	1.5	0.2	1.5	0.2
Val260 (M0)	11.3	16.4	30.9	16.0	31.1	16.5	30.2	15.9
Val260 (M1)	9.2	36.2	9.3	36.4	9.1	36.1	9.4	36.5
Val260 (M2)	34.6	34.7	34.7	34.7	35.0	34.7	34.9	34.7

Val260 (M3)	8.5	9.3	8.6	9.4	8.5	9.3	8.9	9.5
Val260 (M4)	13.0	2.9	13.0	2.9	13.0	2.9	13.3	2.9
Val260 (M5)	2.5	0.5	2.5	0.5	2.4	0.4	2.5	0.5
Val260 (M6)	0.9	0.1	0.9	0.1	0.9	0.1	0.9	0.1
Val288 (M0)								
Val288 (M1)	31.2	16.3	30.8	15.9	31.0	16.5	30.0	15.8
Val288 (M2)	9.1	36.0	9.1	36.1	8.9	35.9	9.1	36.1
Val288 (M3)	26.4	34.5	26.6	34.6	26.8	34.6	26.7	34.6
Val288 (M4)	14.6	9.6	14.7	9.7	14.7	9.4	15.0	9.8
Val288 (M5)	9.2	3.0	9.3	3.1	9.2	3.0	9.5	3.1
Val288 (M6)	7.3	0.5	7.3	0.5	7.3	0.5	7.5	0.5
Val288 (M7)	1.6	0.1	1.6	0.1	1.6	0.1	1.7	0.1
Val288 (M7)	0.5	0.0	0.5	0.0	0.5	0.0	0.5	0.0
Leu274 (M0)								
Leu274 (M1)	22.0	10.2	21.5	9.9	21.6	10.5	20.6	9.7
Leu274 (M2)	15.8	21.7	15.8	21.9	15.8	21.6	15.8	22.1
Leu274 (M3)	24.5	35.1	24.5	35.2	24.8	35.0	24.6	35.3
Leu274 (M4)	18.2	24.1	18.4	24.2	18.3	24.2	18.8	24.1
Leu274 (M5)	11.2	6.6	11.3	6.6	11.2	6.5	11.5	6.7
Leu274 (M6)	6.4	1.9	6.5	1.9	6.4	1.9	6.7	1.9
Leu274 (M7)	1.5	0.3	1.5	0.3	1.5	0.3	1.5	0.3
Leu274 (M7)	0.4	0.0	0.4	0.0	0.4	0.0	0.4	0.0
Ile200 (M0)								
Ile200 (M1)	27.5	15.4	26.8	14.8	27.8	15.9	25.5	14.4
Ile200 (M2)	13.6	31.6	13.9	31.4	13.0	32.1	14.2	31.3
Ile200 (M3)	27.1	35.0	26.9	35.1	27.9	35.0	26.9	35.2
Ile200 (M4)	15.6	14.0	16.0	14.5	15.2	13.3	16.5	14.9
Ile200 (M5)	10.0	3.3	10.1	3.5	10.1	3.1	10.3	3.6
Ile200 (M6)	5.2	0.6	5.3	0.6	5.1	0.5	5.5	0.7
Ile200 (M7)	0.8	0.1	0.8	0.1	0.8	0.1	0.8	0.1
Ile200 (M7)	0.2	0.0	0.2	0.0	0.2	0.0	0.2	0.0
Ile274 (M0)								
Ile274 (M1)	24.7	13.7	24.0	13.2	24.9	14.1	22.8	12.8
Ile274 (M2)	14.0	29.5	14.3	29.2	13.5	30.1	14.5	29.1
Ile274 (M3)	26.2	34.2	26.0	34.3	26.8	34.3	26.0	34.4
Ile274 (M4)	16.3	16.0	16.6	16.5	16.0	15.4	17.2	16.8
Ile274 (M5)	11.0	5.1	11.1	5.3	11.1	4.8	11.4	5.3
Ile274 (M6)	6.0	1.2	6.0	1.3	5.9	1.1	6.2	1.3
Ile274 (M7)	1.4	0.2	1.4	0.2	1.4	0.2	1.5	0.2
Ile274 (M7)	0.4	0.0	0.4	0.0	0.4	0.0	0.4	0.0
Pro258 (M0)								
Pro258 (M1)	27.2	14.8	26.6	14.2	27.0	15.0	25.0	14.0
Pro258 (M1)	16.6	32.3	16.8	32.0	16.1	32.3	17.2	32.2

Pro258 (M2)	29.5	34.7	29.5	34.7	30.1	34.5	29.4	34.7
Pro258 (M3)	12.8	13.4	13.0	13.9	12.6	13.3	13.8	14.0
Pro258 (M4)	10.9	3.9	11.0	4.0	11.1	3.9	11.2	4.1
Pro258 (M5)	2.4	0.8	2.4	0.9	2.4	0.9	2.6	0.9
Pro258 (M6)	0.8	0.1	0.8	0.1	0.8	0.1	0.8	0.1
Met218 (M0)	27.5	16.0	26.7	15.5	27.7	16.4	25.7	15.2
Met218 (M1)	25.7	31.6	25.8	31.5	25.6	32.1	25.9	31.7
Met218 (M2)	22.4	33.1	22.5	33.5	22.4	33.0	23.0	33.5
Met218 (M3)	17.3	14.5	17.7	14.8	17.3	14.1	18.0	14.9
Met218 (M4)	7.1	4.7	7.3	4.7	7.0	4.4	7.5	4.7
Met320 (M0)	22.3	12.7	21.7	12.2	22.5	13.4	20.6	11.9
Met320 (M1)	21.7	26.4	21.4	26.2	21.7	27.1	21.5	26.3
Met320 (M2)	20.8	32.3	20.9	32.5	20.8	32.0	21.2	32.5
Met320 (M3)	18.2	18.7	18.5	19.0	18.2	18.1	18.7	19.1
Met320 (M4)	11.8	7.5	12.0	7.7	11.7	7.2	12.3	7.7
Met320 (M5)	5.3	2.3	5.5	2.4	5.2	2.2	5.6	2.4
Ser390 (M0)	38.3	28.9	37.8	28.8	38.0	28.9	36.6	28.9
Ser390 (M1)	18.5	45.8	19.0	45.8	18.6	45.8	19.5	45.8
Ser390 (M2)	19.3	16.7	19.5	16.7	19.5	16.7	19.9	16.7
Ser390 (M3)	16.4	6.8	16.3	6.8	16.4	6.8	16.5	6.8
Ser390 (M4)	5.5	1.6	5.4	1.5	5.5	1.5	5.5	1.5
Ser390 (M5)	2.0	0.4	2.0	0.3	2.0	0.3	2.0	0.3
Thr376 (M0)	31.8	22.2	31.3	21.7	32.4	22.8	30.2	21.5
Thr376 (M1)	22.1	39.8	22.0	39.7	21.5	40.4	22.5	39.6
Thr376 (M2)	23.7	24.2	23.8	24.6	23.9	23.6	24.1	24.8
Thr376 (M3)	15.4	10.0	15.6	10.1	15.3	9.6	15.9	10.2
Thr376 (M4)	5.3	3.1	5.5	3.2	5.2	3.0	5.5	3.2
Thr376 (M5)	1.8	0.7	1.8	0.8	1.7	0.7	1.8	0.8
Thr404 (M0)	28.6	19.4	27.8	18.9	29.4	20.3	26.9	18.7
Thr404 (M1)	19.2	36.9	19.3	36.5	18.8	37.6	19.4	36.6
Thr404 (M2)	21.7	26.6	21.9	27.0	21.7	25.9	22.2	27.2
Thr404 (M3)	16.1	11.9	16.4	12.1	16.3	11.3	16.6	12.1
Thr404 (M4)	9.9	4.0	10.1	4.1	9.6	3.7	10.3	4.1
Thr404 (M5)	3.4	1.1	3.4	1.1	3.2	1.0	3.4	1.1
Thr404 (M6)	1.1	0.2	1.1	0.2	1.0	0.2	1.1	0.2
Phe308 (M0)	30.1	6.0	29.5	5.6	29.6	6.3	28.6	5.3
Phe308 (M1)	9.9	12.1	9.9	12.2	9.7	12.1	9.8	12.4

Phe308 (M2)	33.1	34.8	33.1	35.0	33.6	34.7	33.3	35.3
Phe308 (M3)	9.6	33.8	9.8	33.9	9.6	33.7	10.0	33.7
Phe308 (M4)	12.8	9.7	12.9	9.7	12.8	9.6	13.2	9.7
Phe308 (M5)	3.1	3.0	3.2	3.0	3.1	2.9	3.4	3.0
Phe308 (M6)	1.1	0.5	1.2	0.5	1.2	0.5	1.3	0.5
Phe308 (M7)	0.2	0.1	0.3	0.1	0.2	0.1	0.3	0.1
Phe308 (M8)	0.1	0.0	0.1	0.0	0.1	0.0	0.2	0.0
Phe336 (M0)	29.8	6.0	29.3	5.7	29.5	6.4	28.4	5.4
Phe336 (M1)	9.8	12.1	9.9	12.2	9.7	12.2	9.7	12.5
Phe336 (M2)	25.5	34.4	25.3	34.7	25.7	34.3	25.5	34.9
Phe336 (M3)	15.1	33.5	15.3	33.7	15.2	33.4	15.5	33.5
Phe336 (M4)	9.4	9.9	9.6	9.9	9.5	9.8	9.8	9.9
Phe336 (M5)	7.5	3.2	7.6	3.1	7.5	3.1	7.8	3.1
Phe336 (M6)	2.1	0.6	2.1	0.5	2.1	0.6	2.3	0.6
Phe336 (M7)	0.7	0.1	0.7	0.1	0.7	0.1	0.8	0.1
Phe336 (M8)	0.1	0.0	0.2	0.0	0.2	0.0	0.2	0.0
Phe336 (M9)	0.1	0.0	0.1	0.0	0.1	0.0	0.1	0.0
Asp390 (M0)	32.0	22.0	31.4	21.5	32.5	22.5	30.5	21.4
Asp390 (M1)	22.1	39.7	22.3	39.5	21.6	40.1	22.5	39.5
Asp390 (M2)	23.6	24.3	23.8	24.7	23.8	23.8	24.0	24.8
Asp390 (M3)	15.2	10.0	15.4	10.2	15.1	9.8	15.8	10.2
Asp390 (M4)	5.3	3.1	5.3	3.2	5.2	3.0	5.4	3.2
Asp390 (M5)	1.8	0.8	1.8	0.8	1.7	0.8	1.8	0.8
Asp418 (M0)	28.7	19.6	28.2	19.1	29.4	20.4	27.0	18.8
Asp418 (M1)	19.5	36.8	19.6	36.5	19.0	37.5	19.7	36.5
Asp418 (M2)	21.8	26.4	21.9	26.8	21.8	25.7	22.2	27.0
Asp418 (M3)	16.0	11.8	16.1	12.1	16.0	11.4	16.3	12.1
Asp418 (M4)	9.7	4.0	9.9	4.1	9.6	3.8	10.2	4.2
Asp418 (M5)	3.2	1.1	3.3	1.1	3.2	1.0	3.4	1.1
Asp418 (M6)	1.0	0.2	1.1	0.2	1.0	0.2	1.1	0.2
Glu330 (M0)	26.4	14.1	25.9	13.8	26.4	14.3	24.9	13.7
Glu330 (M1)	16.9	31.9	17.1	31.8	16.2	32.0	17.3	31.9
Glu330 (M2)	29.1	34.5	29.1	34.5	29.8	34.5	29.2	34.5
Glu330 (M3)	13.2	14.0	13.4	14.3	13.0	13.8	13.9	14.3
Glu330 (M4)	10.9	4.3	10.9	4.4	11.1	4.2	11.1	4.4
Glu330 (M5)	2.7	1.0	2.7	1.0	2.7	1.0	2.7	1.0
Glu330 (M6)	0.8	0.2	0.8	0.2	0.9	0.2	0.9	0.2
Glu432 (M0)	21.1	11.4	20.6	11.0	21.1	11.8	19.6	10.9

Glu432 (M1)	14.8	26.5	14.9	26.3	14.4	26.9	14.9	26.2
Glu432 (M2)	25.0	33.0	24.9	33.0	25.5	33.1	24.9	33.1
Glu432 (M3)	17.4	18.6	17.6	18.9	17.2	18.1	18.0	19.0
Glu432 (M4)	12.0	7.5	12.1	7.7	12.1	7.2	12.4	7.7
Glu432 (M5)	6.8	2.3	6.9	2.4	6.8	2.2	7.2	2.4
Glu432 (M6)	2.2	0.6	2.3	0.6	2.2	0.5	2.3	0.6
Glu432 (M7)	0.7	0.1	0.7	0.1	0.7	0.1	0.7	0.1
Lys329 (M0)	24.0	13.6	23.6	13.2	24.3	14.1	22.4	13.0
Lys329 (M1)	15.1	28.6	15.2	28.4	14.7	28.9	15.3	28.5
Lys329 (M2)	25.1	33.3	25.3	33.5	26.0	33.5	25.3	33.6
Lys329 (M3)	16.3	16.8	16.9	17.1	16.4	16.3	17.4	17.2
Lys329 (M4)	10.8	5.6	11.0	5.8	11.0	5.4	11.4	5.8
Lys329 (M5)	6.4	1.5	6.2	1.5	5.9	1.4	6.4	1.5
Lys329 (M6)	2.3	0.6	1.9	0.4	1.7	0.4	1.8	0.4
Lys431 (M0)	20.6	11.7	19.8	11.3	20.5	12.0	18.9	11.1
Lys431 (M1)	14.4	25.4	14.4	25.2	14.0	25.8	14.1	25.2
Lys431 (M2)	21.0	32.0	21.0	32.0	21.4	32.2	21.0	32.1
Lys431 (M3)	17.4	19.4	17.7	19.8	17.6	18.8	18.1	19.8
Lys431 (M4)	12.5	8.0	12.9	8.2	12.6	7.9	13.2	8.3
Lys431 (M5)	8.1	2.6	8.3	2.7	8.2	2.5	8.5	2.6
Lys431 (M6)	4.1	0.7	4.2	0.7	4.0	0.6	4.4	0.7
Lys431 (M7)	1.4	0.1	1.4	0.2	1.4	0.1	1.4	0.2
Lys431 (M8)	0.5	0.1	0.4	0.1	0.4	0.0	0.5	0.0
Tyr302 (M0)	48.0	71.6	47.6	71.8	47.9	72.0	47.2	71.6
Tyr302 (M1)	25.0	19.5	25.1	19.4	25.1	19.2	25.0	19.5
Tyr302 (M2)	21.7	7.6	21.9	7.5	21.7	7.5	22.3	7.5
Tyr302 (M3)	5.3	1.3	5.4	1.3	5.4	1.3	5.5	1.3
Tyr302 (M4)	0.0	0.0	0.0	0.0	0.0	0.0	0.0	0.0
RNA_Rib173 (M0)	90.4	6.6	90.1	6.0	90.0	6.6	89.9	6.1
RNA_Rib173 (M1)	8.4	86.5	8.5	87.0	8.7	86.5	8.6	87.0
RNA_Rib173 (M2)	1.3	6.9	1.4	7.0	1.4	6.9	1.5	6.9
RNA_Rib284 (M0)	7.0	84.5	6.7	84.2	6.4	84.5	6.9	84.3
RNA_Rib284 (M1)	79.2	12.7	79.4	12.8	79.5	12.6	78.7	12.8

RNA_Rib284 (M2)	11.2	2.0	11.3	2.0	11.3	2.0	11.6	2.1
RNA_Rib284 (M3)	2.3	0.7	2.3	0.8	2.3	0.7	2.4	0.7
RNA_Rib284 (M4)	0.3	0.1	0.3	0.2	0.4	0.1	0.4	0.1
Glycogen_Gluc1 73 (M0)	90.4	15.2	90.0	12.2	89.9	15.9	89.8	13.2
Glycogen_Gluc1 73 (M1)	8.4	78.3	8.7	81.0	8.8	77.7	8.8	80.3
Glycogen_Gluc1 73 (M2)	1.2	6.4	1.3	6.7	1.3	6.3	1.4	6.5
Glycogen_Gluc3 70 (M0)	14.5	13.8	11.6	11.0	11.7	14.4	12.9	11.9
Glycogen_Gluc3 70 (M1)	3.5	70.5	3.1	72.8	3.2	70.0	3.3	72.1
Glycogen_Gluc3 70 (M2)	67.9	12.9	70.6	13.3	70.4	12.8	69.3	13.1
Glycogen_Gluc3 70 (M3)	11.6	2.3	12.1	2.4	12.1	2.3	11.9	2.3
Glycogen_Gluc3 70 (M4)	2.2	0.4	2.3	0.4	2.3	0.4	2.2	0.4
Glycogen_Gluc3 70 (M5)	0.3	0.1	0.3	0.1	0.3	0.1	0.3	0.1

Table B.7 Mass isotopomer distributions from parallel labeling experiments with GX50 grown on glucose and xylose at the specified ratio.

- Tracer: A) [1,2-¹³C]glucose + [1,2-¹³C]xylose
 B) [1,6-¹³C]glucose + [5-¹³C]xylose
 C) [1,2-¹³C]glucose
 D) [1,6-¹³C]glucose
 E) [1,2-¹³C]xylose
 F) [5-¹³C]xylose

Ratio	1:0		2:0		0:1		0:2	
Tracer	C	D	C	D	E	F	E	F
Ala232 (M0)	44.2	12.3	43.7	12.1	48.8	31.9	48.6	31.5
Ala232 (M1)	14.7	66.7	14.8	66.8	13.0	50.6	12.9	50.6
Ala232 (M2)	32.4	14.5	32.7	14.6	30.2	12.5	30.4	12.8
Ala232 (M3)	6.2	5.7	6.3	5.7	5.7	4.3	5.8	4.4
Ala232 (M4)	2.4	0.8	2.5	0.8	2.2	0.6	2.3	0.7
Ala260 (M0)	43.6	11.7	43.0	11.5	47.6	31.2	47.4	30.9
Ala260 (M1)	12.7	66.0	12.7	66.1	12.7	50.0	12.6	49.9
Ala260 (M2)	33.3	15.2	33.8	15.3	7.1	13.2	7.0	13.2
Ala260 (M3)	7.2	6.0	7.4	6.0	25.5	4.7	25.8	5.0
Ala260 (M4)	2.7	0.9	2.8	0.9	5.0	0.7	5.0	0.8
Ala260 (M5)	0.4	0.2	0.4	0.2	2.1	0.1	2.1	0.2
Gly218 (M0)	49.4	76.0	48.9	76.0	51.2	76.1	50.9	76.1
Gly218 (M1)	38.1	16.4	38.5	16.4	36.6	16.3	36.9	16.3
Gly218 (M2)	9.6	6.6	9.7	6.7	9.4	6.6	9.4	6.7
Gly218 (M3)	2.9	1.0	2.9	0.9	2.8	0.9	2.8	0.9
Gly246 (M0)	46.6	74.3	46.1	74.5	49.9	74.8	49.7	74.7
Gly246 (M1)	38.8	17.3	39.2	17.2	12.0	17.0	11.9	17.0
Gly246 (M2)	10.8	7.0	10.9	7.0	30.1	7.0	30.4	7.0
Gly246 (M3)	3.3	1.1	3.3	1.1	5.6	1.0	5.7	1.1
Gly246 (M4)	0.5	0.2	0.5	0.2	2.3	0.2	2.3	0.2
Val260 (M0)	26.8	7.8	25.9	8.0	31.7	15.2	31.3	14.9
Val260 (M1)	11.9	10.5	11.9	10.8	10.6	35.4	10.4	35.6
Val260 (M2)	32.5	60.8	32.9	60.3	33.8	35.6	34.1	35.7
Val260 (M3)	11.1	14.4	11.3	14.4	9.1	10.0	9.1	10.1
Val260 (M4)	13.9	5.4	14.2	5.5	11.8	3.1	12.0	3.1
Val260 (M5)	2.8	0.9	2.8	0.8	2.3	0.5	2.3	0.5
Val260 (M6)	1.0	0.1	1.0	0.1	0.8	0.1	0.8	0.1
Val288 (M0)	26.6	7.8	25.7	8.0	31.2	15.1	30.8	14.8
Val288 (M1)	10.7	10.0	10.7	10.3	10.2	35.0	10.1	35.2
Val288 (M2)	32.8	60.5	33.1	60.1	19.8	35.5	19.9	35.5
Val288 (M3)	10.8	14.8	11.1	14.8	19.5	10.4	19.7	10.5
Val288 (M4)	14.6	5.7	14.8	5.7	6.4	3.3	6.4	3.3
Val288 (M5)	3.2	0.9	3.3	0.9	10.2	0.6	10.4	0.6
Val288 (M6)	1.1	0.2	1.2	0.2	2.0	0.1	2.0	0.1
Val288 (M7)	0.2	0.0	0.2	0.0	0.8	0.0	0.8	0.0

Leu274 (M0)	18.5	7.8	17.4	8.3	22.0	9.7	21.6	9.4
Leu274 (M1)	16.1	3.2	16.1	3.5	16.7	21.0	16.7	21.2
Leu274 (M2)	22.7	13.6	23.0	14.1	25.0	35.0	25.1	35.1
Leu274 (M3)	20.3	56.3	20.7	55.4	18.0	24.9	18.1	24.9
Leu274 (M4)	12.5	13.2	12.7	13.0	10.8	7.0	10.9	7.1
Leu274 (M5)	7.7	5.0	7.8	4.9	5.8	2.0	5.9	2.0
Leu274 (M6)	1.7	0.7	1.8	0.7	1.3	0.3	1.4	0.3
Leu274 (M7)	0.5	0.1	0.5	0.1	0.4	0.1	0.4	0.1
Ile200 (M0)	24.4	8.9	23.5	9.2	26.9	14.7	26.4	14.3
Ile200 (M1)	13.8	8.4	13.9	8.6	15.1	32.0	15.1	32.0
Ile200 (M2)	28.6	47.4	28.9	47.3	25.0	35.9	25.1	35.9
Ile200 (M3)	15.1	26.7	15.4	26.4	17.4	13.5	17.6	13.8
Ile200 (M4)	12.7	7.0	12.9	6.9	8.8	3.3	8.8	3.4
Ile200 (M5)	4.4	1.4	4.5	1.3	5.8	0.6	5.9	0.6
Ile200 (M6)	0.8	0.2	0.8	0.2	0.8	0.1	0.9	0.1
Ile200 (M7)	0.2	0.1	0.2	0.0	0.2	0.0	0.2	0.0
Ile274 (M0)	21.9	8.0	21.0	8.1	24.1	13.2	23.6	12.7
Ile274 (M1)	14.0	7.9	14.0	8.2	15.4	29.8	15.4	29.8
Ile274 (M2)	27.5	43.7	27.7	43.6	24.3	35.0	24.4	35.0
Ile274 (M3)	16.0	27.6	16.3	27.5	17.9	15.7	18.1	15.9
Ile274 (M4)	13.5	9.7	13.7	9.5	9.9	5.0	10.0	5.1
Ile274 (M5)	5.4	2.5	5.5	2.5	6.4	1.2	6.6	1.2
Ile274 (M6)	1.4	0.5	1.4	0.5	1.5	0.2	1.5	0.2
Ile274 (M7)	0.3	0.1	0.4	0.1	0.4	0.1	0.5	0.1
Pro258 (M0)	22.9	8.0	22.6	8.0	26.4	13.7	26.1	13.4
Pro258 (M1)	16.6	9.5	16.5	9.8	17.3	31.8	17.2	31.9
Pro258 (M2)	28.7	50.1	29.3	50.0	29.4	35.3	29.6	35.4
Pro258 (M3)	15.1	23.0	14.9	23.0	13.3	13.9	13.4	14.1
Pro258 (M4)	12.7	7.3	12.7	7.3	10.3	4.2	10.5	4.2
Pro258 (M5)	3.2	1.7	3.1	1.8	2.5	0.9	2.5	1.0
Pro258 (M6)	0.9	0.3	0.9	0.3	0.8	0.2	0.8	0.2
Met218 (M0)	25.0	15.4	24.1	9.4	27.5	15.9	27.0	15.5
Met218 (M1)	24.7	33.0	25.0	12.4	26.2	32.9	26.4	32.9
Met218 (M2)	24.5	33.7	24.8	45.5	20.9	33.7	21.0	33.8
Met218 (M3)	19.1	13.5	19.2	24.5	17.6	13.2	17.7	13.5
Met218 (M4)	6.8	4.4	6.9	8.2	7.8	4.2	7.9	4.3
Met320 (M0)	20.7	12.5	20.0	7.7	21.9	12.9	21.5	12.6
Met320 (M1)	20.7	27.9	20.7	9.8	22.4	28.1	22.5	28.0

Met320 (M2)	23.6	32.9	23.8	36.7	18.4	33.0	18.5	32.9
Met320 (M3)	20.1	17.6	20.4	29.1	17.3	17.2	17.3	17.5
Met320 (M4)	10.3	6.9	10.3	12.5	13.5	6.8	13.7	6.9
Met320 (M5)	4.6	2.3	4.7	4.2	6.4	2.0	6.5	2.2
Ser390 (M0)	35.1	11.4	34.9	11.3	39.5	28.0	39.1	27.8
Ser390 (M1)	19.7	57.7	19.3	57.7	16.8	46.5	16.9	46.7
Ser390 (M2)	30.3	19.7	30.7	19.8	11.0	16.8	11.0	16.9
Ser390 (M3)	9.9	8.9	10.0	8.8	22.6	6.8	22.8	6.8
Ser390 (M4)	4.1	2.0	4.1	2.0	7.0	1.5	7.1	1.5
Ser390 (M5)	0.9	0.5	0.9	0.5	3.1	0.3	3.1	0.3
Thr376 (M0)	30.4	22.1	29.5	9.3	31.4	22.5	30.9	22.1
Thr376 (M1)	20.9	40.8	21.4	41.7	23.0	41.1	23.1	41.3
Thr376 (M2)	27.7	23.4	28.0	30.5	21.1	23.4	21.3	23.4
Thr376 (M3)	14.0	9.7	14.4	13.3	16.9	9.3	16.9	9.6
Thr376 (M4)	5.5	3.1	5.2	4.2	5.6	2.8	5.8	2.9
Thr376 (M5)	1.6	0.9	1.5	1.0	2.0	0.8	2.0	0.7
Thr404 (M0)	28.1	19.8	27.1	8.5	28.0	20.3	27.5	19.8
Thr404 (M1)	17.8	38.6	17.8	35.2	20.3	38.6	20.2	38.6
Thr404 (M2)	27.9	25.4	28.5	33.4	17.7	25.2	17.8	25.5
Thr404 (M3)	14.4	11.3	14.7	15.8	16.8	11.1	16.8	11.3
Thr404 (M4)	8.4	3.8	8.3	5.5	11.9	3.6	12.1	3.7
Thr404 (M5)	2.5	1.0	2.6	1.3	4.0	1.0	4.2	0.9
Thr404 (M6)	0.9	0.3	0.8	0.3	1.4	0.2	1.4	0.2
Phe308 (M0)	20.2	7.6	19.6	7.6	5.7	6.8	5.4	6.5
Phe308 (M1)	10.4	2.9	10.3	2.9	24.1	14.4	24.3	14.4
Phe308 (M2)	26.7	10.3	26.9	10.3	8.0	34.4	7.9	34.7
Phe308 (M3)	13.1	57.0	13.2	57.1	28.9	31.9	29.2	31.8
Phe308 (M4)	16.6	15.4	17.1	15.3	11.4	9.0	11.3	9.2
Phe308 (M5)	7.0	5.6	6.8	5.6	11.5	2.8	11.6	2.8
Phe308 (M6)	4.2	1.0	4.1	1.0	6.8	0.5	6.7	0.5
Phe308 (M7)	1.4	0.2	1.4	0.2	1.9	0.1	1.9	0.1
Phe308 (M8)	0.4	0.1	0.4	0.1	1.8	0.1	1.7	0.1
Phe336 (M0)	20.5	7.4	19.5	7.6	5.6	7.0	5.3	6.6
Phe336 (M1)	9.7	3.1	9.7	3.2	23.9	14.5	24.0	14.4
Phe336 (M2)	26.5	10.0	27.3	10.3	7.8	34.2	7.9	34.4
Phe336 (M3)	12.8	56.7	13.0	56.3	16.2	31.6	16.4	31.6
Phe336 (M4)	16.8	15.6	17.1	15.7	20.8	9.2	20.8	9.4
Phe336 (M5)	7.2	5.9	7.0	5.8	6.5	2.9	6.3	3.0

Phe336 (M6)	4.3	1.0	4.3	1.0	11.6	0.5	11.6	0.5
Phe336 (M7)	1.5	0.2	1.6	0.2	4.6	0.1	4.6	0.1
Phe336 (M8)	0.4	0.0	0.4	0.0	1.5	0.0	1.5	0.0
Phe336 (M9)	0.1	0.0	0.1	0.0	1.5	0.0	1.5	0.0
Asp390 (M0)	30.5	9.6	30.0	9.3	31.6	22.5	31.5	22.1
Asp390 (M1)	21.1	41.6	21.0	41.9	22.8	41.5	22.8	41.3
Asp390 (M2)	27.8	30.2	27.9	30.2	21.2	23.0	21.2	23.4
Asp390 (M3)	14.0	13.2	14.3	13.2	16.8	9.5	16.9	9.5
Asp390 (M4)	5.2	4.4	5.2	4.4	5.6	2.8	5.6	2.9
Asp390 (M5)	1.5	1.1	1.6	1.1	2.0	0.7	2.1	0.7
Asp418 (M0)	28.3	9.1	27.5	8.8	28.0	20.4	27.7	20.0
Asp418 (M1)	18.0	35.1	18.2	35.3	20.5	38.8	20.5	38.7
Asp418 (M2)	28.0	32.6	28.2	32.8	17.7	25.0	17.8	25.3
Asp418 (M3)	14.4	15.8	14.7	15.6	16.7	11.0	16.7	11.2
Asp418 (M4)	8.2	5.6	8.2	5.6	11.7	3.6	11.9	3.7
Asp418 (M5)	2.4	1.6	2.5	1.6	4.0	1.0	4.1	1.0
Asp418 (M6)	0.8	0.3	0.8	0.3	1.4	0.2	1.4	0.2
Glu330 (M0)	23.1	7.6	22.3	7.4	26.5	13.6	26.3	13.3
Glu330 (M1)	16.5	9.3	16.6	9.5	17.2	31.9	17.1	32.0
Glu330 (M2)	28.8	49.9	29.2	50.2	29.3	35.1	29.5	35.2
Glu330 (M3)	14.9	23.3	15.0	23.0	13.2	13.8	13.2	14.0
Glu330 (M4)	12.6	7.6	12.7	7.6	10.5	4.3	10.6	4.3
Glu330 (M5)	3.2	2.0	3.2	1.9	2.6	1.0	2.6	1.1
Glu330 (M6)	1.0	0.4	1.0	0.4	0.8	0.2	0.8	0.2
Glu432 (M0)	19.0	6.6	18.1	6.4	20.5	11.2	20.2	10.8
Glu432 (M1)	14.2	7.6	14.2	7.7	15.5	27.0	15.5	27.0
Glu432 (M2)	25.8	38.9	26.1	39.2	23.4	33.7	23.5	33.8
Glu432 (M3)	17.1	28.3	17.3	28.4	18.6	17.9	18.8	18.3
Glu432 (M4)	14.3	12.8	14.4	12.7	11.4	7.3	11.4	7.3
Glu432 (M5)	6.6	4.3	6.7	4.3	7.4	2.2	7.5	2.2
Glu432 (M6)	2.3	1.1	2.3	1.1	2.3	0.5	2.4	0.5
Glu432 (M7)	0.7	0.2	0.7	0.2	0.8	0.1	0.8	0.1
Lys329 (M0)	22.0	13.5	21.0	9.3	24.0	14.1	23.7	13.3
Lys329 (M1)	14.6	28.7	14.9	8.9	16.1	28.8	16.3	29.0
Lys329 (M2)	26.3	34.0	26.8	40.9	23.7	33.8	23.6	34.0
Lys329 (M3)	16.3	16.5	16.5	27.2	17.9	16.2	18.0	16.3
Lys329 (M4)	13.3	5.5	13.4	10.1	10.0	5.4	10.1	5.6
Lys329 (M5)	5.6	1.5	5.8	2.9	6.5	1.3	6.6	1.4

Lys329 (M6)	1.9	0.4	1.7	0.7	1.8	0.4	1.8	0.4
Lys431 (M0)	19.0	11.5	17.9	7.9	20.3	12.1	19.7	11.5
Lys431 (M1)	13.1	25.4	13.4	8.1	15.0	25.8	15.0	25.7
Lys431 (M2)	24.8	32.5	25.3	34.9	17.0	32.4	17.1	32.6
Lys431 (M3)	16.2	19.1	16.6	29.0	18.8	18.7	18.8	18.9
Lys431 (M4)	15.1	8.0	15.2	13.7	12.5	7.8	12.7	8.0
Lys431 (M5)	7.3	2.6	7.4	4.7	8.6	2.4	8.7	2.5
Lys431 (M6)	3.1	0.7	3.1	1.3	5.5	0.6	5.6	0.7
Lys431 (M7)	1.0	0.2	1.0	0.3	1.8	0.1	1.8	0.1
Lys431 (M8)	0.3	0.0	0.2	0.1	0.6	0.0	0.6	0.0
Tyr302 (M0)	44.9	71.6	44.4	71.6	48.8	71.7	48.7	71.6
Tyr302 (M1)	39.4	19.5	39.6	19.4	13.6	19.5	13.5	19.5
Tyr302 (M2)	12.1	7.5	12.3	7.6	30.6	7.5	30.8	7.6
Tyr302 (M3)	3.6	1.3	3.7	1.3	6.9	1.3	7.0	1.3
Tyr302 (M4)	0.0	0.0	0.0	0.0	0.0	0.0	0.0	0.0
RNA_Rib173 (M0)	66.7	10.5	67.1	9.8	79.9	17.5	80.1	16.5
RNA_Rib173 (M1)	9.6	82.8	9.7	83.4	7.6	76.3	7.7	77.2
RNA_Rib173 (M2)	23.6	6.7	23.3	6.7	12.5	6.2	12.2	6.2
RNA_Rib284 (M0)	8.6	76.3	7.6	76.6	5.4	84.3	4.8	84.3
RNA_Rib284 (M1)	52.9	19.6	54.2	19.3	2.3	12.7	2.2	12.7
RNA_Rib284 (M2)	29.2	3.0	29.1	3.0	70.1	2.1	71.0	2.1
RNA_Rib284 (M3)	8.2	0.9	7.9	0.9	9.5	0.7	9.6	0.7
RNA_Rib284 (M4)	1.2	0.2	1.2	0.2	12.7	0.2	12.4	0.1
Glycogen_Glu c173 (M0)	83.2	21.2	83.0	22.7	70.7	42.0	71.8	38.9
Glycogen_Glu c173 (M1)	8.8	72.8	9.1	71.4	7.6	53.4	7.5	56.3
Glycogen_Glu c173 (M2)	8.0	6.1	7.9	5.9	21.8	4.6	20.7	4.8

Glycogen_Glu c370 (M0)	18.4	22.3	18.4	23.6	17.9	79.6	20.2	79.7
Glycogen_Glu c370 (M1)	6.0	63.3	5.9	62.3	3.9	16.7	4.3	16.6
Glycogen_Glu c370 (M2)	56.8	11.8	57.3	11.5	2.5	3.0	2.5	3.0
Glycogen_Glu c370 (M3)	15.2	2.1	14.8	2.1	47.4	0.5	46.0	0.5
Glycogen_Glu c370 (M4)	3.0	0.4	3.0	0.4	8.5	0.1	8.2	0.1
Glycogen_Glu c370 (M5)	0.5	0.1	0.5	0.2	19.8	0.1	18.9	0.1

Ratio	1:1		2:2		1:2		2:1	
	A	B	A	B	A	B	A	B
Ala232 (M0)	44.6	15.7	44.7	15.5	45.1	18.1	44.6	13.7
Ala232 (M1)	14.7	63.7	14.4	64.1	14.5	62.0	14.6	65.6
Ala232 (M2)	32.0	14.3	32.2	14.1	31.8	13.9	32.1	14.3
Ala232 (M3)	6.2	5.5	6.2	5.5	6.2	5.3	6.2	5.6
Ala232 (M4)	2.4	0.8	2.4	0.8	2.4	0.7	2.4	0.8
Ala260 (M0)	43.8	15.2	43.9	14.9	44.3	17.5	43.8	13.1
Ala260 (M1)	12.0	63.0	11.8	63.5	11.9	61.3	12.0	65.0
Ala260 (M2)	29.5	15.0	28.1	14.8	27.4	14.6	29.9	15.0
Ala260 (M3)	10.7	5.8	12.0	5.8	12.1	5.6	10.3	5.9
Ala260 (M4)	3.3	0.9	3.4	0.9	3.4	0.8	3.2	0.9
Ala260 (M5)	0.7	0.2	0.8	0.2	0.9	0.1	0.7	0.2
Gly218 (M0)	49.4	75.9	49.3	76.1	49.7	76.1	49.7	76.2
Gly218 (M1)	38.1	16.5	38.1	16.3	37.9	16.3	37.8	16.3
Gly218 (M2)	9.6	6.7	9.6	6.6	9.6	6.7	9.6	6.6
Gly218 (M3)	2.9	1.0	2.9	0.9	2.9	0.9	2.9	0.9
Gly246 (M0)	46.1	74.3	46.0	74.6	46.3	74.6	46.4	74.6
Gly246 (M1)	35.0	17.3	33.7	17.1	33.1	17.1	35.2	17.1
Gly246 (M2)	14.3	7.1	15.4	7.0	15.7	7.0	13.9	7.0
Gly246 (M3)	3.8	1.1	3.9	1.1	3.9	1.1	3.7	1.1
Gly246 (M4)	0.8	0.2	0.9	0.2	1.0	0.2	0.8	0.2
Val260 (M0)	26.9	7.4	27.0	8.2	27.5	8.4	26.9	7.1
Val260 (M1)	11.9	17.8	11.7	16.4	11.8	20.7	11.9	14.5
Val260 (M2)	33.0	55.3	33.3	56.1	33.1	52.4	33.1	58.4
Val260 (M3)	11.0	13.7	10.8	13.5	10.7	13.0	11.0	13.9

Val260 (M4)	13.5	5.0	13.6	5.0	13.3	4.7	13.6	5.2
Val260 (M5)	2.7	0.8	2.7	0.8	2.6	0.7	2.7	0.8
Val260 (M6)	1.0	0.1	1.0	0.1	0.9	0.1	1.0	0.1
Val288 (M0)	26.8	7.3	26.8	8.1	27.3	8.3	26.7	7.0
Val288 (M1)	10.3	17.4	10.1	16.0	10.2	20.4	10.3	14.1
Val288 (M2)	31.2	55.0	30.7	55.9	30.3	52.2	31.5	58.3
Val288 (M3)	12.1	14.0	12.6	13.8	12.6	13.3	11.9	14.2
Val288 (M4)	13.3	5.2	13.0	5.2	12.7	4.9	13.5	5.4
Val288 (M5)	4.6	0.8	5.1	0.8	5.1	0.8	4.4	0.8
Val288 (M6)	1.3	0.2	1.4	0.1	1.4	0.1	1.3	0.2
Val288 (M7)	0.3	0.0	0.3	0.0	0.3	0.0	0.3	0.0
Leu274 (M0)	18.3	6.5	18.3	7.3	18.8	7.1	18.3	6.5
Leu274 (M1)	16.5	5.8	16.4	5.0	16.5	7.5	16.4	4.1
Leu274 (M2)	23.4	22.9	23.7	20.9	23.6	25.8	23.4	18.9
Leu274 (M3)	20.1	48.0	20.0	49.9	19.8	44.2	20.1	52.7
Leu274 (M4)	12.3	11.9	12.2	11.9	12.1	10.9	12.3	12.4
Leu274 (M5)	7.2	4.2	7.2	4.3	7.1	3.8	7.3	4.6
Leu274 (M6)	1.7	0.6	1.7	0.6	1.6	0.6	1.7	0.7
Leu274 (M7)	0.5	0.1	0.5	0.1	0.5	0.1	0.5	0.1
Ile200 (M0)	24.2	8.1	24.2	9.1	24.7	9.2	24.3	7.9
Ile200 (M1)	14.1	14.8	14.0	13.7	14.1	17.8	14.0	12.1
Ile200 (M2)	28.3	46.3	28.2	47.8	28.1	45.7	28.5	49.0
Ile200 (M3)	15.7	23.4	15.8	22.5	15.7	21.0	15.5	23.7
Ile200 (M4)	12.0	6.1	11.9	5.6	11.7	5.2	12.1	5.9
Ile200 (M5)	4.7	1.2	4.9	1.1	4.8	1.0	4.6	1.1
Ile200 (M6)	0.8	0.2	0.8	0.1	0.8	0.1	0.8	0.2
Ile200 (M7)	0.2	0.0	0.2	0.0	0.2	0.1	0.2	0.1
Ile274 (M0)	21.6	7.2	21.6	8.1	22.1	8.1	21.8	7.1
Ile274 (M1)	14.3	13.8	14.2	12.9	14.3	16.5	14.2	11.3
Ile274 (M2)	27.2	43.1	27.2	44.4	27.0	42.8	27.4	45.3
Ile274 (M3)	16.5	24.8	16.6	24.1	16.5	22.6	16.3	25.2
Ile274 (M4)	12.9	8.5	12.7	8.1	12.5	7.6	13.0	8.5
Ile274 (M5)	5.7	2.2	5.8	2.1	5.7	1.9	5.6	2.2
Ile274 (M6)	1.4	0.4	1.4	0.4	1.4	0.3	1.4	0.4
Ile274 (M7)	0.4	0.1	0.4	0.1	0.4	0.1	0.4	0.1
Pro258 (M0)	24.2	7.7	24.2	8.1	24.7	8.6	23.9	7.1
Pro258 (M1)	16.7	16.6	16.4	15.0	16.5	19.5	16.6	13.2
Pro258 (M2)	29.7	47.6	29.9	49.1	29.8	45.9	29.6	50.3

Pro258 (M3)	14.0	20.2	13.9	19.9	13.8	18.7	14.2	21.0
Pro258 (M4)	11.9	6.2	12.0	6.3	11.8	5.8	12.1	6.6
Pro258 (M5)	2.6	1.4	2.6	1.4	2.6	1.3	2.7	1.5
Pro258 (M6)	0.8	0.2	0.8	0.2	0.8	0.2	0.9	0.2
Met218 (M0)	24.8	9.3	24.8	9.9	25.3	10.2	24.9	8.7
Met218 (M1)	25.0	18.3	25.2	17.1	25.2	20.6	25.1	15.8
Met218 (M2)	24.2	43.5	23.9	45.0	23.9	42.9	24.3	46.3
Met218 (M3)	18.8	21.7	18.9	21.0	18.5	19.7	18.7	22.0
Met218 (M4)	7.2	7.2	7.2	7.1	7.1	6.5	7.0	7.3
Met320 (M0)	20.4	7.5	20.2	8.0	20.8	8.3	20.6	7.0
Met320 (M1)	20.7	14.4	20.9	13.8	21.2	17.0	21.0	12.6
Met320 (M2)	22.6	36.8	22.3	38.0	22.1	37.1	22.6	38.7
Met320 (M3)	19.9	26.1	19.9	25.5	19.5	24.1	19.9	26.7
Met320 (M4)	11.3	11.3	11.5	10.8	11.3	10.1	11.0	11.2
Met320 (M5)	5.0	3.9	5.2	3.8	5.1	3.3	4.9	3.7
Ser390 (M0)	36.0	14.2	36.0	13.9	36.5	16.0	36.0	12.5
Ser390 (M1)	18.2	55.7	18.0	56.0	17.7	54.6	18.1	56.9
Ser390 (M2)	27.7	19.3	26.8	19.3	26.4	18.8	28.2	19.5
Ser390 (M3)	12.2	8.5	13.0	8.5	13.1	8.3	12.0	8.7
Ser390 (M4)	4.6	1.9	4.8	1.9	4.9	1.9	4.6	1.9
Ser390 (M5)	1.3	0.4	1.4	0.4	1.4	0.4	1.3	0.4
Thr376 (M0)	30.2	11.5	30.1	11.8	30.5	13.3	30.3	10.4
Thr376 (M1)	21.6	42.4	21.5	43.6	21.4	43.1	21.3	43.9
Thr376 (M2)	26.5	28.7	26.4	28.1	26.2	27.5	27.0	28.8
Thr376 (M3)	14.7	12.4	15.1	11.8	14.9	11.5	14.6	12.1
Thr376 (M4)	5.3	4.0	5.3	3.8	5.3	3.7	5.2	3.9
Thr376 (M5)	1.7	1.0	1.7	1.0	1.7	0.9	1.6	1.0
Thr404 (M0)	27.4	10.2	27.3	10.5	27.8	11.9	27.7	9.2
Thr404 (M1)	18.0	36.9	18.2	38.2	18.2	38.3	18.0	38.0
Thr404 (M2)	26.0	31.3	25.4	31.0	25.0	30.0	26.3	31.6
Thr404 (M3)	15.9	14.8	16.2	14.0	16.1	13.6	15.6	14.5
Thr404 (M4)	8.9	5.2	9.1	4.8	9.0	4.7	8.7	5.1
Thr404 (M5)	2.9	1.4	2.9	1.3	2.9	1.3	2.8	1.3
Thr404 (M6)	0.9	0.3	0.9	0.2	0.9	0.2	0.8	0.3
Phe308 (M0)	14.2	6.1	12.8	6.9	12.9	6.4	14.5	6.3
Phe308 (M1)	14.0	4.1	14.9	3.8	15.3	5.1	13.8	3.3
Phe308 (M2)	18.6	18.4	17.3	16.8	17.1	20.8	19.2	15.0

Phe308 (M3)	20.2	51.5	21.8	52.6	21.9	48.8	19.8	54.7
Phe308 (M4)	13.9	13.9	13.4	13.9	13.2	13.2	14.0	14.4
Phe308 (M5)	11.3	5.0	11.8	5.0	11.7	4.6	11.0	5.2
Phe308 (M6)	4.6	0.8	4.6	0.8	4.6	0.8	4.5	0.9
Phe308 (M7)	2.5	0.1	2.5	0.1	2.4	0.1	2.4	0.1
Phe308 (M8)	0.8	0.0	0.8	0.1	0.8	0.1	0.8	0.2
Phe336 (M0)	14.1	6.1	12.7	7.0	12.9	6.5	14.4	6.2
Phe336 (M1)	13.5	4.3	14.4	4.1	14.8	5.4	13.1	3.4
Phe336 (M2)	17.7	18.1	16.2	16.6	15.8	20.6	18.3	14.7
Phe336 (M3)	19.5	51.1	20.5	51.8	20.6	48.3	19.3	54.2
Phe336 (M4)	14.2	14.3	14.0	14.3	13.9	13.4	14.4	14.8
Phe336 (M5)	11.5	5.1	11.8	5.1	11.6	4.8	11.2	5.4
Phe336 (M6)	5.6	0.9	6.0	0.9	6.0	0.9	5.4	1.0
Phe336 (M7)	2.8	0.2	2.9	0.2	2.9	0.1	2.7	0.2
Phe336 (M8)	1.0	0.0	1.1	0.0	1.1	0.0	1.0	0.0
Phe336 (M9)	0.3	0.0	0.4	0.0	0.4	0.0	0.3	0.0
Asp390 (M0)	30.3	11.5	30.4	11.5	30.8	13.3	30.5	10.2
Asp390 (M1)	21.5	42.3	21.4	43.7	21.4	43.2	21.3	43.8
Asp390 (M2)	26.7	28.6	26.3	28.0	26.1	27.3	26.8	28.7
Asp390 (M3)	14.6	12.5	14.9	12.0	14.8	11.6	14.6	12.3
Asp390 (M4)	5.2	4.1	5.3	3.8	5.3	3.7	5.2	3.9
Asp390 (M5)	1.6	1.0	1.7	0.9	1.6	0.9	1.6	1.0
Asp418 (M0)	27.8	10.7	27.6	10.9	28.1	12.4	27.9	9.7
Asp418 (M1)	18.3	36.7	18.4	38.1	18.5	38.2	18.2	38.0
Asp418 (M2)	25.8	31.0	25.2	30.6	24.9	29.6	26.1	31.3
Asp418 (M3)	15.7	14.7	16.0	14.0	15.9	13.6	15.5	14.4
Asp418 (M4)	8.7	5.2	9.0	4.8	8.9	4.7	8.6	5.0
Asp418 (M5)	2.8	1.4	2.9	1.3	2.9	1.2	2.8	1.4
Asp418 (M6)	0.9	0.3	0.9	0.3	0.9	0.3	0.8	0.3
Glu330 (M0)	23.7	7.6	23.9	8.1	24.4	8.6	23.7	7.1
Glu330 (M1)	16.9	16.3	16.6	14.8	16.7	19.2	16.7	13.0
Glu330 (M2)	29.1	46.6	29.4	48.4	29.3	45.3	29.2	49.8
Glu330 (M3)	14.5	20.9	14.3	20.3	14.1	19.0	14.4	21.2
Glu330 (M4)	11.9	6.8	11.9	6.6	11.7	6.1	12.0	6.9
Glu330 (M5)	3.0	1.7	3.0	1.6	2.9	1.5	3.0	1.7
Glu330 (M6)	0.9	0.3	0.9	0.3	0.9	0.3	0.9	0.3
Glu432 (M0)	19.0	6.4	19.0	6.9	19.5	7.2	19.1	6.0
Glu432 (M1)	14.6	13.1	14.5	12.1	14.6	15.7	14.5	10.6

Glu432 (M2)	25.7	38.5	25.6	40.0	25.6	38.6	25.8	40.6
Glu432 (M3)	17.4	25.8	17.5	25.4	17.3	23.9	17.3	26.4
Glu432 (M4)	13.6	11.3	13.5	11.0	13.3	10.3	13.7	11.5
Glu432 (M5)	6.7	3.7	6.8	3.5	6.7	3.3	6.7	3.7
Glu432 (M6)	2.3	1.0	2.3	0.9	2.3	0.8	2.3	1.0
Glu432 (M7)	0.7	0.2	0.7	0.2	0.7	0.2	0.7	0.2
Lys329 (M0)								
Lys329 (M1)	20.9	7.4	21.1	9.0	21.6	8.3	21.3	8.5
Lys329 (M2)	15.1	13.9	15.0	13.1	15.0	16.5	14.9	11.6
Lys329 (M3)	26.4	41.3	26.6	42.2	26.5	41.2	26.9	42.7
Lys329 (M4)	16.8	25.1	16.9	24.2	16.8	23.2	16.6	25.2
Lys329 (M5)	12.8	9.1	12.6	8.6	12.5	8.1	12.8	9.0
Lys329 (M6)	6.0	2.5	6.0	2.4	5.9	2.2	5.8	2.4
Lys329 (M6)	1.9	0.6	1.8	0.6	1.7	0.5	1.7	0.6
Lys431 (M0)								
Lys431 (M1)	18.0	6.4	18.0	7.7	18.3	7.2	18.1	7.2
Lys431 (M1)	13.3	12.2	13.3	11.7	13.5	14.5	13.3	10.4
Lys431 (M2)	23.7	36.3	23.5	37.1	23.5	36.6	24.3	37.3
Lys431 (M3)	17.5	27.0	17.6	26.6	17.4	25.4	17.2	27.4
Lys431 (M4)	14.4	12.4	14.3	11.7	14.2	11.3	14.5	12.2
Lys431 (M5)	8.0	4.3	8.1	3.9	8.0	3.8	7.9	4.2
Lys431 (M6)	3.6	1.1	3.7	1.0	3.6	1.0	3.4	1.1
Lys431 (M7)	1.1	0.3	1.2	0.2	1.2	0.2	1.1	0.2
Lys431 (M8)	0.3	0.1	0.3	0.1	0.3	0.0	0.3	0.0
Tyr302 (M0)								
Tyr302 (M1)	44.9	71.8	44.9	72.0	45.1	72.0	44.8	71.9
Tyr302 (M1)	35.5	19.4	34.2	19.2	33.7	19.2	36.0	19.3
Tyr302 (M2)	15.4	7.5	16.4	7.4	16.6	7.4	15.0	7.5
Tyr302 (M3)	4.3	1.3	4.5	1.3	4.5	1.3	4.2	1.3
Tyr302 (M4)	0.0	0.0	0.0	0.0	0.0	0.0	0.0	0.0
RNA_Rib173 (M0)								
RNA_Rib173 (M1)	71.7	11.0	71.4	11.6	73.5	11.6	73.2	12.0
RNA_Rib173 (M1)	9.2	82.4	9.4	81.9	9.2	81.8	9.1	81.4
RNA_Rib173 (M2)	19.1	6.6	19.3	6.6	17.3	6.6	17.7	6.5
RNA_Rib284 (M0)								
RNA_Rib284 (M0)	5.5	81.6	5.6	80.8	5.2	82.7	5.0	81.6
RNA_Rib284 (M1)	29.2	15.0	30.5	15.7	24.9	14.1	25.4	15.0

RNA_Rib284 (M2)	45.9	2.5	44.8	2.5	49.5	2.3	49.2	2.5
RNA_Rib284 (M3)	15.5	0.8	15.2	0.8	15.6	0.8	15.8	0.8
RNA_Rib284 (M4)	4.0	0.1	3.8	0.2	4.8	0.1	4.6	0.2
Glycogen_Glu c173 (M0)	82.8	27.1	82.9	18.0	83.0	28.4	82.4	20.9
Glycogen_Glu c173 (M1)	8.6	67.4	8.7	75.8	8.7	66.2	8.6	73.2
Glycogen_Glu c173 (M2)	8.6	5.5	8.5	6.1	8.3	5.4	9.0	5.9
Glycogen_Glu c370 (M0)	22.3	34.9	19.6	23.0	25.4	38.9	19.9	26.8
Glycogen_Glu c370 (M1)	5.7	53.2	5.3	62.9	6.2	50.0	5.2	59.9
Glycogen_Glu c370 (M2)	46.8	9.8	50.1	11.6	42.6	9.2	47.0	11.0
Glycogen_Glu c370 (M3)	17.5	1.7	17.5	2.0	17.6	1.6	19.0	1.9
Glycogen_Glu c370 (M4)	5.4	0.3	5.4	0.4	5.5	0.3	5.9	0.3
Glycogen_Glu c370 (M5)	2.4	0.1	2.1	0.1	2.8	0.0	2.9	0.1

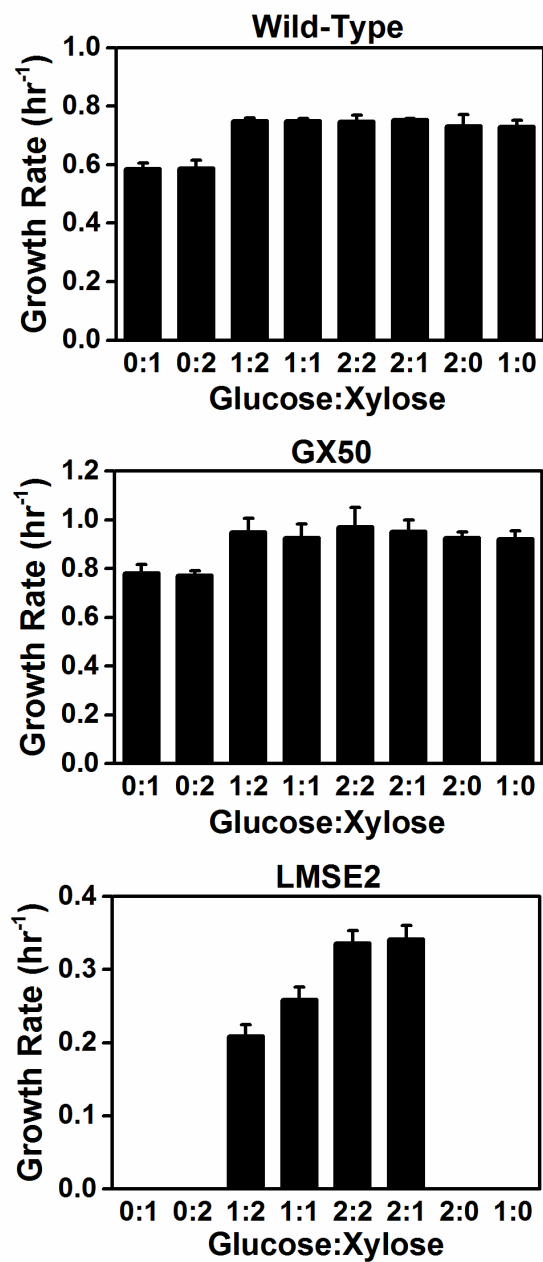


Figure B.1 Growth rates for wild-type *E. coli*, GX50 and LMSE2 for various glucose:xylose concentrations. Error bars indicate standard error (n>3).

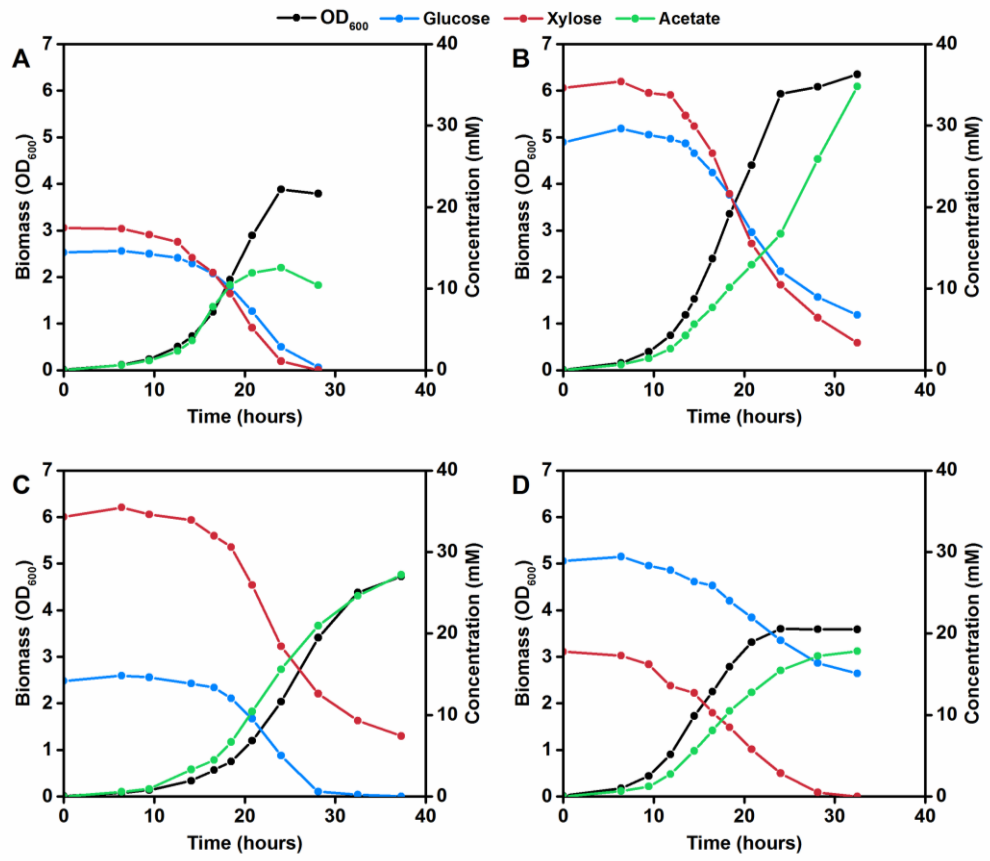


Figure B.2 Representative growth curves for LMSE2 grown on a (A) 1:1, (B) 2:2, (C) 1:2, or (D) 2:1 ratio of glucose to xylose.

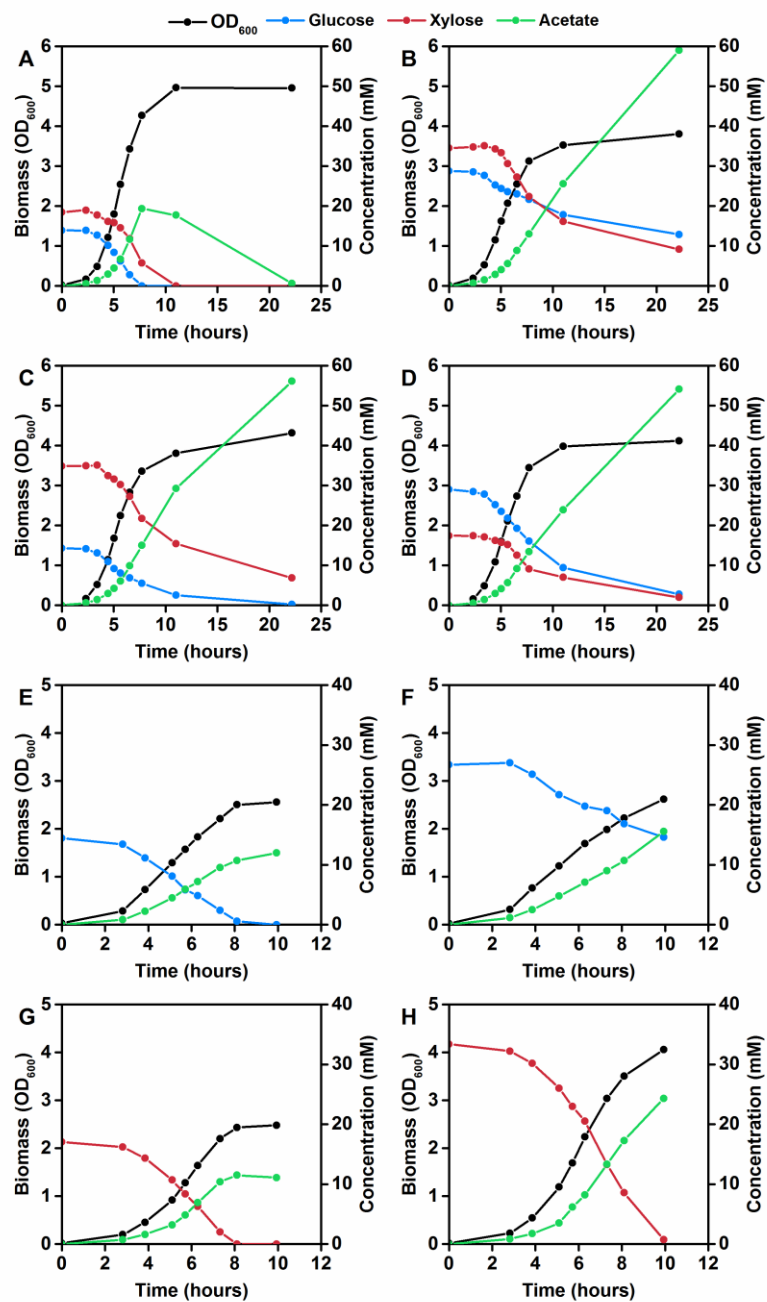


Figure B.3 Representative growth curves for GX50 grown on a (A) 1:1, (B) 2:2, (C) 1:2, (D) 2:1, (E) 1:0, (F) 2:0, (G) 0:1, or (H) 0:2 ratio of glucose to xylose.

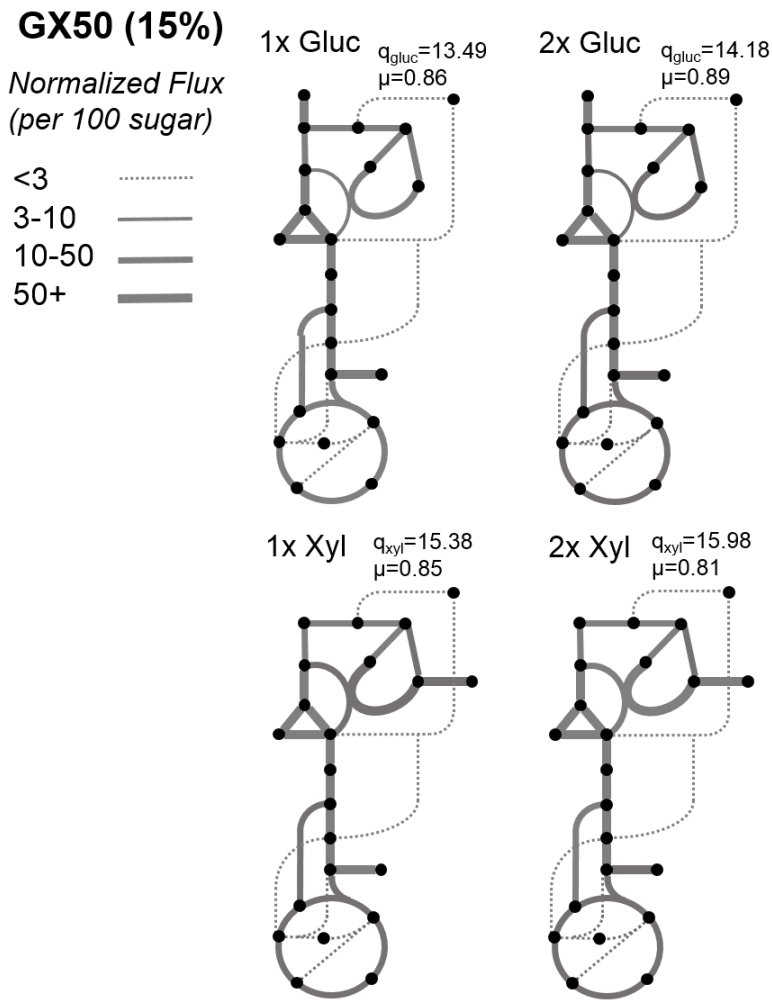


Figure B.4 Comparison of estimated fluxes for various glucose/xylose mixtures. Highlighted changes indicate at least a 15% relative difference compared to the fluxes estimated for the 1x case. Fluxes highlighted blue indicate a flux increase while fluxes highlighted red indicate a flux decrease. No significant change was observed when the glucose or xylose concentration was doubled.

Appendix C

SUPPLEMENTARY DATA FOR CHAPTER 4

Table C.1 ^{13}C -labeling (%) in biomass components during growth on glucose, yeast extract, casamino acids, or tryptone and ^{13}C -methanol (average of two replicates).

Co-substrate	Glucose		Yeast Extract		Casamino Acids		Tryptone	
	24	48	24	48	24	48	24	48
Avg	1	1	2	3	1	1	2	2
Ala260(M0)	99	98	96	95	98	98	97	96
Ala260 (M1)	1	1	2	3	1	1	2	2
Ala260 (M2)	0	0	1	2	1	1	1	1
Ala260 (M3)	0	0	1	1	0	0	0	0
Avg	0	0	0	0	0	0	0	0
Val288 (M0)	99	99	100	100	100	100	100	100
Val288 (M1)	1	1	0	0	0	0	0	0
Val288 (M2)	0	0	0	0	0	0	0	0
Val288 (M3)	0	0	0	0	0	0	0	0
Val288 (M4)	0	0	0	0	0	0	0	0
Val288 (M5)	0	0	0	0	0	0	0	0
Avg	0	0	0	0	0	0	0	0
Leu274 (M0)	98	98	100	100	100	100	100	100
Leu274 (M1)	2	2	0	0	0	0	0	0
Leu274 (M2)	0	0	0	0	0	0	0	0
Leu274 (M3)	0	0	0	0	0	0	0	0
Leu274 (M4)	0	0	0	0	0	0	0	0
Leu274 (M5)	0	0	0	0	0	0	0	0
Avg	1	1	0	0	0	0	0	0
Ile274 (M0)	97	98	100	100	100	100	99	100
Ile274 (M1)	2	2	0	0	0	0	0	0
Ile274 (M2)	0	0	0	0	0	0	0	0
Ile274 (M3)	0	0	0	0	0	0	0	0
Ile274 (M4)	0	0	0	0	0	0	0	0
Ile274 (M5)	0	0	0	0	0	0	0	0

Avg	0	0	3	4	1	1	1	2
Ser390 (M0)	99	99	94	91	98	97	98	96
Ser390 (M1)	1	1	4	6	1	2	1	3
Ser390 (M2)	0	0	1	2	0	1	0	1
Ser390 (M3)	0	0	1	1	0	0	0	0
Avg	0	0	1	1	0	0	0	0
Thr404 (M0)	99	99	98	98	100	100	100	100
Thr404 (M1)	1	1	1	1	0	0	0	0
Thr404 (M2)	0	0	1	1	0	0	0	0
Thr404 (M3)	0	0	0	0	0	0	0	0
Thr404 (M4)	0	0	0	0	0	0	0	0
Avg	0	1	2	2	1	1	1	1
Asp418 (M0)	99	98	96	94	98	98	97	97
Asp418 (M1)	1	2	2	4	1	1	2	2
Asp418 (M2)	0	0	1	2	1	1	1	1
Asp418 (M3)	0	0	0	0	0	0	0	0
Asp418 (M4)	0	0	0	0	0	0	0	0
Avg	1	1	2	3	1	1	1	1
Glu432 (M0)	97	97	94	92	98	98	97	97
Glu432 (M1)	3	3	4	5	1	1	2	2
Glu432 (M2)	0	0	2	3	1	1	1	1
Glu432 (M3)	0	0	0	1	0	0	0	0
Glu432 (M4)	0	0	0	0	0	0	0	0
Glu432 (M5)	0	0	0	0	0	0	0	0
Avg	1	1	5	5	5	7	7	9
RNA_Rib284 (M0)	98	98	86	85	84	80	79	75
RNA_Rib284 (M1)	1	1	9	9	12	14	15	17
RNA_Rib284 (M2)	1	1	4	4	3	5	5	7
RNA_Rib284 (M3)	0	0	1	1	0	1	1	1
RNA_Rib284 (M4)	0	0	0	0	0	0	0	0
Avg	3	3	16	17	12	17	16	22

Glycogen_Glu c370 (M0)	89	90	56	57	58	48	50	39
Glycogen_Glu c370 (M1)	9	7	22	18	26	29	27	28
Glycogen_Glu c370 (M2)	2	2	14	14	11	16	16	21
Glycogen_Glu c370 (M3)	0	0	7	8	3	6	6	10
Glycogen_Glu c370 (M4)	0	0	2	3	0	1	1	2
Glycogen_Glu c370 (M5)	0	0	1	1	0	0	0	0

Table C.2 OD₆₀₀ for growth on co-substrates both with and without ¹³C-methanol (average of two replicates)

Time (hours)	(-) MeOH				(+) MeOH			
	0	24	48	72	0	24	48	72
Co-substrate								
His	0.047	0.040	0.036	0.035	0.056	0.056	0.056	0.055
Tyr	0.055	0.049	0.048	0.046	0.056	0.060	0.059	0.052
Met	0.044	0.035	0.035	0.030	0.041	0.044	0.047	0.043
Arg	0.051	0.043	0.040	0.041	0.050	0.049	0.053	0.052
Val	0.050	0.043	0.042	0.040	0.042	0.047	0.046	0.043
Ile	0.043	0.037	0.038	0.035	0.037	0.042	0.045	0.042
Leu	0.043	0.037	0.037	0.036	0.045	0.051	0.055	0.052
Phe	0.041	0.038	0.036	0.037	0.047	0.053	0.056	0.054
Lys	0.042	0.044	0.042	0.039	0.041	0.048	0.053	0.052
Gly	0.045	0.049	0.048	0.049	0.048	0.060	0.064	0.066
Cys	0.045	0.051	0.047	0.048	0.044	0.046	0.042	0.041
Trp	0.047	0.061	0.053	0.058	0.047	0.068	0.060	0.063
Ser	0.042	0.062	0.063	0.060	0.048	0.071	0.070	0.068
Pro	0.042	0.043	0.042	0.044	0.048	0.057	0.066	0.065
Glut	0.049	0.055	0.059	0.059	0.051	0.069	0.076	0.078
Asn	0.044	0.050	0.057	0.063	0.044	0.059	0.070	0.079
Thr	0.041	0.047	0.048	0.049	0.047	0.074	0.087	0.090
Gln	0.044	0.084	0.117	0.146	0.043	0.080	0.130	0.173
Ala	0.040	0.089	0.332	0.296	0.039	0.175	0.384	0.373
Asp	0.049	0.085	0.202	0.446	0.050	0.111	0.318	0.596

Ac	0.040	0.088	0.215	0.196	0.041	0.117	0.255	0.246
Pyr	0.037	0.311	0.271	0.258	0.042	0.354	0.330	0.326
Suc	0.040	0.459	0.409	0.383	0.040	0.515	0.500	0.497
Xyl	0.041	0.931	0.803	0.774	0.037	0.963	0.910	0.889
Gluc	0.041	1.166	1.088	1.046	0.042	1.244	1.206	1.196

Table C.3 ^{13}C -labeling (%) in biomass components during growth on a co-substrate and ^{13}C -methanol after 72 hours for the non-degradable amino acids (average of two replicates).

Co-substrate	His	Tyr	Val	Met	Arg	Ile	Leu	Phe	Lys
Avg	2	1	0	1	3	1	1	2	2
Ala260(M0)	97	98	100	98	96	98	98	98	97
Ala260 (M1)	1	1	0	1	2	1	1	1	1
Ala260 (M2)	1	1	0	1	2	1	1	1	1
Ala260 (M3)	1	1	0	0	1	1	1	1	1
Avg	1	0	0	0	0	0	0	0	0
Val288 (M0)	99	100	101	100	100	100	100	100	100
Val288 (M1)	0	0	0	0	0	0	0	0	0
Val288 (M2)	0	0	0	0	0	0	0	0	0
Val288 (M3)	0	0	0	0	0	0	0	0	0
Val288 (M4)	0	0	0	0	0	0	0	0	0
Val288 (M5)	0	0	0	0	0	0	0	0	0
Avg	0	0	0	0	0	0	0	0	0
Leu274 (M0)	100	100	100	100	100	100	100	100	100
Leu274 (M1)	0	0	0	0	0	0	0	0	0
Leu274 (M2)	0	0	0	0	0	0	0	0	0
Leu274 (M3)	0	0	0	0	0	0	0	0	0
Leu274 (M4)	0	0	0	0	0	0	0	0	0
Leu274 (M5)	0	0	0	0	0	0	0	0	0
Avg	0	0	0	0	0	0	0	0	0
Ile274 (M0)	100	100	100	99	100	100	100	100	100
Ile274 (M1)	0	0	0	1	0	0	0	0	0
Ile274 (M2)	0	0	0	0	0	0	0	0	0
Ile274 (M3)	0	0	0	0	0	0	0	0	0
Ile274 (M4)	0	0	0	0	0	0	0	0	0

Ile274 (M5)	0	0	0	0	0	0	0	0	0
Avg	5	4	3	5	5	4	4	5	4
Ser390 (M0)	92	93	95	91	92	92	93	92	93
Ser390 (M1)	3	3	2	4	4	4	4	4	4
Ser390 (M2)	3	2	2	3	3	3	2	3	3
Ser390 (M3)	2	1	1	2	1	1	1	1	1
Avg	3	2	2	2	3	2	2	2	3
Thr404 (M0)	95	97	97	97	94	96	96	96	94
Thr404 (M1)	0	0	0	0	0	0	0	0	0
Thr404 (M2)	3	3	2	3	4	3	3	3	4
Thr404 (M3)	0	0	0	0	0	0	0	0	0
Thr404 (M4)	1	0	0	0	1	0	1	1	1
Avg	5	3	3	3	4	4	4	5	4
Asp418 (M0)	92	94	94	94	92	93	93	92	92
Asp418 (M1)	1	1	1	0	1	1	1	1	1
Asp418 (M2)	6	4	4	5	5	5	5	6	5
Asp418 (M3)	1	0	1	0	1	1	0	1	0
Asp418 (M4)	1	1	1	1	1	1	1	1	1
Avg	4	2	2	2	2	4	3	4	3
Glu432 (M0)	91	94	94	94	94	90	93	92	94
Glu432 (M1)	2	2	2	1	2	3	2	2	2
Glu432 (M2)	4	2	2	3	2	4	3	3	3
Glu432 (M3)	2	1	1	1	1	2	1	2	1
Glu432 (M4)	1	0	0	0	0	1	1	1	0
Glu432 (M5)	0	0	0	0	0	0	0	0	0
Avg	7	11	7	7	9	8	8	9	9
RNA_Rib284 (M0)	87	80	87	86	83	85	85	84	82
RNA_Rib284 (M1)	3	5	4	5	6	4	4	4	5
RNA_Rib284 (M2)	5	8	6	6	7	6	6	6	7
RNA_Rib284 (M3)	3	4	2	2	3	3	3	4	3
RNA_Rib284 (M4)	2	3	1	2	2	2	2	2	2
Avg	46	39	40	42	43	42	46	46	43

Glycogen_Gluc 370 (M0)	21	27	23	19	20	20	16	17	17
Glycogen_Gluc 370 (M1)	10	13	15	15	13	14	13	12	15
Glycogen_Gluc 370 (M2)	20	22	24	25	23	24	24	23	25
Glycogen_Gluc 370 (M3)	25	22	22	25	24	24	26	25	24
Glycogen_Gluc 370 (M4)	15	10	11	11	12	12	13	14	12
Glycogen_Gluc 370 (M5)	9	6	5	6	7	6	8	8	6

Table C.4 ¹³C-labeling (%) in biomass components during growth on a co-substrate and ¹³C-methanol at 72 hours for degradable amino acids (average of two replicates)

Co-substrate	Cys	Trp	Pro	Gly	Ser	Glu	Asn	Thr	Gln	Ala	Asp
Avg	0	1	2	2	1	2	2	5	3	1	2
Ala260(M0)	99	98	96	97	99	96	95	92	93	98	95
Ala260 (M1)	0	1	1	1	0	2	3	3	4	1	3
Ala260 (M2)	0	1	2	1	0	1	1	3	2	1	1
Ala260 (M3)	0	0	1	1	0	0	0	1	0	0	0
Avg	0	0	0	1	0	0	1	5	3	0	2
Val288 (M0)	100	100	100	98	100	99	96	87	90	99	92
Val288 (M1)	0	0	0	1	0	0	3	5	6	1	6
Val288 (M2)	0	0	0	1	0	0	1	5	3	0	2
Val288 (M3)	0	0	0	0	0	0	0	2	1	0	0
Val288 (M4)	0	0	0	0	0	0	0	1	0	0	0
Val288 (M5)	0	0	0	0	0	0	0	0	0	0	0
Avg	0	0	0	0	0	0	1	4	3	0	2
Leu274 (M0)	100	100	100	100	100	100	97	90	87	99	90
Leu274 (M1)	0	0	0	0	0	0	2	5	10	1	8
Leu274 (M2)	0	0	0	0	0	0	1	4	3	0	2
Leu274 (M3)	0	0	0	0	0	0	0	1	0	0	0
Leu274 (M4)	0	0	0	0	0	0	0	0	0	0	0
Leu274 (M5)	0	0	0	0	0	0	0	0	0	0	0

Avg	0	0	0	0	0	0	1	3	2	1	1
Ile274 (M0)	100	99	100	99	100	99	98	90	92	97	95
Ile274 (M1)	0	0	0	0	0	0	2	5	6	2	4
Ile274 (M2)	0	0	0	0	0	0	0	3	2	0	1
Ile274 (M3)	0	0	0	0	0	0	0	0	0	0	0
Ile274 (M4)	0	0	0	0	0	0	0	0	0	0	0
Ile274 (M5)	0	0	0	0	0	0	0	0	0	0	0
Avg	1	2	3	0	0	3	3	0	4	2	3
Ser390 (M0)	99	96	94	100	101	94	93	100	91	94	92
Ser390 (M1)	1	3	3	0	0	4	5	0	6	4	6
Ser390 (M2)	0	1	2	0	0	1	1	0	2	1	2
Ser390 (M3)	0	0	1	0	0	1	0	0	1	0	0
Avg	1	1	2	3	1	1	1	0	1	1	0
Thr404 (M0)	98	97	97	95	98	98	99	101	97	96	99
Thr404 (M1)	0	2	0	1	1	0	1	-1	1	3	1
Thr404 (M2)	1	1	2	3	1	1	1	0	2	1	0
Thr404 (M3)	0	0	0	0	0	0	0	0	0	0	0
Thr404 (M4)	0	0	0	0	0	0	0	0	0	0	0
Avg	1	2	2	4	1	1	1	4	1	2	1
Asp418 (M0)	97	96	96	92	97	97	99	90	97	94	99
Asp418 (M1)	1	2	1	2	2	1	1	4	1	4	1
Asp418 (M2)	2	1	3	4	1	2	1	5	2	2	1
Asp418 (M3)	0	0	0	1	0	0	0	1	0	0	0
Asp418 (M4)	0	0	0	1	0	0	0	0	0	0	0
Avg	2	2	1	5	2	0	3	6	1	2	2
Glu432 (M0)	95	94	97	88	92	99	90	83	98	92	92
Glu432 (M1)	2	3	0	4	4	0	6	8	1	5	5
Glu432 (M2)	2	2	1	5	3	0	3	7	1	2	2
Glu432 (M3)	1	0	1	2	1	0	1	2	0	0	0
Glu432 (M4)	0	0	0	1	0	0	0	1	0	0	0
Glu432 (M5)	0	0	0	0	0	0	0	0	0	0	0
Avg	3	4	8	8	6	7	8	12	10	8	8
RNA_Rib284 (M0)	92	89	83	84	85	82	80	73	73	75	77
RNA_Rib284 (M1)	4	6	7	6	8	9	12	12	17	18	16

RNA_Rib284 (M2)	3	4	6	6	5	6	6	10	8	6	6
RNA_Rib284 (M3)	1	1	3	3	1	2	2	4	1	1	1
RNA_Rib284 (M4)	0	0	1	1	0	1	0	1	0	0	0
Avg	12	15	36	41	19	28	25	35	19	18	12
Glycogen_Gluc 370 (M0)	69	56	22	20	46	30	32	23	43	46	61
Glycogen_Gluc 370 (M1)	14	23	20	16	27	26	31	20	29	29	23
Glycogen_Gluc 370 (M2)	9	14	26	24	17	25	23	26	19	17	12
Glycogen_Gluc 370 (M3)	5	5	20	23	8	14	11	20	8	7	4
Glycogen_Gluc 370 (M4)	1	1	8	12	2	4	3	8	1	1	1
Glycogen_Gluc 370 (M5)	2	0	3	5	0	1	1	2	0	0	0

Table C.5 ¹³C-labeling (%) in biomass components during growth on a co-substrate and ¹³C-methanol at 72 hours for non-amino acids (average of two replicates)

Co-substrate	Ac	Pyr	Suc	Xyl	Gluc
Avg	4	1	2	1	1
Ala260(M0)	92	97	96	97	98
Ala260 (M1)	5	2	3	3	2
Ala260 (M2)	2	1	1	0	0
Ala260 (M3)	1	0	0	0	0
Avg	3	0	1	1	0
Val288 (M0)	90	99	97	97	98
Val288 (M1)	7	1	2	3	2
Val288 (M2)	3	0	0	0	0
Val288 (M3)	1	0	0	0	0
Val288 (M4)	0	0	0	0	0
Val288 (M5)	0	0	0	0	0
Avg	2	0	1	1	1

Leu274 (M0)	91	98	97	96	97
Leu274 (M1)	7	2	3	3	3
Leu274 (M2)	2	0	0	0	0
Leu274 (M3)	0	0	0	0	0
Leu274 (M4)	0	0	0	0	0
Leu274 (M5)	0	0	0	0	0
Avg	2	1	1	1	1
Ile274 (M0)	93	97	98	96	97
Ile274 (M1)	6	2	2	3	3
Ile274 (M2)	2	0	0	0	0
Ile274 (M3)	0	0	0	0	0
Ile274 (M4)	0	0	0	0	0
Ile274 (M5)	0	0	0	0	0
Avg	5	2	3	2	1
Ser390 (M0)	89	95	93	96	97
Ser390 (M1)	8	4	5	4	2
Ser390 (M2)	2	1	1	1	0
Ser390 (M3)	1	0	0	0	0
Avg	2	1	1	1	1
Thr404 (M0)	96	96	97	97	98
Thr404 (M1)	2	2	1	3	2
Thr404 (M2)	1	1	1	1	0
Thr404 (M3)	0	0	0	0	0
Thr404 (M4)	0	0	0	0	0
Avg	2	2	2	2	1
Asp418 (M0)	95	95	95	95	96
Asp418 (M1)	3	3	3	4	3
Asp418 (M2)	2	2	1	1	1
Asp418 (M3)	0	0	0	0	0
Asp418 (M4)	0	0	0	0	0
Avg	3	2	2	2	1
Glu432 (M0)	92	93	93	92	94
Glu432 (M1)	4	4	5	6	5
Glu432 (M2)	3	2	2	2	1
Glu432 (M3)	1	0	0	0	0
Glu432 (M4)	0	0	0	0	0
Glu432 (M5)	0	0	0	0	0

Avg	10	7	5	1	1
RNA_Rib284 (M0)	71	80	84	96	98
RNA_Rib284 (M1)	18	14	13	2	1
RNA_Rib284 (M2)	8	5	3	1	1
RNA_Rib284 (M3)	2	1	0	0	0
RNA_Rib284 (M4)	0	0	0	0	0
Avg	23	21	11	6	2
Glycogen_Gluc 370 (M0)	36	45	64	81	93
Glycogen_Gluc 370 (M1)	30	24	22	12	5
Glycogen_Gluc 370 (M2)	20	18	9	5	2
Glycogen_Gluc 370 (M3)	11	10	4	2	0
Glycogen_Gluc 370 (M4)	3	2	1	0	0
Glycogen_Gluc 370 (M5)	1	1	0	0	0

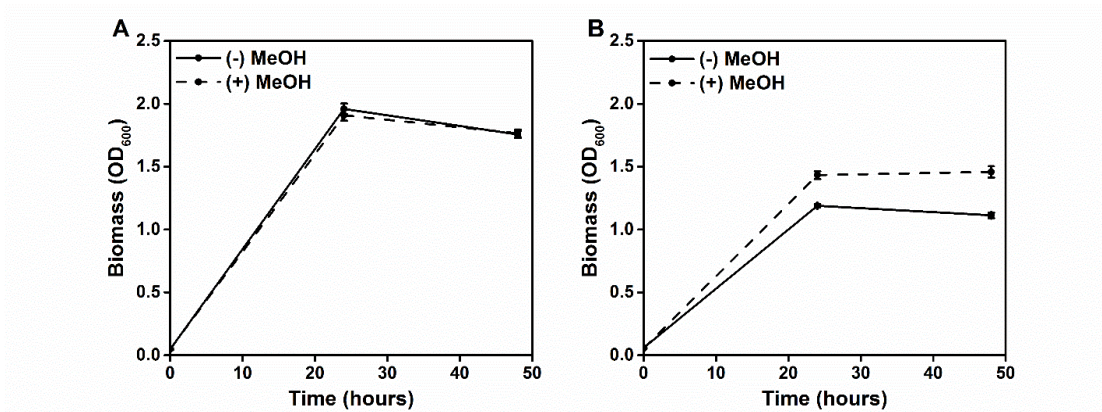


Figure C.1 Yeast extract as a co-substrate results in improved growth when methanol is present. Growth was characterized in medium containing 1.5 g/L glucose (A) or 1.5 g/L yeast extract with (dashed line) or without (solid line) 60 mM ¹³C-methanol. A substantial improvement in growth was observed when yeast extract was the co-substrate. Error bars indicate standard error ($n = 2$).

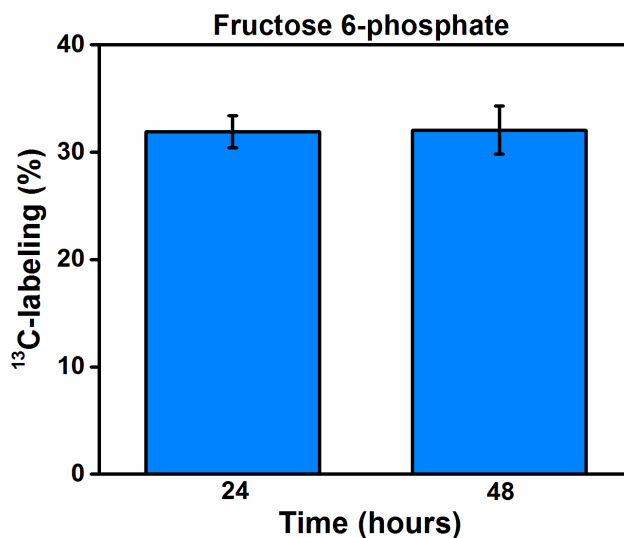


Figure C.2 High ¹³C-labeling is observed in fructose 6-phosphate, a key intermediate in methanol assimilation via the RuMP pathway. ¹³C-labeling of fructose 6-phosphate was measured for the base strain grown on 1.5 g/L yeast extract and 60 mM ¹³C-methanol at 24 and 48 hour timepoints. Error bars indicate standard error ($n = 2$).

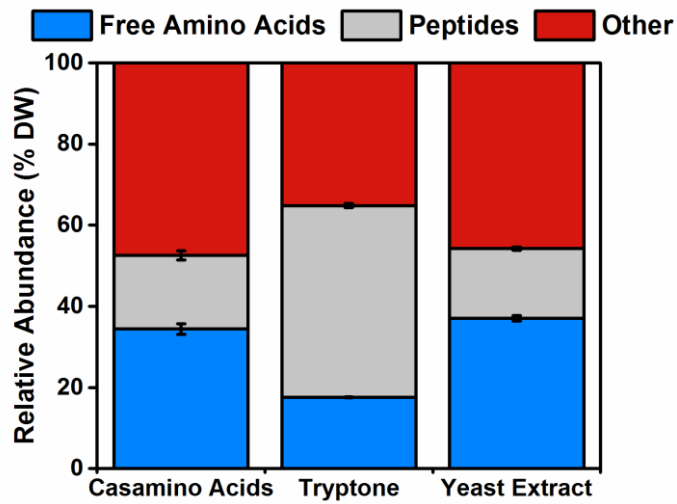


Figure C.3 Amino acids are the major components of casamino acids, tryptone, and yeast extract. The relative amount of amino acids, both as free amino acids and in peptide form, was measured for casamino acids, tryptone, and yeast extract. Amino acids composed >52% of the total dry weight. Error bars indicate standard error ($n = 4$).

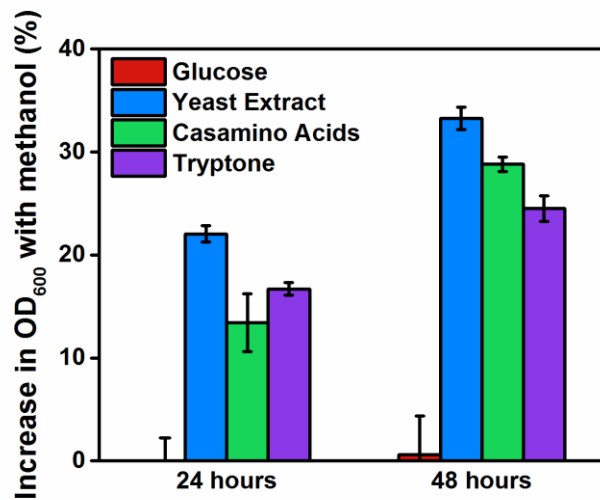


Figure C.4 Casamino acids, tryptone, and yeast extract affect growth similarly when methanol is present. The increase in OD₆₀₀ in the presence of methanol was compared to control experiments without methanol. Error bars indicate standard error ($n = 2$).

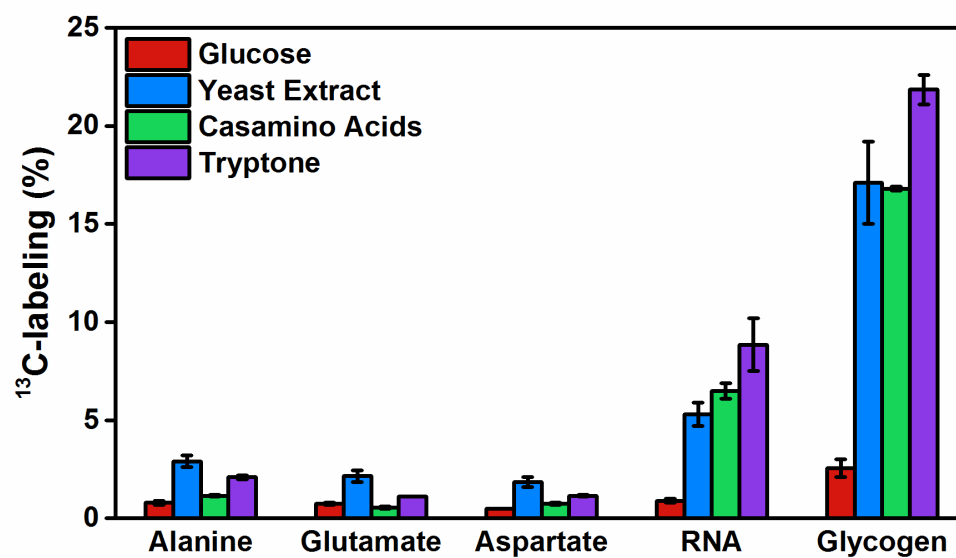


Figure C.5 ¹³C-methanol assimilation is enhanced when casamino acids, tryptone, or yeast extract are used as co-substrates. ¹³C-labeling of biomass components from ¹³C-methanol was measured for each co-substrate at 48 hours. Error bars indicate standard error ($n = 2$).

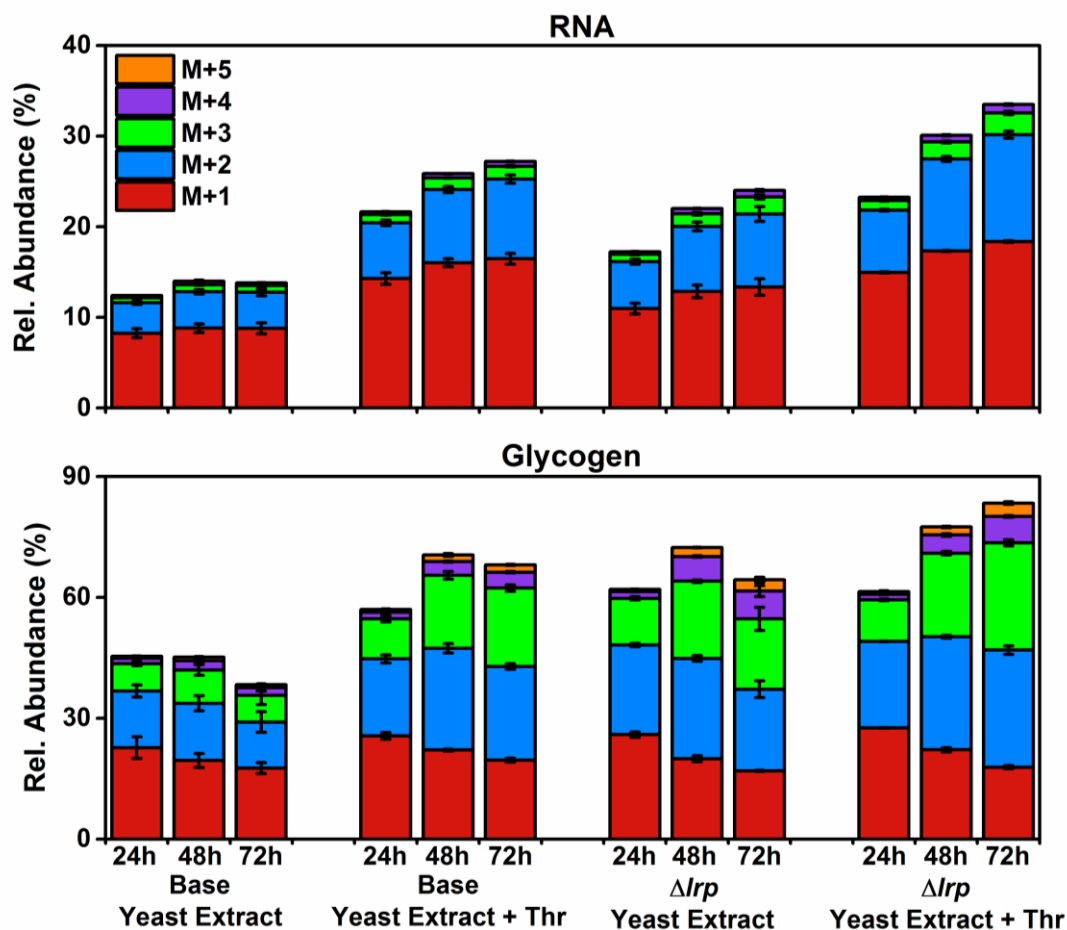


Figure C.6 Deletion of *lrp* has a similar effect as adding threonine to yeast extract in the base strain. The base strain and the Δlrp strain were both grown in 1.5 g/L yeast extract + 60 mM ^{13}C -methanol, or 1.5 g/L yeast extract + 5 mM threonine (Thr) + 60 mM ^{13}C -methanol. The ^{13}C -labeling of RNA and glycogen were measured by GC-MS. Adding threonine to yeast extract in the base strain resulted in similar labeling as Δlrp strain grown in yeast extract alone as the co-substrate. Error bars indicate standard error ($n = 3$).

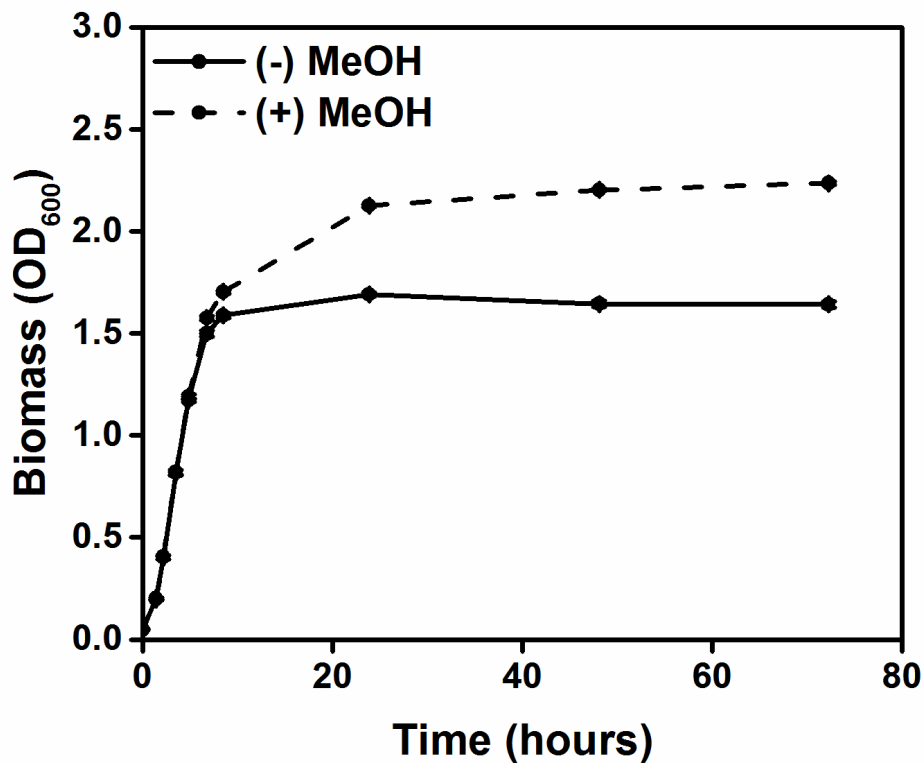


Figure C.7 Yeast extract and threonine as co-substrates also results in improved growth with methanol present. Growth of the base strain was characterized in medium containing 1.5 g/L yeast extract and 5 mM threonine with (dashed line) or without (solid line) 60 mM methanol. An improvement in growth was observed when methanol was present. Error bars indicate standard error ($n = 3$).

Appendix D

SUPPLEMENTARY DATA FOR CHAPTER 5

Table D.1 Metabolic network model used for ^{13}C -metabolic flux analysis in *M. acetivorans*. “2e” represents two electrons.

Glycolysis

- (1) G6P (abcdef) \rightleftharpoons F6P (abcdef)
- (2) FBP (abcdef) \rightleftharpoons F6P (abcdef) + P_i
- (3) FBP (abcdef) \rightleftharpoons DHAP (cba) + GAP (def)
- (4) DHAP (abc) \rightleftharpoons GAP (abc)
- (5) GAP (abc) \rightleftharpoons 3PG (abc) + ATP + 2e
- (6) 3PG (abc) \rightleftharpoons PEP (abc)
- (7) Pyr (abc) + 2ATP \rightarrow PEP (abc)

Pentose Phosphate Pathway

- (8) Ru5P (abcde) \rightleftharpoons R5P (abcde)
- (9) F6P (abcdef) \rightleftharpoons H6P (abcdef)
- (10) FAH (a) + Ru5P (bcdef) \rightleftharpoons H6P (abcdef)
- (11) R5P + 2ATP \rightarrow RuBP
- (12) RuBP + CO₂ \rightarrow 2 3PG

Amphibolic Reactions

- (13) Pyr (abc) + CO₂ (d) + ATP \rightarrow OAC(abcd)

TCA Cycle

- (14) AcCoA (ab) + 2e \rightleftharpoons PFOR-C2 (ab)
- (15) PFOR-C2 (bc) + CO₂ (a) \rightleftharpoons Pyr (abc)
- (16) OAC (abcd) + AcCoA (ef) \rightarrow Cit (dcbfea)
- (17) Cit (abcdef) \rightleftharpoons ICit (abcdef)
- (18) ICit (abcdef) \rightarrow AKG (abcde) + CO₂ (f) + 2e
- (19) AKG (abcde) \rightarrow SucCoA (bcde) + CO₂ (a) + 2e
- (20) SucCoA (abcd) \rightleftharpoons Suc ($\frac{1}{2}$ abcd + $\frac{1}{2}$ dcba) + ATP
- (21) Suc ($\frac{1}{2}$ abcd + $\frac{1}{2}$ dcba) \rightleftharpoons Fum ($\frac{1}{2}$ abcd + $\frac{1}{2}$ dcba) + 2e
- (22) Fum ($\frac{1}{2}$ abcd + $\frac{1}{2}$ dcba) \rightleftharpoons Mal (abcd)
- (23) Mal (abcd) \rightleftharpoons OAC (abcd) + 2e

Fermentation Reactions

- (24) AcCoA (ab) \rightleftharpoons Ac (ab) + ATP

Amino Acid Biosynthesis

- (25) Glu (abcde) + ATP + NH₃ -> Gln (abcde)
(26) Glu (abcde) + AKG (fghij) -> CO₂ (e) + Glu (fghij) + 2e + SucCoA(bcde)
(27) OAC (abcd) + Glu (efghi) -> Asp (abcd) + AKG (efghi)
(28) Thr (abcd) -> Gly (ab) + AcCoA (cd) + 2e
(29) Ser (abc) + THS <=> Gly (ab) + MEETHS (c)
(30) LL-DAP (½ abcdefg + ½ gfedcba) -> Lys (abcdef) + CO₂ (g)
(31) Asp (abcd) + 2 ATP + Gln (efghi) -> Asn (abcd) + Glu (efghi)
(32) Cys (abc) -> Ala (abc)
(33) AKG (abcde) + 2e + NH₃ -> Glu (abcde)
(34) Glu (abcde) + ATP + 2 2e -> Pro (abcde)
(35) Glu (abcde) + CO₂ (f) + Gln (ghijk) + Asp (lmno) + AcCoA (pq) + 5 ATP + 2e -> Arg (abcdef) + AKG (ghijk) + Fum (lmno) + Ac (pq)
(36) 3PG (abc) + Glu (defgh) -> Ser (abc) + AKG (defgh) + 2e
(37) Asp (abcd) + 2 ATP + 2 2e -> Thr (abcd)
(38) Asp (abcd) + Pyr (efg) + Glu (hijkl) + ATP + 2 2e -> LL-DAP (½ abcdgfe + ½ efgdcba) + AKG (hijkl)
(39) AcCoA(ab) + Pyr (cde) + Pyr (fgh) + Glu (ijklm) + 2e -> Ile (abgdeh) + CO₂ (a) + CO₂ (c) + AKG (ijklm)
(40) Asp (abcd) + GAP (efg) + FBP (hijklm) + PEP (nop) + 2ATP + Glu (qrstu) + 2e -> GAP (klm) + DHAP (jih) + CO₂ (a) + Phe (nopbcdefg) + AKG (qrstu) + NH₃
(41) Asp (abcd) + GAP (efg) + FBP (hijklm) + PEP (nop) + 2ATP + Glu (qrstu) + 2e -> GAP (klm) + DHAP (jih) + CO₂ (a) + AKG (qrstu) + Tyr (nopbcdefg) + NH₃
(42) Asp (abcd) + GAP (efg) + FBP (hijklm) + PEP (nop) + Gln (qrstu) + R5P(vwxyz) + Ser (aabbcc) + 4ATP + 2e -> GAP (klm) + DHAP (jih) + CO₂ (a) + GAP (wzvw) + Pyr (nop) + Glu (qrstu) + Trp (aabbccybgfedcx)
(43) Ser (abc) + AcCoA (de) + 3 ATP + 4 2e + SO₄ -> Cys (abc) + Ac (de)
(44) Pyr (abc) + Pyr (def) + Glu (ghijk) + 2e -> Val (abcef) + CO₂ (d) + AKG (ghijk)
(45) AcCoA (ab) + Pyr (cde) + Pyr (fgh) + Glu (ijklm) + 2e -> Leu (abdghe) + CO₂ (c) + CO₂ (f) + AKG
(46) Asp (abcd) + METHS (e) + AcCoA (fg) + ATP + 2e -> Met (abcde) + Ac (fg) + THS
(47) R5P (abcde) + METHS (f) + Gln (ghijk) + 2 ATP -> His (edcbaf) + AKG (ghijk) + 2 2e + THS

Isoprene Synthesis

- (48) AcCoA (ab) + AcCoA (cd) + AcCoA (ef) + 2 2e + 3 ATP -> IPP (bcfed) CO₂ (a)

Biomass Formation

- (49) 0.49 Ala + 0.267 Arg + 0.27 Asn + 0.27 Asp + 0.087 Cys + 0.46 Glu + 0.46 Gln + 0.466 Gly + 0.076 His + 0.297 Ile + 0.39 Leu + 0.343 Lys + 0.167 Met + 0.167 Phe + 0.205 Pro + 0.295 Ser + 0.301 Thr + 0.054 Trp + 0.172 Tyr + 0.356 Val +

0.463 G6P + 0.552IPP + 0.069 GAP + 0.271 3PG + 0.206 OAC + 0.476 R5P +
31.214 ATP + 0.254 2e -> 31.214 ADP + 31.214 Pi + 37.1 Biomass

Methanogenesis

- (50) E-CH₃ (a) + CO (b) <=> AcCoA (b)
 (51) CO₂ (a) + 2 2e + THS <=> MEETHS (a)
 (52) FAH (a) + THS <=> MEETHS (a)
 (53) METHS (a) <=> MeCoM (a) + THS
 (54) METHS (a) <=> E-CH₃ (a) + THS
 (55) MeOH (a) <=> MeCoM (a)
 (56) MeCoM (a) + 2e <=> CH₄ (a)
 (57) CO₂ (a) + 2e <=> CO (a)
 (58) MEETHS (a) + 2e <=> METHS (A)

Transport

- (59) CO₂ (a) -> CO₂.ext (a)
 (60) NH₃.ext -> NH₃
 (61) SO₄.ext -> SO₄
 (62) MeOH.ext -> MeOH
 (63) CH₄ -> CH₄.ext

Labeling dilution from CO₂ and external acetate

- (64) CO₂.unlabeled (abc) + CO₂ (def) -> CO₂ (abc) + CO₂.out (def)
 (65) AcCoA.unlabeled (ab) + AcCoA (cd) -> AcCoA (ab) + AcCoA.out (cd)

Table D.2 Results from ¹³C-MFA of *M. acetivorans* grown on methanol and methanol + acetate. The reaction numbers correspond to the reactions listed in Table D.1. The fluxes are normalized to a methanol uptake rate of 1000. 95% confidence intervals of fluxes (LB95 = lower bound, UB95 = upper bound) were determined by evaluating the sensitivity of the minimized SSR to flux variations. Data from a ¹³C-methanol + acetate and methanol + [U-¹³C]acetate were fit simultaneously to estimate fluxes.

Condition	Methanol			Methanol + Acetate		
SSR	132			262		
Net Fluxes						
Reaction No.	Best Fit	LB95	UB95	Best Fit	LB95	UB95
(1)	-2.5	-2.8	-2.2	-3.4	-4.2	-2.6
(2)	5.7	5.0	6.6	8.0	6.2	9.9
(3)	-7.8	-8.9	-6.9	-10.9	-13.4	-8.4
(4)	-5.7	-6.6	-5.0	-8.0	-9.9	-6.2

(5)	-13.5	-15.5	-11.9	-19.1	-23.5	-14.7
(6)	-18.9	-21.3	-16.6	-31.0	-38.0	-23.8
(7)	21.0	18.4	23.6	33.9	26.1	41.5
(8)	3.2	2.8	3.9	4.6	3.5	5.8
(9)	3.2	2.8	3.9	4.6	3.5	5.8
(10)	-3.2	-3.9	-2.8	-4.6	-5.8	-3.5
(11)	0.0	0.0	0.6	0.1	0.0	0.6
(12)	0.0	0.0	0.6	0.1	0.0	0.6
(13)	21.3	18.7	23.9	24.8	19.1	30.4
(14)	54.9	48.4	61.4	76.1	58.8	93.2
(15)	54.9	48.4	61.4	76.1	58.8	93.2
(16)	7.4	6.5	8.3	10.4	8.0	12.7
(17)	7.4	6.5	8.3	10.4	8.0	12.7
(18)	7.4	6.5	8.3	10.4	8.0	12.7
(19)	0.0	0.0	0.4	0.1	0.0	0.4
(20)	0.0	0.0	0.4	0.1	0.0	0.4
(21)	0.0	0.0	0.4	0.1	0.0	0.4
(22)	1.4	1.3	1.8	2.1	1.6	2.6
(23)	1.4	1.3	1.8	2.1	1.6	2.6
(24)	-5.4	-6.0	-4.7	-7.5	-9.1	-5.8
(25)	6.0	5.3	6.7	8.3	6.4	10.2
(26)	0.0	0.0	0.4	0.1	0.0	0.4
(27)	14.2	12.4	16.1	14.9	11.5	18.6
(28)	3.5	2.6	4.4	0.1	0.0	1.4
(29)	-1.0	-1.8	-0.2	3.3	1.9	4.2
(30)	1.8	1.6	2.0	2.5	2.0	3.1
(31)	1.4	1.3	1.6	2.0	1.5	2.4
(32)	2.6	2.3	2.9	3.6	2.8	4.4
(33)	36.5	32.2	40.8	50.6	39.1	62.0
(34)	1.1	1.0	1.2	1.5	1.2	1.9
(35)	1.4	1.3	1.6	2.0	1.5	2.4
(36)	3.9	3.1	4.9	10.2	7.7	12.6
(37)	5.1	4.1	6.1	2.3	1.7	3.8
(38)	1.8	1.6	2.0	2.5	2.0	3.1
(39)	1.6	1.4	1.8	2.2	1.7	2.7
(40)	0.9	0.8	1.0	1.2	1.0	1.5
(41)	0.9	0.8	1.0	1.3	1.0	1.6
(42)	0.3	0.3	0.3	0.4	0.3	0.5
(43)	3.1	2.7	3.4	4.3	3.3	5.2
(44)	1.9	1.7	2.1	2.6	2.0	3.2
(45)	2.1	1.8	2.3	2.9	2.2	3.5
(46)	0.9	0.8	1.0	1.2	1.0	1.5
(47)	0.4	0.4	0.5	0.6	0.4	0.7

(48)	2.9	2.6	3.3	4.1	3.1	5.0
(49)	5.3	4.7	5.9	7.4	5.7	9.0
(50)	71.3	62.8	79.7	103.7	80.0	127.0
(51)	-284.3	-288.3	-280.2	-296.4	-306.9	-285.8
(52)	3.2	2.8	3.9	4.6	3.5	5.8
(53)	-354.6	-367.0	-342.3	-394.0	-426.1	-361.2
(54)	71.3	62.8	79.7	103.7	80.0	127.0
(55)	1000.0	999.8	1000.2	1000.0	999.9	1000.1
(56)	645.4	633.0	657.7	606.0	573.9	638.8
(57)	71.3	62.8	79.7	103.7	80.0	127.0
(58)	-282.1	-286.0	-278.2	-288.5	-297.3	-279.7
(59)	158.9	148.2	169.7	122.5	93.9	151.5
(60)	40.7	35.9	45.5	56.5	43.6	69.1
(61)	3.1	2.7	3.4	4.3	3.3	5.2
(62)	1000.0	999.8	1000.2	1000.0	999.9	1000.1
(63)	645.4	633.0	657.7	606.0	573.9	638.8
(64)	8797.7	5976.4	10622.4	6824.3	6210.2	8754.4
(65)		Not in model		194.5	148.8	253.2
Exchange Fluxes						
(1)	968.9	0.0	Inf	>1000	0.0	Inf
(3)	227.4	0.0	Inf	>1000	0.0	Inf
(4)	386.9	0.0	Inf	>1000	0.0	Inf
(5)	0.0	0.0	Inf	0.0	0.0	Inf
(6)	0.3	0.0	Inf	Inf	0.0	Inf
(8)	672.5	0.0	Inf	>1000	0.0	Inf
(9)	691.6	0.0	Inf	>1000	>1000	Inf
(10)	394.5	0.0	Inf	>1000	>1000	Inf
(14)	661.2	0.0	Inf	>1000	0.0	Inf
(15)	619.2	0.0	Inf	>1000	0.0	Inf
(17)	189.8	0.0	Inf	>1000	0.0	Inf
(18)	956.7	0.0	Inf	>1000	0.0	Inf
(20)	47.3	0.0	Inf	>1000	0.0	Inf
(21)	854.3	0.0	Inf	>1000	0.0	Inf
(22)	107.0	1.6	Inf	4.2	1.6	7.6
(23)	2.6	1.6	Inf	>1000	>1000	Inf
(24)	359.7	0.0	Inf	>1000	153.1	Inf
(29)	0.0	0.0	0.9	0.0	0.0	0.1
(50)	Inf	507.1	Inf	44.3	34.6	67.6
(51)	>1000	396.9	Inf	79.8	67.3	175.0
(52)	280.2	0.0	Inf	>1000	>1000	Inf
(53)	>1000	0.0	Inf	0.0	0.0	Inf
(54)	0.0	0.0	9.2	2.6	0.0	64.6
(55)	659.1	0.0	Inf	>1000	0.0	Inf

(56)	841.1	0.0	Inf	562.8	0.0	Inf
(57)	830.1	103.4	Inf	Inf	>1000	Inf
(58)	425.0	152.4	>1000	Inf	>1000	Inf

Table D.3 Mass isotopomer distributions from labeling experiments using ^{13}C -methanol, ^{13}C -methanol + acetate, or methanol + $[\text{U-}^{13}\text{C}]$ acetate as substrates.

Tracer	^{13}C -Methanol	^{13}C -Methanol + Acetate	Methanol + $[\text{U-}^{13}\text{C}]$ Acetate
Ala232 (M0)	39.5	60.6	49.5
Ala232 (M1)	43.4	27.5	15.3
Ala232 (M2)	12.5	9.3	27.8
Ala232 (M3)	3.9	2.2	5.4
Ala232 (M4)	0.7	0.4	2.1
Ala260 (M0)	38.6	58.7	48.8
Ala260 (M1)	42.0	28.1	15.6
Ala260 (M2)	14.0	9.9	27.5
Ala260 (M3)	4.4	2.8	5.7
Ala260 (M4)	0.9	0.5	2.1
Ala260 (M5)	0.1	0.1	0.3
Gly218 (M0)	73.5	75.1	54.0
Gly218 (M1)	18.3	17.0	34.1
Gly218 (M2)	7.0	6.8	9.2
Gly218 (M3)	1.2	1.1	2.7
Gly246 (M0)	70.1	72.1	53.2
Gly246 (M1)	20.5	19.0	34.0
Gly246 (M2)	7.7	7.4	9.6
Gly246 (M3)	1.5	1.3	2.8
Gly246 (M4)	0.2	0.2	0.4
Val260 (M0)	27.2	49.9	39.7
Val260 (M1)	26.5	30.6	12.9
Val260 (M2)	32.0	14.2	20.0
Val260 (M3)	10.2	4.0	8.7
Val260 (M4)	3.3	1.1	14.6

Val260 (M5)	0.6	0.2	3.0
Val260 (M6)	0.1	0.0	1.1
Val288 (M0)	26.9	48.8	39.5
Val288 (M1)	25.8	30.5	13.0
Val288 (M2)	31.5	14.8	19.9
Val288 (M3)	11.2	4.4	8.8
Val288 (M4)	3.6	1.2	14.3
Val288 (M5)	0.9	0.3	3.2
Val288 (M6)	0.2	0.1	1.2
Val288 (M7)	0.0	0.0	0.2
Leu274 (M0)	23.3	42.8	35.0
Leu274 (M1)	15.5	30.0	13.7
Leu274 (M2)	25.6	18.1	12.6
Leu274 (M3)	24.6	6.6	14.2
Leu274 (M4)	7.9	1.9	10.2
Leu274 (M5)	2.5	0.5	11.0
Leu274 (M6)	0.5	0.1	2.4
Leu274 (M7)	0.1	0.0	0.8
Ile200 (M0)	25.8	47.3	38.7
Ile200 (M1)	15.4	29.7	12.1
Ile200 (M2)	26.4	16.3	11.8
Ile200 (M3)	24.6	5.2	14.4
Ile200 (M4)	6.1	1.1	9.8
Ile200 (M5)	1.4	0.3	11.2
Ile200 (M6)	0.2	0.0	1.6
Ile200 (M7)	0.1	0.1	0.6
Ile274 (M0)	23.2	42.6	34.7
Ile274 (M1)	15.6	30.2	13.6
Ile274 (M2)	25.7	18.1	12.6
Ile274 (M3)	24.6	6.7	14.2
Ile274 (M4)	8.0	1.9	10.2
Ile274 (M5)	2.5	0.5	11.3
Ile274 (M6)	0.5	0.1	2.5
Ile274 (M7)	0.1	0.0	0.9
Met218 (M0)	25.9	36.9	50.0
Met218 (M1)	25.6	35.3	13.9
Met218 (M2)	34.9	20.0	28.3
Met218 (M3)	9.6	5.8	5.1

Met218 (M4)	3.4	1.7	2.3
Met320 (M0)	22.7	32.4	44.4
Met320 (M1)	24.0	33.5	16.0
Met320 (M2)	33.3	22.0	28.0
Met320 (M3)	12.9	8.4	7.2
Met320 (M4)	5.3	2.8	3.5
Met320 (M5)	1.4	0.7	0.7
Ser362 (M0)	32.4	52.3	43.6
Ser362 (M1)	43.7	30.7	18.8
Ser362 (M2)	17.3	13.0	28.9
Ser362 (M3)	6.6	4.0	8.6
Ser390 (M0)	30.7	49.7	41.0
Ser390 (M1)	41.4	30.7	18.2
Ser390 (M2)	18.4	13.7	27.6
Ser390 (M3)	7.3	4.5	8.8
Ser390 (M4)	1.9	1.1	3.6
Ser390 (M5)	0.4	0.3	0.8
Thr376 (M0)	31.5	50.3	41.9
Thr376 (M1)	41.1	30.4	18.4
Thr376 (M2)	18.0	13.3	26.7
Thr376 (M3)	7.0	4.4	8.4
Thr376 (M4)	1.8	1.1	3.4
Thr376 (M5)	0.1	0.6	1.2
Thr404 (M0)	31.2	48.8	41.3
Thr404 (M1)	39.7	30.8	19.0
Thr404 (M2)	19.0	14.1	26.6
Thr404 (M3)	7.4	4.6	8.5
Thr404 (M4)	2.1	1.3	3.6
Thr404 (M5)	0.5	0.3	0.8
Thr404 (M6)	0.1	0.1	0.2
Phe302 (M0)	67.6	69.4	52.6
Phe302 (M1)	22.4	21.1	33.9
Phe302 (M2)	8.3	7.9	10.6
Phe302 (M3)	1.7	1.5	3.0
Phe308 (M0)	22.6	39.9	35.1
Phe308 (M1)	14.6	29.4	11.8

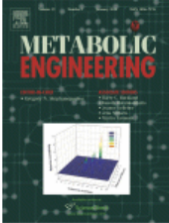
Phe308 (M2)	23.3	19.2	13.3
Phe308 (M3)	24.3	8.1	8.0
Phe308 (M4)	10.6	2.6	14.2
Phe308 (M5)	3.5	0.7	6.9
Phe308 (M6)	0.9	0.1	8.2
Phe308 (M7)	0.2	0.0	1.9
Phe308 (M8)	0.2	0.1	0.8
Phe336 (M0)	22.4	39.0	34.8
Phe336 (M1)	14.3	29.0	12.0
Phe336 (M2)	22.6	19.4	13.3
Phe336 (M3)	23.9	8.5	8.0
Phe336 (M4)	11.3	2.8	14.0
Phe336 (M5)	4.0	0.8	6.9
Phe336 (M6)	1.0	0.2	8.1
Phe336 (M7)	0.3	0.1	2.0
Phe336 (M8)	0.1	0.1	0.7
Phe336 (M9)	0.2	0.1	0.2
Asp302 (M0)	64.6	67.9	49.5
Asp302 (M1)	23.4	21.9	35.9
Asp302 (M2)	8.9	8.4	11.3
Asp302 (M3)	2.2	1.8	3.3
Asp390 (M0)	30.5	49.8	40.6
Asp390 (M1)	41.7	30.8	18.1
Asp390 (M2)	18.4	13.7	28.1
Asp390 (M3)	7.2	4.4	8.8
Asp390 (M4)	1.9	1.1	3.6
Asp390 (M5)	0.4	0.2	0.8
Asp418 (M0)	21.0	48.2	40.4
Asp418 (M1)	27.8	31.1	18.4
Asp418 (M2)	34.3	14.4	27.7
Asp418 (M3)	12.1	4.7	8.9
Asp418 (M4)	3.9	1.3	3.7
Asp418 (M5)	0.8	0.3	0.8
Asp418 (M6)	0.1	0.1	0.2
Glu330 (M0)	21.0	44.3	31.0
Glu330 (M1)	27.8	33.1	13.4
Glu330 (M2)	34.3	16.0	22.0
Glu330 (M3)	12.1	5.0	12.0

Glu330 (M4)	3.9	1.3	16.2
Glu330 (M5)	0.8	0.2	4.0
Glu330 (M6)	0.1	0.0	1.4
Glu432 (M0)	18.5	38.8	27.5
Glu432 (M1)	25.5	32.5	13.4
Glu432 (M2)	32.8	18.7	21.9
Glu432 (M3)	15.1	7.2	11.8
Glu432 (M4)	6.0	2.2	17.1
Glu432 (M5)	1.7	0.6	5.5
Glu432 (M6)	0.4	0.1	2.3
Glu432 (M7)	0.1	0.0	0.5
Lys329 (M0)	25.3	45.3	38.2
Lys329 (M1)	25.7	31.7	15.0
Lys329 (M2)	31.3	16.0	19.9
Lys329 (M3)	12.5	5.2	9.5
Lys329 (M4)	4.1	1.4	12.9
Lys329 (M5)	1.0	0.3	3.4
Lys329 (M6)	0.3	0.1	1.1
Lys431 (M0)	22.5	40.1	34.1
Lys431 (M1)	24.4	31.6	16.2
Lys431 (M2)	30.1	18.3	19.9
Lys431 (M3)	14.8	7.1	10.5
Lys431 (M4)	5.9	2.3	12.9
Lys431 (M5)	1.7	0.6	4.3
Lys431 (M6)	0.4	0.1	1.7
Lys431 (M7)	0.1	0.0	0.4
Lys431 (M8)	0.0	0.0	0.1
Tyr302 (M0)	67.5	69.4	51.4
Tyr302 (M1)	22.5	21.2	34.9
Tyr302 (M2)	8.3	7.9	10.7
Tyr302 (M3)	1.7	1.5	3.1

Appendix E

REPRINT PERMISSION LETTERS

  [Home](#) [Account Info](#) [Help](#) 



Title: Comprehensive analysis of glucose and xylose metabolism in *Escherichia coli* under aerobic and anaerobic conditions by 13C metabolic flux analysis

Author: Jacqueline E. Gonzalez, Christopher P. Long, Maciek R. Antoniewicz

Publication: Metabolic Engineering

Publisher: Elsevier

Date: January 2017

© 2016 International Metabolic Engineering Society. Published by Elsevier Inc. All rights reserved.

Logged in as:
Jacqueline Gonzalez
[LOGOUT](#)

Please note that, as the author of this Elsevier article, you retain the right to include it in a thesis or dissertation, provided it is not published commercially. Permission is not required, but please ensure that you reference the journal as the original source. For more information on this and on your other retained rights, please visit: <https://www.elsevier.com/about/our-business/policies/copyright#Author-rights>

[BACK](#)

[CLOSE WINDOW](#)

Copyright © 2018 [Copyright Clearance Center, Inc.](#) All Rights Reserved. [Privacy statement.](#) [Terms and Conditions.](#)
Comments? We would like to hear from you. E-mail us at customercare@copyright.com

  [Home](#) [Account Info](#) [Help](#) 



Title: Tracing metabolism from lignocellulosic biomass and gaseous substrates to products with stable-isotopes

Author: Jacqueline E Gonzalez, Maciek R Antoniewicz

Publication: Current Opinion in Biotechnology

Publisher: Elsevier

Date: February 2017

© 2016 Elsevier Ltd. All rights reserved.

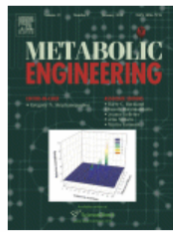
Logged in as:
Jacqueline Gonzalez
[LOGOUT](#)

Please note that, as the author of this Elsevier article, you retain the right to include it in a thesis or dissertation, provided it is not published commercially. Permission is not required, but please ensure that you reference the journal as the original source. For more information on this and on your other retained rights, please visit: <https://www.elsevier.com/about/our-business/policies/copyright#Author-rights>

[BACK](#)

[CLOSE WINDOW](#)

Copyright © 2018 [Copyright Clearance Center, Inc.](#) All Rights Reserved. [Privacy statement.](#) [Terms and Conditions.](#)
Comments? We would like to hear from you. E-mail us at customercare@copyright.com



Title: Methanol assimilation in Escherichia coli is improved by co-utilization of threonine and deletion of leucine-responsive regulatory protein

Author: Jacqueline E. Gonzalez, R. Kyle Bennett, E. Terry Papoutsakis, Maciek R. Antoniewicz

Publication: Metabolic Engineering

Publisher: Elsevier

Date: January 2018

© 2017 International Metabolic Engineering Society.
Published by Elsevier Inc. All rights reserved.

Logged in as:
Jacqueline Gonzalez
Account #:
3001284577

LOGOUT

Please note that, as the author of this Elsevier article, you retain the right to include it in a thesis or dissertation, provided it is not published commercially. Permission is not required, but please ensure that you reference the journal as the original source. For more information on this and on your other retained rights, please visit: <https://www.elsevier.com/about/our-business/policies/copyright#Author-rights>

BACK

CLOSE WINDOW

Copyright © 2018 [Copyright Clearance Center, Inc.](#) All Rights Reserved. [Privacy statement](#). [Terms and Conditions](#).
Comments? We would like to hear from you. E-mail us at customercare@copyright.com